University of Surrey
Faculty of Engineering and Physical Sciences

Modelling chassis flexibility in vehicle dynamics simulation

by Enrico Sampò

Supervisors:
Dr. Aldo Sorniotti
Prof. Andrew Crocombe

Submitted for the Degree of Doctor of Philosophy

Declaration

I hereby declare that the work contained in this thesis is my own original work and has not been previously submitted, in its entirety or in part, to any University for a degree.

Guildford, March 2011

Enrico Sampò

Abstract

This thesis deals with the development of advanced mathematical models for the assessment of the influence of chassis flexibility on vehicle handling qualities.

A review of the literature relevant to the subject is presented and discussed in the first part of the thesis. A preliminary model that includes chassis flexibility is then developed and employed for a first assessment of the significance of chassis flexibility. In the second part of the thesis a symbolic multibody library for vehicle dynamics simulations is introduced. This library constitutes the basis for the development of an advanced 14-degrees-of-freedom vehicle model that includes chassis flexibility. The model is then demonstrated using a set of data relative to a real vehicle. Finally, simulation results are discussed and conclusions are presented.

The advanced model fully exploits a novel multibody formulation which represent the kinematics and the dynamics of the system with a level of accuracy which is typical of numeric multibody models while retaining the benefits of purpose-developed hand-derived models. More specifically, a semi-recursive formulation, a velocity projection technique and a symbolic development are, for the first time, coupled with flexible body modelling.

The effect of chassis flexibility on vehicle handling is observed through the analysis of open- and closed-loop manoeuvres. Results show that chassis flexibility induces variations of lateral load transfer distribution and suspension kinematics that sensibly affect the steady-state behaviour of the vehicle. Further effects on dynamic response and high-speed stability are demonstrated. Also, optimal control theory is employed to demonstrate the existence of a strict correlation between chassis flexibility and driver behaviour.

The research yields new insights into the dynamics of vehicles with a flexible chassis and highlights critical aspects of chassis design. Although the focus is on sports and race cars, both the modelling approach and the results can be extended to other vehicles.

Acknowledgements

I would like to express here my gratitude to my supervisors Aldo and Andy for their uninterrupted support and advice throughout the years. Also, I gratefully acknowledge the funding provided by the University Research Committee. In addition, I thank all the members of the SAVAG, EnFlo and TFS UTC groups who have helped me enjoy these years at the University.

Contents

List of figures viii

List of tables ix

Nomenclature x

1 Introduction 1
- 1.1 Context . . . 1
- 1.2 Scope of the research . . . 2
- 1.3 Outline of the thesis . . . 3

2 Vehicle chassis and vehicle dynamics 5
- 2.1 The chassis . . . 5
  - 2.1.1 Introduction . . . 5
  - 2.1.2 Notes on chassis evolution . . . 6
  - 2.1.3 Loads and deformations . . . 8
  - 2.1.4 Chassis properties . . . 9
- 2.2 Vehicle dynamics modelling . . . 14
  - 2.2.1 Introduction . . . 14
  - 2.2.2 Purpose-designed models . . . 15
  - 2.2.3 Multibody packages . . . 20
  - 2.2.4 Toolkits . . . 20
- 2.3 Modelling of vehicles with a flexible chassis . . . 20
  - 2.3.1 Introduction . . . 20
  - 2.3.2 Models for lateral load transfer analysis . . . 21
  - 2.3.3 Models for stability analysis . . . 23
  - 2.3.4 Multi-purpose vehicle models . . . 24
  - 2.3.5 Ride models . . . 27
- 2.4 Driver modelling . . . 27
- 2.5 Concluding remarks . . . 29

3 A preliminary vehicle model with a flexible chassis 31
3.1 Lateral load transfer distribution . . . 31
3.1.1 Rigid vehicle . . . 31
3.1.2 Flexible vehicle . . . 33
3.2 Roll steer . . . 36
3.2.1 Rigid vehicle . . . 36
3.2.2 Flexible vehicle . . . 37
3.3 Vehicle dynamics . . . 40
3.3.1 Equations of motion . . . 40
3.3.2 Steady-state vehicle behaviour . . . 43
3.3.3 Transitory dynamics . . . 45
3.3.4 Root locus analysis . . . 46
3.3.5 Frequency response . . . 48
3.3.6 Optimal controls . . . 49
3.4 Concluding remarks . . . 54

4 Multibody dynamics 56
4.1 Overview . . . 56
4.2 Fundamentals of multibody simulation . . . 58
4.3 System coordinates . . . 58
4.3.1 Introduction . . . 58
4.3.2 Reference point coordinates . . . 59
4.3.3 Relative coordinates . . . 61
4.3.4 Natural coordinates . . . 61
4.3.5 Mixed coordinates . . . 62
4.4 System constraints . . . 62
4.5 Equations of motion . . . 63
4.6 Deformable bodies . . . 64
4.6.1 Overview . . . 64
4.6.2 Floating frame of reference formulation . . . 65
4.6.3 Absolute nodal coordinate formulation . . . 67
4.7 Recursive algorithms . . . 67
4.8 Reduction techniques . . . 68
4.8.1 Index reduction techniques . . . 69
4.8.2 Coordinate partitioning . . . 70
4.8.3 Coordinate reduction . . . 71
4.8.4 Other formulations . . . 73
4.9 Symbolic generation of the equations of motions . . . 74
4.10 Numerical integration of the equations of motion . . . 75
4.10.1 Solution of ODEs . . . 75

4.10.2 Solution of DAEs . . . 76
4.11 Concluding remarks . . . 77

5 A symbolic library for flexible multibody modelling 79
5.1 Introduction . . . 79
5.2 Kinematics . . . 80
5.2.1 Rigid body . . . 80
5.2.2 Flexible body . . . 82
5.3 Constraints . . . 83
5.3.1 Spherical joint . . . 83
5.3.2 Link joint . . . 84
5.3.3 Revolute joint . . . 84
5.4 Dynamics . . . 84
5.4.1 Rigid body . . . 84
5.4.2 Flexible body . . . 87
5.5 Dynamic formulation . . . 89
5.5.1 Newton-Euler equations . . . 89
5.5.2 Semi-recursive formulation . . . 89
5.5.3 Coordinate reduction technique . . . 91
5.6 Implementation . . . 93
5.7 Example . . . 96
5.8 Concluding remarks . . . 98

6 A vehicle model with a flexible chassis 100
6.1 Model description . . . 100
6.1.1 Introduction . . . 100
6.1.2 Kinematics . . . 101
6.1.3 Constraints . . . 103
6.1.4 Dynamics . . . 105
6.1.5 External loads . . . 107
6.2 Vehicle data . . . 113
6.2.1 General data . . . 113
6.2.2 Chassis . . . 113
6.3 Model Implementation . . . 118
6.3.1 Main program . . . 118
6.3.2 ODE Solver . . . 118
6.4 Rigid model verification . . . 119
6.4.1 Adams/Car model . . . 119
6.4.2 Suspension kinematics . . . 120
6.4.3 Vehicle behaviour . . . 123

6.4.4 Computational efficiency . . . 125
6.5 Concluding remarks . . . 125

7 Chassis flexibility and vehicle dynamics 127
7.1 Steady-state behaviour . . . 127
7.1.1 Analysis of modal coordinates . . . 127
7.1.2 Lateral load transfer distribution . . . 128
7.1.3 Suspension kinematics . . . 130
7.1.4 Handling characteristics . . . 134
7.2 Transient dynamics . . . 136
7.3 Root locus analysis . . . 137
7.4 Frequency response . . . 139
7.4.1 Driver input . . . 139
7.4.2 Road input . . . 141
7.5 Optimal controls . . . 143
7.6 Computational aspects . . . 144
7.6.1 Effect of chassis deformation on inertial forces . . . 144
7.6.2 Influence of coordinate reduction . . . 145
7.6.3 Computational efficiency . . . 145
7.7 Concluding remarks . . . 146

8 Conclusions and future work 148
8.1 Conclusions . . . 148
8.2 Future work . . . 151

A Input data for the preliminary model of Chapter 3 153

B Input data for the vehicle model of Chapter 4 155

References 159

List of figures

2.1 Chassis assembly for torsional stiffness testing 12

3.1 Rigid model for lateral load transfer 32
3.2 Flexible model for lateral load transfer 33
3.3 Effect of chassis torsional stiffness on lateral load transfer distribution 35
3.4 Effect of chassis torsional stiffness on understeer gradient through roll steer mechanism 39
3.5 Five-degrees-of-freedom vehicle model 40
3.6 Vehicle steady-state characteristics during a skid-pad test 43
3.7 Effect of chassis torsional stiffness on vehicle behaviour adjustment . . 44
3.8 Effect of chassis flexibility on steering step response 46
3.9 System root locus plot 47
3.10 Comparison between frequency response of the vehicle when chassis torsional compliance is included or neglected 48
3.11 Effect of chassis torsional stiffness on TI-optimal preview gains 53

4.1 Types of available coordinate systems for multibody systems 60

5.1 Yaw-pitch-roll sequence for rigid bodies 80
5.2 Compound planar double pendulum. 97

6.1 Coordinate reference systems 102
6.2 Double wishbone suspension geometry and hard points. 103
6.3 Transmission of lateral forces over a suspension wishbone 104
6.4 Lower wishbone geometry 107
6.5 Rocker arm geometry 109
6.6 Lower wishbone free body diagram 110
6.7 Finite element model of the chassis 114
6.8 Six lowest modes of the chassis 115
6.9 Comparison between modal truncation and component mode synthesis 117
6.10 Adams/Car multibody model of the vehicle. 119

6.11 Comparative responses of the 14 d.o.f. model and Adams/Car during a bump test of the front suspension 120
6.12 Comparison between of the 14 d.o.f. model and Adams/Car during a steering test 121
6.13 Comparative responses of the 14 d.o.f. model and Adams/Car during a ramp steer manoeuvre at 40 km/h 122
6.14 Comparative responses of the 14 d.o.f. model and Adams/Car during a step-steer manoeuvre at 40 km/h 123
6.15 Comparison between the frequency response of the vehicle obtained by using the 14 d.o.f. model and Adams/Car 124

7.1 Modal coordinates 128
7.2 Effect of chassis flexibility on lateral load transfer distribution 129
7.3 Sparsity pattern for reduction matrices 131
7.4 Effect of chassis flexibility on suspension kinematics 134
7.5 Vehicle steady-state characteristics during skid-pad test 135
7.6 Effect of chassis flexibility on steering step response 136
7.7 Root locus plots 138
7.8 Frequency response to steering input 140
7.9 Frequency response to road input 142
7.10 Effect of chassis flexibility on TI-optimal controls 143

B.1 Tyre force characteristics 158

List of tables

2.1 Indicative values of chassis torsional stiffness for different vehicles . . . 11
2.2 Comparison of some of the key features of the software packages available for vehicle dynamics studies . . . 15
2.3 Comparison of the most representative models for vehicle dynamics studies . . . 16

5.1 Available commands for the definition of multibody systems . . . 94
5.2 Available commands for the generation of the equations of motion of the multibody system . . . 95
5.3 Computational routines . . . 96

6.1 Vehicle bodies . . . 101
6.2 Hard points of the front left suspension. . . . 104
6.3 Links of the double wishbone suspension. . . . 105
6.4 Natural frequencies and modes of vibration of the chassis. . . . 116
6.5 Comparison of CPU time for different solvers. . . . 118
6.6 Comparison of CPU time, 14-degrees-of-freedom model versus Adams/Car 125

7.1 Kinematic gradients from projection matrix analysis. . . . 133
7.2 Comparison of computational efficiency . . . 146

A.1 Vehicle data . . . 153

B.1 Vehicle data . . . 155
B.2 Front left suspension hard points . . . 156
B.3 Rear left suspension hard points . . . 157
B.4 Tyre data . . . 157

Nomenclature

a	distance of vehicle c.g. from front axle
a_y	vehicle lateral acceleration
$\boldsymbol{A}$	rotation matrix
b	distance of vehicle c.g. from rear axle
$\boldsymbol{b}$	time-dependent vector for velocities projection
$\boldsymbol{B}$	velocity Jacobian matrix
c_C	chassis torsional damping
c_F, c_R	front and rear roll damping
$\boldsymbol{c}$	second order time dependent vector for velocities projection
C_F, C_R	front and rear cornering stiffness
$\boldsymbol{C}$	position-dependent matrix for recursive formulation
$\boldsymbol{D}$	joint-dependent matrix for recursive formulation
$\boldsymbol{e}$	vector of independent generalised speeds
F_x	tyre longitudinal force
F_y	tyre lateral force
F_z	tyre vertical force
$\boldsymbol{g}$	vector of gravity acceleration
$\boldsymbol{G}$	inverse velocity Jacobian matrix
h_G	complete vehicle c.g. height
h_{uF}, h_{uR}	front and rear height of unsprung mass c.g.
h_{sF}, h_{sR}	height of front and rear part of sprung mass c.g.
$\boldsymbol{I}$	identity matrix
J_{rF}, J_{rR}	front and rear roll inertia
J_{xs}	sprung mass moment of inertia about $x-x$ axis
J_{xuF}, J_{xuR}	front and rear unsprung mass cambering moment of inertia
J_{xzs}	sprung mass moment xz product of inertia
J_{yuF}, J_{yuR}	front and rear unsprung mass pitching moment of inertia
J_{ys}	sprung mass moment of inertia about $y-y$ axis
J_{wF}, J_{wR}	front and rear wheel spin moment of inertia
J_z	vehicle yaw inertia

J_{zs}	sprung mass moment of inertia about $z-z$ axis
J_{zuF}, J_{zuR}	front and rear unsprung mass yawing moment of inertia
k	tyre longitudinal slip
k_C	chassis torsional stiffness
k_F, k_R	front and rear roll stiffness
k_{stw}	steer ratio
k_u	understeer gradient
$\boldsymbol{K}$	generalised stiffness matrix
$\boldsymbol{K}_p$	vector of preview gains
l	vehicle wheelbase
L	Lagrangian
L_p	preview distance
m	vehicle mass
m_{uF}, m_{uR}	front and rear unsprung mass
m_s	sprung mass
M_z	tyre self-aligning moment
$\boldsymbol{M}$	generalised mass matrix
$\boldsymbol{P}$	constant projection matrix
$\boldsymbol{q}$	vector of generalised coordinates
$\boldsymbol{Q_e}$	vector of external forces
$\boldsymbol{Q_i}$	vector of internal forces
r	yaw rate
$\boldsymbol{R}$	coordinate-dependent reduction matrix
$\boldsymbol{s}$	vector of independent joint coordinates
$\boldsymbol{S}$	time-dependent reduction matrix
t_F, t_R	front and rear track widths
T	kinetic energy
$\boldsymbol{T}$	global recursion matrix
U	potential energy
$\boldsymbol{v}$	vector of generalised velocities
$\boldsymbol{y}$	vector of joint velocities
$\boldsymbol{z}$	vector of independent joint velocities
z_F, z_R	front and rear roll centre height
α	tyre slip angle
β	vehicle slip angle
γ_R, γ_R	static front and rear camber angles
δ_F, δ_R	front and rear steer angle
δ_{sw}	steering wheel angle
$\Delta F_{zF}, \Delta F_{zR}$	front and rear lateral load transfer

$\varepsilon_F, \varepsilon_R$	front and rear roll steer coefficients
ζ	roll moment distribution
ϑ	pitch angle
$\boldsymbol{\theta}$	Euler angles
λ	roll stiffness distribution
$\boldsymbol{\lambda}$	vector of Lagrange multipliers
μ	normalised chassis torsional stiffness
φ	roll angle
φ_y	roll gradient
$\boldsymbol{\Phi}$	vector of constraint equations
$\boldsymbol{\Phi_q}$	Jacobian of constraint equations
$\boldsymbol{\Phi}_t$	derivative of constraint equations with respect to time
χ	lateral load transfer distribution
ψ	yaw angle
$\boldsymbol{\Psi}$	modal shapes
$\boldsymbol{\omega}$	vector of angular speed

Subscripts

I	inertial reference system
B	body reference system
FL	front left
FR	front right
RL	rear left
RR	rear right

Others

$\boldsymbol{x}$	vector $\boldsymbol{x}$
$\boldsymbol{X}$	matrix $\boldsymbol{X}$
$\bar{\boldsymbol{x}}$	vector is expressed in the local reference system
$\tilde{\boldsymbol{x}}$	skew symmetric matrix of vector $\boldsymbol{x}$
$\boldsymbol{x}^{(i)}$	referred to the i-th body

Chapter 1

Introduction

1.1 Context

When a new racing or sports car is released, technicians tend to praise the quality of its chassis by giving figures of its lightness and its stiffness. Indeed, from the vehicle dynamics point of view, these are the most important qualities of an automotive chassis. Targets of low weight and high stiffness however are generally in conflict each with other and with cost limits.

The importance of chassis lightness and stiffness is nowadays also recognised outside the racing and sporting community. During the last 30 years, the automotive industry has seen a steady increment of size and power of road vehicles; weight has increased more than 20 percent while power almost doubled, [1]. Part of this weight increment is due to the addition of many energy-consuming accessories and capabilities; another part however is due to a substantial increment of chassis weight. For many years, increment of chassis weight has been the only viable option towards the fulfilment of stringent targets in terms of safety, handling and comfort while keeping the final product cost effective. Until the mid 1990s, improvement of engine efficiency has compensated the increment of chassis weight with the result of a continuous improvement in vehicle fuel efficiency; in the last 15 years however, the progress in engine efficiency has no longer been sufficient to improve fuel efficiency, [1].

Recent financial instability and environmental awareness, however, are now inducing the automotive industry to develop more efficient vehicles at affordable costs. Reduction of the overall vehicle weight represents one of the keys for reaching this goal. On the other hand, requirements on chassis stiffness generally make any weight reduction difficult and expensive. The problem of finding the best compromise between chassis stiffness, weight and cost is therefore of high importance for the development of both high-performance race cars and cost-effective fuel-efficient road vehicles. This requires the engineering community to understand all the implications of chassis compliance on the overall vehicle behaviour. Despite this fact however, no general

consensus on the amount of stiffness required exists.

Nowadays modelling plays a very important role in vehicle dynamics analysis. Several modelling approaches exist; the choice is not only related to the level of detail involved, but also to the particular aspect of vehicle handling under investigation. For limited values of lateral acceleration, manually-derived models of moderate complexity can be used. These models would include body lateral, yaw and roll motions, main suspension elasto-kinematic effects, steering system and aerodynamic forces. Such models have been successfully used in practice for a long time. When high values of lateral acceleration are considered, the derivation of non-linear equations is generally too complicated to do manually and it is now common practice to employ multibody codes, [2]. It is in the non-linear region of the vehicle characteristics that chassis compliance plays a major role. This, together with the complexity of the mathematics involved, makes it impracticable any attempt to use detailed, hand-derived vehicle models to study the effect of chassis flexibility on vehicle dynamics.

Multibody codes have proven to be an efficient tool for analysis of ground vehicles and are nowadays used both in academia and in the industry. Most of the commercially available codes for modelling and simulating multibody systems are based on a numerical approach. However, it has been shown that, when fundamental problems are analysed and/or high computational efficiency is desired, symbolic codes provide a better option, [3, 4]. These systems allow the user to derive the equations of motion in a symbolic form and to apply to them any desired manipulation or simplification. For simulation purposes, equations are then exported and a numeric solver is employed. Although many of the available numeric codes offer the possibility of modelling elastic components, this is not the case for symbolic codes. To the author's knowledge, none of the available symbolic multibody codes offers the possibility of modelling elastic bodies while leaving the user the freedom to choose the level of simplification acceptable for the analysis.

1.2 Scope of the research

Given the context depicted in Section 1.1, aim of the research is the development of a novel mathematical model for the analysis of the effects of chassis flexibility on the handling performance of sports and racing vehicles.

The model implements a set of characteristics that make it unique. First, it is based on a multibody formulation that combines a semi-recursive formulation and velocity projection technique; these techniques not only improve its computational efficiency and stability, but also they provide a valuable tool for the analysis of suspension kinematics and dynamics. Furthermore, they offer a novel approach by which the existing gap between multibody and traditional vehicle models can be at least partially covered.

Second, the entire vehicle model has been derived by means of a symbolic multibody library implemented within the Computer Algebra Software Maple®. Although it has been developed with the objective of creating the vehicle model, the library can be used for modelling any mechanical system. Features of the library are the capability of including flexible bodies, of implementing several advanced computational techniques and the capability of generating efficient computational routines for the numeric integration.

Third, the model describes the non-linear dynamics and kinematics of the vehicle system, it includes both large body motion and the elastodynamics of the frame and several complementary subsystems like tyres, driver and powertrain systems. Chassis elasticity is included in the symbolic code so that all the advantages of adopting a symbolic code are retained.

The model is suitable for simulation of vehicle handling during steady-state and dynamic manoeuvres, for chassis and vehicle set-up optimisation. Furthermore, it can be used for the analysis and optimization of the interaction with the driver and for evaluation of the dynamic loads on the vehicle frame. Some of these applications are exploited in the research, others are only suggested.

Besides the advanced model, hand-derived simplified vehicle models for a preliminary assessment of the influence of chassis torsional stiffness on vehicle behaviour are presented and discussed. Despite the simplifications introduced, these models are capable of predicting important aspects of vehicle behaviour; limitations are discussed and analysed.

Simulations show that there are several aspects of vehicle dynamics that are affected by chassis flexibility. More specifically, the influence on lateral load transfer distribution, on the steady and unsteady response of the vehicle, on its stability and its controllability is found. Mechanisms underlying these effects are investigated through the use of the developed model. Guidelines for chassis design and optimisation have been drawn from the analysis.

1.3 Outline of the thesis

This work consists of eight main chapters, not counting annex and references. The present chapter includes an introduction into the thematic area of this dissertation and a brief explanation of the work; Chapter 2 highlights the fundamentals and background of the main themes covered as well as previous work which is connected to these topics. In particular, literature relevant to chassis properties, vehicle dynamics and driver modelling is presented.

Chapter 3 introduces an analytical vehicle model capable of taking account of chassis torsional stiffness. The main purpose of the model is a preliminary assessment of the importance of chassis flexibility on vehicle dynamics. A non-linear model is

employed in order to analyse the influence of chassis stiffness on vehicle steady-state characteristics. From this, a linear dynamic model is derived and employed for the evaluation of the frequency response of the vehicle and its interaction with the driver. Qualitative conclusions and model limitations are discussed.

A review of the literature on multibody systems is presented in Chapter 4. While several aspects of multibody kinematics and dynamics are considered, particular attention is focused on all those techniques that can be successfully employed for an efficient vehicle dynamics simulation.

Chapter 5 describes the development of a multibody library based on a symbolic approach. The library implements several advanced modelling techniques and permits the inclusion of flexible bodies. The library is suitable for modelling generic mechanical systems and vehicles in particular.

The description of a vehicle model created by means of the multibody library is presented in Chapter 6. Besides a detailed modelling of vehicle kinematics and dynamics, the model includes a tyre model, a powertrain unit and a driver routine. Also, data of a real vehicle are introduced and a preliminary validation of the model is included.

Chapter 7 contains results obtained from the vehicle model. Simulations that permit a detailed assessment of the influence of chassis compliance on vehicle dynamics are presented. Furthermore, comparisons against the preliminary model of Chapter 3 are included and an analysis of the achieved computational efficiency is presented.

Chapter 8 summarises the contents of this work and highlights the contributions to the research area. Suggestions for further activities are also included.

Chapter 2

Vehicle chassis and vehicle dynamics

The purpose of this chapter is to offer an overview of the literature relevant to the research. First, the chassis properties relevant to vehicle dynamics are analysed and their significance is discussed. The literature relating to the mathematical modelling of rigid and flexible vehicles is then presented and reviewed. Finally, a section is dedicated to the review of the available driver models.

2.1 The chassis

2.1.1 Introduction

The chassis is defined as the base frame of a motor vehicle or as the structure on which the vehicle is built. In this sense, it constitutes the backbone of the vehicle and it keeps it together in the truest sense of the word. Furthermore, it forms the survival cell for the driver, [5].

The term chassis comes from Latin "capsa" or "capsum" which mean box or case, [6]. In this sense, the chassis is that part of the vehicle that has the function of containing, supporting and connecting the other parts. The word chassis is nowadays often used with a more general meaning, in which not only the frame but also the suspension; the tyres and the steering system of the vehicle are included. If the latter definition is adopted, the supporting structure of the vehicle is named "frame". The original meaning of the word "frame" was "established order, plan" or "building". Starting from 1870s, it can be found in the literature to indicate structures of bicycles and, from 1900s, of motor cars, [6]. In this thesis the terms "chassis" and "frame" are considered equivalent. If road cars are considered, the chassis can be identified as the vehicle body and is often called body-in-white.

In the first lines of their book on chassis design, Costin and Phipps, [7], state that

"ideally, the first purpose of a motor car chassis is to connect all four wheels with a structure which is rigid in bending and torsion – that is one which will never sag nor twist. It must be capable of supporting all components and should absorb all loads without deflecting unduly". From [5], a vehicle chassis fulfils several purposes that can be summarised as:

- connection of the suspension system;
- transmission of the work loads;
- protection of the driver during crash events;
- it accommodates the powertrain system and its ancillary components;
- it accommodates the cockpit and the driver.

2.1.2 Notes on chassis evolution

In 1920s, typical cars had a separate "body-on-chassis" construction which consisted of a wooden or metal body mounted on a separate chassis that contained all the mechanical components. Early bodies were built by carpenters out of timber and had very low values of stiffness. Frames were of the ladder type, so named for its resemblance to a ladder. They consisted of two symmetrical rails, or beams, and perpendicular crossmembers connecting them. These frames had a good bending stiffness but poor values of torsional stiffness, [8].

The importance of torsional behaviour of the structure was still not understood in 1925, [9]. In the body-on-chassis scheme, the detached body and chassis work as torsion springs in parallel and share torsion load according to their relative stiffness. This causes problems of rattling and squeaking between the two structures. This problem was solved in 1930s either by installing flexible mountings between the frame and the body or by increasing the chassis stiffness through the introduction of cruciform bracing or the use of closed cross-members, [8].

The importance of chassis stiffness was recognised in the next decade, [10]. As an evolution of the ladder type chassis, twin- and multi-tube frames first and space frames later, were developed. Due to the tubular closed section of their members, these chassis offered much higher chassis stiffness. According to Costin, [7], a true space frame is a complete structure in which all the joints could be flexible without the chassis loosing any of its stiffness. Theoretically, it is possible to build a stiff and light space frame chassis in which no tubes are subject to bending loads. However, the need to accommodate the driver, the powertrain unit and other components makes the practical realisation of such a chassis impossible and the stiffness of a real chassis is usually far from the theoretically achievable one.

During the early 1950s, these types of chassis were suitable for Formula One racing. However, towards the end of the decade engine power and cornering speed had increased, and improvements in both the strength of the chassis and safety were needed. Furthermore, a more precise control of suspension kinematics was required. Colin Chapman, chief designer of Lotus, introduced the monocoque chassis to Formula One by placing thin plates which acted as shear panels around the bars of the space frame chassis. This increased the stiffness without increasing mass significantly. In 1961, Chapman used a complete "tub" in the design of the Lotus 49. The tub was constructed entirely from aluminium sheeting and it marked an evolution of the space-frame; it was lighter, stiffer and with a smaller frontal area.

In 1978 Lotus created an aluminium honeycomb chassis, which, like the "49", was a fully enclosed monocoque. However, instead of just using aluminium panels, sheets of aluminium honeycomb with skins of thin aluminium sheet were used. The result was that, again, the chassis was lighter and more rigid.

During the 1970s the aero revolution was introduced into Formula One. The use of wings and ground effects dramatically increased the speeds and the loadings through the chassis, with the consequence that a stronger and safer chassis was required. During the early 1980s, the chassis designers found that the aerodynamic loads were flexing the chassis with the consequence that not only was the efficiency of these devices reduced but also fatigue failure was accelerated.

In 1981 John Barnard from McLaren, together with the American company Hercules Aerospace, designed and constructed the first carbon fibre Formula One chassis for the MP4/1 car. The performance gain over the conventional aluminium honeycomb chassis was enormous and subsequent developments led to the MP4/4 winning 15 out of 16 races in 1988. Since then, carbon fibre chassis has become the standard technique, not only for the realisation of Formula One chassis, but also for many high-performance sports cars.

During the historical development of race and sports cars, two important phenomena can be noticed. First, the structural function of supporting and connecting different components has been assigned, as a secondary function, to other parts. For example the powertrain units of the modern Formula One cars are used to connect the rear suspension to the front part of the vehicle. This is an extreme example, in which these components substitute the rear part of the chassis. Less obvious is the case in which non structural components, like the windscreen or the engine, are used to add stiffness to the frame. It is therefore impossible, when certain vehicles are considered, to identify a structure that has the only purpose of supporting the other components of the car. Hence, the term "chassis" is used to identify the assembly of parts that contribute to support the vehicle.

Secondly, other functions have been assigned to the chassis, mainly related to safety issues. Again, if a Formula One vehicle is considered, the chassis constitutes

the driver compartment, it plays an important safety role and it contributes to the aerodynamic performance of the vehicle. More details on chassis construction types and evolution can be found in [5, 7, 9].

It is not among the objectives of the present research to investigate how, from the design point of view, chassis stiffness is obtained. An interesting example of chassis design and optimisation can be found in [11]. Design of a lightweight chassis for a land speed record vehicle is described and analysed in the paper. Several of the available construction techniques, from space frame to full monocoque are discussed and analysed through the use of structural parameters such as ratios of torsional and bending stiffness over mass and values of chassis natural frequencies.

2.1.3 Loads and deformations

While accomplishing its functions, the chassis is subject to a number of loads that can be categorised according to the following scheme [5, 7]:

- rear suspension loads: because of the higher weight applied to the rear axle and because of the driving torque, these are the highest load applied to the chassis (a rear wheel drive vehicle is assumed). They can be applied on a few points or on many points, according to the kind of suspension employed and consist of longitudinal, lateral and normal forces;
- front suspension and steering loads: the applied loads are similar to those of the rear suspension but, because of the front to rear weight distribution of racing cars, they usually have a smaller magnitude;
- engine, gearbox and final drive: these usually are the most cumbersome components of the vehicle, therefore their location defines the architecture of the vehicle. The induced loads are usually transmitted through a set of brackets and include reactions from driving torque and engine vibrations;
- aerodynamic loads from wings, bodywork;
- seats and controls: depending on the vehicle they can be integrated into the chassis or built as a separate unit. The induced loads are usually of small intensity.
- other parts: fuel tank, minor components, battery.

The nature of these loads may be static or dynamic. During cornering for example the lateral acceleration introduces a centrifugal force and hitting a bump may result in significant dynamic forces in the suspension and on the chassis. It is therefore necessary to evaluate the load inputs into the frame by means of a careful analysis of the vehicle behaviour.

Loads generate deformations on the chassis structure. A generic deformation can be seen as the superposition of global and local deformation modes. Local deformations are typical of suspension brackets and attachments; they are largely dependent on the local properties of the chassis and they cannot easily be included under a general classification. Global deformations instead can be described by the following principal deformation modes, [12]:

- longitudinal torsion. This occurs when, because of cornering, road irregularities or obstacles, tyres have different normal loads. In this case, the frame can be thought of as a torsion spring connecting the front and the rear suspensions;
- vertical bending. Any chassis under static load is subject to a bending deformation in the vertical plane due to its own weight and to the weight of the components it supports. During motion, vertical acceleration and pitch moments modify the load status and can cause significant deformations;
- lateral bending. Lateral bending can occur when the vehicle is subject to a lateral load. This can be due to a lateral acceleration during cornering, to the aerodynamics or to the road banking;
- horizontal lozenging. This distortion consists of a deformation of the chassis into a parallelogram shape. This phenomenon occurs when a chassis is loaded by forward and backward forces applied to opposite wheels. These forces may be caused by vertical variations in the pavement or by small impacts.

According to Brown, [9], the most important deformations on vehicle structures are the bending one due to the weight of the components and to symmetrical bump load and the torsion one. These two load situations are very often combined; the principle of superposition is generally used for deformation analysis.

2.1.4 Chassis properties

The chassis represents a connecting structure with several purposes, its properties therefore have to be defined with one aspect or another in mind. Requirements dictated by vehicle dynamics, safety, packaging, aerodynamics, ride quality, cost, accessibility are very often in conflict with each other. From the structural point of view for example, the main criteria by which the performance of the chassis is judged are crashworthiness, inertial properties, static and dynamic stiffness, [13]. Inertial and stiffness properties are the most important areas of interest from the vehicle dynamics point of view.

Inertial properties

Inertial properties include mass and its distribution, parameters that have always been fundamental for any design activity related to motor sports. Strictly speaking, these parameters are not just related to the chassis but to the whole vehicle. However, because of its connecting function, the chassis plays an important role for the definition of the inertial properties of the vehicle.

Together the importance of chassis lightness, the importance of moments of inertia, and in particular the yaw moment of inertia was soon recognised in the racing community. Low values of yaw inertia are generally preferable for sports and road cars. Interestingly, it has been shown that for modern Formula One cars the sensitivity of the performance with respect to yaw inertia is often negligible and increasing the yaw moment of inertia makes the car easier to control without penalising the performance, see for example [14] and [15]. The importance of chassis inertial properties is not treated here.

Chassis stiffness

Both the handling and the vibrational behaviour of a vehicle are sensibly affected by the stiffness of its chassis. Generally speaking, it is required that deflections due to external loads do not impair the functioning of the vehicle. As an example, chassis deflection should not prevent the doors to be closed and the suspension to work properly.

By referring to the global deformation modes described in previous sections, it is possible to define static values of torsion, vertical and lateral bending and of lozenging stiffness. Bending and torsion stiffness however are more often used as benchmarks of vehicle structural performance, [9]. Bending stiffness is usually defined as the symmetrical vertical deflection of a point near the centre of the wheelbase when static loads are applied to the vehicle. Torsion stiffness instead relates to the torsional deflection of the structure when it is subject to an applied pure torque acting about the longitudinal axis of the vehicle.

It is usually found that a chassis that has enough torsional stiffness usually has ample rigidity in bending; as a consequence torsional rigidity represents the main criterion of chassis design, and the primary function of a high-performance chassis, [7, 9]. As an example, typical values of chassis torsional stiffness are reported in Table 2.1.

Stiffness measurement

Chassis torsional stiffness can be measured by using specific test rigs. This can be done with a real chassis or with a finite element model of the chassis itself. The design

Table 2.1: Indicative values of chassis torsional stiffness for different vehicles, from [5, 16–20].

Vehicle	Chassis torsional stiffness [Nm/deg]
Formula SAE car	300 - 3000
Passenger car	5000 - 25000
Winston Cup racing car	15000 - 30000
Sports car	5000 - 50000
Formula One car	5000 - 10000

of a standard test rig to measure torsion stiffness can follow one of three configurations. Each configuration is a variant of the basic principle of fixing one end of the chassis and applying a load at the other end so that twist is generated and measured. The first two configurations require the frame to be supported at three points, two rigidly at the rear end and one pivotally on a knife-edge respectively at the centre and at one side of a front cross member. An off-centre vertical load is then applied to the front end, [10]. According to the third configuration instead, only the rear part of the chassis is constrained and two opposite vertical loads are applied at the front end so that a torque is generated, [18, 21]. Although it might result in an overestimation of the torsional stiffness, the latter configuration is the most widespread to measure torsional stiffness. Detailed description of a rig for chassis testing can be found in [22].

A different layout was described in [20] and further analysed in [17]. The paper highlights the fact that loads applied to the chassis during one of the described tests are not strictly representative of the actual loading of the frame during its working conditions. A more realistic load condition is achieved through the inclusion of the suspension in the measure so that an overall chassis stiffness, known as "hub-to-hub" stiffness is obtained. Both a finite element implementation and an experimental test were reported by the authors. An example of chassis assembly for torsional stiffness testing is reported in Figure 2.1.

While static analysis describes how the body deforms under load and is related to vehicle dynamics qualities and to durability, dynamic or modal analysis refers to structural vibrations and it mainly affects the NVH behaviour of the vehicle. Although the natural frequencies of the whole vehicle are more of interest than the natural frequencies of the chassis, values of natural frequency related to global bending and torsional vibration are used as benchmark for vehicle structural performance, [9]. If trimmed body and full vehicle are analysed, the values of static stiffness obtained are similar to those of body-in-white analyses while natural frequencies are lower.

Full vehicle analysis is performed to assess the modal alignment of the vehicle

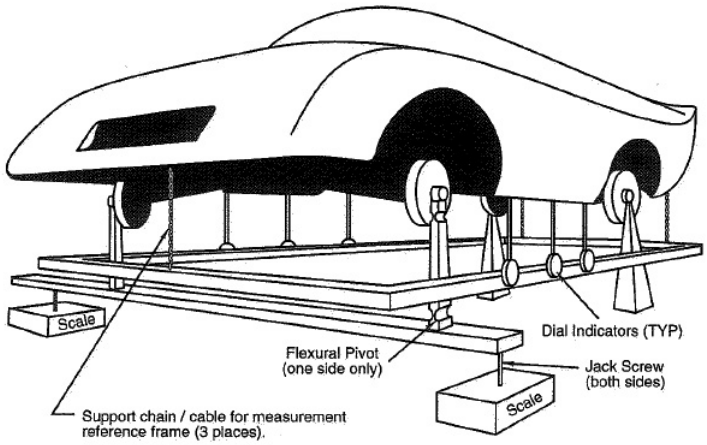

Figure 2.1: Chassis assembly for torsional stiffness testing, from [20].

and to ensure that no overlap exists between the modal shapes. Modal frequencies are a better measure of chassis refinement than static stiffness because they can be compared with natural frequency of engine, road wheels and suspension. Modal alignment analysis is performed early in the design process to mitigate risk of structural resonance issues in automotive structures, [13].

Following [13], good design criteria for a body-in-white of a passenger car require the first mode to appear at a frequency not lower than 45-60 Hz. The first two modes are typically global torsion and global bending. Other common modes are a front lateral and vertical deformation. No local mode should appear at frequencies lower than the first global mode.

Similarly to that described for static analysis, experimental and simulation techniques are available. When experimental methods are considered, classical modal analysis or operational modal analysis techniques can be used. Classical modal analysis involves the process of extracting dynamic characteristics of a vibrating system from measured force inputs and vibratory responses, whereas operational modal analysis extracts the dynamic characteristics of a vibrating system in its operating environment solely from vibratory responses. Both of these methods offer distinct advantages and disadvantages in designing and developing today's automotive structures and their systems and components. Further details can be found in [23].

Simulation techniques for modal analysis are based on finite element models usually employed for static analysis. In this case however, no constraints are applied to the body and an eigenvalue or model reduction analysis is performed. Output of the analysis are the natural frequencies and the related modal shapes of the structure. As the body is unconstrained, six zero-energy modes, corresponding to the rigid motion of the structure, appear in the solution, [13].

The importance of chassis stiffness

Different categories of deformation modes play different roles in the definition of the behaviour of the vehicle. Symmetrical deformations, like the bending ones, mainly affect the ride qualities while the skew-symmetrical ones, for example those induced by the torsional flexibility, have their main impact on vehicle handling, [24]. This fact, together with the fact that torsional stiffness is the most difficult target to achieve during chassis design, justifies the fact that chassis stiffness is often represented by torsion stiffness.

There are several factors that make the rigidity of the chassis an important figure in vehicle dynamics, especially when racing vehicles are considered, [19, 25]. Effects of compliances are often unknown and tend to make vehicles unresponsive to the standard changes to which other cars respond. As a consequence, they make the prediction of the performance of a race car difficult, [20]. Karts constitute an exception because they generally do not have any suspension and the flexibility of the chassis is used as substitute.

Problems induced by insufficient chassis rigidity can be briefly described as:

- the control of lateral load distribution is difficult;
- unwanted displacements of the suspension attachment points occur, so that the desired control of the movement of the tyres cannot be guaranteed;
- dynamic effects and vibrations can occur;
- generally, it makes the vehicle behaviour unpredictable and difficult to tune;
- it does not inspire confidence to the driver;
- fatigue phenomena are more marked;
- ride quality is poor.

Depending on the kind of vehicle considered, these aspects can be more or less important. For sports and race cars, control of lateral load transfer and of the suspension kinematics, as well as the dynamic effects, are particularly relevant.

Body flexibility cannot be neglected when sports cars and, above all, Formula One cars are considered, [24]. For these vehicles, in fact, suspension roll stiffness and chassis torsional stiffness are similar.

Clear evidence of the importance of chassis stiffness for race vehicles comes from shaker rig testing. Conventional 7-post rigs consist of four actuators that support the four tyres and three actuators, known as aeroloaders, that reproduce the effects of aerodynamic downforce and the motions resulting from lateral and longitudinal acceleration on the chassis. Both specific excitation profiles and racetrack simulations

can be applied to the car. Compared to track testing, rig testing is more repeatable and more cost effective.

If the chassis is infinitely rigid, the use of three aeroloaders is sufficient to reproduce the exact behaviour of the car. It has however been shown that, even for highly competitive Nascar and Formula One vehicles, the use of a fourth aeroloader is necessary in order to reproduce the behaviour of the vehicle on the track with good fidelity, [26, 27]. While a seven-post rig requires the creation of roll conditions in order to create chassis deformation, an eight-post rig can create pure chassis deformation without creating roll and vice versa. As a consequence, chassis deformation can be reproduced in a more accurate manner.

2.2 Vehicle dynamics modelling

2.2.1 Introduction

Modelling plays an important role in vehicle dynamics analysis. Sharp, from Blundell, [28], states that "models do not possess intrinsic value. They are for solving problems. They should be thought of in relation to the problem or range of problems which they are intended to solve. The ideal model is that with minimum complexity which is capable of solving the problems of concern with an acceptable risk of the solution being wrong. This acceptable risk is not quantifiable and it must remain a matter of judgement. However, it is clear that diminishing returns are obtained for model elaboration."

According to Crolla, [2], the choice of the model is not only related to the level of detail involved, but also to the particular aspect of vehicle handling under investigation. For limited values of lateral acceleration a manually-derived model of moderate complexity can be used. Models of this kind usually include body lateral, yaw and roll motions, main suspension elasto-kinematic effects, steering system and aerodynamic forces. Such models have been successfully used in practice for a long time. When high values of lateral acceleration are considered, the derivation of non-linear equations is generally too complicated to be carried out manually and it is now common practice to employ multibody codes.

In the same paper the author identified the main categories of simulation tools as purpose-designed simulation tools, numeric and algebraic multibody packages and general purpose toolkits. According to the author, it is possible to identify advantages and disadvantages for each of these solutions, as reported in Table 2.2. The following sections briefly describe the categories of vehicle models which can be found in literature; an extended literature review on the subject can be found in [29] and in [28]. The principal properties of the discussed models are summarised in Table 2.3.

Table 2.2: Comparison of some of the key features of the software packages available for vehicle dynamics studies, adapted from [2].

Category	Advantages	Disadvantages
Purpose-designed	Inexpensive Models already proven Suitable for specific problems rather then for investigation of design issues	Limited flexibility
Numeric multibody	Industry standard Powerful packages available High animation capabilities Linked to CAD packages	Expensive High computing cost Limited value for analysis of design issues
Symbolic multibody	High computational efficiency Inexpensive Powerful for solving complex problems	Limited flexibility High level of training required
Toolkits	Inexpensive Suitable for investigation of design issues Tailored to the application Existing models can be used	Model must be available Inappropriate for very complex systems

2.2.2 Purpose-designed models

Purpose-designed models have for a long time been the standard approach for the simulation of vehicle dynamics. By the middle of the 1950s the groundwork for a mathematical model of the vehicle had been laid. A basic understanding of the behaviour of the tyres had been achieved and relatively accurate tyre models were available. Following earlier papers from Rieckert and Shunck, [30], and Rocard, [31], three extremely influential papers on vehicle handling were published by Milliken, Whitcomb and Segel of the Cornell Aeronautic Laboratory in 1956, [32–34]. These works formed the basis for research in the area of automotive stability and control for the next three decades and are still frequently referenced in the current literature.

In the first of the papers Milliken and Whitcomb, [32], provided a historical overview of the field: “The major effort in handling research to date has been in the recognition of individual effects, their isolation, and examination as separate

Table 2.3: Comparison of the most representative models for vehicle dynamics studies.

Property (x: implemented)	single track	single track with roll	14-d.o.f	IDFSC	VDANL	FASIM	VDAS	single track with flex. chassis	CarSim - VehicleSim	ADAMS/CAR
Analysis:										
linear	x	x	x	x	x	x	x	x	x	x
non-linear			x	x	x	x	x		x	x
d.o.f. number	2	3	14	17	var.	var.	var.	4	var.	var.
Model implementation:										
conventional	x	x	x	x	x			x		
numeric multibody						x				x
symbolic multibody							x		x	
Suspension kinematics:										
none	x	x						x		
look-up tables			x	x	x		x		x	
exact						x	x		x	x
Chassis flexibility:										
none	x	x	x	x	x	x	x		x	x
simplified								x		x
complete										x

entities. This work naturally started out as qualitative and in some instances has become quantitative. It has been conceptual in character; it has been pioneering and not infrequently intuitive and inspired, but it can hardly be viewed as an end in itself. Rather, it is a substantial beginning. All the individual effects now known need quantitative analytical expression. More significant, however, is the need for comprehensive, integrated analysis methods, for such overall theories will enable the prediction of the actual motion by rationally and simultaneously taking into account all the separate effects."

They also recognised that, although a great deal of progress had been made

in understanding tyre behaviour, more research was needed. In spite of the recent developments, that observation is still true today. At that time, no universally accepted set of reference axes were available and measured tyre data of the period were rather incomplete. This made translation of the data from one set of axes to another difficult if not impossible. Furthermore, the effects of tyre design on handling were largely unknown. Also, the need to perform testing on a wide variety of common passenger car tyres to determine the effects of the various design parameters was recognised. Discussing the future objectives of the Cornell Aeronautics Lab research program, Milliken emphasised the need to concentrate on the analysis of car stability and control. Important distinctions between stability and control and between performance and ride were also made.

A two-degrees-of-freedom vehicle model, also known as the single track model was described by Whitcomb and Milliken in [33]. In the model, only the yaw and sideslip degrees of freedom were considered and the tyres were assumed on the centreline of the vehicle. A set of linearised differential equations was derived using stability derivatives and the transient response of the vehicle was studied. In studying the yaw response of the car at a constant vehicle side slip angle, the concept of static margin was developed. Also, the fact that with a negative static margin a critical speed exists was recognised.

In the third paper of the series, Segel, [34], presented a derivation of a three-degrees-of-freedom model for stability and control studies. The considered degrees of freedom were lateral motion, yaw and roll; the bounce and pitch of the chassis were ignored and a fixed longitudinal roll axis parallel to the ground was considered. Several other simplifying assumptions were introduced: constant forward velocity, fixed driving thrust divided equally between the rear wheels, decoupling of longitudinal and lateral tyre forces. The unsprung mass was modelled as a single non-rolling lumped mass. An experimental validation of the model was performed. The model was validated against experimental data relative to pulse steering and step steering manoeuvres. Furthermore, the theoretical predictions of the model were compared to the experimental data taken in a series of frequency response curves; good correlation was found.

More detailed models began to be developed with research carried out in the early 1960s, [35, 36]. Among these, a general mathematical model and computer simulation of the dynamic responses of automobiles was developed at the Cornell Aeronautical Laboratory, [37]. The mathematical model, which was subsequently named Highway Vehicle Object Simulation Model (HVOSM), included eleven degrees of freedom, empirical relationships to generate tire forces, and was capable of dealing with traversals of terrain irregularities and collisions with certain types of roadside obstacles. The development of the HVOSM included an extensive validation effort within which a series of repeated full-scale tests with instrumented vehicles was

performed.

A 14-degrees-of-freedom vehicle model was presented in 1969 by Sharp and Goodall, [38]. The equations of motion of the vehicle were derived by means of Lagrange's method; six degrees of freedom of the vehicle body, vertical motion of the unsprung masses and wheel spin were included. Suspension kinematics was completely modelled by means of the suspension derivatives concept. The main advantage of the model over its predecessors was that inertial contributions of the unsprung masses were included and that the coupling between ride and handling motions was realistically represented.

By the early 1970s simulations of vehicle dynamics were becoming more complex and realistic. This was primarily due to advances in computing technology. Prior to the 1970s most simulations were performed on analogue computers; these machines were capable of solving the vehicle dynamics problems in real time since the differential equations were modelled by equivalent electrical component networks in a cost effective manner. On the other hand, it was very difficult to model non-linear functions of more than one variable. Since this is the case for most of the models, the accuracy of the simulations was compromised by limitations in the computing equipment.

A vehicle dynamics simulation code for a hybrid computer was created by the research staff at the Bendix Corporation Research Laboratories, [39]. The model was based on the 10-degrees-of-freedom model developed at the Cornell Aeronautics Laboratory. The original model was improved by adding four spin coordinates for the wheels and a three-degrees-of-freedom steering system. The original model had six coordinates for the sprung mass, one vertical coordinate for each front wheel, and one vertical and one rotational coordinate for the rear axle. At the time of publication the model had been partially validated by comparison of simulation results with the other models.

The advent of digital computers allowed researchers to create more complex models containing non-linear functions. This brought higher levels of realism in the simulations; however the slow speed of the digital machines meant increased computing time. As digital computers gradually replaced analogue and hybrid machines, primarily as a result of economic concerns, it became necessary to create vehicle dynamics models which were completely digital. The combination of the cost of computer time and the slower solution speed of the digital machines made it desirable to create computationally efficient models.

In 1973 Speckhart, [40], published a paper in which he presented a digital 14-degrees-of-freedom vehicle model. Six degrees of freedom were assigned to the sprung mass, four degrees of freedom were associated with the suspension movement at the four corners of the vehicle, and four rotational degrees of freedom were assigned to the wheels. A Lagrangian approach was used for the derivation of the equations. Models were presented for several different suspension configurations. The sprung mass was restricted to pivot about a specified roll axis and, according to the author, this

guaranteed a sufficiently accurate representation of the kinematics involved. The results of computer simulations for J-turn manoeuvres were compared with experimentally measured data for two different speeds and steering inputs, good agreement was found.

By the early 1980s a partial shift in vehicle modelling process was taking place. The demand for accurate vehicle dynamics models combined with the difficulty in deriving the equations of motion for large systems led to the use of general-purpose numeric multibody simulation codes. These codes, however, as shown in Table 2.2, did not and partially still do not, completely satisfy the needs of the research community. Indeed, the availability of inexpensive computers encouraged the creation of several purpose-developed simulation codes, and, alongside single vehicle models, complete packages that included different suspension systems and other vehicle components were developed. Among them, it is worth mentioning the IDSFC, VDANL, FASIM, VDAS codes.

The IDSFC code was developed at the University of Michigan in the early 1980s, [41], and contained a model with 17 degrees of freedom. In order to reduce computational costs, the steering system was described statically and wheel spin dynamics was modelled in an algebraic form. The package contained numerous additional features such as an anti-lock braking system, several tyre models, optional activation of non-linear kinematic terms, solid rear axle or independent rear suspension and interactive capability. The program was constructed in a modular fashion to enable future enhancements and upgrades.

The VDANL model was developed by System Technology and is presented by Allen et al., [42]. The model includes lateral, directional and longitudinal dynamics, tyre forces and wheel spin dynamics. The basic equations were derived from earlier dynamics models; some improvements however were introduced. For example, the model was capable of considering a moving roll axis and the suspension model was capable of reflecting camber change with body roll. The model was capable of running on standard computers and was used by many authors in order to study the importance of tyre lags [43], of lateral load transfer distribution, [44] and of the driver-vehicle interaction, [45].

A more sophisticated package, called FaSim, was developed by Bosch and the University of Duisburg, [46, 47]. The code was based on object oriented programming concepts and was formed of a set of subroutines for the initialisation and the calculation of the kinematics and of the dynamics of the vehicle. The underlying mathematics was based on a numeric multibody formulation of the D'Alembert's principle; by means of the kinematic differential concept, a minimum order description of the system was obtained. The model offered the user the possibility of choosing the level of desired complexity, and included many additional modules, including models of vehicle dynamics control systems (ABS, ASR, VDC).

The package VDAS, developed at the University of Leeds, [48], has been successfully

used for several years for ride and handling analyses. The code was particularly interesting because it incorporated a preprocessor based an external algebraic package capable of performing a symbolic manipulation of the equations of motion. The generated code was then particularly efficient. The package was used to develop several vehicle models, including multi-axle models, vehicle combinations and various forms of suspension systems. It was also used for hardware-in-the-loop simulations.

2.2.3 Multibody packages

Multibody packages, in particular numeric ones, are nowadays the most widespread tools for the analysis of vehicle dynamics. They permit the building of detailed models of systems with a large degree of complexity which is as close as possible to the real system. Despite the apparent advantage of this approach, a great amount of input data and a high computational power are required. Due to the development of more powerful computers, the latter problem is now partly resolved. The task of collecting the data required by a detailed multibody model however makes the use of such models of limited use outside the industrial environment, [49]. Symbolic multibody codes represent a valid alternative, especially for academic purposes. Because of their importance, a more complete survey of the literature relevant to multibody systems is presented in Chapter 5.

2.2.4 Toolkits

Purposely developed models are generally implemented by using native code or toolkits. Because of their ease of use, general simulation toolkits are nowadays very common. Among them Simulink®, from The MathWorks, is perhaps the most widely used. This tool includes a large amount of libraries of functions and algorithms for matrix operations, simulation, controller design and a graphic interface which makes its use intuitive. Simulink and similar simulation environments may be successfully employed for vehicle dynamics studies; however they do not help the user to build the model or to develop the necessary equations, but only to solve them. The equations could be either derived by hand in the case of simple models or obtained from one of the packages described above. Furthermore, toolkits are usually characterised by a low computational efficiency.

2.3 Modelling of vehicles with a flexible chassis

2.3.1 Introduction

Most of the analysis on the effects of chassis flexibility on vehicle dynamics in the past has been based on the use of purpose-developed models. Specific tools for the analysis

of lateral load transfer distribution, for stability and for ride studies can be found in the literature. Beside them, more generic models, mainly based on numeric multibody codes can be found. A more detailed review of the available models is presented in the following sections.

2.3.2 Models for lateral load transfer analysis

Every time a vehicle is engaged in a turning manoeuvre a lateral load transfer occurs. The load transfer is usually not equally distributed between the front and the rear axles. Furthermore, because of the non-linear dependency between the cornering force and the normal load of the tyres, an increase of the lateral load applied to an axle decreases the axle cornering stiffness and therefore influences the handling of the vehicle. The behaviour of tyres, in fact, is such that when the normal load is increased, an increase in the lateral load is obtained, but the gain becomes smaller as the normal load grows, [20]. As a consequence, two tyres having fixed slip angles can globally produce less lateral force when they are unequally loaded than when they are equally loaded. If an axle is required to generate a constant lateral force, its slip angle, considered as an average of those of the two tyres, is increased by the presence of a lateral load transfer. The handling behaviour of a vehicle strongly depends on the difference between front and rear slip angles and, in turn, on the load transfer distribution.

Lateral load transfer is a function of roll stiffness distribution, of unsprung mass and of roll axis position. A literature review on this subject can be found in [44]. The first studies on load transfer of heavy lorries showed that the oversteer behaviour of trucks was primarily due to the rearward-biased roll stiffness distribution. Also, it was recognised that the introduction of a front anti-roll bar improved stability and yaw response of the vehicle.

More recently, Chu and Jones, [50], investigated the steady-state behaviour of a vehicle subjected to lateral load transfer and suggested a novel criterion for determining the influence of lateral load transfer on the vehicle characteristics. In the paper, a theoretical procedure for the evaluation of the vehicle behaviour based on the stability factor concept was proposed and the results were compared with those obtained by using a linear and a non-linear model. Good correlation was found for low values of lateral acceleration; some discrepancies were found for values of lateral acceleration close to 1g.

Chassis stiffness and in particular chassis torsional stiffness plays an important role in the mechanism of lateral load transfer. Chassis compliance introduces what can be called a “fifth spring” that interacts with the suspension and modifies the lateral load transfer distribution.

The influence of chassis torsional stiffness on the control of lateral load distribution

on a Formula Student vehicle was analysed by Deakin et al., [16]. The paper uses the concept of vehicle balancing in order to analyse the importance of lateral load transfer control and therefore of the chassis stiffness. Two vehicle models were introduced, the first being a purpose-developed static model and the second a multibody one. The first model describes the vehicle as an assembly composed of two point masses connected by a torsion spring and two suspensions characterised by two different roll stiffnesses. The effect of chassis stiffness on lateral load transfer distribution was analysed for different values of roll stiffness and static weight distribution. The aim was to find the chassis stiffness that ensures a large percentage of the difference in front to rear lateral load transfer (a percentage of 80% was suggested) to be controlled by the difference in front to rear roll stiffness. For example, a minimum chassis torsional stiffness of 3000 Nm/deg was suggested for a vehicle with a roll stiffness of 1500 Nm/deg, that is, a ratio of chassis stiffness over roll stiffness equal to 2. It was also stressed that, as the vehicle does not have an evenly distributed mass and moment of inertia, the model could be improved by modelling the chassis by means of a series of masses and torsional springs. It was also reported that other effects, for example suspension compliances, could affect the results of the analysis. The paper however, does not consider the fact that load transfer distribution is partially controlled by roll axis position and that as a consequence, only a fraction of it can be controlled by the roll stiffness distribution.

The second part of the paper describes a multibody model based on Adams Flex®. A modal neutral file, derived by means of the finite element package Ansys®, was used for the description of the chassis stiffness and external loads were applied to the suspension mounts. The model showed that the stiffness distribution along the wheelbase was not constant and that, as a consequence, the idealised models were not capable of describing the problem correctly. Skid-pad simulations showed that the vehicle behaviour was sensibly affected by the chassis torsion stiffness.

The influence of chassis stiffness on roll stiffness distribution was analysed by Thompson et al., [18]. A finite element model of the chassis of a Winston Cup race car was employed in order to evaluate the influence of different manufacturing details. The value of suspension roll stiffness evaluated by means of a model that included a flexible body was compared with the theoretical value. It was found that, when the baseline configuration of the vehicle was used, the effective roll stiffness was sensibly smaller than the theoretical one. Similar results were obtained for camber stiffness. In the second part of the paper it was shown how, adding different reinforcement structures, the torsional stiffness was improved and, as a consequence, the suspension roll stiffness obtained was closer to the ideal one. The authors concluded that both the effective roll stiffness and the camber stiffness reached a value within 3% of the ideal ones when the chassis torsional stiffness was increased by 130% over the baseline configuration and that any further increase did not produce any significant improvement. The

corresponding chassis torsional stiffness to roll stiffness ratio was about 10. The authors also showed how, because of the low spring rates used on the rear suspension of the car, the effective roll stiffness was marginally affected by the stiffness of the rear part of the chassis.

The importance of local deformation effects on roll stiffness was highlighted by the same authors in a similar paper, [51], in which the same FEM model was employed in order to evaluate the influence of different manufacturing details on the behaviour of the chassis. Effective roll stiffness, camber and steer response of the suspension installed on the flexible chassis were analysed and detailed conclusions useful for chassis manufacturing were drawn.

Riley and George presented a paper in 2002 in which they described the design of a Formula SAE car chassis, [17]. In the first part of the paper, a linear steady-state model which included suspension and chassis flexibility was introduced. The authors demonstrated that the response of a wheel subjected to a vertical load can be seen as the response of a system composed of suspension and chassis torsional stiffness. The equivalent stiffness of the system was called, improperly, vehicle stiffness. A normalised graph was produced in which the role played by the frame stiffness and the suspension compliances was demonstrated. None of the consequences of chassis flexibility on vehicle dynamics were however considered. A finite element model of the chassis of a Formula SAE vehicle and the derivation of its natural frequencies were introduced in the second part of the paper; an experimental procedure for chassis testing was also presented.

A multibody model for the analysis of lateral load transfer distribution of a kart was presented in [52]. Simulation and experimental results showed how the dynamic performance of karts is mainly determined by the elastic deformation of its chassis. It was furthermore demonstrated that in many cases, simplified models can predict the effect of frame configuration on the performance of the vehicle in a sufficiently accurate manner. A similar work can be found in [53].

2.3.3 Models for stability analysis

The influence of body torsional stiffness on the stability of medium duty trucks was studied by Hasegawa et al., [54, 55], by means of a purpose-developed model. Roll dynamics was considered as the most important characteristics for vehicle stability and controllability. Basis for the analysis was a five-degrees-of-freedom model in which, in addition to lateral motion, yaw and steering system dynamics, roll of the front and of the rear part of the body were included. A steady-state analysis showed that when the torsional stiffness of the frame is not sufficient, the roll gradient of one of the two parts of the vehicle may be excessive and create stability problems. The frequency response of the roll motion was investigated; results showed that roll natural frequency

is not affected by the chassis stiffness.

The model proposed by Hasegawa et al. can be adopted for the analysis of passenger vehicles. Substantial differences between trucks and passenger cars are however present and conclusions valid for one category of vehicles might not be valid for the other. More specifically, ratios of roll centre height to track width of a truck is much bigger than that of a passenger car and roll angle, and not spin or drift, limits the controllability or the stability of the vehicle. Similar results were obtained by Miki, [56], by means of simulation results and experimental tests.

2.3.4 Multi-purpose vehicle models

Lateral load transfer is only one of the mechanisms through which chassis compliance affects the vehicle behaviour; unwanted changes of suspension geometry can be similarly important. Global torsion compliance affects suspension geometry through roll steer and roll camber, mechanisms that are usually employed to control the cornering behaviour of the car. In presence of lateral acceleration the front and the rear part of the chassis give rise to roll angles that are different from those evaluated neglecting chassis torsional compliance; as a consequence roll steer and roll camber mechanisms control the tyre angles in a different manner. As a consequence, an effect of chassis flexibility on toe variation is present and, in turn, vehicle behaviour is affected.

Besides global chassis compliances, local suspension compliances play a very important role in the definition of vehicle characteristics. From this point of view, there is a marked difference between the goals facing designers of suspension systems for track racing and those of road counterparts. When road cars are considered, a compromise between comfort and handling requirements is necessary. Passenger comfort generally requires low values of longitudinal suspension stiffness; vehicle handling implies high values of lateral, toe and camber stiffness. Optimal solutions require the use of specific bushes or the use of advanced suspension concepts, see for example [57]. Driver comfort is of secondary importance for racing cars; as a consequence no bushes are employed and high suspension stiffness is desired in such a manner that a precise control of the tyre kinematics is obtained.

As this thesis is focused on sports and racing vehicles, desired suspension compliances due to flexible components as bushes are neglected. Also, flexibility of wishbones and wheel hubs is not considered.

A model capable of including local compliances was presented by Genta in [20]. The model describes suspension kinematics by means of the roll centre concept and introduces a modelling approach based on the implementation of a modal approach where the deformations of the sprung mass are described as linear functions of modal shapes. The modes of the chassis were divided into symmetrical and skew-symmetrical modes and a different mathematical treatment was derived for each of the two groups.

According to the author, the first ones, like the bending modes on the longitudinal plane of the vehicle, can affect the ride comfort but are not relevant to the vehicle handling. Skew-symmetrical modes however, especially the torsion ones, can affect the vehicle behaviour, especially for sports and race cars. The mathematics related to the representation of the modal shapes was described and the problem related to the damping of the structure was analysed; no simulation results were however presented.

A comparison between the behaviour of vehicle with rigid and flexible chassis was presented by Tong, [58]. Three multibody vehicle models were considered: one with a finite element description of the chassis based on nodal coordinates, one with a finite element description based on modal coordinates and one with a rigid chassis model. In the first part of the paper the behaviour of a vehicle travelling over a sinusoidal road profile at various speeds was analysed. In absence of lateral forces, no significant difference was found between the dynamic responses obtained by using the rigid and flexible models while a significant discrepancy was found when a lateral force was applied. In particular, it was shown how both the vertical dynamics and the trajectory of the vehicle were affected by chassis flexibility. It was also shown that an important deflection occurred at the front suspension spring attachment point. Close agreement between the two flexible models was found.

The second part of the paper describes some open-loop pulse steering simulations. The results showed that, as high lateral loads are generated during the manoeuvre, the lateral deformation of the suspension attachment point is important and that, as a consequence, the vehicle behaviour is strongly modified. The final part of the paper focuses on the comparison between complete and incomplete modal representations of the chassis. It was shown that the use of an increasing number of modal shapes of the chassis improves the accuracy of the simulations but also that, especially in terms of vehicle dynamics, good results can be obtained with a few modes.

Ambrósio and Gonçalves presented a paper in 2000 on flexible multibody systems with application to vehicle dynamics, [59]. Two multibody models of a Lancia Stratos composed of 17 bodies were presented; the first one included a rigid chassis, the second a flexible chassis. A complete finite element model of the chassis was created and its ten lowest natural frequencies; the corresponding modes of vibrations were obtained and included in the multibody formulation. Structural damping was introduced in order to improve numerical performances. The simulation of the ride of the vehicle over a bump did not reveal any significant differences between the two models. In accordance with the results obtained by Tong, no significant differences between the two models could be found in absence of lateral forces. An obstacle avoidance manoeuvre however highlighted significant differences between the two models. Although very briefly, it was shown how both the directional response and the stability of the vehicle were affected by the chassis flexibility. The flexible model was capable of lower values of lateral acceleration and exhibited a higher tendency to oversteer. The authors however

stated that no definitive conclusions regarding the vehicle dynamics could be reached.

More recently, a paper was published in which a vehicle model that includes chassis flexibility is employed in order to design and optimise a vehicle dynamic control system, [60]. In the first part of the paper a complete multibody vehicle model built in the Adams/Car environment is described. The model includes a McPherson front suspension, a torsion beam rear suspension, braking and steering systems and a flexible body. A finite element model of the vehicle is built and a modal neutral file is prepared. The modal neutral file includes information on the geometry and mass properties of the body. The first 36 modes of the body, up to a frequency of 51 Hz were imported and included in the multibody model. Two torsion modes of the body-in-white structure were found at 18 and 21 Hz while the first bending mode was found at about 20 Hz. The model was validated against experimental results under different tests. Agreement between simulation and experimental results was found; no comparison between a model with rigid and one with flexible chassis was however included.

In the second part of the paper, an optimal control strategy for the design of a vehicle stability control system was presented. The controller is based on a standard two-degrees-of-freedom vehicle model that does not include chassis flexibility. The efficiency of the controller is evaluated under different conditions in which a rigid or a flexible chassis is considered. Results showed that in case of a flexible chassis, the implementation of a vehicle stability control system sensibly improves safety and handling qualities of the vehicle.

Similar vehicle models are described in [61]. In this case however, design iterations were generated through the modification of modal properties instead of physical properties and a multibody code was used for the assessment of their impact on vehicle behaviour. First, modal shapes of the body were derived and a parametrisation of the vehicle structure was introduced; ride and handling simulations were then carried out. Results showed that an increment of torsional stiffness led to a significant improvement of the controllability of the car. A similar vehicle model was described in [62].

The relationship between global chassis stiffness and local compliances was discussed in [63]. The paper describes a finite element model of the whole chassis from which torsional, stiffness and bending stiffness are evaluated. Two design iterations are then introduced. The first one consists of a set of reinforcement members that help increasing static torsional stiffness by 25%; the second one is obtained through the use of a reinforced front subframe that gives origin to an increment of lateral stiffness of the front suspension by 10%. Prototypes were then built and experiments were run in order to assess the impact of the design iterations on vehicle dynamics behaviour and on the NVH performance.

Results showed that the increment of chassis torsional stiffness was not beneficial for the vehicle handling performance; a significant reduction of noise level in the

passenger compartment was however measured. The increment of lateral stiffness of the front suspension instead, introduced significant subjective improvements on the on-centre feel, on the yaw response and a more linear understeer behaviour. Objective evaluation was carried out through yaw rate measurements during an open-loop pulse response test; it was found that both the design improvements, in particular the second iteration, contributed to a sensible reduction of yaw rate phase lag, leading to a more responsive and predictable vehicle behaviour.

2.3.5 Ride models

Lack of torsional stiffness is felt by the driver in a number of ways. The classic manifestation is what is called "scuttle shake". In presence of a scuttle shake phenomenon due to low torsional stiffness, it is possible to notice that, when the vehicle is driven over rough road surfaces, the whole body tends to twist and to flex as a consequence of the shocks.

In 1994 Ibrahim et al., [64], studied the effects of the frame flexibility on ride performance of trucks. The results obtained by means of a model with rigid chassis were compared with those obtained by means of a model which included the chassis flexibility. The first model had six degrees of freedom (displacement and pitch of body and cab and vertical displacement of the two axles) while the second one included a flexible chassis. First, the modal masses, stiffness and damping parameters were calculated separately by means of a finite elements tool. The displacements, velocities and accelerations of the attachment points of the suspensions were calculated by means of the modal superposition method. The first three flexible vibration modes were used and different values of structural damping were considered. A random road profile was generated and the power spectral density of the accelerations of different parts of the vehicle was obtained. It was found that the frame flexibility strongly affects the driver vertical acceleration, the cab pitch dynamics and the acceleration of the different points of the frame. Interestingly, recent activities have shown that ride qualities of flexible vehicles can be improved by implementing active vibration systems, see for example [65]. Ride quality is not among the research themes of this activity and therefore it is not discussed further.

2.4 Driver modelling

The aim of racing vehicle design is to develop and set up a car so that the driver can complete a given set of manoeuvres, usually a circuit lap, in the minimum possible time, [66]. Circuit racing requires most of the controls to be applied in an open-loop manner, with minor trim closed-loop corrections. When approaching a race, the driver learns braking, turning and accelerating points through rehearsal and tuning of the car.

In this sense, circuit racing is very different from rally, where control and adaptation to the continuously changing track conditions are required, [28].

Race car driving was described by Moss: "...once one has presented the car to a very high-speed corner it's rather like throwing a dart - when it has left your hand you can't do a thing about its path. If you present a car accurately to such a corner it will track through in a long drift on a virtually predestined trajectory. You can make tiny adjustments, but once you have presented it to the corner you can only adjust the trim, not make major changes of direction - not if you are on the limit. Steering is used to present the car, then to compensate for the throttle, because as one opens the throttle, and car starts to slide you may have to use the steering wheel to compensate - to balance the power. I would describe the steering wheel as the presenter and balancer really", [67].

From the vehicle dynamics point of view, a racing car should be capable of the largest g-g diagram while maintaining sufficient control and stability so that a skilled driver can operate it as close as possible to the limits. The role of the car therefore is to facilitate the task of the driver and of its team, [20]. The role of the driver is to apply controls in such a manner that lap time is minimised; the best drivers have the ability to find and develop the best driving technique for a given vehicle on a given circuit. During the rehearsing process they learn how to drive the vehicle and how to improve the overall vehicle performance. Thanks to the driver's ability, vehicles that theoretically have limited capabilities are very often seen to perform as well as the most capable ones.

Since it is generally difficult to represent the behaviour of a driver within a mathematical model, despite his fundamental role, the driver is usually left out of the loop and the behaviour of the car is analysed independent of the driver. On the other hand, a review of the relevant literature seems to suggest that no general consensus on the importance of chassis torsional stiffness exists. In practice, this means that drivers can adapt to both "soft" and "stiff" vehicles. As a consequence, the adaptive behaviour of the driver reflects the handling characteristics of the vehicle and can be analysed to estimate the handling qualities of the vehicle, [68].

Under this perspective, optimal control theory seems to be the most promising path along which to develop a driver model for vehicle dynamics analysis. It is not among the scopes of this thesis to analyse the theory involved; more details can be found in [69]. Seminal work on the application of optimal control theory to vehicle steering control is presented in [70] and in [71]. Driver models introduced were based on the use of a multi-point path preview. This was obtained through the projection of an imaginary optical lever forward from the vehicle; preview information is obtained by comparing points on the ideal vehicle path with points on the optical lever. Steering control input is then evaluated as a weighted sum of the preview samples.

Both the papers refer to a previously developed work that permits the reformulation

of the small-perturbation path-tracking control problem into a constant-coefficients linear plant that includes the vehicle model and a shift register for road samples. Vehicle and driver systems are therefore represented as a standard discrete-time linear-quadratic optimal regulator in which the control input is represented by the steering wheel angle and road samples are the external disturbance.

The optimal control problem is obtained through the definition of a cost function that includes both tracking error and attitude error. In case of infinite horizon and Gaussian disturbance case, the problem is also time-invariant. In this case, the solution of the optimal control problem is derived straightforwardly from the algebraic Riccati equation and permits to evaluate the weighting coefficients.

A novel hypothesis is also included in [71]. First, given a certain vehicle velocity and balance between tracking accuracy and control power, the author derives a set of TI-optimal preview gains that only depend on the distance ahead of the car. The preview distance is then defined as the minimum distance ahead of the car for which most of the area subtended by the curve of the full preview gains is contained. As a consequence, the preview distance defines the minimum length of the preview needed by an optimal driver in order to control the car along a given path. The paper suggests the use of the preview distance as a parameter for the description of the handling qualities of the vehicle. It is implied that the shorter the distance, the more responsive the car is to steering control. More advanced models that include non-linear vehicle models were used for the evaluation of optimal controls at cornering trim states in [72] or for the generation of time-optimal trajectories for a model of a Formula One racing car, [66].

2.5 Concluding remarks

A review of the literature relevant to the relationship between chassis stiffness and vehicle dynamics has been presented in this chapter. The analysis reveals that although the importance of chassis stiffness is generally recognised, a systematic and complete work on its effects on vehicle dynamics is not available.

Literature shows that chassis torsional stiffness is generally modelled by connecting the axles of the vehicle by means of a torsion spring. It is likely that this model is suitable for the analysis of the effect of chassis compliance on lateral load transfer distribution at limited values of lateral acceleration; in the other cases however, suspension attachment points might undergo significant displacements that require a more complex modelling of the chassis compliances. As shown, the interaction with suspension kinematics is particularly important when highly dynamic events occur and when the vehicle is subjected to high lateral forces. Despite the fact that these are the typical operating conditions of sports and racing cars, this interaction has never been thoroughly investigated.

On one hand, it emerges from the literature that the complexity of the effects of chassis compliance on vehicle behaviour requires the use of an advanced analysis tool. On the other hand, it seems that a simplified purposely-developed vehicle model could be of great advantage for an initial assessment of the magnitude of the problem. As a consequence, both the options are explored, respectively in Chapters 3 and 5.

Apart from the difficulties encountered whilst tuning or optimising the behaviour of a vehicle having excessive compliance, the literature shows that subjectivity plays an important role in the definition of the minimum amount of chassis stiffness which is desirable. Despite the amount of information they can deliver, it seems that conventional open- or closed-loop analysis methods are not capable of capturing this aspect. As shown, optimal control theory offers an understanding of the relationship between the vehicle and the driver and it permits to study the behaviour of the vehicle when driven by "the best" driver. It is therefore intended to develop a vehicle model that can be included within the existing framework of optimal control theory and to employ it as a tool for the evaluation of the impact of chassis flexibility on the handling performance of the vehicle.

Chapter 3

A preliminary vehicle model with a flexible chassis

The present chapter describes a preliminary study carried out in order to obtain an estimate of the influence of the chassis torsional compliance on the vehicle behaviour. In the first section the correlation between torsional stiffness and lateral load transfer and roll steer mechanisms is analysed through the use of analytical models. A four-degrees-of-freedom mathematical model is then presented and employed for the steady-state and transient analysis of vehicle dynamics. A linearised version of the model is then introduced and employed for root locus and frequency response analyses. Finally, the impact of chassis compliance on vehicle behaviour is observed through the use of optimal control theory.

3.1 Lateral load transfer distribution

3.1.1 Rigid vehicle

Lateral load transfer control is a primary key for tuning vehicle behaviour. Control of the repartition of the lateral load transfer between the two axles however is only possible if the chassis is sufficiently stiff, [16].

Consider a vehicle having mass m, centre of mass height $h_{_G}$ and wheel tracks equal to t. Under the effect of a lateral acceleration $a_{_y}$, the total lateral load transfer $\Delta F_{_z}$ is equal to:

$$\Delta F_{_z} = \frac{m\, h_{_G}\, a_{_y}}{t} \tag{3.1}$$

A model for the evaluation of the lateral load transfer distribution between the two axles under steady-state conditions is described by Milliken, [20]. The following assumptions are introduced:

- a lateral load applied along the roll axis does not produce roll;

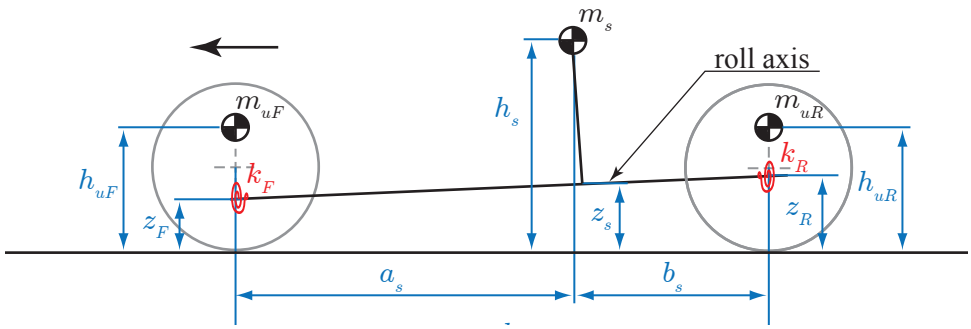

Figure 3.1: Rigid model for lateral load transfer.

- front and rear roll rates are measured independently;
- solid axle roll relative to the ground is not considered;
- the gravity term associated with roll angle is neglected;
- all the lines normal to the roll axis are considered vertical.

Referring to Figure 3.1, front and rear lateral load transfer can be written as:

$$\begin{aligned} \Delta F_{zF} &= \left(\frac{k_F}{k_F + k_R} d_s m_s + z_F m_{sF} + h_{uF} m_{uF} \right) \frac{a_y}{t} \\ \Delta F_{zR} &= \left(\frac{k_R}{k_F + k_R} d_s m_s + z_R m_{sR} + h_{uR} m_{uR} \right) \frac{a_y}{t} \end{aligned} \tag{3.2}$$

where k_F and k_R represent the front and rear roll stiffness, $d_s = h_s - z_s$ is the distance between the centre of gravity of the sprung mass m_s and the roll axis, z_F and z_R are the front and rear roll centre heights, $m_{sF} = b_s/l$ and $m_{sF} = a_s/l$ are the front and rear parts of the sprung mass. Front and rear unsprung masses, located at heights h_{uF} and h_{uR}, are represented by masses m_{uF} and m_{uR}.

A roll stiffness proportion $\lambda = k_F/(k_F + k_R)$ and a lateral load transfer proportion $\chi = \Delta F_{zF}/\Delta F_z$ are here defined. From Equations (3.2), the following relationship holds:

$$\chi_0 = \lambda \frac{d_s}{h_G} \frac{m_s}{m} + \frac{z_F}{h_G} \frac{m_{sF}}{m} + \frac{h_{uF}}{h_G} \frac{m_{uF}}{m} \tag{3.3}$$

where the suffix 0 is used to denote vehicle with a rigid chassis. Equation (3.3) shows that three terms contribute to the lateral load transfer distribution. The first one depends on the fraction of the roll moment generated by the sprung mass and withstood by the front axle; the second on the lateral force applied to the axle while the third term includes the effect of the unsprung mass. It is the first of the three terms that is more often adjusted by changing the roll stiffness proportion λ.

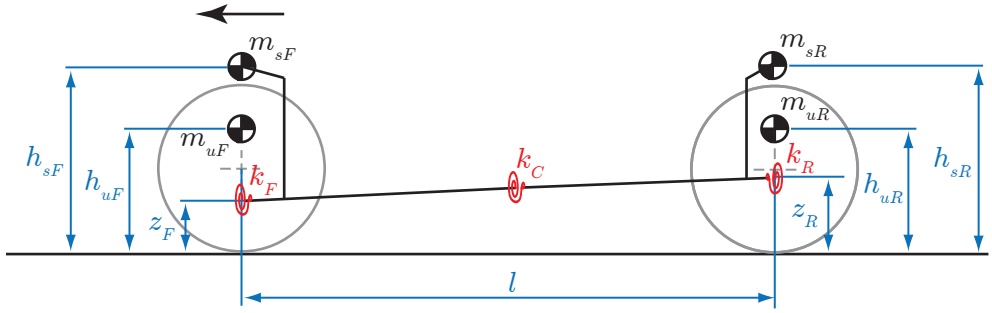

Figure 3.2: Flexible model for lateral load transfer.

It is possible to demonstrate that the described model is equivalent to a system in which the sprung mass is divided in two parts, equal to m_{sF} and m_{sR} placed on the front and rear axle and having heights from the ground equal to h_{sF} and h_{sR}. Equations (3.2) can be rewritten in the equivalent form:

$$\begin{aligned} \Delta F_{zF} &= \left(\frac{k_F}{k_F + k_R} d_{sF} m_{sF} + \frac{k_F}{k_F + k_R} d_{sR} m_{sR} + z_F m_{sF} + z_{uF} m_{uF} \right) \frac{a_y}{t} \\ \Delta F_{zR} &= \left(\frac{k_R}{k_F + k_R} d_{sF} m_{sF} + \frac{k_R}{k_F + k_R} d_{sR} m_{sR} + z_R m_{sR} + z_{uR} m_{uR} \right) \frac{a_y}{t} \end{aligned} \tag{3.4}$$

where $d_{sF} = h_{sF} - z_F$ and $d_{sR} = h_{sR} - z_R$.

3.1.2 Flexible vehicle

If the initial assumption of rigid chassis is relaxed, Equations (3.4) are no longer valid. Deakin et al., [16], presented an analytical model in order to evaluate the chassis torsional stiffness that ensures a good handling sensitivity when the roll stiffness distribution is changed. Some figures were given, inconsistencies however were found in the equations and in their comments. Furthermore, the model described in the paper does not consider the fact that load transfer distribution is partially controlled by roll axis position and by unsprung masses.

A model that includes chassis torsional stiffness can be developed by substituting the link which connects the front and the rear axles by means of a torsion spring of stiffness k_C. The model, represented in Figure 3.2, can be derived from Equations (3.4). According to this approach, the fraction of the lateral load transfer generated by the front part of the vehicle and transmitted to the rear axle, encounters along its load path, the torsional spring which represents the chassis stiffness. As a consequence the spring which represents the chassis stiffness can be seen as in series with the rear axle roll stiffness. A similar argument is valid for the fraction of the lateral load generated by the rear half of the vehicle. It is therefore possible to write the equation for the

lateral load transfer as:

$$\begin{aligned}
\Delta F_{zF} &= \left(\frac{k_F\, d_{sF} m_{sF}}{k_F + \dfrac{k_R\, k_C}{k_R + k_C}} + \frac{\dfrac{k_F\, k_C}{k_F + k_C}\, d_{sR} m_{sR}}{\dfrac{k_F\, k_C}{k_F + k_C} + k_R} + z_F m_{sF} + h_{uF} m_{uF} \right) \frac{a_y}{t_F} \\
\Delta F_{zR} &= \left(\frac{\dfrac{k_R\, k_C}{k_R + k_C}\, d_{sF} m_{sF}}{k_F + \dfrac{k_R\, k_C}{k_R + k_C}} + \frac{k_R\, d_{sR} m_{sR}}{\dfrac{k_F\, k_C}{k_F + k_C} + k_R} + z_R m_{sR} + h_{uR} m_{uR} \right) \frac{a_y}{t_R}
\end{aligned} \tag{3.5}$$

By introducing the non-dimensional parameter $\mu = k_C/(k_F + k_R)$, expression for lateral load transfer proportion reads:

$$\chi = \frac{\lambda^2 - (\mu + 1)\lambda}{\lambda^2 - \lambda - \mu} \frac{d_{sF}}{h_G} \frac{m_{sF}}{m} - \frac{\mu\lambda}{\lambda^2 - \lambda - \mu} \frac{d_{sR}}{h_G} \frac{m_{sR}}{m} + \frac{z_F}{h_G} \frac{m_{sF}}{m} + \frac{z_{uF}}{h_G} \frac{m_{uF}}{m} \tag{3.6}$$

As an example, the effect of chassis torsional compliance for a Formula Student vehicle is presented in Figure 3.3. Vehicle data are presented in Appendix A.

Figure 3.3a reports values of lateral load transfer proportion χ versus roll stiffness proportion λ for different values of chassis torsional stiffness. The effect of chassis torsional compliance consists of the introduction of a non-linearity in the relationship between χ and λ. Figure 3.3a shows that three different configurations in which the value of μ does not affect the lateral load transfer distribution exist. Two of them consist of limit configurations, characterized by $\lambda = 0$ and $\lambda = 1$, that is when either the front or the rear roll stiffness is null. From Equation (3.6), the third value corresponds to the condition:

$$\frac{\lambda}{1 - \lambda} = \frac{d_{sF}\, m_{sF}}{d_{sR}\, m_{sR}} \tag{3.7}$$

The right hand side of Equation (3.7) can be considered as the ratio of front to rear roll moment. It is therefore possible to say that the chassis torsional stiffness is irrelevant when the ratio of front to rear roll stiffness is equal to the ratio of front to rear roll moment. If the non-dimensional parameter $\zeta = d_{sF}\, m_{sF}/(d_{sF}\, m_{sF} + d_{sR}\, m_{sR})$ is introduced, relationship (3.7) can be expressed as $\lambda = \zeta$.

Lateral load transfer proportion χ tends to its asymptotic value for increasing values of normalised chassis torsional stiffness μ, see Figure 3.3b. The graph shows that the effect of μ is small when values of λ are close to satisfying Equation (3.7) while higher values of chassis torsional stiffness are required if this is not the case.

A map of $|\chi - \chi_0|$ normalised over χ_0 versus λ and μ is presented in Figure 3.3c. The graph therefore reports the error committed in the evaluation of the lateral load transfer distribution if chassis torsional compliance is neglected. Errors up to 60% can be noticed for low values of chassis stiffness and rear-biased roll stiffness distribution;

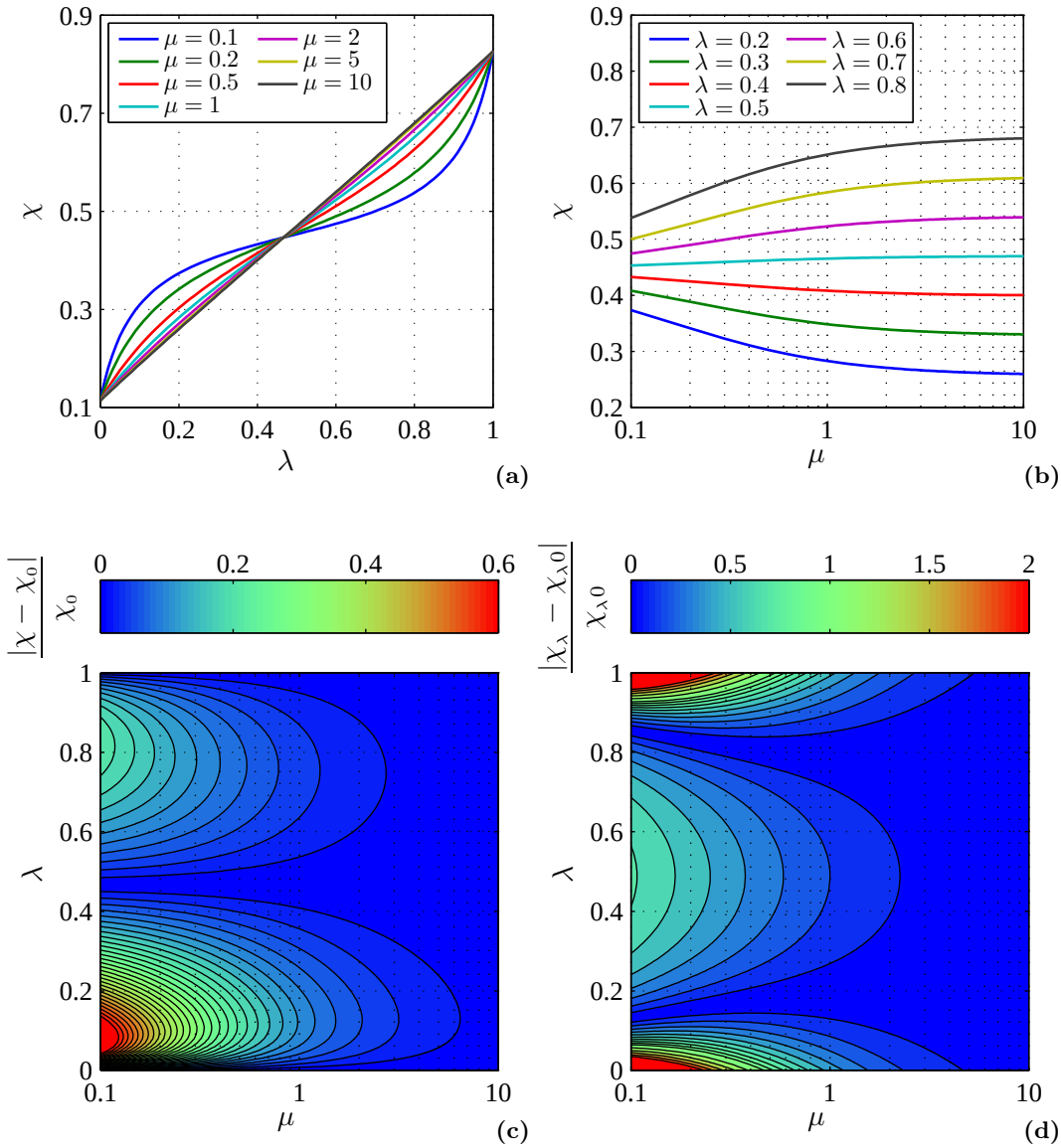

Figure 3.3: Effect of chassis torsional stiffness on lateral load transfer distribution. (a) Lateral load transfer proportion versus roll stiffness distribution for different values of normalised chassis torsional stiffness. (b) Lateral load transfer distribution versus normalised chassis torsional stiffness for different values of roll stiffness distribution. (c) Effect of chassis torsional compliance on lateral load transfer proportion versus normalised chassis torsional stiffness and roll stiffness proportion. (d) Effect of chassis torsional compliance on lateral load transfer distribution sensitivity versus normalised chassis torsional stiffness and roll stiffness distribution.

errors up to 25% can be found for high values of λ. This difference is due to different values of roll moment generated by the front and rear part of the unsprung mass.

Two values of λ for which the error is maximum can be found for each value of torsional stiffness. As expected, the error tends to disappear for high values of μ. The graph can be successfully used to determine the minimum stiffness required in order to control lateral load transfer proportion to a desired level. Let us suppose, for example, that a maximum error on lateral load transfer distribution of 2% is desired over a range of roll stiffness distribution $\lambda = 0.3 - 0.7$. From Figure 3.3c, a minimum value of $\mu \approx 3$ is found.

Lateral load transfer distribution is usually controlled by tuning roll stiffness distribution. As a consequence, an important role is played by the sensitivity of χ towards λ, that is the partial derivative $\chi_\lambda = \partial\chi/\partial\lambda$. Figure 3.3d reports a map of the sensitivity error over a wide range of μ and λ. In presence of an infinitely rigid chassis, a linear relationship between the two quantities exists, see Equation (3.3). As a consequence, a sensitivity error map can be interpreted as a non-linear map of the relationship between roll stiffness distribution and lateral load transfer distribution. Interestingly, high non-linearity errors can be found not only in regions where $\lambda = 0$ and $\lambda = 1$ but also where $\lambda = \zeta$. Chassis compliance therefore introduces a non-linearity effect that makes tuning of the vehicle difficult. The graph represents a useful tool for the designer. Again, if a maximum non-linearity error of 5% is desired over a range of $\lambda = 0.3 - 0.7$, from Figure 3.3d, a minimum value of $\mu \approx 5$ is found.

3.2 Roll steer

3.2.1 Rigid vehicle

Suspension kinematics is generally designed in such a manner that, when bump or roll movements occur, desired variations of tyre working angles are obtained. Amongst other characteristics, the effect of roll steer in presence of chassis torsional compliance is here analysed.

Roll steer can be described as the variation of the steering angle of a wheel that is kinematically linked to the roll angle of the sprung mass. For small roll and steer angles, it is possible to assume that the dependency between the steering angle variation induced by roll steer and roll angle φ is linear. Front and rear axle steer angles can therefore be written as:

$$\delta_F = \delta + \varepsilon_F \varphi \qquad \delta_R = \varepsilon_R \varphi \tag{3.8}$$

where δ is the steer angle commanded by the steering system, φ is the roll angle and ε_F and ε_R are the front and rear roll steer coefficients.

Neglecting the contribution of the gravity, roll angle of the sprung mass of a rigid vehicle subject to a lateral acceleration a_y can be evaluated as:

$$\varphi = \frac{m_s d_s}{k_F + k_R} a_y = \varphi_y a_y \tag{3.9}$$

where the term $\varphi_y = (m_s d_s)/(k_F + k_R)$ is the roll gradient.

A linear bicycle model is here adopted in order to evaluate the influence of roll steer on the steady-state behaviour of the vehicle in its linear region. A detailed derivation of the model can be found in [20, 25]; only the necessary assumptions are here reported:

- no longitudinal forces are considered;
- the dependency of the cornering force on the slip angle is considered linear;
- tyre cornering stiffness is considered constant;
- no aerodynamic effects are considered;
- sideslip and steering angles are considered small.

Under these assumptions, steady state-vehicle behaviour can be described by an analytical relationship between the front axle steering angle δ and lateral acceleration a_y:

$$\delta = \frac{l}{R} + \left(\frac{m}{l} \left(\frac{b}{C_F} - \frac{a}{C_R} \right) - (\varepsilon_F - \varepsilon_R)\, \varphi_y \right) a_y \tag{3.10}$$

where l represents the vehicle wheelbase, m its total mass, a and b respectively the front and rear semi-wheelbases, C_F and C_R represent the front and rear axle cornering stiffness and ε_F and ε_R the corresponding roll steer coefficients. The first component of Equation 3.10, l/R, expresses the steering angle required to drive a pure rolling vehicle along a circular path of radius R; for this reason it is also known as kinematic steering angle, δ_k. The second term of the equation (3.10), also known as dynamic steering angle, δ_d, expresses the part of the steering angle that depends on lateral acceleration. The gradient of δ versus a_y, known as understeer gradient, plays an important role in the definition of the handling behaviour of the vehicle. Under the given assumptions, the understeer gradient only depends on vehicle mass distribution, on tyre cornering stiffness and on roll steer coefficients ε_F and ε_R and can be expressed as:

$$k_{u0} = \frac{\mathrm{d}\delta}{\mathrm{d}a_y} = \frac{m}{l} \left(\frac{b}{C_F} - \frac{a}{C_R} \right) - (\varepsilon_F - \varepsilon_R)\, \varphi_y \tag{3.11}$$

where the subscript 0 refers to a rigid chassis vehicle.

3.2.2 Flexible vehicle

In presence of chassis torsional compliance, front and rear roll angles will differ. Referring to Figure 3.2, it is possible to derive steady-state roll equilibrium equations for the front and rear part of the sprung mass. Equations read:

$$\begin{cases} m_{sF} d_{sF} a_y = k_F \varphi_F + k_C (\varphi_F - \varphi_R) \\ m_{sR} d_{sR} a_y = k_R \varphi_R - k_C (\varphi_F - \varphi_R) \end{cases} \tag{3.12}$$

where φ_F and φ_R represent the roll angles of the front and rear parts of the sprung mass. Solution of Equations (3.12) leads to:

$$\begin{aligned}\varphi_F &= \frac{k_C(m_{sF}d_{sF} + m_{sR}d_{sR}) + k_R m_{sF}d_{sF}}{k_F k_R + k_R k_C + k_C k_F} a_y \\ \varphi_R &= \frac{k_C(m_{sF}d_{sF} + m_{sR}d_{sR}) + k_F m_{sR}d_{sR}}{k_F k_R + k_R k_C + k_C k_F} a_y\end{aligned} \tag{3.13}$$

By substituting the already introduced non-dimensional quantities $\lambda = k_F/(k_F + k_R)$, $\mu = k_C/(k_F + k_R)$ and $\zeta = (m_{sF}d_{sF})/(m_{sF}d_{sF} + m_{sR}d_{sR})$ and the definition of roll gradient derived for the rigid case, Expressions (3.13) can be rewritten as:

$$\begin{aligned}\varphi_F &= \frac{\mu + (1-\lambda)\zeta}{\mu + \lambda - \lambda^2}\varphi_y a_y \\ \varphi_R &= \frac{\mu + (1-\zeta)\lambda}{\mu + \lambda - \lambda^2}\varphi_y a_y\end{aligned} \tag{3.14}$$

Chassis twist angle, defined as $\varphi_C = \varphi_F - \varphi_R$, can be evaluated as:

$$\varphi_C = \frac{\lambda - \zeta}{\mu + \lambda - \lambda^2}\varphi \tag{3.15}$$

From Equation (3.15) it is possible to see that chassis twist angle is proportional to the lateral acceleration, to the roll gradient and to the difference between roll stiffness and roll moment proportions $\lambda - \zeta$. Also, φ_C is inverse in proportion to the normalised chassis torsional stiffness μ. Given roll angles of Equation (3.14), understeer gradient can be written as:

$$k_u = \frac{m}{l}\left(\frac{b}{C_F} - \frac{a}{C_R}\right) - \left(\frac{\mu + (1-\lambda)\zeta}{\lambda + \mu - \lambda^2}\varepsilon_F - \frac{\mu + \lambda(1-\zeta)}{\lambda + \mu - \lambda^2}\varepsilon_R\right)\varphi_y \tag{3.16}$$

Equation (3.16) demonstrates that, thanks to the roll stiffness mechanics, chassis torsional compliance introduces a direct dependency between understeer gradient k_u and roll stiffness distribution λ.

As an example, the significance of the interaction between chassis torsional stiffness and roll steer mechanism is analysed for the vehicle described in Appendix A. This is a moderately understeer vehicle with an understeer gradient, in the linear region, of about 0.74 deg/g. Front and rear roll steer coefficients are set, respectively, equal to 0.05 and 0.1.

The relationship between the understeer gradient k_u and the lateral load transfer proportion λ is shown in Figure 3.4a. The graph suggests that a significant fraction of k_u is controlled by parameter λ. The dependency of understeer gradient k_u on

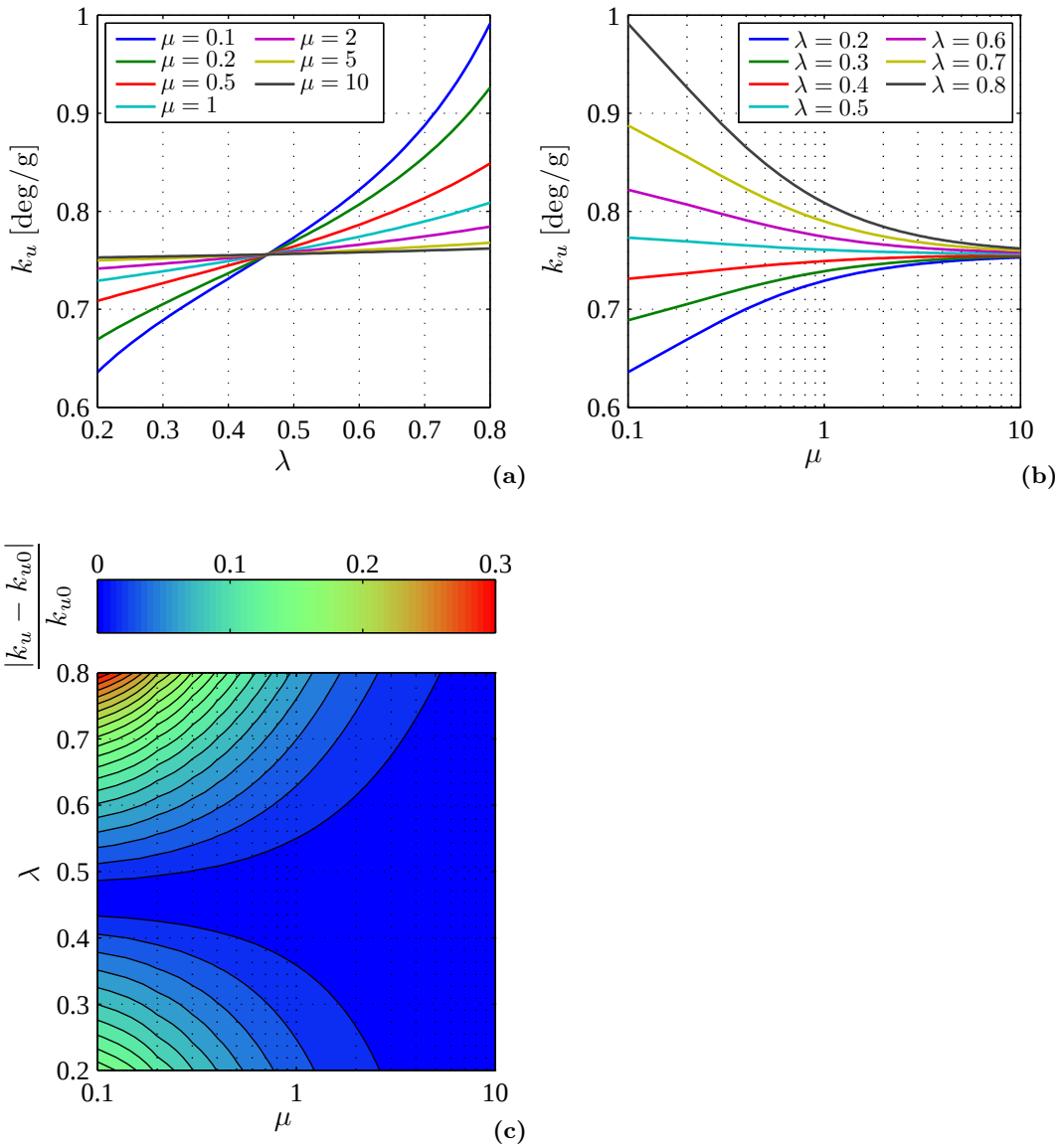

Figure 3.4: Effect of chassis torsional stiffness on understeer gradient through roll steer mechanism. (a) Understeer gradient versus roll stiffness distribution for different values of normalised chassis torsional stiffness. (b) Understeer gradient versus normalised chassis torsional stiffness for different values of roll stiffness distribution. (c) Effect of chassis torsional compliance on understeer gradient as a function of normalised chassis torsional stiffness and roll stiffness distribution.

chassis torsional stiffness μ is reported in Figure 3.4b. The graph reveals that values of $\mu \approx 2 - 3$ are required in order to minimize the variation of k_u introduced by chassis compliance.

The map of Figure 3.4c describes the relative error committed in the evaluation

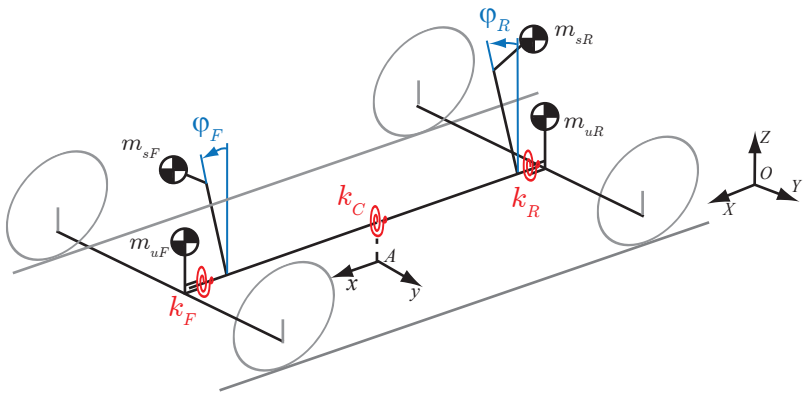

Figure 3.5: Five-degrees-of-freedom vehicle model.

of the understeer gradient when chassis flexibility is neglected. Errors up to 50% can be found for extreme values of λ and low values of μ. The map can be used for the evaluation of design solutions in a way that is similar to the one described for Figures 3.3b and 3.3c. If a target of maximum error on understeer gradient of 2% is desired in the range of $\lambda = 0.3 - 0.7$, a mimum value of chassis torsional stiffness $\mu \approx 8$ can be found from the graph.

It is worth noting that the presented analysis is only valid for limited values of lateral acceleration, for which the assumption of tyre linearity holds. A more detailed non-linear model is presented in Section 3.3.

3.3 Vehicle dynamics

3.3.1 Equations of motion

Equations of motion of the vehicle are derived from the system of Figure 3.5. Cartesian coordinates X and Y of reference point A, yaw angle ψ and front and rear roll angles φ_F and φ_R are used as state variables.

Position of unsprung masses can be derived from expressions:

$$\begin{cases} X_{uF} = X + a\cos\psi \\ Y_{uF} = Y + a\sin\psi \end{cases} \qquad \begin{cases} X_{uR} = X - b\cos\psi \\ Y_{uR} = Y - b\sin\psi \end{cases} \tag{3.17}$$

where a and b represent the front and rear semi-wheelbases. Similarly, positions of

sprung masses are described as:

$$\begin{cases} X_{sF} = X + a\cos\psi + d_{sF}\varphi_F \sin\psi \\ Y_{sF} = Y + a\sin\psi - d_{sF}\varphi_F \cos\psi \end{cases} \qquad \begin{cases} X_{sR} = X - b\cos\psi + d_{sR}\varphi_R \sin\psi \\ Y_{sR} = Y - b\sin\psi - d_{sR}\varphi_R \cos\psi \end{cases} \tag{3.18}$$

Differentiation of Equations (3.17) and (3.18) leads to the evaluation of the velocities of the bodies, not reported here for sake of brevity.

Equations of motions are written using Lagrange's equation:

$$\frac{\mathrm{d}}{\mathrm{d}t}\left(\frac{\partial T}{\partial \dot{\boldsymbol{q}}}\right) - \frac{\partial T}{\partial \boldsymbol{q}} + \frac{\partial F}{\partial \dot{\boldsymbol{q}}} + \frac{\partial U}{\partial \dot{\boldsymbol{q}}} = \boldsymbol{Q_e} \tag{3.19}$$

where $\boldsymbol{q} = [X\ Y\ \psi\ \varphi_F\ \varphi_R]^T$ is used as a set of generalised coordinates. Terms T, F and U represent respectively the total kinetic energy, the dissipative Rayleigh function and the potential energy of the system while vector $\boldsymbol{Q_e}$ represents the external forces.

Total kinetic energy is evaluated as a sum of the kinetic energy of the sprung and unsprung masses:

$$T = T_{sF} + T_{sR} + T_{uF} + T_{uR} \tag{3.20}$$

Kinetic energy associated with the front sprung mass m_{sF} can be written as:

$$T_{sF} = \frac{1}{2}m_{sF}\left(\dot{X}_{sF}^2 + \dot{Y}_{sF}^2\right) + \frac{1}{2}J_{zsF}\dot{\psi}^2 + \frac{1}{2}J_{xsF}\dot{\varphi}_F^2 \tag{3.21}$$

where J_{zsF} and J_{xsF} represent, respectively, the yaw and roll inertia. Cross inertia products are here ignored. Similar equations can be written for the rear sprung mass and for the unsprung masses. For the front unsprung mass, it is:

$$T_{uF} = \frac{1}{2}m_{uF}\left(\dot{X}_{uF}^2 + \dot{Y}_{uF}^2\right) + \frac{1}{2}J_{zuF}\dot{\psi}^2 \tag{3.22}$$

Rayleigh dissipation function includes the damping effect of shock absorbers and the internal damping of the chassis:

$$F = \frac{1}{2}c_F\dot{\varphi}_F^2 + \frac{1}{2}c_R\dot{\varphi}_R^2 + \frac{1}{2}c_C\left(\dot{\varphi}_F - \dot{\varphi}_R\right)^2 \tag{3.23}$$

where c_F and c_R are the roll damping coefficients of front and rear axle and c_C is the damping coefficient of the torsional damper associated with the torsional stiffness of the chassis.

Potential energy includes elastic energy stored in springs, here assumed linear:

$$U = \frac{1}{2}k_F\varphi_F^2 + \frac{1}{2}k_R\varphi_R^2 + \frac{1}{2}k_C\left(\varphi_F - \varphi_R\right)^2 \tag{3.24}$$

where k_F is the roll stiffness of the front axle, k_R the roll stiffness of the rear axles and k_C the chassis torsional stiffness.

The vector of external forces $\boldsymbol{Q_e}$ contains the components of the tyre forces acting along the axes of the inertial frame. Introducing Equations (3.20), (3.23), (3.24) into Equation (3.19), the equations of motion can be derived as a function of $\ddot{\boldsymbol{q}}$. It is however more convenient to express the vehicle velocities in the moving reference frame. The following relationship holds between the two sets of velocities:

$$\begin{cases} \dot{X} = u\cos\psi - v\sin\psi \\ \dot{Y} = u\sin\psi + v\cos\psi \\ \dot{\psi} = r \\ \dot{\varphi}_F = p_F \\ \dot{\varphi}_R = p_R \end{cases} \tag{3.25}$$

where u and v and r are respectively the longitudinal, lateral and yaw velocities while p_F and p_R represent the front and rear roll velocities. Velocity u is here considered constant and the relevant degree of freedom is therefore removed. From this, equations of motion can be written as:

$$\begin{cases} m(\dot{v} + ru) - d_{sF}m_{sF}\dot{p}_F - d_{sR}m_{sR}\dot{p}_R = F_{yF} + F_{yR} \\ J_z\dot{r} - d_{sF}m_{sF}a\,\dot{p}_F + d_{sR}m_{sR}b\,\dot{p}_R = F_{yF}\,a - F_{yR}\,b \\ J_{rF}\dot{p}_F - d_{sF}m_{sF}(\dot{v} + ru - a\dot{r}) + k_F\varphi_F + c_F p_F + \\ \qquad\qquad +k_C(\varphi_F - \varphi_R) + c_C(p_F - p_R) = 0 \\ J_{rR}\dot{p}_R - d_{sR}m_{sR}(\dot{v} + ru + b\dot{r}) + k_R\varphi_R + c_R p_R + \\ \qquad\qquad -k_C(\varphi_F - \varphi_R) - c_C(p_F - p_R) = 0 \end{cases} \tag{3.26}$$

where J_z is the total yaw inertia of the vehicle and J_{rF} and J_{rR} are the front and rear roll moments of inertia. Neglecting the terms that depend on chassis twist, the value of J_z can be considered constant and evaluated as $J_z = J_{zsF} + J_{zsR} + J_{zuF} + J_{zuR} + a^2(m_{sF} + m_{uF}) + b^2(m_{sR} + m_{uR})$ while $J_{rF} = J_{xsF} + d_{sF}^2 m_{sF}$ and $J_{rR} = J_{xsR} + d_{sR}^2 m_{sR}$. In case of infinite chassis stiffness, Equations (3.21) can be reduced to equations of motion widely used for vehicle dynamic studies, see for example [34].

Tyre forces are represented by their cornering components, F_{yF} and F_{yR} evaluated by means of a simplified version of Pacejka Magic formula, [73], in which both camber and combined longitudinal and lateral slip effects are neglected. Given an axle slip angle α_F, tyre cornering force of the front axle can be expressed as:

$$F_{yF} = f(\alpha_F, F_{zsF} + dF_{zF}) + f(\alpha_F, F_{zsF} - dF_{zF}) \tag{3.27}$$

where F_{zsF} represents the tyre static load and dF_z is the lateral load transfer evaluated according to Equation (3.5) under the assumption of steady-state lateral acceleration $a_y = ru$. Similar equations can be derived for the rear axle. Tyre sideslip angles are evaluated according to the equations:

$$\alpha_F = \delta_F + \frac{v + ar}{u} \qquad \alpha_R = \delta_R - \frac{v - br}{u} \tag{3.28}$$

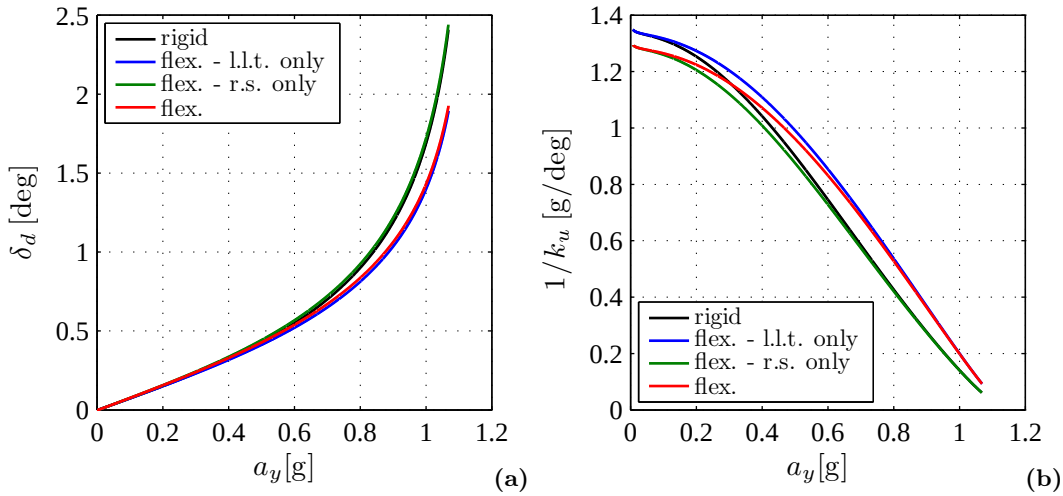

Figure 3.6: Vehicle steady-state characteristics during a skid-pad test. Comparison between results obtained under the assumptions: rigid chassis, flexible chassis with inclusion effect of chassis compliance on lateral load transfer distribution only, flexible chassis with inclusion effect of chassis compliance on roll steer mechanism only, flexible chassis with inclusion of the effect of chassis compliance on lateral load transfer distribution and on roll steer mechanism. (a) Dynamic steer angle versus lateral acceleration. (b) Steering sensitivity versus lateral acceleration.

In presence of roll steer, steering angles δ_F and δ_R are evaluated as in Equation (3.8).

Numerical integration of Equations (3.25) and (3.26) permits the simulation the dynamic behaviour of the vehicle. Longitudinal speed u is considered constant; steering angle δ is controlled by a driver routine. Data used for the simulations can be found in Appendix A, results are presented and discussed in the following sections.

3.3.2 Steady-state vehicle behaviour

Steady-state behaviour is observed through the analysis of a skid-pad test with a constant radius of 50 m. A normalised chassis torsional stiffness $\mu = 1$, a roll stiffness distribution parameter $\lambda = 0.54$ and a roll moment distribution $\zeta = 0.46$ are assumed. Figure 3.6 reports a comparison between the results obtained by means of four variants of the described model. While the first one does not consider any effects of chassis flexibility, the second and the third variants only considers its effects, respectively, on lateral load transfer and on roll steer mechanism. Both the effects are included in the fourth version of the model.

A plot of the dynamic steering angle versus lateral acceleration is presented in Figure 3.6a. The graph confirms that the effect of chassis flexibility cannot be neglected, especially when high values of lateral acceleration are considered. Also, it reveals that

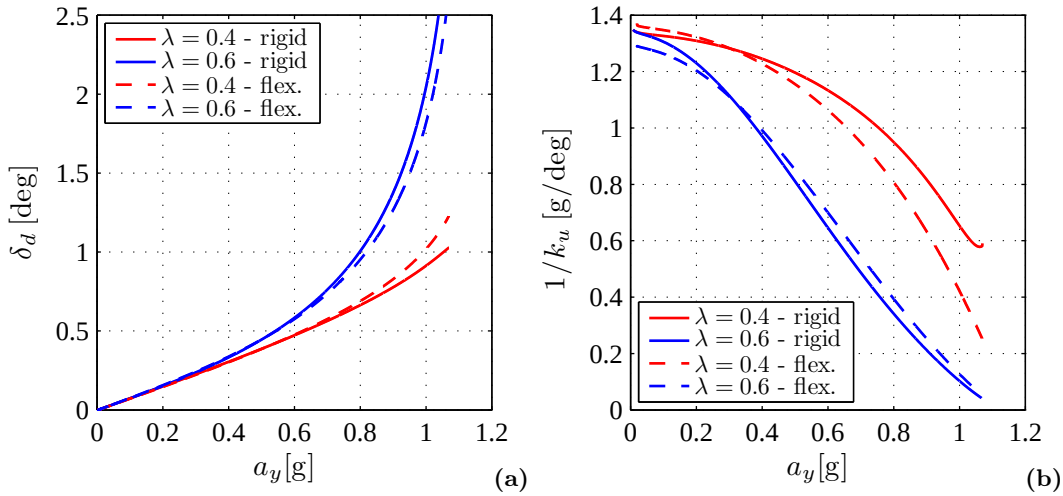

Figure 3.7: Effect of chassis torsional stiffness on vehicle behaviour adjustment during a skid-pad test. Comparison between the results obtained under the hypotheses of rigid and flexible chassis for $\lambda = 0.4$ and $\lambda = 0.6$. (a) Dynamic steering angle versus lateral acceleration. (b) Steering sensitivity versus lateral acceleration.

lateral load transfer distribution is the primary mechanism through which chassis compliance affects the behaviour of the vehicle. This is confirmed by the graph of Figure 3.6b where the inverse of the understeer gradient, also known as steering sensitivity, is plotted. At low values of lateral acceleration, the curve that represents the results obtained considering only the effect of chassis torsional stiffness on lateral load transfer distribution is coincident with the curve obtained with a rigid chassis model. At high values of lateral acceleration it is coincident with the curve obtained with a complete model. The opposite can be noticed for the curve obtained considering the only effect of chassis torsional stiffness on roll steer. It is therefore possible to say that at low values of lateral acceleration, the effect of chassis compliance on suspension geometry is more important than the effect on lateral load transfer distribution; the opposite holds at high levels of lateral acceleration.

Ease of adjustment is another important characteristic of race vehicles. Without considering aerodynamic and tyre pressure effects, roll stiffness distribution is one of the main parameters for the optimisation of the limit behaviour of the vehicle. Figure 3.7 shows a comparison between the results obtained under the assumptions of rigid and flexible chassis when the roll stiffness distribution parameter λ is varied. The dynamic steering angle is plotted against lateral acceleration in Figure 3.7a. The graph confirms that, under both the assumptions, it is the limit behaviour of the vehicle that is mainly affected by the roll stiffness distribution parameter λ.

From the graph of Figure 3.7a it is possible to see that lines corresponding to a flexible chassis vehicle delimit an area that is smaller than the area delimited

by the lines corresponding to a rigid chassis vehicle. This fact demonstrates that chassis compliance reduces the sensitivity of the vehicle behaviour towards roll stiffness distribution and that, if the available range of λ is limited, it might not be possible to obtain a particular set-up of the vehicle. This fact is confirmed by the graph of Figure 3.7b where steering sensitivity is plotted against lateral acceleration.

A second effect of chassis compliance can be deduced from Figure 3.7b. In case of a rigid chassis, the variation of roll stiffness distribution does not affect the value of the steering sensitivity at zero lateral acceleration; the opposite holds in case of a flexible chassis. This behaviour is due to the roll steer mechanism described in Section 2. Chassis flexibility therefore not only limits the number of possible set-ups that can be obtained by tuning roll stiffness distribution but it also makes impossible to tune separately the behaviour of the car at low and high values of lateral acceleration.

3.3.3 Transitory dynamics

A steering step input is employed to characterise the transitory behaviour of the vehicle. The manoeuvre is carried out at a constant speed of 90 km/h, steering amplitude is set equal to 1.5 deg. Steering input is generated through the use of a cubic polynomial that, while being a good approximation of the Heaviside step function, has continuous first derivative.

Time histories obtained under the assumption of a rigid and flexible chassis are reported in Figure 3.8. While the steering input is represented in Figure 3.8a, time history of lateral acceleration is plotted in Figure 3.8b. As anticipated by the previous analysis, a slight difference in the steady-state value of the lateral acceleration exists. The graph however also shows a less damped vehicle behaviour with a greater overshoot ratio. This can be more markedly noticed in Figure 3.8c where the yaw rate time history is reported. Analysis of the results shows that chassis compliance induces an increment of the yaw rate response time from 0.17 s to 0.22 s and of overshoot ratio from 9.5% to 14.5%. Similar effect is noticed on the roll angle of the sprung mass, evaluated as average value between the roll angle of the front and of the rear parts of the sprung mass; for sake of brevity the relative graph is not reported here.

Chassis torsional deformation is reported in Figure 3.8d. The consequent oscillations appear to have high peak values and to be highly underdamped. This is testified by a relatively long settling time of 1.2 s, measured as the time elapsed from the application of the step input to the time at which the value of the output enters and remains within a 2% error band of its steady-state value.

Results displayed in Figure 3.8 have been obtained neglecting chassis damping. It could be argued that, although low, materials used for chassis construction generally exhibit a certain internal damping. Simulation trials however, have shown that the impact of such damping on chassis oscillations and on vehicle dynamics is negligible.

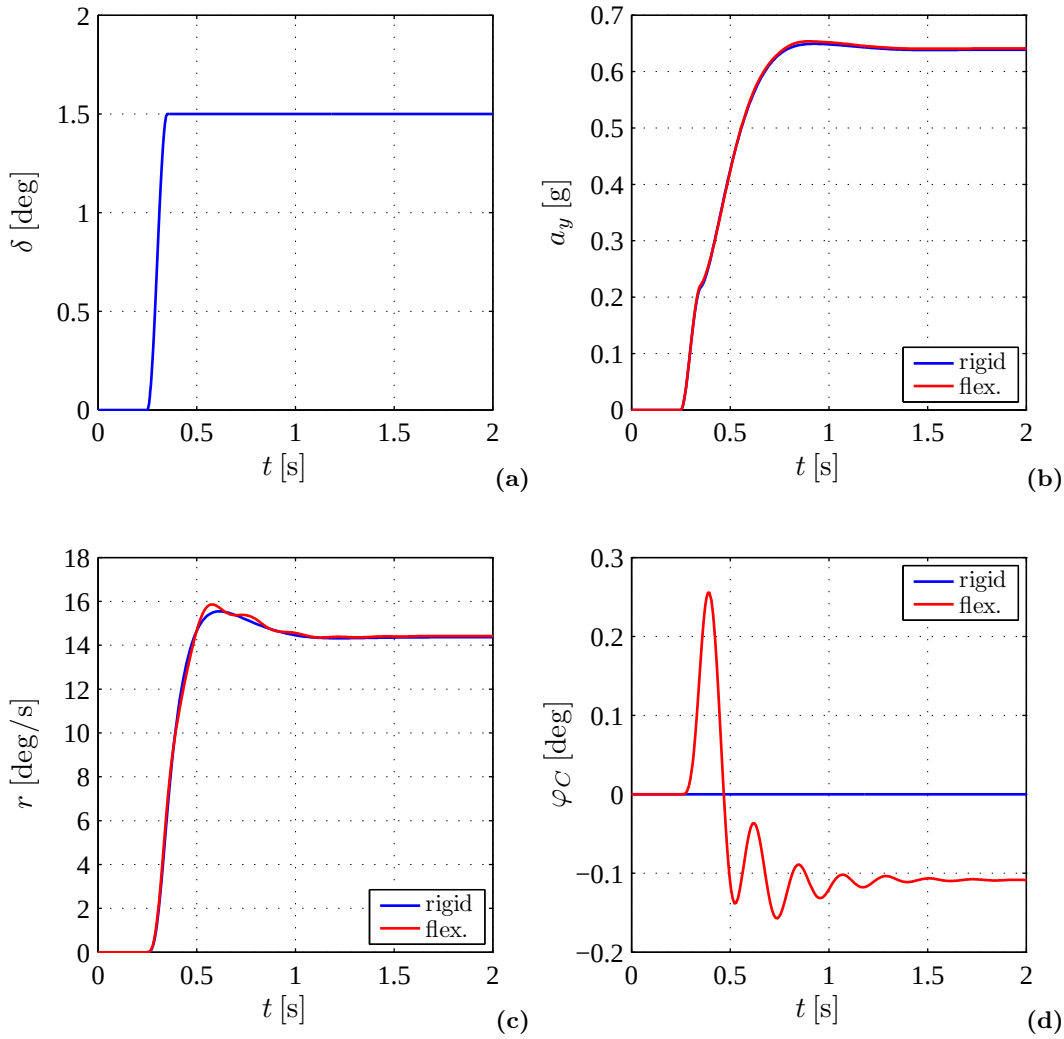

Figure 3.8: Effect of chassis flexibility on steering step response at 50 km/h. (a) Steering input. (b) Lateral acceleration. (c) Yaw rate. (d) Chassis torsion angle.

3.3.4 Root locus analysis

The dynamic model presented in Equations (3.26) can be linearised around trim state at null lateral acceleration by using constant values of tyre cornering stiffness. This permits the study of the positioning of the eigenvalues of the system and its frequency response.

In general, the motion of a rigid vehicle can be described by using two modes, the first of which can be approximated as a yaw and sideslip motion while the second mainly consists of a roll motion, [34]. For models including chassis flexibility, various coordinates participate in a single modal motion; identification of modal shapes it therefore more complex. In this case, however, a third mode mainly corresponding to

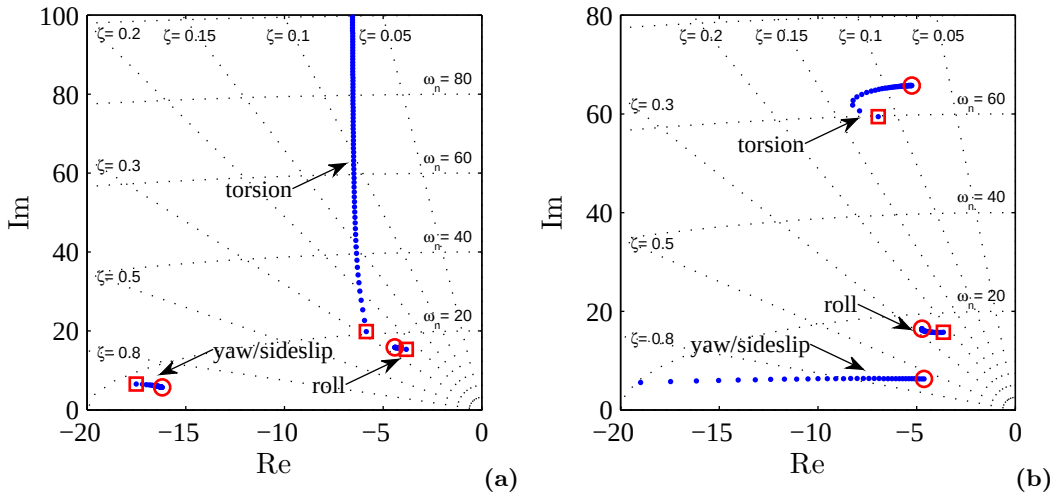

Figure 3.9: System root locus plot. (a) Root locus at constant speed as a function of chassis torsional stiffness; μ varied from 0.1 (□) to 10 (○). (b) Root locus as function of vehicle longitudinal velocity; velocity varied from 5 (□) to 120 km/h (○).

an out-of-phase roll motion of the two halves of the chassis can be observed.

The analysis of the positioning of the eigenvalues of the system permits the analysis of the natural frequency and the damping associated with the modes of motion of the vehicle. Results are displayed in Figure 3.9. The real and the imaginary part of the eigenvalues, as well as straight lines representing constant values of damping and concentric arches corresponding to constant values of undamped natural frequencies, are plotted.

Figure 3.9a reports a root locus plot obtained at a fixed speed of 50 km/h while the chassis torsional stiffness is increased. An increment of chassis stiffness generates an increment of the imaginary part of the eigenvalue corresponding to the torsion mode while no substantial variation is noticed on its real part. In other words, the natural frequency of the torsion mode is increased while its damping coefficient is decreased.

The maximum value of the damping coefficient is obtained for very low values of torsional stiffness and it is equal to the damping of the roll mode. Furthermore, the graph seems to suggest that low values of chassis torsional stiffness promote an increment of the natural frequency and a reduction of the damping coefficient associated with the yaw and sideslip mode of the vehicle. No substantial variation of the positioning of the eigenvalue related to the pure roll mode can be noticed when chassis stiffness is changed.

An analysis of the effect of vehicle velocity on the positioning of the eigenvalues is reported in Figure 3.9b. A variation of both the natural frequency and the damping

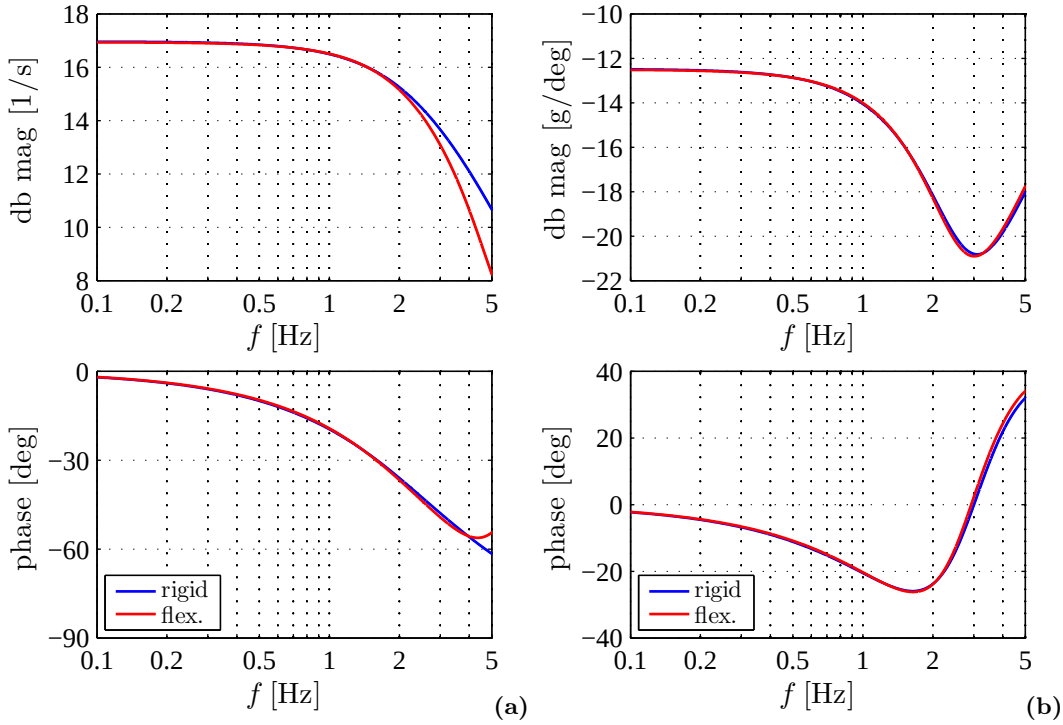

Figure 3.10: Comparison between frequency response of the vehicle when chassis torsional compliance is included or neglected at 50 km/h. (a) Yaw rate frequency response versus steering wheel input. (b) Lateral acceleration frequency response versus steering wheel input.

of the mode associated with chassis torsion can be observed when the vehicle speed is increased. In particular, speed increase generates a slight increment of the natural frequency of the torsion mode and a sensible reduction of its damping coefficient. A careful choice of chassis stiffness is therefore required in order to obtain high speed vehicle stability. No unexpected variation of the positioning of the eigenvalues related to the yaw and sideslip and roll mode can be noticed.

3.3.5 Frequency response

The analysis of the frequency response permits the study of the dynamic behaviour of the vehicle when subject to a small perturbation input from the driver. To this purpose, Bode magnitude and phase plots of the response of the system to a steering angle input for frequencies up to 5 Hz are shown in Figure 3.10.

Experimental analysis has shown that the spectrum of the steering wheel input a normal road driver is capable of constantly decreases up to a frequency of 0.5 Hz and is practically null for higher frequencies, [28]. If a professional driver is however considered, it is possible to notice that the spectrum is approximatively flat up to a

frequency of 1 Hz, after which it decreases slowly until 5 Hz. Furthermore, the high-frequency content of the driver input undergoes a significant rise during emergency manoeuvres. Because of this, input frequencies up to 5 Hz are considered.

Yaw rate frequency response is reported in Figure 3.10a. Although the natural frequency of the torsion mode of the chassis, equal to about 10 Hz, lies outside the plotted range of frequency, an effect on the response of the vehicle in the 2-5 Hz range is noticed. In particular, starting from 2 Hz, chassis compliance increases the rate of the response decay. Phase delay is instead increased for frequencies up to 4 Hz and then abruptly decreased.

Lateral acceleration frequency response is reported in Figure 3.10b. The graph shows that the effect of chassis compliance on lateral acceleration response is smaller than the one on yaw rate response; a minor variation on the phase delay can however be noticed for frequencies close to 5 Hz.

3.3.6 Optimal controls

The present section introduces an attempt at applying the optimal control theory framework presented in [71] and discussed in Section 2.4 to the developed vehicle model. The standard non-rolling bicycle vehicle model used in the mentioned paper is substituted with a linearised version of the equations of motion (3.26). Linearisation is evaluated at trim point corresponding to a null lateral acceleration. In order to align the problem form with the discrete-time linear-quadratic- regulator theory available, equations of motion (3.26) need to be coupled with the linear kinematic relationships:

$$\begin{cases} \dot{Y} = u\,\psi + v \\ \dot{\psi} = r \\ \dot{\varphi}_F = p_F \\ \dot{\varphi}_R = p_R \end{cases} \tag{3.29}$$

Equations (3.29) can be derived from (3.25) under the assumption of small yaw angles and neglecting the position of the vehicle along the X axis.

The complete set of equations is written in a matrix form:

$$\begin{bmatrix} \boldsymbol{I} & \boldsymbol{0} \\ \boldsymbol{0} & \boldsymbol{M} \end{bmatrix} \begin{bmatrix} \dot{\boldsymbol{q}} \\ \boldsymbol{v} \end{bmatrix} = \begin{bmatrix} \boldsymbol{T} & \boldsymbol{I} \\ \boldsymbol{K} & \boldsymbol{D} \end{bmatrix} \begin{bmatrix} \boldsymbol{q} \\ \boldsymbol{v} \end{bmatrix} + \begin{bmatrix} \boldsymbol{0} \\ \boldsymbol{Y} \end{bmatrix} \delta_{stw} \tag{3.30}$$

in which the first part of the state vector contains the vehicle lateral position and the front and rear roll angles: $\boldsymbol{q} = [Y \quad \psi \quad \varphi_F \quad \varphi_R]^T$. Vehicle velocities, expressed in the moving reference system, are contained in the second part of the state vector $\boldsymbol{v} = [v \quad r \quad p_F \quad p_R]^T$. Steering wheel input δ_{stw} is evaluated as $\delta_{stw} = k_{stw}\delta$ where k_{stw} represents the steering ratio. Mass matrix $\boldsymbol{M}$ is obtained from (3.26) and can be

written as:

$$\boldsymbol{M} = \begin{bmatrix} m & 0 & -m_{sF}d_{sF} & -m_{sR}d_{sR} \\ 0 & J_z & -a\,m_{sF}d_{sF} & b\,m_{sR}d_{sR} \\ -m_{sF}d_{sF} & -a\,m_{sF}d_{sF} & J_{sF}+m_{sF}d_{sF}^2 & 0 \\ -m_{sR}d_{sR} & b\,m_{sR}d_{sR} & 0 & J_{sR}+m_{sR}d_{sR}^2 \end{bmatrix} \tag{3.31}$$

Inertial and geometrical properties have been defined in Section 3.1 and 3.2. Matrix $\boldsymbol{T}$ is derived from Equation (3.29) and helps defining a linearised relationship between velocities expressed in the moving and in the inertial reference frames:

$$\boldsymbol{T} = \begin{bmatrix} 0 & u & 0 & 0 \\ 0 & 0 & 0 & 0 \\ 0 & 0 & 0 & 0 \\ 0 & 0 & 0 & 0 \end{bmatrix} \tag{3.32}$$

where u is the vehicle longitudinal velocity. Matrices $\boldsymbol{K}$ and $\boldsymbol{D}$ are written as:

$$\boldsymbol{K} = \begin{bmatrix} 0 & 0 & \varepsilon_F C_F & \varepsilon_R C_R \\ 0 & 0 & \varepsilon_F C_F a & -\varepsilon_R C_R b \\ 0 & 0 & -k_C - k_F & k_C \\ 0 & 0 & k_C & -k_C - k_R \end{bmatrix} \tag{3.33}$$

$$\boldsymbol{D} = \begin{bmatrix} -\dfrac{C_F + C_R}{u} & -mu - \dfrac{C_F a - C_R b}{u} & 0 & 0 \\ -\dfrac{C_F a - C_R b}{u} & -\dfrac{C_F a^2 + C_R b^2}{u} & 0 & 0 \\ 0 & m_{sF}d_{sF}u & -c_C - c_F & c_C \\ 0 & m_{sR}d_{sR}u & c_C & -c_C - c_R \end{bmatrix} \tag{3.34}$$

Input matrix $\boldsymbol{Y}$ is derived as:

$$\boldsymbol{Y} = \frac{1}{k_{stw}} \begin{bmatrix} C_F \\ aC_F \\ 0 \\ 0 \end{bmatrix} \tag{3.35}$$

From Equation (3.30), continuous-time state space equation for vehicle dynamics is written as:

$$\dot{\boldsymbol{x}}_c = \boldsymbol{A}_c \boldsymbol{x}_c + \boldsymbol{B}_c \delta_{stw} \tag{3.36}$$

with $\boldsymbol{x}_c = [\boldsymbol{q} \quad \boldsymbol{v}]^T$ and

$$\boldsymbol{A}_c = \begin{bmatrix} \boldsymbol{I} & \boldsymbol{0} \\ \boldsymbol{0} & \boldsymbol{M} \end{bmatrix}^{-1} \begin{bmatrix} \boldsymbol{T} & \boldsymbol{I} \\ \boldsymbol{K} & \boldsymbol{C} \end{bmatrix} \qquad \boldsymbol{B}_c = \begin{bmatrix} \boldsymbol{I} & \boldsymbol{0} \\ \boldsymbol{0} & \boldsymbol{M} \end{bmatrix}^{-1} \begin{bmatrix} \boldsymbol{0} \\ \boldsymbol{Y} \end{bmatrix} \tag{3.37}$$

A discrete-time form of the equations of motion is derived from the continuous-time form of Equation (3.36) using a zero-order hold discretisation of the input and a sample time t_s. It is therefore:

$$\boldsymbol{x}_d(k+1) = \boldsymbol{A}_d\boldsymbol{x}_d(k) + \boldsymbol{B}_d\delta_{stw}(k) \tag{3.38}$$

In addition to the linear vehicle model, a shift register that models road dynamics and a low pass-filter are included in the plant, [71]. The shift register represents the process in which road samples ahead of the car are moved, at each iteration, one step nearer to the car. The low-pass filter permits the reduction of the high frequency content of the white-noise that simulates road input disturbance, leading to a more realistic representation.

Filter dynamics, written in the discrete-time state space form, is represented by the equations:

$$\begin{aligned} \boldsymbol{x}_f(k+1) &= \boldsymbol{A}_f\boldsymbol{x}_f(k) + \boldsymbol{B}_f y_{ri}(k) \\ y_f(k) &= \boldsymbol{C}_f\boldsymbol{x}_f(k) + \boldsymbol{D}_f y_{ri}(k) \end{aligned} \tag{3.39}$$

where $\boldsymbol{x}_f$ represents the state vector of the filter, y_{ri} is the road disturbance and matrices $\boldsymbol{A}_f$, $\boldsymbol{B}_f$, $\boldsymbol{C}_f$ and $\boldsymbol{D}_f$ depend on the order and on the type of filter employed.

Given q preview points, the road shift register process is described by the equations:

$$\boldsymbol{y}_r(k+1) = \boldsymbol{A}_r\boldsymbol{y}_r(k) + \boldsymbol{B}_r y_f(k) \tag{3.40}$$

where matrix $\boldsymbol{A}_r$ is a square matrix of order $q+1$ with the q elements of its first upper diagonal equal to one while all the other elements are null. Also vector $\boldsymbol{B}_r$ is formed by null elements, apart from the last one which is unitary.

The time-invariant discrete-time linear optimal regulator problem can therefore be written as:

$$\begin{aligned} \boldsymbol{z}(k+1) &= \boldsymbol{A}\boldsymbol{z}(k) + \boldsymbol{B}\delta_{stw}(k) + \boldsymbol{E}y_{ri}(k) \\ \boldsymbol{y}(k) &= \boldsymbol{C}\boldsymbol{z}(k) \end{aligned} \tag{3.41}$$

where $\boldsymbol{z} = \begin{bmatrix} \boldsymbol{x}_f & \boldsymbol{x}_d & \boldsymbol{y}_r \end{bmatrix}^T$ while:

$$\begin{aligned} \boldsymbol{A} &= \begin{bmatrix} \boldsymbol{A}_f & \boldsymbol{0} & \boldsymbol{0} \\ \boldsymbol{0} & \boldsymbol{A}_d & \boldsymbol{0} \\ \boldsymbol{B}_r\boldsymbol{C}_f & \boldsymbol{0} & \boldsymbol{A}_r \end{bmatrix} & \boldsymbol{B} &= \begin{bmatrix} \boldsymbol{0} \\ \boldsymbol{B}_d \\ \boldsymbol{0} \end{bmatrix} \\ \boldsymbol{E} &= \begin{bmatrix} \boldsymbol{B}_f \\ \boldsymbol{0} \\ \boldsymbol{B}_r\boldsymbol{D}_f \end{bmatrix} & \boldsymbol{C} &= \begin{bmatrix} \boldsymbol{0} & \boldsymbol{C}_d & \boldsymbol{C}_r \end{bmatrix} \end{aligned} \tag{3.42}$$

where matrices $\boldsymbol{A}_f$, $\boldsymbol{A}_d$, $\boldsymbol{A}_r$, $\boldsymbol{B}_r$, $\boldsymbol{C}_f$, $\boldsymbol{B}_d$ and $\boldsymbol{B}_f$ have been defined in Equations (3.38), (3.39) and (3.40). Matrices $\boldsymbol{C}_d$ and $\boldsymbol{C}_r$ define the cost function to be minimised. In this case, only the path-following error is of interest. As a consequence, vector $\boldsymbol{C}_d$ is defined as $\boldsymbol{C}_d = [1\ 0\ 0\ 0\ 0\ 0\ 0\ 0]$ while $\boldsymbol{C}_r = [-1\ 0\ \ldots\ 0]$.

Given the weighting factors $\boldsymbol{Q}$ and $\boldsymbol{R}$ the cost function J is defined as:

$$J = \lim_{n\to\infty} \sum_{k=0}^{n} \left(\boldsymbol{z}(k)^T \boldsymbol{Q}\, \boldsymbol{z}(k) + \boldsymbol{u}(k)^T \boldsymbol{R}\, \boldsymbol{u}(k) \right) \tag{3.43}$$

Given the plant of (3.41) and a disturbance input $y_{ri}(k)$ which is a sample from a white-noise random sequence, the state-feedback time-invariant optimal control that minimises the quadratic cost function of Equation (3.43) is evaluated as:

$$u(k)^* = -\boldsymbol{K}\boldsymbol{z}(k) \tag{3.44}$$

where $\boldsymbol{K} = \left(\boldsymbol{R} + \boldsymbol{B}^T \boldsymbol{P} \boldsymbol{B}\right)^{-1} \boldsymbol{B}^T \boldsymbol{P} \boldsymbol{A}$ and matrix $\boldsymbol{P}$ is obtained from the solution of the matrix-difference-Riccati equation:

$$\boldsymbol{P} = \boldsymbol{A}^T \boldsymbol{P} \boldsymbol{A} - \boldsymbol{A}^T \boldsymbol{P} \boldsymbol{B} \left(\boldsymbol{R} + \boldsymbol{B}^T \boldsymbol{P} \boldsymbol{B}\right)^{-1} \boldsymbol{B}^T \boldsymbol{P} \boldsymbol{A} + \boldsymbol{C}^T \boldsymbol{Q} \boldsymbol{C} \tag{3.45}$$

Optimal controls are calculated using data reported in Appendix A. Results are obtained by using a fourth-order low-pass Butterworth filter with a cut-off frequency of 2 Hz while discretisation is carried out with a time step Δt of 0.01 s. Because of adopted definition of the cost function, weighting factors $\boldsymbol{Q}$ and $\boldsymbol{R}$ are scalars. Values of $Q = 1000$ and $R = 1$ are chosen in order to guarantee sufficient control tightness on the tracking accuracy. Trials have shown that a complete preview is obtained over a vast range of configurations using $q = 200$ preview points.

Vector $\boldsymbol{K}$ obtained from the solution of the optimal preview problem contains the gains relative to the filter states, named $\boldsymbol{K}_f$, to the car states, named $\boldsymbol{K}_d$ and the preview gains $\boldsymbol{K}_p$.

Low-pass filter gains vanish when complete preview is considered, [71]. Car state feedback relative to lateral position and yaw angle disappear when the problem is transformed into a moving reference frame fixed with the vehicle. Also, lateral velocity, yaw rate, roll angle and roll rate gains are not analysed here.

Figures 3.11a and 3.11b report plots of the obtained time-invariant preview gains $\boldsymbol{K}_p$ respectively at 40 and 100 km/h for the rigid and the flexible vehicle. A small difference between the two curves can be noticed in the first case; a more substantial one is present in the second case. High-speed travelling and chassis compliance therefore imply a more oscillatory gain sequence and therefore a different, if not a more demanding, driving technique.

Plots of Figures 3.11c and 3.11d report values of high and low speed preview distances required for full control of the car versus normalised chassis torsional stiffness. In accordance with [71], the preview distance L_p is defined as the minimum distance ahead of the car for which 98 per cent of the area subtended by the curve of the preview gains is contained. It is therefore $L_p = n\, u\, \Delta t$ with:

$$n = \min \left(\sum_{i=1}^{n} |\boldsymbol{K}_{p,i}| > 0.98 \sum_{i=1}^{q} |\boldsymbol{K}_{p,i}| \right) \tag{3.46}$$

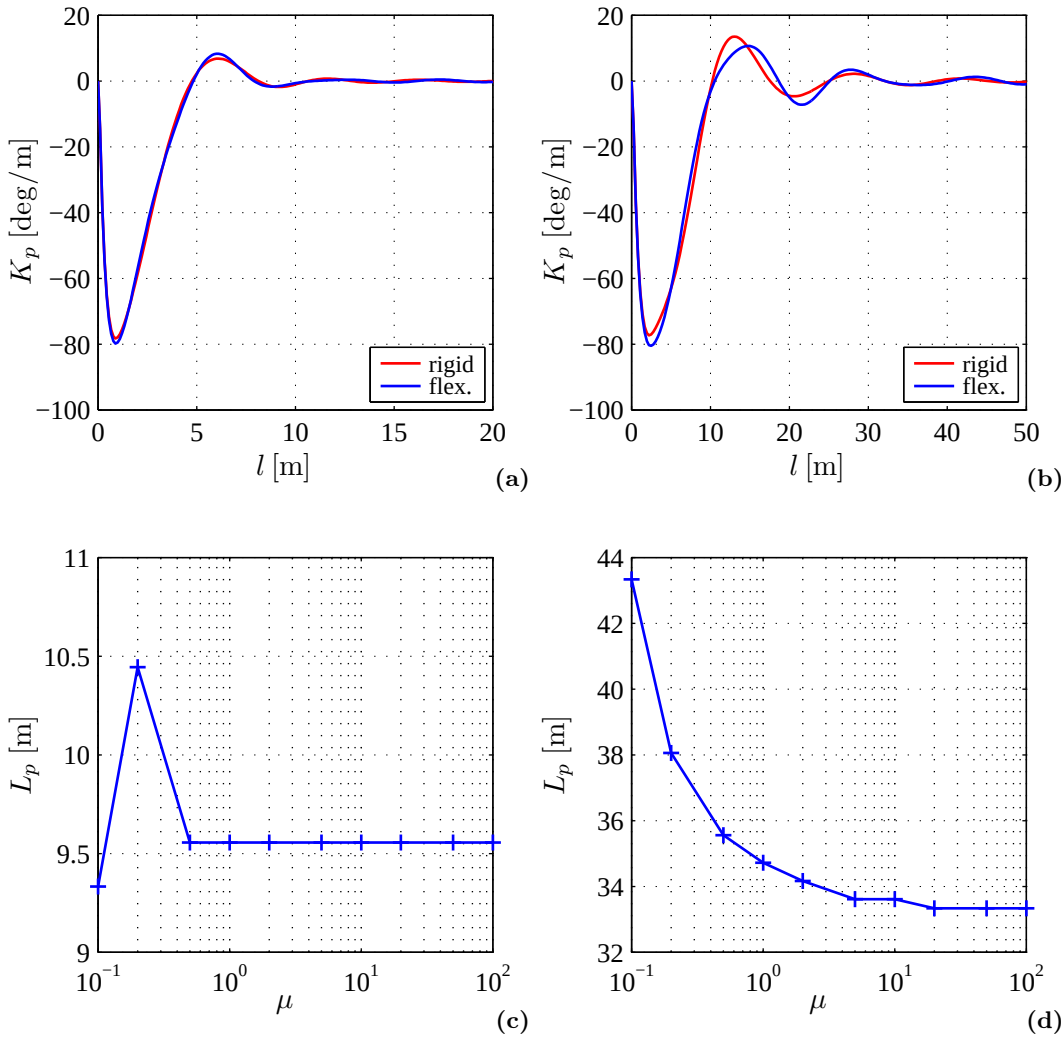

Figure 3.11: Effect of chassis torsional stiffness on TI-optimal preview gains. (a) Comparison between TI-optimal preview gains in the rigid and flexible chassis cases at 40 km/h. (b) Comparison between TI-optimal preview gains in the rigid and flexible chassis cases at 100km/h. (c) Effect of chassis torsional stiffness on preview distance at 40 km/h. (d) Effect of chassis torsional stiffness on preview distance at 100 km/h.

Results show that preview distance is scarcely affected by torsional stiffness at low speed, see Figure 3.11c. When the vehicle is travelling at high speed instead, in presence of chassis compliance, longer preview distance is required, see Figure 3.11d. Chassis torsional compliance causes a substantial increment of the preview distance, with an increment up to 30 % for extremely low values of chassis torsional stiffness.

In presence of chassis compliance, not only a different driving technique is required, but also a greater preview distance is needed for high-speed. As the curve

of Figure 3.11d is asymptotically convergent to its minimum value, given the vehicle maximum speed, it is possible to define the minimum value of chassis torsional stiffness for which the preview length lies within a desired threshold, for example 2 % of its asymptotic value. For the considered vehicle, it is $\mu \approx 8$.

3.4 Concluding remarks

A preliminary analysis of the effects of chassis compliance on vehicle behaviour has been introduced in the present chapter.

A simplified model for the analysis of the influence of the chassis stiffness on lateral load transfer distribution has been introduced. Results confirm that chassis torsional flexibility plays an important role in the repartition of lateral load transfer between the two axles. As a consequence, its knowledge is required for a precise estimate of loads acting on the tyres. Effects of chassis deformation on suspension geometry have been analysed through a detailed modelling of roll steer mechanism in presence of chassis compliance.

A four-degrees-of-freedom non-linear vehicle model that includes the previously analysed effects has been introduced in the second part of the chapter. Steady-state simulations have shown that, while chassis compliance mainly affects the linear region of the vehicle characteristics through the roll steer mechanism, the limit behaviour is mainly controlled through the effect on lateral load transfer distribution. Furthermore, the model is capable of highlighting the complications encountered during the set-up of a vehicle with unknown chassis compliance. The analysis of the transitory behaviour of the vehicle has revealed that simulation models with rigid chassis tend to overestimate the dynamic performance of the vehicle.

A linear version of the developed model has then been introduced in order to analyse the root locus and the frequency response of the vehicle. The former has shown that the damping of the chassis torsional oscillations is generally lower than the damping associated with the roll motion of the vehicle and, more significantly, that a decay of the damping at high speed occurs. The analysis has shown that effects of chassis compliance can be found in the frequency response of the vehicle even though chassis natural frequency is well beyond the frequency of the input the driver is capable of.

Finally, a linear version of the four-degrees-of-freedom model has been introduced within an existing framework that permits the evaluation of optimal controls for path-tracking. Results have shown that the optimal driver is capable of adapting its driving technique to a vehicle with a flexible chassis. Furthermore, it has been shown that chassis compliance implies the need of a longer preview distance for high-speed tracking accuracy.

The preliminary results obtained confirm the importance of a thorough investigation

on the effects of chassis flexibility on vehicle dynamics. The analysis has shown that the use of simplified analytical models is of great advantage in the definition of the research and that design criteria can be deduced from each of the analysed aspects.

Limitations inherent to the adopted modelling approach are however also apparent. For example, a detailed description of the suspension kinematics is not included. Also, while only one deformation is considered, it seems extremely complicated to further develop the model so that other compliances are included. Furthermore, mass and stiffness distribution are represented in a very idealised manner that might not be sufficiently realistic. For these reasons, a more detailed model which overcomes these limitations is necessary. As the literature suggests, this can be obtained by means of a more advanced multibody model.

Chapter 4

Multibody dynamics

The present chapter offers a review of the multibody formulations and techniques available in the literature. Various aspects of multibody dynamics, in particular the techniques that permit the development of efficient models, are reviewed. Conclusions and recommendations for the development of a multibody vehicle model are included.

4.1 Overview

Multibody dynamics represents an efficient tool for the simulation of the linear and non-linear dynamic behaviour of complex mechanical systems. Multibody systems can be regarded as a virtual test bench for mathematical representations of real systems. The consequent analysis permits the evaluation of the performance of the entire system, or of its major components, often long before the first prototype of the system is ready for field tests.

The origin of multibody systems can be found in the classical mechanical problem of translational and rotational motion of rigid bodies. Apart from a limited use for the analysis of industrial mechanisms in the 19^{th} and early 20^{th} centuries however, the potential of the works from d'Alembert, Euler and Lagrange remained long unexploited. The need of tools for the analysis of dynamic systems, e.g. high speed mechanisms and spacecraft, promoted the development of more complex analysis tools. A major role in this area has also been played by the development of more efficient and cost-effective computational systems.

Starting from 1977, when the first symposium on multibody dynamics was held in Munich, a vast literature on this subject has been developed. In the same year, the first textbook dedicated to multibody dynamics was published by Wittenburg, [74]. Texts from Nikravesh, [75], Haug, [76], Schiehlen, [77], Von Schwerin, [78], Schwertassek and Wallrapp, [79], Huston, [80], Shabana, [81–83] and García de Jalón and Bayo, [84], followed. A review of the roots, of the state-of-the-art and of the perspectives of

multibody dynamics can be found in [85].

In 1985 Kortüm and Schiehlen, [86], presented a paper in which they illustrated the desirable qualities of a multibody program and, after analysing two contemporary examples of codes, employed them to generate basic vehicle models. The first program discussed was Neweul, a code capable of generating the equations of motion in symbolic form and of using both Cartesian and generalised coordinates, non-holonomic constraints and moving reference frames. The second program, based on numeric formalism, was Medyna.

The development of some of the most widely used multibody codes like ADAMS and DADS (now LMS Virtual.Lab) began in the early 1970s, many others followed. Modern general-purpose multibody codes are characterised by a wide variety of capabilities, including the possibility of using non-inertial reference frames, to incorporate flexible elements, to utilise generalised coordinates and to symbolically generate the equations of motion.

Since the beginning of their development, multibody codes have been employed to generate vehicle models. The capabilities of 27 currently available multibody and vehicle simulation codes were presented and reviewed in [87]. A comparison of the capabilities of the various codes was provided. The desirable traits of a multibody code were described and a brief discussion of the contemporary numerical methods applicable to vehicle dynamics simulation was given. A benchmark analysis was also carried out. The programs discussed include Compamm, FaSim, Adams, AutoSim, Medyna, Neweul, Simpack, DADS and others. Many of the reviewed codes were general-purpose, numeric codes. Still nowadays, most of these codes are focused on the development of the final product and offer the possibility of modelling several details using a large number of degrees of freedom. They are often integrated with complex CAD packages and FEM codes and they embed models for important subsystems (e.g. tires, sensors and others).

In 1994 Sharp, [3], focused on the comparison between the capabilities of the major multibody codes with emphasis on those which generate the equations of motion symbolically. The codes reviewed were selected on the basis of their applicability to automotive simulation. The methods used by each code in deriving the equations of motion with attention to the limitations of each method were discussed. Some guidelines for the development of highly efficient code were given: the employment of moving reference axes, the omission of insignificant detail, the efficient treatment of the constraints and of small quantities and the optimisation of the repeated calculations. The limitations of each code with respect to the types of constraint equations that could be handled were also discussed. A substantial reference list was also given. A similar paper was published by the same author in 1998, [88].

Some of the general purpose packages now include particular tools that ease the study of vehicles. For example, Adams/Car constitutes a template-based simulation

tool that helps the user to speed-up and simplify the vehicle modelling process. AutoSim (now VehicleSim) constitutes an interesting example of multi-purpose symbolic multibody code. Differently from the numeric multibody codes, it does not solve the equations, but it creates a set of optimised routines that can be solved by means of a generic solver. A brief review of the state of art of multibody modelling is presented in the next sections.

4.2 Fundamentals of multibody simulation

A multibody system can be defined as an assembly of interconnected rigid or flexible bodies which can move relative to one another when forces are applied, [82].

A rigid body is defined by its reference frame, its mass and its inertia tensor. Additional frames, known as markers, are usually employed to help define attachment points of joints, of acting points or of external forces. The definition of flexible bodies implies the use of an additional set of degrees of freedom for modelling the deformation of the body. This is generally done under the assumption of small, elastic and reversible deformations that derive from linear superposition of pre-calculated modal shapes.

Interconnections between bodies are generally defined by joints. While they are usually assumed as ideal, backlash-free and weightless, more advanced models are available. Force elements define forces and torques that are applied to the bodies. Forces can be generated by internal elements, e.g. springs, actuators, shock absorbers or by external entities as the gravitation field or interaction with fluids.

Starting from bodies, joints and force elements properties defined by the user, multibody tools are capable of generating the equations of motion of the system. Equations are usually non-linear and in the form of a system of differential algebraic equations (DAE). A variety of solvers is available to generate solutions numerically.

4.3 System coordinates

4.3.1 Introduction

The location and the orientation of the bodies of a multibody system are described by means of a set of variables called generalised coordinates. These coordinates may or may not form a set of independent variables. If they do, the system is said to be represented in a minimal form and the coordinates are independent; if some of the coordinates are dependent on others the system is said to be described by means of a descriptor form, [78].

According to the dependent coordinates technique, the configuration of the system is identified by using a set of Cartesian coordinates that describe the locations and orientations of the bodies, resulting in six or more coordinates for each body to account

for the six degrees of freedom of rigid body motion. The connections between bodies are introduced by an additional set of algebraic constraint equations, thus forming a set of DAEs.

The minimal coordinates technique automatically accounts for the reduction of the degrees of freedom by describing the location and orientation of a body in reference to the neighbouring body which has a lower level in the kinematic topology of the system. Thus, only the actual degrees of freedom of the connecting joint, and consequently of the body in question, are added to the system.

The description of a system by means of the dependent coordinates form has many advantages. It is intuitive and transparent, but it also treats the constraints in a way that eases an automatic handling and the evaluation of the reaction forces. Furthermore, depending on the coordinates used, it allows the use of sparse matrix techniques so that a good efficiency can be achieved.

On the other hand, the differential equations of motion obtained need to be augmented by a set of algebraic constraint equations; the consequent equations form a differential algebraic equation (DAE). The solution of this kind of differential equations requires particular solvers and it is often characterised by low stability and low efficiency. The obtained DAE is therefore usually transformed into a lower index DAE or into an ordinary differential equation (ODE) by means of index or coordinate reduction methods.

The minimal coordinates formulation avoids the use of DAEs and generates a smaller set of equations. This advantage is however at least partially impaired by the comparatively increased complexity of the equations of motion and more complex generation of the Jacobian matrix. Furthermore, the computation of constraint forces is generally not possible and closed loop topologies give origin to numerical singularities. As a consequence, the direct building of a minimal model is not recommended even for very simple mechanical systems, [78].

Available types of dependent and independent coordinates are represented in Figure 4.1 and described in the following sections.

4.3.2 Reference point coordinates

Reference point coordinates provide a description of the position of a body by means of the Cartesian coordinates of one of its points and of the angular orientation of a reference frame rigidly fixed on the body. The description of the body location is usually carried out with respect to an inertial reference frame and the centre of mass is employed as the reference point, see Figure 4.1a. By definition, reference point coordinates generate a set of dependent coordinates.

The position of a single body is described by means of at least six parameters: three for the position of the centre of gravity and three for the angular orientation. A

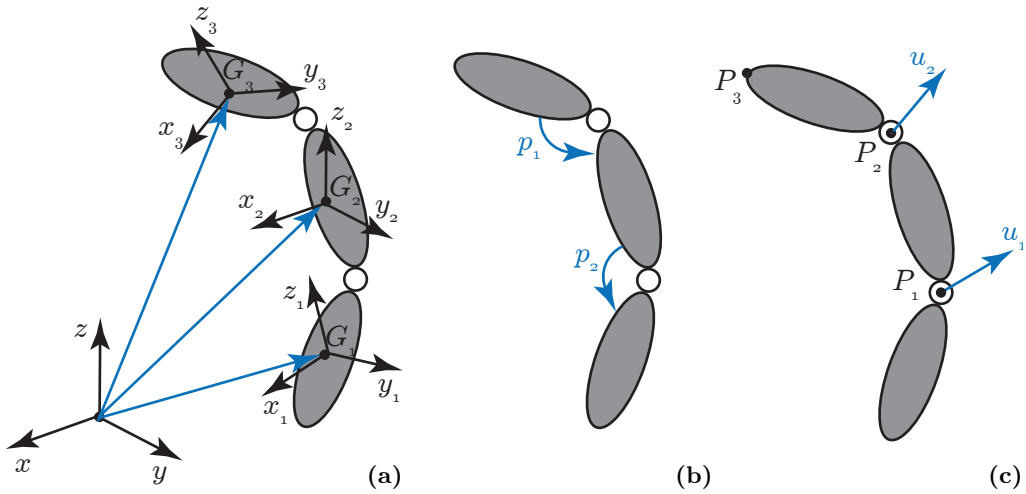

Figure 4.1: Types of available coordinate systems for multibody systems. (a) Reference point coordinates. (b) Relative coordinate. (c) Natural coordinates.

set of three rotation parameters by itself is not capable of unequivocally representing the orientation of the moving frame at any possible position but additional information about the rotation axis corresponding to the rotation angles is required. The most common parameter sets are the Euler angles. Several different sets of Euler angles are used in the analysis of mechanical and aerospace systems. They all involve three successive rotations about three axes that are not, in general, perpendicular.

An important aspect is related to the uniqueness of the representation of the position of the body. It can be shown that a reference point system based on three angular parameters is not capable of uniquely defining the position of the body when particular configurations are found. As a solution, alternative sets of angles can be defined when singular positions are detected or four angular parameters can be used instead of three. Many of the codes developed adopt this latter solution and use a set of four parameters known as Euler parameters. The main properties of Euler parameters can be found in [74], [75] and [76]. It is worth noting that the use of Euler parameters directly implies the presence of algebraic relationships between the body coordinates.

Because of their simplicity and their direct link to the equations to Newton-Euler, Jordan, Hamilton or Lagrange equations, reference point coordinates are the most widely used. Furthermore, they permit the direct evaluation of the position of each body during the solution of the equations of motion; hence no particular pre- or post-processing routines are required.

Another important characteristic of reference point coordinates is that the definition of a single joint only involves the coordinates of the bodies which the joint connects.

As a consequence, constraint equations can be established at a local level and the automatic generation of the equations of motion for an arbitrarily complex model is straightforward.

The main disadvantages of reference point coordinates are that the number of required parameters is quite large (six for each body) and that they do not exploit the topology of the system. This disadvantage can however be partially compensated by exploiting the particular structure present in the dynamic formulation, [84].

4.3.3 Relative coordinates

Relative coordinates define the position of each body in relation to the previous one in the kinematic tree by using the coordinates corresponding to the relative degrees of freedom allowed by the joint linking the two bodies. An example of relative coordinates is shown in Figure 4.1b. As a consequence, relative coordinates build up a system with a minimum number of coordinates and their number is equal to the number of degrees of freedom; no constraint equations are therefore required. Robotics is a specific field in which relative coordinates are particularly advantageous and effective, [89]. In other cases however, for example when closed-loop systems are involved, the computational effort required by this technique is often prohibitive.

According to García de Jalón et al., [84], the main advantages of this approach are the reduced number of coordinates, the efficiency for open-loop configurations and the fact that, due to the presence of a strict correlation between the coordinates and the degrees of freedom of the joints, it is possible to directly control the motion of the joints involved. It is worth noting that relative coordinates usually require a pre-processing routine and that, if one is interested in the absolute position of the bodies, some post-processing analysis of the results of the simulation is required.

4.3.4 Natural coordinates

Natural coordinates were introduced by Serna et al. in 1982 for planar cases, [90], and by García de Jalón and Bayo in 1986 for spatial systems, [84]. For planar systems they can be seen as an evolution of reference point coordinates in which the reference points have been moved to the joint. In this case, natural coordinates are made up of the Cartesian coordinates of the basic points, see Figure 4.1c. For three-dimensional systems, the Cartesian coordinates of the basic points are augmented with a set of unit vectors related to the joints of the system. A detailed analysis of the methodology can be found in [84].

The number of parameters necessary to describe a system using natural coordinates tends to be an average between the number of relative coordinates and the number of reference point coordinates. This is due to the fact that no angular coordinates are necessary and that joint vectors are required. These coordinates have the advantage,

compared to reference point ones, that they introduce a formulation in which the mass matrix is constant so that no Coriolis or centrifugal forces appear in the equations of motion. Furthermore, they lead to a constraint Jacobian matrix which reduces the computational burden associated with constraint equations. Natural coordinates have the disadvantage that they do not directly reflect their associated degrees of freedom and that, as for relative coordinates, pre-processing and post-processing routines are necessary.

4.3.5 Mixed coordinates

Mixed coordinates are obtained by adding to natural or reference point coordinates other variables corresponding to the degrees of freedom of the system. If relative coordinates are considered, it is clear that they offer the possibility of directly accounting for the relative degree of freedom of the joints and that no other system can offer this advantage. Mixed coordinates try to combine the advantages of natural or reference point coordinates with this characteristic of relative coordinates, [84].

4.4 System constraints

Joints are represented by a set of constraint equations. These are algebraic equations that have to be satisfied by the system. Each joint is described by a certain number of constraint equations, depending on the number of degrees of freedom removed and on the coordinates used. For example, three degrees of freedom are removed by each spherical joint. It is possible to define several kinds of joints, the spherical, revolute, prismatic, cylindrical, universal, rigid ones being the most diffused ones. For a detailed and exhaustive description, see the texts of Shabana, [82] and García de Jalón et al., [84].

Constraint equations of a generic multibody system can be expressed as:

$$\boldsymbol{\Phi} = \begin{bmatrix} \Phi_1 & \dots \Phi_i & \dots & \Phi_m \end{bmatrix}^T = 0 \tag{4.1}$$

where Φ_i represents the i-th constraint equation; m is the number of constraint equations introduced. Given a system described by a set of generalised coordinates $\boldsymbol{q}$, constraint equations are classified on the basis of the variables included in their definitions:

- holonomic constraints: the constraint equations involve relationships between displacements. If they merely depend on the position vector $\boldsymbol{q}$ they are said to be scleronomic:

$$\boldsymbol{\Phi}(\boldsymbol{q}) = \boldsymbol{0} \tag{4.2}$$

if instead they also depend explicitly the time variable t, they are said to be rheonomic:

$$\boldsymbol{\Phi}(\boldsymbol{q}, t) = \mathbf{0} \tag{4.3}$$

- non-holonomic constraints: the constraint equations involve non integrable relationships between velocities:

$$\boldsymbol{\Phi}(\boldsymbol{q}, \dot{\boldsymbol{q}}, t) = \mathbf{0} \tag{4.4}$$

In order to be defined as non-holonomic, constraint equations must not be transformable into holonomic ones by integration.

An important role in the equations of motion is played by the Jacobian of the constraint equations with respect to the generalised coordinates $\boldsymbol{q}$, named $\boldsymbol{\Phi}_{\boldsymbol{q}}$. For a system described by n generalised coordinates and m constraint equations, it is an $m \times n$ matrix. The rank of $\boldsymbol{\Phi}_{\boldsymbol{q}}$ represents the number of degrees of freedom removed by the constraints; therefore it determines the number of degrees of freedom of the system. If the rank of $\boldsymbol{\Phi}_{\boldsymbol{q}}$ is r, the number of degrees of freedom of the system is given by the equation, sometimes called the Kutzbach criterion, [82]:

$$d.o.f = n - r \tag{4.5}$$

If the rank of $\boldsymbol{\Phi}_{\boldsymbol{q}}$ is maximum, $r = m$ and therefore the number of degrees of freedom is equal to $n - m$. When two rows of matrix $\boldsymbol{\Phi}_{\boldsymbol{q}}$ are not independent, the corresponding constraints work on the same degree of freedom with the consequence that it is impossible to define the force applied by each of them, but only their sum. It is therefore good practice to build the model in such a way that the rank of $\boldsymbol{\Phi}_{\boldsymbol{q}}$ is always maximum.

4.5 Equations of motion

Equations of motion of multibody systems are written in a form that depends on the type of coordinates adopted. If a set of dependent reference point coordinates is used, equations of motion can be derived from principles of classical mechanics through the use of Lagrange's equation, virtual work, virtual power principle or Hamilton's equations. Further details can be found in [78, 84]. Also, they can be written in a fixed or in a moving reference frame.

According to this approach, each body is assigned at least six degrees of freedom. The connections between bodies are introduced by a set of non-linear algebraic constraint equations, which are usually adjoined to the system equations by a set Lagrangian multipliers. All the methods lead to a form of the equations of motion

known as descriptor form that can be expressed, in the most general form as:

$$\begin{cases} \boldsymbol{M}(\boldsymbol{q})\ddot{\boldsymbol{q}} + \boldsymbol{\Phi}_{\boldsymbol{q}}(\boldsymbol{q})^T\boldsymbol{\lambda} = \boldsymbol{Q}(\boldsymbol{q}, \dot{\boldsymbol{q}}, t) \\ \boldsymbol{\Phi}(\boldsymbol{q}, t) = \boldsymbol{0} \end{cases} \tag{4.6}$$

where $\boldsymbol{q}$ is the vector of generalised coordinates, $\boldsymbol{M}$ represents the inertial matrix of the system, $\boldsymbol{\lambda}$ is the vector of Lagrange multipliers while vector $\boldsymbol{Q}$ represents the external and the internal forces of the system. Equation (4.6), which is generally valid for both rigid and flexible multibody systems, forms a set of differential algebraic equation of index three.

When relative coordinates are employed, a minimal formulation that eliminates the constraints from the equations of motion is directly obtained. Equations are written as a set of ODEs. Despite the apparent advantage, however, the direct generation of equations of motion in a minimal form is complex and inefficient, especially for systems with closed loops. Furthermore, a separate formulation for the evaluation of the constraint forces is required. A more convenient approach involves the development of the equations of motion by using dependent coordinates and the numerical generation of a minimal form, see Section 4.8.

4.6 Deformable bodies

4.6.1 Overview

Deformable bodies that undergo rigid body motion and elastic deformation can be included into the existing framework through the introduction of flexible multibody dynamics. In the 1970s, development of new light materials and the demand of higher operating speeds in the automotive, aerospace and precision machinery fields, required the development of more accurate methods for modelling the deformation of components.

Techniques were developed that permitted the use of the latest developments in rigid body dynamics and to add to the rigid body methodologies the capability of treating flexible bodies. On the other hand, finite element methods had emerged in the 1960s as a powerful tool for the analysis of deformable bodies. From this, procedures were developed that enabled the inclusion of large body displacements, including rigid body ones. Most of these methods are based on an incremental formulation; others however have been recently proposed, [83]. A thorough review on the implementation of elastic bodies into multibody systems can be found in [79, 82, 85, 91, 92]; only the most important concepts are here reported.

As far as concern the inclusion of flexible bodies in vehicle dynamics, many of the examples found in literature are related to design problems. Non-linear finite element models are commonly employed for crashworthiness studies while linear models are

employed for vehicle dynamics or ride studies. Among others, the previously discussed paper of Ambrósio and Gonçalves, [59], is of particular interest.

4.6.2 Floating frame of reference formulation

The floating frame of reference formulation implies that the configuration of a deformable body can be expressed by means of a set of reference and elastic coordinates. While reference coordinates define the location and the orientation of a selected body reference frame, the elastic ones describe the deformation field with respect to the local frame, [74].

Reference and elastic coordinates permit the evaluation of the global position of any arbitrary point on the body. From this, equations for evaluation of the kinetic energy of the deformable body, as well as the coupling inertia terms, can be derived.

The original set of partial differential equations representing the dynamics of the deformable body is generally converted into a set of ordinary differential equations through the use of Bernoulli's principle of separation of variables. According to this principle, the state- and time-dependant displacement field of the deformable body can be described by a set of state-dependent base functions and of time-dependent elastic coordinates. The deformation field is therefore represented in terms of an infinite series where some components, called coordinates, are time-dependent while other components, called base functions, are state-dependent, [93]. The infinite series obtained are capable of describing the exact configuration of the deformable body; a finite number of coordinates is however required for any numerical implementation. Approximations like the finite element method or the modal method were therefore developed, [93].

Finite element representation

The most popular approach for the description of flexibility of multibody systems is the inclusion of a finite element model. This method was first proposed by Song and Haug, [94] and later developed by Shabana and others, [49, 82, 83]. According to this approach, the position and the orientation of each finite element is described through the use of a local reference frame attached to the finite element itself. A set of independent coordinates describing the location of the local reference frames is then introduced.

This formulation involves the use of a large number of elastic degrees of freedom; as a consequence it is inadequate for applications in which a good computational efficiency is required. Furthermore, it is not capable of exactly describing any rigid motion of the body and, in case of lumped masses, it leads to a non-diagonal mass matrix that further reduces the computational efficiency, [82].

Modal representation

Modal representation is based on Rayleigh-Ritz approximation. According to this approach, local deformations are approximated by a linear combination of a finite number of known assumed functions, known as modal shapes, and of time-dependant elastic coordinates. With the introduction of base functions, the equations of motion of the deformable body contain state-independent volume integrals which are responsible for the coupling between rigid body motion and elastic deformation. These integrals are usually computed prior to integration of the equations of motion.

The quality of the results obtained through modal representation strongly depends upon the quality of the base functions, [95]. The choice of the shape functions however is tied with the definition of the body reference frame. A very common choice, known as the tangent frame formulation, implies that a zero deformation is assigned to a single point of the body. The centre of gravity is often used. Other approaches have been developed, see for example the Buckens-, Gylden-, Tisserand-frames, [82, 93, 95].

Base functions are generally derived from a complete finite element model of the deformable body by means of reduction techniques. The problem of modal basis optimisation has been widely discussed in the literature, [95]. Among other methods, Guyan reduction, dynamic reduction, Component Mode Synthesis and the SEREP methods are the most widely used, [96].

Most of the reduction methods belong to a class of reduction methods based on the theory of master and slave degrees of freedom. During modal reduction the master degrees of freedom, also called external or interface degrees of freedom are preserved; no loss of resolution when higher order modes are truncated is present. All the non-master degrees of freedom, known as slave or internal degrees of freedom are more or less well described by the modal basis depending on the number of truncated higher modes. The choice of the master nodes is not straightforward; while this is usually done on the basis of the engineer's experience, analytical criteria have also been recently developed. When multibody systems are considered, the connection nodes between the deformable body and the complete model are usually selected as master nodes, [96].

Of particular interest is the Component Mode Synthesis method, also known as Craig-Bampton method, [97]. According to this method, the modal basis is formed by a set of constraint modes and of substructure normal-mode modes. The first ones are static shapes obtained by giving each boundary degree of freedom a unit displacement while holding all other boundary degrees of freedom fixed. The basis of constraint modes completely spans all possible motions of the boundary DOFs, with a one-to-one correspondence between the modal coordinates of the constraint modes and the displacement in the corresponding boundary degrees of freedom. Normal modes are instead related to free vibration of the body and define the modal expansion of the

interior degrees of freedom. While the number of constraint modes depends on the number of boundary nodes, the number of fixed-boundary normal modes is defined by the user. One of the drawbacks of the method is that its effectiveness is highly dependent on the set of master nodes and on the number of internal modes retained, [95].

The evaluation of the quality of the reduction method implies the introduction of comparison criteria, generally known as Modal Correlation Criteria. The relative error between the natural frequencies of the original and of the reduced model (NRDF), the normalised correlation between the modal shapes (MAC and modMAC), and the differences between mass- or stiffness-normalised eigenvectors (MNVD and SNVD) are generally employed, [96].

Although modal reduction is often used to model component flexibility within vehicle dynamics studies, a comparison between the available techniques cannot be found in the literature. This is mainly due to the fact that commercial finite element codes usually offer routines that only implement one or another of the available methods for modal extraction. The finite element code Ansys for example includes a module capable of creating proprietary formatted files that can be imported into the commercial multibody code Adams.

4.6.3 Absolute nodal coordinate formulation

More recently, the absolute nodal coordinate has been developed by Shabana et al., [83]. According to this approach, nodal coordinates are formed by absolute slopes and displacements of the nodal points. Compared to the finite element formulation employed within the floating frame of reference, this technique allows an exact description of rigid body motion. Further details on this formulation can be found in [82].

Because of these characteristics, the absolute nodal coordinate formulation is suitable for large deformation problems. On the other hand, the high number of degrees of freedom introduced makes it unsuitable for efficient vehicle dynamics simulations.

4.7 Recursive algorithms

Within the context of multibody dynamics, a recursive formulation is a procedure in which elementary relationships between an arbitrary pair of contiguous bodies as part of a system of bodies can be re-used all along the system, [82]. As discussed, relative or natural coordinates are generally available for the description of multibody systems. As relative coordinates describe the motion of a body relative to an adjacent one, they make a recursive formulation possible.

The formulation, first introduced by Haug, [98, 99], exploits the topology of systems

with a tree-like structure for the definition of computational recursive sequences. Using a variational form of the equations of dynamics, inertia and right-hand side terms of the equations of motions are reduced from outboard body centroidal reference frames to an inboard body centroidal reference frame.

Relative coordinate formulation of open-chain systems avoids constraint equations. In this case, several fully recursive formulations that are capable of solving the direct and inverse dynamic problem in an efficient manner exist. It has been shown that these methods are the most efficient when chains have a large number of bodies, [98]. In case of closed-loop systems, relative coordinates cannot be independent and semi-recursive formulations are therefore employed. According to this approach, one of the joints of the loop is cut and the dynamic analysis is carried out by applying additional constraints.

Some formulations have been developed that permit to employ reference point Cartesian coordinates to formulate the dynamic equations of the bodies; a velocity transformation is then applied at a latter stage. As a result, the number of differential equations is reduced and equations of motion are written in terms of relative joint variables, [82, 89].

Recursive formulations are of great advantage when chain-like topologies are present. Furthermore, they permit the development of subsystem synthesis techniques. In [100] for example, a technique was proposed that permitted the development of effective models of subsystems for vehicle dynamic analysis. This method is based on the characteristics that relative motion of an independent system, e.g. a suspension system, only depends on the relative coordinates associated with the subsystem itself. As a consequence, a subsystem model can be analysed and synthesised before it is introduced into a more complex vehicle model. A similar technique is presented in [101]. In this case, suspension systems are analysed through the use of a macro joint approach which is substantially equivalent to the mentioned subsystem synthesis techniques. The paper also proposes several simplification steps and analyses their effects on simulation accuracy. Results showed that the technique is suitable for real time simulation.

Despite the need for a more complex modelling of the joints involved, recursive formulation are also suitable for flexible multibody systems, see for example [102, 103].

4.8 Reduction techniques

Differential algebraic equations of index three naturally arise from the coupling of equations of motion and constraint equations. A DAE is said to be of differentiation index equal to n if n is the number of analytical differentiations necessary to transform it into an explicit ordinary differential system, known as underlying ODE, [104]. The index of a DAE can also be interpreted as a perturbation index which is a measure

of the sensitivity of the solution to perturbations applied to the numerical problem. In case of the problem expressed by Equation (4.6), both differentiation index and perturbation index are equal to three. As a consequence, the numerical solution of the problem of Equation (4.6) is affected by the second derivative of any perturbation introduced in its solution, [104]. As any numerical scheme introduces small errors in the solution, both index three and index two formulations are ill-posed and generally unsuitable for direct integration.

Techniques have been developed which avoid the solution of index three DAEs. Generally speaking, they consist of index or coordinate reduction techniques. Index reduction techniques permit the transformation of the original index three DAE into a new low index DAE or an ODE which contains the same coordinates as the original problem; coordinate reduction techniques instead transform the original problem into an ODE which contains a smaller set of independent coordinates. An extensive review of the available techniques can be found in [105] and [106] they are however here briefly explained.

4.8.1 Index reduction techniques

Index reduction can be obtained through differentiation with respect to time of the constraint equation of Equation (4.3). A first differentiation leads to a DAE of index two that can be solved by using specialised solvers, as for example half-explicit methods or the GGL-formulation, [107].

Because of the related numerical problems, it is however generally preferable to further differentiate the constraint equations with time so that a DAE of index one, substantially equivalent to an ODE, can be obtained. Equations of motion are generally obtained in a matrix form:

$$\begin{bmatrix} \boldsymbol{M} & \boldsymbol{\Phi}_{\boldsymbol{q}}^{T} \\ \boldsymbol{\Phi}_{\boldsymbol{q}} & \boldsymbol{0} \end{bmatrix} \begin{bmatrix} \ddot{\boldsymbol{q}} \\ \boldsymbol{\lambda} \end{bmatrix} = \begin{bmatrix} \boldsymbol{Q} \\ \boldsymbol{c} \end{bmatrix} \tag{4.7}$$

in which $\boldsymbol{Q} = \boldsymbol{Q_e} + \boldsymbol{Q_i}$ and $\boldsymbol{c} = -\dot{\boldsymbol{\Phi}}_q \dot{\boldsymbol{q}} - \dot{\boldsymbol{\Phi}}_t$.

The index two DAE is mathematically equivalent to Equation (4.6). During their numerical integration however, it is not possible to guarantee that the constraint equations are satisfied. This problem, known as drift-off phenomenon, is present in every index reduction method that does not involve a stabilisation technique. Furthermore, consistent initial values at the position and velocity levels are required. Techniques capable of stabilising or eliminating the drift-off error have been developed.

Among the constraint violation stabilisation techniques, index one formulation is usually preferred and the Baumgarte approach, [108], is commonly employed. The basic idea is that an artificial feedback in the constraint equations can be provided if, instead of the second derivative of the constraint equations, the following equation is

used:

$$\ddot{\mathbf{\Phi}} + 2\alpha\dot{\mathbf{\Phi}} + \beta^2\mathbf{\Phi} = \mathbf{0} \tag{4.8}$$

where the parameters α and β have to be chosen properly. As a consequence, equation (4.7) becomes:

$$\begin{bmatrix} \boldsymbol{M} & \boldsymbol{\Phi}_{\boldsymbol{q}}^T \\ \boldsymbol{\Phi}_{\boldsymbol{q}} & \mathbf{0} \end{bmatrix} \begin{bmatrix} \ddot{\boldsymbol{q}} \\ \boldsymbol{\lambda} \end{bmatrix} = \begin{bmatrix} \boldsymbol{Q} \\ \boldsymbol{d} \end{bmatrix} \tag{4.9}$$

with $\boldsymbol{d} = -\dot{\boldsymbol{\Phi}}_q\dot{\boldsymbol{q}} - \dot{\boldsymbol{\Phi}}_t - 2\alpha\left(\boldsymbol{\Phi}_{\boldsymbol{q}}\dot{\boldsymbol{q}} + \boldsymbol{\Phi}_t\right) - \beta^2\boldsymbol{\Phi}$.

As Equation (4.8) represents a second order system which tends to the desired solution, Baumgarte stabilisation can be interpreted within the framework of control theory. As a consequence, the system is stable if α and β are positive. Furthermore, if $\alpha = \beta$, critical damping is achieved and the fastest error reduction is obtained. Studies have shown that numerical integration of the equations of motion with Baumgarte stabilisation is much more efficient than the one without it and that this approach is a general, simple and efficient method for the stabilisation of the multibody system. One of the drawbacks of Baumgarte stabilisation is that constraint equations are not statically, but just dynamically, satisfied. Furthermore, artificial stiffness in the system is introduced if the stabilisation parameters are not properly chosen. Since no general criteria for their choice exists, this can easily happen, [109]. Some optimisation and adaptive techniques for the evaluation of the parameters have been recently proposed and, despite these drawbacks, the stabilisation approach works well in many practical applications.

Another constraint violation stabilisation technique, known as penalty formulation, was proposed by Bayo et al., [110]. According to this approach, it is possible to incorporate the constraint equations as a dynamic system, penalised by a large factor, into the equations of motion. As a consequence, Lagrange multipliers are eliminated from the equations of motion and an index one DAE is obtained. It has been proved that this approach guarantees accurate solutions for a wide range of values of the penalty factors; a generalisation for non-holonomic systems has been later developed, [84].

Both the Baumgarte stabilisation and the penalty formulation do not eliminate the violation of the constraints with the consequence that the constraint equations are never completely satisfied. Other stabilisation methods that can guarantee the satisfaction of the constraint equations with machine accuracy have been developed. According to these methods the solution is corrected by using geometric projection or mass orthogonal methods; a review of these methods can be found in [106].

4.8.2 Coordinate partitioning

The coordinate partitioning method, also known as the extraction method, permits the transformation of the equations of motion of Equation (4.6) into a minimal form.

Because of its relative simplicity, coordinate partitioning methods have been widely employed in the past. According to this technique, first proposed by Wehage and Haug, [76, 111], the complete vector of dependent acceleration is calculated from Equation (4.7); only the elements of the vector corresponding to the independent coordinates are however fed into the numerical integrator subroutine. As a result, only the coordinates and the velocities relative to the independent coordinates are found. Dependent coordinate velocities are then calculated in a second step by solving the position problem and the velocity problem.

The subset of accelerations to be integrated is generally chosen by means of Gauss triangularisation with total pivoting of the constraints Jacobian $\boldsymbol{\Phi}_{\boldsymbol{q}}$; other techniques have however been suggested. The numerical integration of the obtained equations requires the solution of the position and velocity problems at each iteration. While the latter does not imply any particular computational burden, the former requires an iterative solution that is generally computationally inefficient. A partial solution to this problem is the evaluation of the system-dependent coordinates through the integration of the complete set of dependent velocities, [84].

4.8.3 Coordinate reduction

As with the coordinate partitioning method, coordinate reduction techniques, also known as coordinate orthogonalisation, transform the original descriptor form into a minimal formulation of the problem. As a consequence, Lagrange's multipliers are eliminated from the equations of motion and Equations (4.6) are transformed into a set of ordinary differential equations.

A coordinate reduction technique was first described in 1896 by Maggi, [112] and again in 1901, [113] and appeared in the English literature for the first time in 1972 in Neimark and Fufaev, [114]. Since then, it has been known under the names of matrix $\boldsymbol{R}$ formulation, [28], Maggi-Kane or Kane's method. The substantial equivalence of Maggi's and Kane's method was outlined by Borri et al., [115] and by Kurdila et al., [116].

The method is based on the projection of dependent velocities $\dot{\boldsymbol{q}}$ over the rows of a constant matrix $\boldsymbol{B}$, [111]. Consider a multibody system described by n generalised coordinates and m constraint equations. A set of $(n - m)$ independent kinematic parameters, also known as independent quasi-velocities, kinematic parameters or generalised speeds, $\boldsymbol{e}$, is defined as:

$$\boldsymbol{e} = \boldsymbol{B}\dot{\boldsymbol{q}} \tag{4.10}$$

where $\boldsymbol{B}$ is an $(n - m) \times n$ matrix the rows of which are linearly independent from one another and from the rows of matrix $\boldsymbol{\Phi}_{\boldsymbol{q}}$.

Combining the time-derivative of the constraint equations and Equation (4.10), it is possible to write:

$$\begin{bmatrix} \boldsymbol{\Phi_q} \\ \boldsymbol{B} \end{bmatrix} \dot{\boldsymbol{q}} = \begin{bmatrix} \boldsymbol{b} \\ \boldsymbol{e} \end{bmatrix} \tag{4.11}$$

where $\boldsymbol{b} = -\boldsymbol{\Phi}_t$ expresses the partial derivative of $\boldsymbol{\Phi}$ with time. Assuming a full rank constraint matrix and a judicious choice of the kinematic parameters, Equation (4.11) is invertible and the vector of generalised velocities $\dot{\boldsymbol{q}}$ can be expressed as a function of vector of independent velocities $\boldsymbol{e}$:

$$\dot{\boldsymbol{q}} = \begin{bmatrix} \boldsymbol{S} & \boldsymbol{R} \end{bmatrix} \begin{bmatrix} \boldsymbol{b} \\ \boldsymbol{e} \end{bmatrix} = \boldsymbol{R}\,\boldsymbol{e} + \boldsymbol{S}\,\boldsymbol{b} \tag{4.12}$$

where $\boldsymbol{S}$ and $\boldsymbol{R}$ are formed, respectively, by the first m and by the last $n-m$ columns of the inverse matrix of equation (4.11). Since Equations (4.10) and (4.12) are the inverse each of the other, the following relationship must be satisfied:

$$\begin{bmatrix} \boldsymbol{\Phi_q} \\ \boldsymbol{B} \end{bmatrix} \begin{bmatrix} \boldsymbol{S} & \boldsymbol{R} \end{bmatrix} = \begin{bmatrix} \boldsymbol{\Phi_q S} & \boldsymbol{\Phi_q R} \\ \boldsymbol{BS} & \boldsymbol{BR} \end{bmatrix} = \begin{bmatrix} \boldsymbol{I} & \boldsymbol{0} \\ \boldsymbol{0} & \boldsymbol{I} \end{bmatrix} \tag{4.13}$$

Equation (4.13) implies that $\boldsymbol{\Phi_q R} = \boldsymbol{0}$. It is therefore possible to say that the columns of $\boldsymbol{R}$ pertain to and generate the nullspace of $\boldsymbol{\Phi_q}$ and that $\boldsymbol{\Phi_q}$ and $\boldsymbol{R}$ are orthogonal. It is also interesting to note that the term $\boldsymbol{R}\,\boldsymbol{e}$ represents a general solution of the homogeneous velocity equation, while the term $\boldsymbol{S}\,\boldsymbol{b}$ represents a particular solution of the complete equation in the case of rheonomic constraints, that is, when the term $\boldsymbol{\Phi}_t$ is not null.

Accelerations are found in a similar way. Equations of motion are therefore rewritten as:

$$\boldsymbol{R}^T \boldsymbol{M} \boldsymbol{R}\,\dot{\boldsymbol{e}} = \boldsymbol{R}^T \boldsymbol{Q} - \boldsymbol{R}^T \boldsymbol{M}\ \boldsymbol{S}\,\boldsymbol{c} \tag{4.14}$$

in which $\boldsymbol{Q} = \boldsymbol{Q_e} + \boldsymbol{Q_i}$ and $\boldsymbol{c} = -\dot{\boldsymbol{\Phi}}_q \dot{\boldsymbol{q}} - \dot{\boldsymbol{\Phi}}_t$.

Equation (4.12), together with the (4.14) forms a system of $2n-m$ first order ODEs in which the unknowns are the kinematic characteristics $\boldsymbol{e}$ and the generalised coordinates $\boldsymbol{q}$. Lagrange multipliers are not present in the formulation, they can however be easily evaluated by solving a system of linear equations.

This technique does not specify how to choose the independent velocities; whereas the generalised velocities are defined, any set of independent vectors can be selected to span the null space, each leading to a different set of kinematic characteristics.

Many ways of generating the projection matrix $\boldsymbol{B}$ and, as a consequence, the kinematic characteristics $\boldsymbol{e}$ have been proposed. Among them, Gaussian elimination, SVD, QR and Schur decomposition are to be mentioned, [28]. It is sometimes possible to identify a set of independent coordinates that always remain independent. In this case, the evaluation of the projection matrix $\boldsymbol{B}$ does not require any analysis of matrix

$\boldsymbol{\Phi_q}$; $\boldsymbol{B}$ is a Boolean matrix formed by a set of ones and zeros, so that it extracts $n-m$ components of $\dot{\boldsymbol{q}}$ as independent coordinates $\dot{\boldsymbol{z}}$. This method is the simplest, and it is almost always the most efficient one, [84].

Further improvements to this formulation have been suggested. It was for example suggested by Serna, [84], that the evaluation of matrix $\boldsymbol{R}$ can be performed without inversion of Equation (4.12). This method is based on the fact that the columns of matrix $\boldsymbol{R}$ form a nullspace of the matrix of Equation (4.11). As a consequence, the columns of $\boldsymbol{R}$ are given by the solutions of the linear system of (4.11) obtained by assigning independent vectors to $\dot{\boldsymbol{e}}$. The simplest way of creating an independent vector is the use of unitary constant vectors.

As the constraint Jacobian $\boldsymbol{\Phi_q}$ is a function of time, the projection matrix $\boldsymbol{R}$ is also time-dependent. As a consequence, matrix $\boldsymbol{R}$ has to be evaluated at each time step. However, some methods in which the null space matrix $\boldsymbol{R}$ is kept constant for a certain number of time steps and is recalculated at regular intervals, have been developed, [105].

The solution of the equation of motion obtained allows the evaluation of the vector of independent velocities $\boldsymbol{e}$, from which it is possible, by means of equation (4.12) to evaluate the vector of the generalised velocities $\dot{\boldsymbol{q}}$ that, integrated, leads to the evaluation of the generalised coordinates $\boldsymbol{q}$. Although being very efficient, this method has the disadvantage of being more difficult to implement than those based on dependent coordinates. Also, numerical errors in the constraint equations may accumulate with the effect of reducing the efficiency of the simulation. A positional error check is therefore necessary.

Despite the different terminology, Equation (4.12) is also the basis of Kane's method, [117]. It has been shown that Kane's method can be considered as an analytical procedure for choosing the null-space basis of the problem; the columns of matrix $\boldsymbol{R}$ correspond to the partial velocities with respect to the generalised coordinates $\boldsymbol{e}$ while the product $\boldsymbol{Sb}$ describes the partial velocities with respect to time, [115].

According to Sharp, [3, 88], Kane's method is particularly advantageous when vehicle dynamics studies are considered and good computational efficiency is required. Several commercial codes are based on Kane's method, among these, AutoSim, [118, 119], is of particular interest. The simulation procedure implemented in AutoSim is very similar to the one described in the previous paragraph, including the generation of the subspace matrix and the positional error correction routine, [117].

4.8.4 Other formulations

Among other formulations, Udwadia and Kalaba's formulation, [120] is rather widespread. This approach uses the Gauss principle of Least Action to demonstrate that

the equations of motion can be expressed as a solution of a quadratic minimization problem subjected to acceleration level constraints. The solution of the equations of motion implies the use of the Moore-Penrose generalised inverse matrix that, unless particular configurations are considered, is generally very costly.

A graph-theoretical algorithm that uses the dependency structure of the equations has been proposed by Pantelides, [121]. The algorithm constitutes a systematic method for determining which equations need to be differentiated and it has been successfully implemented into the commercial code Dymola.

4.9 Symbolic generation of the equations of motions

Regarding the computational procedure, numerical and symbolical formalisms are available. Numerical formalisms directly deliver the equations of motion in a numerical form at each time step of the simulation. Symbolic methods instead, are capable of producing the equations of motion in a symbolic manner, as it would be done manually, [3, 122]. The generation of symbolic equations of motion is generally more complex than generation of numeric equations; however, there is no need to regenerate the equations when a new simulation is run or a simulation parameter is changed.

Furthermore, symbolic preparation of the equations of motion permits the user to omit insignificant details that are not relevant to the problem bandwidth, to treat small quantities in an appropriate manner or to neglect them. Also, equations of motion obtained through the use of symbolic tools are inherently parametric; it is for example possible to assign the same inertial parameters to two identical bodies. All these qualities tend to make models prepared by using symbolic tools particularly efficient and suitable for real time simulation, [3].

General purpose computer algebra software, like Maple or Mathematica can be used to manipulate the symbolic systems mentioned above. After symbolic generation of the equations of motion, symbolic codes are generally capable of exporting computational routines written in Matlab, C or Fortran code.

A variety of symbolic code exists. Among others, AutoSim, MBSymba and Neweul are the most significant ones. AutoSim has provided the basis for the commercial simulation codes CarSim, BikeSim and TruckSim and has been extensively used to create vehicle models for driver and path optimisation, see for example [14, 123, 124]. The code is based on a form of Kane's equations and is characterised by the fact that it automates the generation of the equations of motion by applying extensive algebraic and programming optimisations. The user is responsible for choosing the generalised coordinates which describe the configuration of the system; it is not necessary to use Cartesian coordinates and numerous constraint equations to formulate the equations of motion are available. Further information on AutoSim can be found in [118, 119, 125].

A paper describing a 14-degrees-of-freedom model built utilising Autosim was

presented in 1991 by Mousseau et al., [125]. One of the peculiarities of the model was that the location and orientation of the wheel spindle was expressed in terms of four generalised coordinates; the generalised coordinates were specified as prescribed cubic polynomial functions of the suspension deflection using a quasi-static approximation. The cubic polynomials were obtained from a kinematic suspension model. The effects of suspension geometry and suspension bushing compliance were included in the suspension model by means of look-up tables. Integration of the resulting Fortran model produced good correlation with measured data.

The developed vehicle model was later included in the commercial software CarSim. AutoSim was described in many papers, for example it was in 1996 applied to the Iltis benchmark model, [119]. A full and a reduced model were described, the first one being capable of describing the complete suspension kinematics, the second using look-up tables. A step steer input manoeuvre was simulated at three vehicle speeds and good agreement, except for roll angle, was found between the two models. An eigenvalue analysis showed good agreement with results obtained using other multibody codes. Computational efficiency was and still is one of the key characteristics of AutoSim, which is therefore suitable for real-time simulations, [118]. It is not however capable of including flexible bodies.

MBSymba is a Maple package for the symbolic modelling of multibody systems developed at the University of Padua. The library provides an object-oriented language for multibody systems, contains procedures for defining the elements of the multibody systems and a set of additional procedures that enable the user to derive and manipulate the equations of motion. The package has been extensively used for the analysis of motorcycle dynamics, [4, 126, 127].

To the author's knowledge, Neweul-M^2 is the only recent symbolic package that permits a detailed modelling of deformable bodies. The code is a research package based on Newton-Euler equations and the principles of d'Alembert and Jourdain. It is capable of generating equations of motion in minimal form for open-loop systems and differential form for closed-loop systems, [122]. No recursive formulation is however available. Furthermore, the entire symbolic program is based on the Matlab symbolic engine, which has limited capabilities.

4.10 Numerical integration of the equations of motion

4.10.1 Solution of ODEs

Equations of motion need to be solved numerically. Depending on the formulation adopted, either a set of ODEs or of DAEs is obtained. In case of ODEs, several methods are available; a detailed review on the available methods can be found in [128]. In general, two distinctive groups of algorithms exist for the solution of stiff

and non-stiff initial value ODEs problems. Several attempts at a rigorous definition of stiffness appear in the literature; a pragmatic definition is however generally accepted. According to this approach, stiff problems are those for which certain implicit methods perform sensibly better than explicit ones, [104].

Runge-Kutta methods are the most widely used one-step methods for solving non-stiff ODEs. These formulas have the advantage that they do not need any special starting procedure or for the generation of past values when the step size is changed. Also, in their explicit form, they do not involve the solution of non-linear equations at each step. In contrast to one-step methods, multi-step methods offer higher efficiency by using the information from several previous solution approximations. In this class, Adams and Adams-Moulton and the predictor-corrector schemes are the most important. A complete review on numerical methods for ODEs can be found in [129].

Stability properties of the classical Adams and explicit Runge-Kutta methods is generally not adequate for the solution of stiff systems. Furthermore, while many implicit formulas do have adequate stability properties, they require the solution of a set of non-linear equations at each step. An inexpensive method for solving non-linear equations, such as an iteration method, can be used when an implicit formula is used to solve non-stiff ODEs but cannot be used when the equations are stiff. The most commonly used algorithms for the solution of stiff ODEs are the backward differentiation formulas (BDFs), [130]. One of the first and most successful routines for the solution of stiff problems was implemented by Gear in 1971, [107]. The routine, known as DIFSUB, consisted of a variable-order, variable-step size BDF formula and under different forms it is still in widespread use.

More advanced algorithms were later developed. For example, Petzold proposed an algorithm capable of detecting the stiffness of the considered system and of automatically selecting between a method based on backward differentiation formulas or on Adams formula, [131]. Under different variants, the algorithm is known as LSODE.

4.10.2 Solution of DAEs

Solution of DAEs requires the use of appropriate solvers. An overview on DAEs, on their properties and on their numerical solution, can be found in the texts of Hairer, [104], and Brenan, [132]. The problem of the numerical integration of DAEs is the instability due to the index three formulation found for mechanical systems, [85]. In addition to error control techniques, such as the Baumgarte stabilisation, schemes capable of solving index-three DAEs have been proposed. According to some authors, [133], the sparsity of the system allows the use of particular techniques that improve the efficiency of the developed solvers. However, numerically dissipative time integrators have to be used and the difficulties associated with the solution of the index-three

formulations have not been overcome. Gear and Petzold, [134], suggested that if the index of a DAE is greater than one, it is strongly recommended to reduce it.

Fundamental contributions to the development of methods for the integration of index two DAEs are due to Gear, [135–137], Petzold, [138, 139], Gear and Petzold [134], Burrage and Petzold, [140] and Ascher et al., [109, 141, 142]. A widely used code based on a backward difference formula (BDF) is DASSL, implemented by Petzold in 1982, [132]. Other approaches are based on implicit or explicit Runge-Kutta methods or on the Gear-Gupta-Leimkuhler formulation (GGL), [143]. The GGL method implies a coupling of the velocity to the differential part of the descriptor form by means of additional multipliers. This method is known to be reliable but, as additional multipliers are required, it is generally not efficient.

Beside the mentioned generic DAE solvers, particular solvers have been developed that exploit the structure of the equations that arise from multibody systems. Among others, the extrapolation code MEXX is to be noted, [144].

4.11 Concluding remarks

A survey of the available techniques for multibody simulation has been presented in this chapter. It appears from the literature that there exists a great variety of methods and techniques for multibody analysis. As a comment, it is surprising that commercial multibody codes generally offer the possibility of using only a very limited set of these methods. The choice of the approach to be adopted in order to successfully build a multibody model for the problem considered is not trivial. Among the reviewed techniques however, it is possible to identify some that appear to be preferable.

Early attempts at creating a vehicle model based on minimal coordinates have confirmed that not only is its development a very complex task but also that poor computational efficiency is obtained. The choice of reference Cartesian coordinates is therefore recommended.

Another advantage bound to the use of Cartesian coordinates is that they permit the development of the equations of motion using conventional, existing formulations. As suggested, the use of a moving reference frame is beneficial from the efficiency point of view. Furthermore, equations of motion for flexible bodies are available in the literature and have been proven to be reliable.

The use of a modal technique is particularly suitable for modelling chassis compliance for vehicle dynamic studies. In fact, not only has it already been proven to be valid, but also it permits the development of computationally efficient models.

Because of their topology, vehicle models are generally suitable for recursive formulations. As it is intended to model the exact kinematics of the suspension through the use of a closed-loop chain, the use of fully recursive formulation is not possible. Furthermore, as chains are not particularly long, the gain in computational

efficiency would be limited. However, the use of relative coordinates at the velocity level, as suggested by the velocity transformation method, not only offers a computational advantage, but, combined with a coordinate reduction technique, it also offers a valid tool for the understanding of the effects of chassis compliance on suspension kinematics.

Literature has shown that techniques that transform the DAE that originates from the equations of motion written in the descriptor form into a set of ODEs are available. This approach provides higher computational efficiency and stability and allows the use of standard and more robust solvers. Furthermore, this approach is compatible with a semi-recursive formulation based on velocity transformation.

Finally, it emerges from the literature that the symbolic development of the equations of motion not only is of great advantage from the point of view of the computational efficiency but also it permits a deeper understanding of the systems analysed.

To the author's knowledge, a tool in which all the stated techniques are implemented is not available. Furthermore, it appears that only a purpose-developed tool that permits manipulation, inspection, simplification of the equations employed would be of use in this work. On the other hand, available computer algebra tools, e.g. Maple, permit the development and the implementation of the models in an efficient and effective manner. A symbolic multibody library which implements the described techniques is presented in Chapter 5.

Chapter 5

A symbolic library for flexible multibody modelling

The present chapter describes a multibody library that permits the symbolic generation of the equations of motion of a generic multibody system. The library implements several of the previously discussed techniques and is intended to provide a tool for the analysis of generally complex multibody systems. An example of an application of the library is included.

5.1 Introduction

The analysis of the literature review presented in Chapter 4 has revealed that several options for multibody modelling exist. However, when vehicle dynamics modelling of flexible vehicles is considered, it is possible to identify a set of techniques that are preferable. Briefly, they can be summarised as:

- the use of dependent reference point Cartesian coordinates;
- the use of equations of motion written according to a Newton-Euler formulation using a moving reference frame;
- the representation of flexible bodies through the use of a modal approach;
- the use of a velocity transformation technique in order to obtain a semi-recursive formulation;
- the implementation of a coordinate reduction technique;
- the use of a symbolic tool for the generation of the equations of motion.

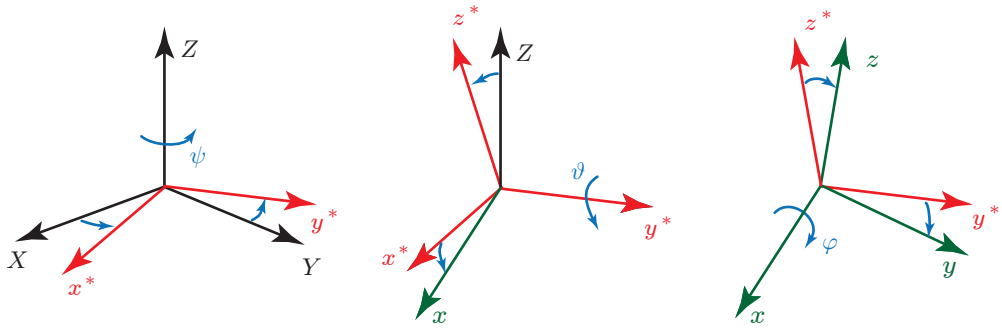

Figure 5.1: Yaw-pitch-roll sequence for rigid bodies.

A library containing a set of routines and methods that permit the implementation of these techniques is presented below. In addition to other existing libraries, the possibility of including flexible bodies, the implementation of the velocity transformation technique and the completely symbolic development constitute elements of novelty. The package is based on the computer algebra software Maple and contains a set of commands that allow the user to build a desired model and to obtain its equations of motion. Details on the kinematic and dynamic formulations adopted are given in the following sections.

5.2 Kinematics

5.2.1 Rigid body

Rigid body kinematics is described by means of a set of Cartesian coordinates relative to a reference point and three Euler angles. When compared with other possible sets, for example Euler parameters or quaternions, Euler angles have the drawback that they can only be used if singular positions are avoided. For vehicle studies, this is only possible if a particular set of the Euler angles sequence is employed, [25].

The coordinates of the body reference point, generally coincident with its centre of gravity, are described by means of the variables $x^{(i)}$, $y^{(i)}$ and $z^{(i)}$ and the three rotation parameters are $\varphi^{(i)}$, $\vartheta^{(i)}$ and $\psi^{(i)}$, so that a vector of generalised coordinates $\boldsymbol{q}^{(i)}$ for the i-th body is defined as:

$$\boldsymbol{q}^{(i)} = \left[x^{(i)} \; y^{(i)} \; z^{(i)} \; \varphi^{(i)} \; \vartheta^{(i)} \; \psi^{(i)} \right]^T \tag{5.1}$$

Several rotation sequences are available. The derivation of the particular sequence of Euler angle generally employed in aerospace and vehicle application, based on yaw, roll and pitch angle is presented here. The sequence is also known as the Tait-Bryan one, see Figure 5.1.

The first rotation considered is about the Z-axis of the inertial reference system, and brings the X-axis to coincide with the projection of the x-axis on the XY-plane, which is the x^*-axis. The y-axis is transformed into the y^*-axis. The transformation between the two reference systems is described by the following rotation matrix:

$$\boldsymbol{A}_1^{(i)} = \begin{bmatrix} \cos(\psi^{(i)}) & -\sin(\psi^{(i)}) & 0 \\ \sin(\psi^{(i)}) & \cos(\psi^{(i)}) & 0 \\ 0 & 0 & 1 \end{bmatrix} \tag{5.2}$$

in which the yaw angle $\psi^{(i)}$ represents the rotation angle between the X- and x^*-axes.

The second rotation is about the y^*-axis and it is described by the pitch angle $\vartheta^{(i)}$. The x^*-axis is then coincident with the x-axis. The rotation matrix is:

$$\boldsymbol{A}_2^{(i)} = \begin{bmatrix} \cos(\vartheta^{(i)}) & 0 & \sin(\vartheta^{(i)}) \\ 0 & 1 & 0 \\ -\sin(\vartheta^{(i)}) & 0 & \cos(\vartheta^{(i)}) \end{bmatrix} \tag{5.3}$$

The third rotation takes place about the x-axis and is described by the roll angle $\varphi^{(i)}$. It leads the y^*- and z^*-axes in the position of the y- and z-axes. The corresponding rotation matrix is:

$$\boldsymbol{A}_3^{(i)} = \begin{bmatrix} 1 & 0 & 0 \\ 0 & \cos(\varphi^{(i)}) & -\sin(\varphi^{(i)}) \\ 0 & \sin(\varphi^{(i)}) & \cos(\varphi^{(i)}) \end{bmatrix} \tag{5.4}$$

The global rotation matrix allowing the rotation of any vector from the local frame xyz to the inertial frame XYZ is then the product of the three matrices:

$$\boldsymbol{A}^{(i)} = \boldsymbol{A}_1{}^{(i)} \boldsymbol{A}_2{}^{(i)} \boldsymbol{A}_3{}^{(i)} \tag{5.5}$$

Euler angles have the drawback that the matrix $\boldsymbol{A}^{(i)}$ is singular when $\vartheta^{(i)}$ is a multiple of $\pi/2$; in this case the position of the body cannot be uniquely defined. However, if the particular application of vehicle dynamics is considered, during normal manoeuvres some angles (e.g. roll, pitch, camber, steering angles) are usually small. As a consequence, the proposed angles can be employed without incurring singularities.

Let arrays $\boldsymbol{r}^{(i)} = \begin{bmatrix} x^{(i)} & y^{(i)} & z^{(i)} \end{bmatrix}^T$ and $\boldsymbol{\vartheta}^{(i)} = \begin{bmatrix} \varphi^{(i)} & \vartheta^{(i)} & \psi^{(i)} \end{bmatrix}^T$ represent respectively the translation and the orientation of the origin of the i-th body reference system with respect to the inertial reference frame. The absolute position of a generic point P belonging to the body can be written as:

$$\boldsymbol{x}_P{}^{(i)} = \boldsymbol{r}^{(i)} + \boldsymbol{A}^{(i)} \bar{\boldsymbol{x}}_P{}^{(i)} \tag{5.6}$$

where $\boldsymbol{A}^{(i)}$ represents the transformation matrix from the i-th body reference frame to the inertial one and $\bar{\boldsymbol{x}}^{(i)}$ is the position of point P in the body fixed reference frame.

Generally, all variables denoted with an overbar are to be considered as expressed in the body reference system.

The absolute velocity of the generic point is obtained through differentiation of Equation (5.6) versus time. Under the assumption of a rigid body ($\bar{\boldsymbol{x}}^{(i)}$ constant), it is:

$$\dot{\boldsymbol{x}}_P{}^{(i)} = \dot{\boldsymbol{r}}^{(i)} + \dot{\boldsymbol{A}}^{(i)}\bar{\boldsymbol{x}}_P{}^{(i)} \tag{5.7}$$

Furthermore, it is possible to show that the following relationship holds:

$$\dot{\boldsymbol{A}}^{(i)} = \boldsymbol{A}^{(i)}\tilde{\bar{\boldsymbol{\omega}}}^{(i)} \tag{5.8}$$

where $\bar{\boldsymbol{\omega}}^{(i)}$ is the angular velocity vector defined in the i-th body reference frame. Overhead tilde sign represents the skew operator. Furthermore, vector $\bar{\boldsymbol{\omega}}^{(i)}$ is written as $\bar{\boldsymbol{\omega}}^{(i)} = \boldsymbol{G_r}{}^{(i)}\dot{\boldsymbol{\vartheta}}^{(i)}$ where, given rotation matrix of Equation (5.5), $\boldsymbol{G_r}{}^{(i)}$ is evaluated as:

$$\boldsymbol{G_r}{}^{(i)} = \begin{bmatrix} 1 & 0 & -\sin(\vartheta^{(i)}) \\ 0 & \cos(\varphi^{(i)}) & \sin(\varphi^{(i)})\cos(\vartheta^{(i)}) \\ 0 & -\sin(\varphi^{(i)}) & \cos(\varphi^{(i)})\cos(\vartheta^{(i)}) \end{bmatrix} \tag{5.9}$$

Substituting (5.7) into (5.8) and exploiting the commutation property of the skew operator, it is:

$$\dot{\boldsymbol{x}}_P{}^{(i)} = \dot{\boldsymbol{r}}^{(i)} + \boldsymbol{A}^{(i)}\tilde{\bar{\boldsymbol{\omega}}}^{(i)}\bar{\boldsymbol{x}}_P{}^{(i)} = \dot{\boldsymbol{r}}^{(i)} - \boldsymbol{A}^{(i)}\tilde{\bar{\boldsymbol{x}}}_P{}^{(i)}\bar{\boldsymbol{\omega}}^{(i)} \tag{5.10}$$

Introducing Equation (5.9) into (5.10), expression for the velocity of a generic point belonging to the i-th body is written as:

$$\dot{\boldsymbol{x}}_P{}^{(i)} = \dot{\boldsymbol{r}}^{(i)} - \boldsymbol{A}^{(i)}\tilde{\bar{\boldsymbol{x}}}_P{}^{(i)}\boldsymbol{G_r}{}^{(i)}\dot{\boldsymbol{\vartheta}}^{(i)} \tag{5.11}$$

Expression (5.11) is to be used for the evaluation of the kinetic energy of the body, see Section 1.4, but also for the evaluation of the velocity of a generic marker point attached to the same body.

5.2.2 Flexible body

The following assumptions are made for the modelling of elastic bodies:

- only linear elastic deformation is considered;
- a floating reference frame coincident with the centre of gravity of the body is used;
- total displacement of material points is described by the superposition of the motion of a reference frame and of a local deformation;
- only small deformation is considered;

The implemented approach is derived and adapted from Schwertassek and Wallrapp, [79, 93]; it is however also compatible with [82].

In case of flexible bodies, vector $\bar{\boldsymbol{x}}^{(i)}$ of Equation (5.6) is not constant. Indeed, it is composed by its rigid body part $\bar{\boldsymbol{x}}_{\boldsymbol{0}}{}^{(i)}$ and by a local deformation $\bar{\boldsymbol{u}}^{(i)}$

$$\bar{\boldsymbol{x}}_P{}^{(i)} = \bar{\boldsymbol{x}}_{\boldsymbol{0}P}{}^{(i)} + \bar{\boldsymbol{u}}_P{}^{(i)} \tag{5.12}$$

Local deformation is approximated by means of the Rayleigh-Ritz approach. A set of known modal shapes $\boldsymbol{\Psi}^{(i)}$ and a vector of time-dependent modal coordinates $\boldsymbol{p}^{(i)}$ are defined so that:

$$\bar{\boldsymbol{u}}_P{}^{(i)} = \boldsymbol{\Psi}_P{}^{(i)}\, \boldsymbol{p}^{(i)} \tag{5.13}$$

The vector of generalised coordinates associated to the i-th body is therefore augmented with the vector of modal coordinates $\boldsymbol{p}^{(i)}$. It is therefore $\boldsymbol{q}^{(i)} = \begin{bmatrix} \boldsymbol{r}^{(i)} & \boldsymbol{\vartheta}^{(i)} & \boldsymbol{p}^{(i)} \end{bmatrix}^T$. Introducing Equation (5.12) into Equation (5.6), after differentiation, velocity of generic point P can be expressed as:

$$\dot{\boldsymbol{x}}_P{}^{(i)} = \dot{\boldsymbol{r}}^{(i)} - \boldsymbol{A}^{(i)} \left(\widetilde{\bar{\boldsymbol{x}}_{\boldsymbol{0}P}{}^{(i)} + \boldsymbol{\Psi}_P{}^{(i)}\, \boldsymbol{p}^{(i)}} \right) \boldsymbol{G}_{\boldsymbol{r}}{}^{(i)} \dot{\boldsymbol{\vartheta}}^{(\boldsymbol{i})} + \boldsymbol{A}^{(i)} \boldsymbol{\Psi}_P{}^{(i)} \dot{\boldsymbol{p}}^{(i)} \tag{5.14}$$

As shown in Section 4.6.2, several approaches for derivation of modal functions are available. The present formulation is generic and can be used in combination of any modal reduction technique which is compatible with the stated assumptions. A comparison between modal shapes obtained under the free-free hypothesis and using the Craig-Bampton method is reported in Section 6.2.2.

5.3 Constraints

Constraints equations are written by means of markers located on rigid points according to Equation (5.6) and on flexible bodies according to Equation (5.12). Constraint Jacobians are evaluated symbolically. Several constraint pairs can be introduced; only the spherical, the link and the revolute one are treated here. For further details see [81, 84].

5.3.1 Spherical joint

Two bodies are linked by a spherical joint when they have a point in common. Let $P^{(i)}$ and $Q^{(i)}$ be the two coincident points and $\boldsymbol{x}_P{}^{(i)}$ and $\boldsymbol{x}_Q{}^{(i)}$ the corresponding subsets of the global vector $\boldsymbol{x}$. The joint is defined by the equations:

$$\boldsymbol{x}_P^{(i)} - \boldsymbol{x}_Q^{(j)} = \boldsymbol{0} \tag{5.15}$$

The vectorial expression (5.15) corresponds to three algebraic equations that constrain three degrees of freedom.

5.3.2 Link joint

A link is a particular joint which constrains the distance between two points to be constant. It is often used to model light bodies connecting bigger bodies. It is in fact quite common to find in many mechanical systems some bodies whose inertial properties can be neglected and that can be substituted with sets of massless links. Mathematically, the equation describing a link of length l which connects points P and Q is:

$$\left\| \boldsymbol{x}_P^{(i)} - \boldsymbol{x}_Q^{(j)} \right\| = l \tag{5.16}$$

which represents a second order, non-linear algebraic equation.

5.3.3 Revolute joint

The revolute joint constrains five degrees of freedom allowing the two bodies to rotate about a common axis. The revolute pair consists of imposing the compatibility condition between the axis direction and one common point on this axis. If three orthogonal vectors $\boldsymbol{n_1}^{(i)}$ and $\boldsymbol{n_2}^{(i)}$ and $\boldsymbol{n_3}^{(i)}$ and point P of the i-th body are defined and vector $\boldsymbol{n_1}^{(j)}$ and point Q of the j-th body are defined, it is possible to describe a revolute joint by imposing the coincidence of points P and Q and the coincidence of the axes $\boldsymbol{n_1}^{(i)}$ and $\boldsymbol{n_1}^{(j)}$. The former condition is the same used by a spherical joint, the latter can be expressed by imposing the orthogonality between vectors $\boldsymbol{n_2}^{(i)}$, $\boldsymbol{n_1}^{(j)}$ and $\boldsymbol{n_3}^{(i)}$, $\boldsymbol{n_1}^{(j)}$. As a consequence it is:

$$\begin{cases} \boldsymbol{x}_P^{(i)} - \boldsymbol{x}_Q^{(j)} = \boldsymbol{0} \\ \boldsymbol{n_2}^{(i)} \cdot \boldsymbol{n_1}^{(j)} = 0 \\ \boldsymbol{n_3}^{(i)} \cdot \boldsymbol{n_1}^{(j)} = 0 \end{cases} \tag{5.17}$$

This vectorial equation corresponds to a set of five algebraic equations, hence the revolute joint removes five degrees of freedom. Note that Equation (5.17) allows both right- and left-handed results; although the presence of other constraints generally avoids the system to assume the undesired configuration, additional checks on body relative position might be required.

5.4 Dynamics

5.4.1 Rigid body

Consider a rigid body belonging to a multibody system having, respectively, kinetic and potential energy $T^{(i)}$ and $U^{(i)}$. Its Lagrangian is defined as:

$$L^{(i)} = T^{(i)} - U^{(i)} \tag{5.18}$$

From this, the Lagrange's equation of motion, also known as Euler-Lagrange's equation, can be written as:

$$\frac{\mathrm{d}}{\mathrm{d}t}\left(\frac{\partial L^{(i)}}{\partial \dot{\boldsymbol{q}}^{(i)}}\right) - \frac{\partial L^{(i)}}{\partial \boldsymbol{q}^{(i)}} + \boldsymbol{\Phi}_{\boldsymbol{q}}{}^{(i)T}\boldsymbol{\lambda} = \boldsymbol{Q}_{\boldsymbol{e}}{}^{(i)} \tag{5.19}$$

where $\boldsymbol{\Phi}_{\boldsymbol{q}}{}^{(i)}$ is the Jacobian matrix of the constraints, vector $\boldsymbol{\lambda}$ contains the Lagrange multipliers and $\boldsymbol{Q}_{\boldsymbol{e}}{}^{(i)}$ the generalised external forces. A complete derivation of equation (5.19) from Hamilton's principle can be found in [84] or in [82].

The kinetic energy of the rigid i-th body, having density $\rho^{(i)}$ and volume $V^{(i)}$, is evaluated as:

$$T^{(i)} = \frac{1}{2}\int_{V^{(i)}} \rho^{(i)} \dot{\boldsymbol{x}}^T \dot{\boldsymbol{x}}^{(i)} \mathrm{d}V \tag{5.20}$$

Substituting Equation (5.11) into (5.20), it is possible to show that the kinetic energy of the i-th body can be written as:

$$T^{(i)} = \frac{1}{2}\dot{\boldsymbol{q}}^{(i)T}\boldsymbol{M}^{(i)}\dot{\boldsymbol{q}}^{(i)} \tag{5.21}$$

with:

$$\boldsymbol{M}^{(i)} = \begin{bmatrix} m^{(i)}\boldsymbol{I} & \text{symm.} \\ \boldsymbol{A}^{(i)T} m^{(i)} \tilde{\bar{\boldsymbol{c}}}^{(i)} \boldsymbol{G_r}{}^{(i)} & \boldsymbol{G_r}{}^{(i)T} \bar{\boldsymbol{J}}^{(i)} \boldsymbol{G_r}{}^{(i)} \end{bmatrix} \tag{5.22}$$

where $m^{(i)}$ represents the mass of the body, $\bar{\boldsymbol{c}}^{(i)}$ is the distance between the origin of the body fixed reference frame and the centre of gravity of the body expressed in the body reference frame. In case of centroidal reference system, it is $\bar{\boldsymbol{c}}^{(i)} = \boldsymbol{0}$. Matrix $\bar{\boldsymbol{J}}^{(i)}$ represents the inertia tensor of the body. By introducing matrix $\boldsymbol{G}^{(i)}$, defined as:

$$\boldsymbol{G}^{(i)} = \begin{bmatrix} \boldsymbol{A}^{(i)T} & \boldsymbol{0} \\ \boldsymbol{0} & \boldsymbol{G_r}^{(i)} \end{bmatrix} \tag{5.23}$$

it is possible to redefine the mass matrix of the body as:

$$\boldsymbol{M}^{(i)} = \boldsymbol{G}^{(i)T}\bar{\boldsymbol{M}}^{(i)}\boldsymbol{G}^{(i)} \tag{5.24}$$

where $\bar{\boldsymbol{M}}$ represents the constant mass matrix of the i-th body:

$$\bar{\boldsymbol{M}}^{(i)} = \begin{bmatrix} m^{(i)}\boldsymbol{I} & \text{symm.} \\ m^{(i)}\tilde{\bar{\boldsymbol{c}}}^{(i)} & \bar{\boldsymbol{J}}^{(i)} \end{bmatrix} \tag{5.25}$$

Finally, the kinetic energy of the rigid body expressed in (5.21) can be rewritten as:

$$T^{(i)} = \frac{1}{2}\dot{\boldsymbol{q}}^{(i)T}\boldsymbol{G}^{(i)T}\bar{\boldsymbol{M}}^{(i)}\boldsymbol{G}^{(i)}\dot{\boldsymbol{q}}^{(i)} \tag{5.26}$$

By introducing Expression (5.26) into Equation (5.18), it is possible to obtain the equations of motion of the i-th rigid body as:

$$\boldsymbol{M}^{(i)}\ddot{\boldsymbol{q}}^{(i)} + \boldsymbol{\Phi}_{\boldsymbol{q}}{}^{(i)T}\boldsymbol{\lambda} = \boldsymbol{Q}_{\boldsymbol{e},i} + \boldsymbol{Q}_{\boldsymbol{i},i} \tag{5.27}$$

where $\boldsymbol{M}^{(i)}$ is the mass matrix, $\boldsymbol{\Phi_q}^{(i)}$ is the Jacobian matrix of the constraints, $\boldsymbol{\lambda}^{(i)}$ is the vector of Lagrange multipliers, $\boldsymbol{Q_e}^{(i)} = \begin{bmatrix} \boldsymbol{F}^{(i)} & \boldsymbol{T}^{(i)} \end{bmatrix}^T$ represents the vector of external loads. Vector $\boldsymbol{Q_i}^{(i)}$ includes the components due to gravity and terms quadratic in the velocities with coefficients that may depend on $\boldsymbol{q}^{(i)}$. The terms that involve the presence of a single velocity squared are called centrifugal; those which involve the product of two velocities are called Coriolis terms:

$$\boldsymbol{Q_i}^{(i)} = \begin{bmatrix} \boldsymbol{0} \\ -\boldsymbol{G_r}^{(i)T} \left(\tilde{\bar{\boldsymbol{\omega}}}^{(i)} \bar{\boldsymbol{J}}^{(i)} \bar{\boldsymbol{\omega}}^{(i)} + \bar{\boldsymbol{J}}^{(i)} \dot{\boldsymbol{G}}_{\boldsymbol{r}}^{(i)} \dot{\boldsymbol{\vartheta}}^{(i)} \right) \end{bmatrix} + \begin{bmatrix} m^{(i)} \boldsymbol{g} \\ m^{(i)} \boldsymbol{g} \tilde{\bar{\boldsymbol{c}}}^{(i)} \end{bmatrix} \tag{5.28}$$

where vector $\boldsymbol{g}$ represents the vector of gravitational acceleration. In case of a centroidal reference system, equations of motion can be rewritten as:

$$\begin{bmatrix} m^{(i)} \boldsymbol{I} & \boldsymbol{0} \\ \boldsymbol{0} & \boldsymbol{G_r}^{(i)T} \bar{\boldsymbol{J}}^{(i)} \boldsymbol{G_r}^{(i)} \end{bmatrix} \begin{bmatrix} \ddot{\boldsymbol{r}}^{(i)} \\ \ddot{\boldsymbol{\vartheta}}^{(i)} \end{bmatrix} + \begin{bmatrix} \boldsymbol{\Phi_{qt}}^{(i)} \\ \boldsymbol{\Phi_{qr}}^{(i)} \end{bmatrix}^T \boldsymbol{\lambda} = \begin{bmatrix} \boldsymbol{F}^{(i)} \\ \boldsymbol{T}^{(i)} \end{bmatrix} + \\ - \begin{bmatrix} \boldsymbol{0} \\ \boldsymbol{G_r}^{(i)T} \left(\tilde{\bar{\boldsymbol{\omega}}}^{(i)} \bar{\boldsymbol{J}}^{(i)} \bar{\boldsymbol{\omega}}^{(i)} + \bar{\boldsymbol{J}}^{(i)} \dot{\boldsymbol{G}}_{\boldsymbol{r}}^{(i)} \dot{\boldsymbol{\vartheta}}^{(i)} \right) \end{bmatrix} + \begin{bmatrix} m^{(i)} \boldsymbol{g} \\ \boldsymbol{0} \end{bmatrix} \tag{5.29}$$

Angular accelerations are more conveniently expressed in the body moving reference frame. The obtained equations of motion, known as Newton-Euler equations are written as:

$$\begin{bmatrix} m^{(i)} \boldsymbol{I} & \boldsymbol{0} \\ \boldsymbol{0} & \bar{\boldsymbol{J}}^{(i)} \end{bmatrix} \begin{bmatrix} \ddot{\boldsymbol{r}}^{(i)} \\ \dot{\bar{\boldsymbol{\omega}}}^{(i)} \end{bmatrix} + \begin{bmatrix} \boldsymbol{\Phi_{qt}}^{(i)} \\ \bar{\boldsymbol{\Phi}}_{\boldsymbol{qr}}^{(i)} \end{bmatrix}^T \boldsymbol{\lambda} = \begin{bmatrix} \boldsymbol{F}^{(i)} \\ \bar{\boldsymbol{T}}^{(i)} \end{bmatrix} - \begin{bmatrix} \boldsymbol{0} \\ \tilde{\bar{\boldsymbol{\omega}}}^{(i)} \bar{\boldsymbol{J}}^{(i)} \bar{\boldsymbol{\omega}}^{(i)} \end{bmatrix} + \begin{bmatrix} m^{(i)} \boldsymbol{g} \\ \boldsymbol{0} \end{bmatrix} \tag{5.30}$$

where $\bar{\boldsymbol{\Phi}}_{\boldsymbol{qr}}^{(i)} = \boldsymbol{\Phi_{qr}}^{(i)} \boldsymbol{G_r}^{(i)-1}$ and $\bar{\boldsymbol{T}}^{(i)} = \boldsymbol{G_r}^{(i)-1} \boldsymbol{T}^{(i)}$.

Equation (5.30) can be expressed in a moving reference frame if linear acceleration is written as the first derivative of vector $\bar{\boldsymbol{v}}^{(i)} = \begin{bmatrix} \bar{\boldsymbol{u}}^{(i)} & \bar{\boldsymbol{\omega}}^{(i)} \end{bmatrix}^T$ which expresses the body velocities in the moving reference frame. To this purpose, matrix $\boldsymbol{B}^{(i)} = \boldsymbol{B}^{(i)} = \boldsymbol{G}^{(i)-1}$ is introduced, so that:

$$\dot{\boldsymbol{q}}^{(i)} = \boldsymbol{B}^{(i)} \bar{\boldsymbol{v}}^{(i)} \tag{5.31}$$

Differentiation versus time of equation (5.31) yelds to:

$$\ddot{\boldsymbol{q}}^{(i)} = \boldsymbol{B}^{(i)} \dot{\bar{\boldsymbol{v}}}^{(i)} + \dot{\boldsymbol{B}}^{(i)} \bar{\boldsymbol{v}}^{(i)} \tag{5.32}$$

By substituting Expression (5.32) into (5.22) and premultiplying by $\boldsymbol{B}^{(i)T}$, one obtains:

$$\bar{\boldsymbol{M}}^{(i)} \dot{\bar{\boldsymbol{v}}}^{(i)} + \left(\boldsymbol{\Phi_q}^{(i)} \boldsymbol{B}^{(i)} \right)^T \boldsymbol{\lambda} = \boldsymbol{B}^{(i)T} \boldsymbol{Q_e}^{(i)} + \boldsymbol{B}^{(i)T} \boldsymbol{Q_i}^{(i)} - \bar{\boldsymbol{M}}^{(i)} \boldsymbol{G}^{(i)} \dot{\boldsymbol{B}}^{(i)} \bar{\boldsymbol{v}}^{(i)} \tag{5.33}$$

that can be rewritten as:

$$\bar{\boldsymbol{M}}^{(i)} \dot{\bar{\boldsymbol{v}}}^{(i)} + \bar{\boldsymbol{\Phi}}_{\boldsymbol{q}}^{(i)T} \boldsymbol{\lambda} = \bar{\boldsymbol{Q}}_{\boldsymbol{e}}^{(i)} + \bar{\boldsymbol{Q}}_{\boldsymbol{i}}^{(i)} \tag{5.34}$$

with $\bar{\boldsymbol{\Phi}}_{\boldsymbol{q}}^{(i)} = \boldsymbol{B}^{(i)T}\boldsymbol{\Phi}_{\boldsymbol{q}}^{(i)}$ and $\bar{\boldsymbol{Q}}_{\boldsymbol{e}}^{(i)} = \boldsymbol{B}^{(i)T}\boldsymbol{Q}_{\boldsymbol{e}}^{(i)}$. If a centroidal reference system is adopted, the vector of centrifugal, Coriolis and gravity forces is written as:

$$\bar{\boldsymbol{Q}}_{\boldsymbol{i}}^{(i)} = -\begin{bmatrix} \tilde{\bar{\boldsymbol{\omega}}}^{(i)} m^{(i)} \bar{\boldsymbol{u}}^{(i)} \\ \tilde{\bar{\boldsymbol{\omega}}}^{(i)} \bar{\boldsymbol{J}}^{(i)} \bar{\boldsymbol{\omega}}^{(i)} \end{bmatrix} + \begin{bmatrix} \boldsymbol{m^{(i)} g} \\ \boldsymbol{0} \end{bmatrix} \tag{5.35}$$

From this, Equation (5.34) can be rewritten as:

$$\begin{bmatrix} m^{(i)}\boldsymbol{I} & \boldsymbol{0} \\ \boldsymbol{0} & \bar{\boldsymbol{J}}^{(i)} \end{bmatrix} \begin{bmatrix} \dot{\bar{\boldsymbol{u}}}^{(i)} \\ \dot{\bar{\boldsymbol{\omega}}}^{(i)} \end{bmatrix} + \begin{bmatrix} \bar{\boldsymbol{\Phi}}_{\boldsymbol{qt}}^{(i)} \\ \bar{\boldsymbol{\Phi}}_{\boldsymbol{qr}}^{(i)} \end{bmatrix}^T \boldsymbol{\lambda} = \begin{bmatrix} \bar{\boldsymbol{F}}^{(i)} \\ \bar{\boldsymbol{T}}^{(i)} \end{bmatrix} - \begin{bmatrix} \tilde{\bar{\boldsymbol{\omega}}}^{(i)} m^{(i)} \bar{\boldsymbol{u}}^{(i)} \\ \tilde{\bar{\boldsymbol{\omega}}}^{(i)} \bar{\boldsymbol{J}}^{(i)} \bar{\boldsymbol{\omega}}^{(i)} \end{bmatrix} + \begin{bmatrix} m^{(i)} \bar{\boldsymbol{g}} \\ \boldsymbol{0} \end{bmatrix} \tag{5.36}$$

The equations of motion of a rigid body are included in the multibody library in accordance with Equation (5.36). Advantages of this formulation are the constant mass matrix, the possibility of expressing external forces directly in the body reference system and the fact that, thanks to the moving reference frame, integration quantities are always limited, leading to a more stable numeric integration.

5.4.2 Flexible body

Equations of motion of a flexible body can be derived in a similar manner as those for rigid bodies. The mass matrix is augmented by non-constant components that depend on modal variables $\boldsymbol{p}^{(i)}$:

$$\bar{\boldsymbol{M}}^{(i)} = \begin{bmatrix} m^{(i)}\boldsymbol{I} & & \text{symm.} \\ m^{(i)}\tilde{\bar{\boldsymbol{c}}}^{(i)} & \bar{\boldsymbol{J}}^{(i)} & \\ \boldsymbol{C_t}^{(i)} & \boldsymbol{C_r}^{(i)} & \boldsymbol{M_e}^{(i)} \end{bmatrix} \tag{5.37}$$

where the terms $\boldsymbol{C_t}^{(i)}$, $\boldsymbol{C_r}^{(i)}$ and $\boldsymbol{M_e}^{(i)}$ are due to body flexibility.

In agreement with [59], it is supposed that a finite element model of the deformable body is available. Furthermore, it is supposed that the finite element model is based on a lumped mass formulation so that the mass of the flexible body is distributed by the finite element nodal positions. As a consequence, a nodal mass ${m_k}^{(i)}$ and inertia tensor ${\bar{\boldsymbol{J}}_k}^{(i)}$ are available for each node.

Referring to matrix of Equation (5.37), vector $\bar{\boldsymbol{c}}^{(i)}$ describes the position of the centre of gravity within the body reference and is expressed as a first order Taylor series so that $\bar{\boldsymbol{c}}^{(i)} = \bar{\boldsymbol{c}}_{\boldsymbol{0}}^{(i)} + \bar{\boldsymbol{c}}_{\boldsymbol{1}}^{(i)}$ with:

$$\begin{aligned} m^{(i)}\bar{\boldsymbol{c}}_{\boldsymbol{0}}^{(i)} &= \sum_{k=1}^{n_n} {m_k}^{(i)} {\bar{\boldsymbol{x}}_{\boldsymbol{0},k}}^{(i)} \\ m^{(i)}\bar{\boldsymbol{c}}_{\boldsymbol{1}}^{(i)} &= \sum_{l=1}^{n_m}\sum_{k=1}^{n_n} {m_k}^{(i)} {\boldsymbol{\Psi}_{k,l}}^{(i)} \boldsymbol{p}_l^{(i)} \end{aligned} \tag{5.38}$$

where vector ${\bar{\boldsymbol{x}}_{\boldsymbol{0},k}}^{(i)}$ describes the position of the k-th node, n_n is the number of nodes and n_m the number of modal shapes available, represented by matrix $\boldsymbol{\Psi}$. Vector $\bar{\boldsymbol{c}}_{\boldsymbol{0}}^{(i)}$

only depends on the location of the centre of gravity of the underformed body and, in case of a centroidal reference system, is null. Matrix $\bar{\boldsymbol{c}}_{\mathbf{1}}$ is a $3 \times n_m$ matrix that represents the first order Jacobian of the displacement of centre of gravity due to body deformations.

Similarly, inertia tensor $\bar{\boldsymbol{J}}^{(i)}$ is evaluated as $\bar{\boldsymbol{J}}^{(i)} = \bar{\boldsymbol{J}}_{\mathbf{0}}{}^{(i)} + \bar{\boldsymbol{J}}_{\mathbf{1}}{}^{(i)}$ where $\bar{\boldsymbol{J}}_{\mathbf{0}}{}^{(i)}$ represents the inertia tensor of the undeformed body and $\bar{\boldsymbol{J}}_{\mathbf{1}}{}^{(i)}$ the part dependent on body deformation:

$$\begin{aligned}
\bar{\boldsymbol{J}}_{\mathbf{0}}{}^{(i)} &= \sum_{k=1}^{n_n} \bar{\boldsymbol{J}}_k{}^{(i)} + \tilde{\bar{\boldsymbol{x}}}_{\mathbf{0},k}{}^{(i)^T} m_k{}^{(i)} \tilde{\bar{\boldsymbol{x}}}_{\mathbf{0},k}{}^{(i)} \\
\bar{\boldsymbol{J}}_{\mathbf{1}}{}^{(i)} &= -\sum_{l=1}^{n_m} \left(\boldsymbol{C}_{\mathbf{4},l}{}^{(i)} + \boldsymbol{C}_{\mathbf{4},l}{}^{(i)^T} \right) \boldsymbol{p}_l^{(i)} \quad \text{with } \boldsymbol{C}_{\mathbf{4},l}{}^{(i)} = \sum_{k=1}^{n_n} \tilde{\bar{\boldsymbol{x}}}_{\mathbf{0},k}{}^{(i)} m_k{}^{(i)} \tilde{\boldsymbol{\Psi}}_{k,l}{}^{(i)}
\end{aligned} \tag{5.39}$$

Matrix $\boldsymbol{C}_{\boldsymbol{t}}{}^{(i)}$ is a $3 \times n_m$ constant matrix that represents the coupling term between the reference coordinates and the elastic coordinates:

$$\boldsymbol{C}_{\boldsymbol{t}}{}^{(i)} = \sum_{k=1}^{n_n} m_k{}^{(i)} \boldsymbol{\Psi}_k{}^{(i)} \tag{5.40}$$

The coupling term between the large rotation coordinates of the body and the elastic coordinates is expressed by matrix $\boldsymbol{C}_{\boldsymbol{r}}{}^{(i)} = \boldsymbol{C}_{\boldsymbol{r0}}{}^{(i)} + \boldsymbol{C}_{\boldsymbol{r1}}{}^{(i)}$ with:

$$\begin{aligned}
\boldsymbol{C}_{\boldsymbol{r0}}{}^{(i)} &= \sum_{k=1}^{n_n} m_k{}^{(i)} \tilde{\bar{\boldsymbol{x}}}_{\mathbf{0},k}{}^{(i)} \boldsymbol{\Psi}_{\boldsymbol{t},k}{}^{(i)} + \bar{\boldsymbol{J}}_k{}^{(i)} \boldsymbol{\Psi}_{\boldsymbol{r},k}{}^{(i)} \\
\bar{\boldsymbol{C}}_{\boldsymbol{r1}}{}^{(i)} &= \sum_{l=1}^{n_m} \boldsymbol{C}_{\mathbf{5},l}{}^{(i)} \boldsymbol{p}_l^{(i)} \quad \text{with } \boldsymbol{C}_{\mathbf{5},l}{}^{(i)} = \sum_{k=1}^{n_n} \tilde{\boldsymbol{\Psi}}_{k,l}{}^{(i)} m_k{}^{(i)} \boldsymbol{\Psi}_k{}^{(i)}
\end{aligned} \tag{5.41}$$

Finally, matrix $\boldsymbol{M}_{\boldsymbol{e}}{}^{(i)}$ is the mass matrix corresponding to the pure elastic deformation that is written as:

$$\boldsymbol{M}_{\boldsymbol{e}} = \sum_{k=1}^{n_n} \boldsymbol{\Psi}_{\boldsymbol{t},k}{}^{(i)T} m_k{}^{(i)} \boldsymbol{\Psi}_{\boldsymbol{t},k}{}^{(i)} + \boldsymbol{\Psi}_{\boldsymbol{r},k}{}^{(i)T} \bar{\boldsymbol{J}}_k{}^{(i)} \boldsymbol{\Psi}_{\boldsymbol{r},k}{}^{(i)} \tag{5.42}$$

According to Equations (5.38-5.42), the mass matrix of a flexible body is not constant but it also depends on the modal coordinates. This reflects the fact that the mass distribution of the body is modified by its deformation; it seems however reasonable to assume that this effect is generally very small, especially when large bodies like a vehicle chassis are considered. This hypothesis will be later verified.

The vector of internal forces $\bar{\boldsymbol{Q}}_{\boldsymbol{i}}{}^{(i)} = \boldsymbol{h}_{\boldsymbol{g}}{}^{(i)} + \boldsymbol{h}_{\boldsymbol{e}}{}^{(i)} + \boldsymbol{h}_{\boldsymbol{\omega}}{}^{(i)}$ contains gravity, elastic, damping and gyroscopic forces. Gravity force is introduced as:

$$\boldsymbol{h}_{\boldsymbol{g}}{}^{(i)} = \begin{bmatrix} m^{(i)} \boldsymbol{g} \\ m^{(i)} \, \boldsymbol{g} \, \tilde{\bar{\boldsymbol{c}}}^{(i)} \\ \boldsymbol{C}_{\boldsymbol{t}}^{(i)} \end{bmatrix} \tag{5.43}$$

where $\boldsymbol{g}$ represents the vector of gravitational acceleration. Vector ${\boldsymbol{h_e}}^{(i)}$ contains elastic and damping forces which arise from the inner properties of the material :

$$ {\boldsymbol{h_e}}^{(i)} = \begin{bmatrix} \mathbf{0} \\ \mathbf{0} \\ {\boldsymbol{K_e}}^{(i)}\boldsymbol{p}^{(i)} + {\boldsymbol{D_e}}^{(i)}\dot{\boldsymbol{p}}^{(i)} \end{bmatrix} \tag{5.44} $$

where ${\boldsymbol{K_e}}^{(i)}$ and ${\boldsymbol{D_e}}^{(i)}$ represent the reduced stiffness and damping matrix of the deformable body. A more detailed description on their derivation is reported in Chapter 6. The vector of gyroscopic and Coriolis forces is written as:

$$ {\boldsymbol{h_\omega}}^{(i)} = - \begin{bmatrix} \tilde{\bar{\boldsymbol{\omega}}}^{(i)} m^{(i)} \bar{\boldsymbol{u}}^{(i)} + \tilde{\bar{\boldsymbol{\omega}}}^{(i)} m^{(i)} \tilde{\bar{\boldsymbol{\omega}}}^{(i)} \bar{\boldsymbol{c}}^{(i)} + 2\tilde{\bar{\boldsymbol{\omega}}}^{(i)} \boldsymbol{C_t^{(i)}} \dot{\boldsymbol{p}}^{(i)} \\ \tilde{\bar{\boldsymbol{\omega}}}^{(i)} \bar{\boldsymbol{J}}^{(i)} \bar{\boldsymbol{\omega}}^{(i)} + m^{(i)} \tilde{\bar{\boldsymbol{c}}}^{(i)} \tilde{\bar{\boldsymbol{\omega}}}^{(i)} \bar{\boldsymbol{v}}^{(i)} + \sum_{l=1}^{n_m} {\boldsymbol{G_{r,l}}}^{(i)} \dot{\boldsymbol{p}}_l{}^{(i)} \bar{\boldsymbol{\omega}}^{(i)} \\ \boldsymbol{C_t}^{(i)} \tilde{\bar{\boldsymbol{\omega}}}^{(i)} \bar{\boldsymbol{v}}^{(i)} + \sum_{l=1}^{n_m} {\boldsymbol{G_{e,l}}}^{(i)} \dot{\boldsymbol{p}}_l{}^{(i)} \bar{\boldsymbol{\omega}}^{(i)} + {\boldsymbol{O_e}}^{(i)} \bar{\boldsymbol{\omega}}^{(i)} \end{bmatrix} \tag{5.45} $$

where terms $\boldsymbol{G_r}$, $\boldsymbol{G_e}$ and $\boldsymbol{O_e}$ represent the gyroscopic effects due to rotational and elastic coordinates. For a detailed derivation of Equation (5.45), see [93].

5.5 Dynamic formulation

5.5.1 Newton-Euler equations

Equations of motion of the multibody system can be assembled from the equations of motion of single rigid or flexible bodies. Given a vector of generalised coordinates $\boldsymbol{q} = \left[\boldsymbol{q}^{(1)} \dots \boldsymbol{q}^{(i)} \dots \boldsymbol{q}^{(n_b)}\right]^T$ and a vector of generalised velocities expressed in body reference frame $\bar{\boldsymbol{v}} = \left[\bar{\boldsymbol{v}}^{(1)} \dots \bar{\boldsymbol{v}}^{(i)} \dots \bar{\boldsymbol{v}}^{(n_b)}\right]^T$, matrix $\boldsymbol{B}$ for the definition of velocities in body reference frames and mass matrix $\bar{\boldsymbol{M}}$ are assembled so that Newton-Euler equations for the entire system are written as:

$$ \begin{cases} \dot{\boldsymbol{q}} = \boldsymbol{B}\bar{\boldsymbol{v}} \\ \bar{\boldsymbol{M}}\dot{\bar{\boldsymbol{v}}} + \bar{\boldsymbol{\Phi}}_{\boldsymbol{q}}{}^T \boldsymbol{\lambda} = \bar{\boldsymbol{Q}}_{\boldsymbol{e}} + \bar{\boldsymbol{Q}}_{\boldsymbol{i}} \\ \boldsymbol{\Phi} = \mathbf{0} \end{cases} \tag{5.46} $$

Equations (5.46) form a set of DAEs that can be used for simulation purposes. It has however been shown that in presence of chain-like topologies, typical for example of suspension systems, the use of recursive techniques is of great advantage.

5.5.2 Semi-recursive formulation

A semi-recursive formulation, similar to the velocity transformation technique reviewed in Section 4.7 and described in [81, 89] is here introduced. A set of dependent joint

velocities $\boldsymbol{y}$ is defined so that the velocity of the i-th body can be expressed as a linear combination of the velocity of the preceding body in the topological chain and a joint velocity:

$$\bar{\boldsymbol{v}}^{(i)} = \boldsymbol{C}^{(i)}\bar{\boldsymbol{v}}^{(i-1)} + \boldsymbol{D}^{(i)}\boldsymbol{y}^{(i)} \tag{5.47}$$

where matrix $\boldsymbol{C}^{(i)}$ depends on the relative position of the two bodies and matrix $\boldsymbol{D}^{(i)}$ defines the joint kinematics. For rigid bodies, matrix $\boldsymbol{C}^{(i)}$ is written as:

$$\boldsymbol{C}^{(i)} = \begin{bmatrix} \boldsymbol{A}^{(i,i-1)} & -\boldsymbol{A}^{(i,i-1)}\tilde{\bar{\boldsymbol{r}}}^{(i,i-1)} \\ \boldsymbol{0} & \boldsymbol{A}^{(i,i-1)} \end{bmatrix} \tag{5.48}$$

In Equation (5.48), matrix $\boldsymbol{A}^{(i,i-1)}$ is the rotation matrix between the i-th and $(i-1)$-th body and $\bar{\boldsymbol{r}}^{(i,i-1)}$ represents the distance between the centres of gravities of the same bodies written in the reference system attached to the $(i-1)$-th body. For flexible bodies, matrix $\boldsymbol{C}^{(i)}$ is augmented with a further identity matrix.

If closed-loops are involved, it is not possible to write an explicit reduced form of matrix $\boldsymbol{D}^{(i)}$ so that joint velocities $\boldsymbol{y}$ are independent. As a consequence, matrix $\boldsymbol{D}^{(i)}$ is here assumed as an identity matrix; a coordinate reduction technique is later implemented.

The recursive definition of the velocity vector of Equation (5.47) can be written for each of the bodies of the system. In a matrix form, it is:

$$\bar{\boldsymbol{v}} = \boldsymbol{T}\boldsymbol{y} \tag{5.49}$$

where matrix $\boldsymbol{T}$ is the global recursion matrix. Matrix $\boldsymbol{T}$ depends on the connection between the bodies and defines the topology of the system. For example, for a single chain system composed of n bodies it is:

$$\boldsymbol{T} = \begin{bmatrix} \boldsymbol{D}^{(1)} & \boldsymbol{0} & \boldsymbol{0} & \dots & \boldsymbol{0} \\ \boldsymbol{C}^{(2)}\boldsymbol{D}^{(1)} & \boldsymbol{D}^{(2)} & \boldsymbol{0} & \dots & \boldsymbol{0} \\ \boldsymbol{C}^{(3)}\boldsymbol{C}^{(2)}\boldsymbol{D}^{(1)} & \boldsymbol{C}^{(3)}\boldsymbol{D}^{(2)} & \boldsymbol{D}^{(3)} & \dots & \boldsymbol{0} \\ \vdots & \vdots & \vdots & \ddots & \vdots \\ * & * & * & \dots & \boldsymbol{D}^{(n)} \end{bmatrix} \tag{5.50}$$

By substituting Equation (5.49) into (5.46) and premultiplying by $\boldsymbol{T}^T$, equations of motion can be written as:

$$\begin{cases} \dot{\boldsymbol{q}} = \boldsymbol{B}\boldsymbol{T}\boldsymbol{y} \\ \boldsymbol{T}^T\bar{\boldsymbol{M}}\boldsymbol{T}\dot{\boldsymbol{y}} + \boldsymbol{T}^T\bar{\boldsymbol{\Phi}}_{\boldsymbol{q}}{}^T\boldsymbol{\lambda} = \boldsymbol{T}^T\bar{\boldsymbol{Q}}_{\boldsymbol{e}} + \boldsymbol{T}^T\bar{\boldsymbol{Q}}_{\boldsymbol{i}} - \boldsymbol{T}^T\boldsymbol{M}\dot{\boldsymbol{T}}\boldsymbol{y} \\ \boldsymbol{\Phi} = \boldsymbol{0} \end{cases} \tag{5.51}$$

5.5.3 Coordinate reduction technique

A coordinate reduction technique is implemented in order to obtain a minimal form of the equations of motion. To this purpose, a subset of independent velocities is defined as:

$$\boldsymbol{z} = \boldsymbol{P}\boldsymbol{y} \tag{5.52}$$

where $\boldsymbol{y}$ is the vector of joint velocities defined in Equation (5.47) and matrix $\boldsymbol{P}$ is a constant matrix that helps in defining the independent velocities. Vector $\boldsymbol{z}$ represents a set of independent kinematic parameters, also known as independent quasi-velocities, kinematic parameters or generalised speeds, [84].

Differentiation of the vector of constraints versus time yields:

$$\dot{\boldsymbol{\Phi}} = \boldsymbol{\Phi}_{\boldsymbol{q}}\dot{\boldsymbol{q}} + \boldsymbol{\Phi}_{\boldsymbol{t}} = \boldsymbol{0} \tag{5.53}$$

where $\boldsymbol{\Phi}_{\boldsymbol{q}}$ and $\boldsymbol{\Phi}_t$ are, respectively, the Jacobian of $\boldsymbol{\Phi}$ with respect to $\boldsymbol{q}$ and t.

Coupling of Equations (5.53) and (5.52) permits the definition the following relationship:

$$\begin{bmatrix} \boldsymbol{\Phi}_{\boldsymbol{q}}\boldsymbol{B}\boldsymbol{T} \\ \boldsymbol{P} \end{bmatrix} \boldsymbol{y} = \begin{bmatrix} \boldsymbol{b} \\ \boldsymbol{z} \end{bmatrix} \tag{5.54}$$

where $\boldsymbol{b} = -\boldsymbol{\Phi}_t$.

It is assumed that the transformation defined by Equation (5.54) is invertible. This implies a full rank constraint matrix and a judicious choice of the kinematic parameters. As a consequence, the generalised velocities can be expressed as a function of the kinematic characteristics:

$$\boldsymbol{y} = \begin{bmatrix} \boldsymbol{S} & \boldsymbol{R} \end{bmatrix} \begin{bmatrix} \boldsymbol{b} \\ \boldsymbol{z} \end{bmatrix} = \boldsymbol{S}\boldsymbol{b} + \boldsymbol{R}\boldsymbol{z} \tag{5.55}$$

where matrices $\boldsymbol{S}$ and $\boldsymbol{R}$ express the inverse of matrix of Equation (5.35) in a partitioned form. These matrices are conceptually equivalent to those described in [84] and reviewed in Section 4.8. In this case, however, they are used to project onto relative velocities instead of onto time derivatives of generalised coordinates. Since Equations (5.54) and (5.55) are the inverse each of the other, the following relationship must be satisfied:

$$\begin{bmatrix} \boldsymbol{\Phi}_{\boldsymbol{q}}\boldsymbol{B}\boldsymbol{T} \\ \boldsymbol{P} \end{bmatrix} \begin{bmatrix} \boldsymbol{S} & \boldsymbol{R} \end{bmatrix} = \begin{bmatrix} \boldsymbol{\Phi}_{\boldsymbol{q}}\boldsymbol{B}\boldsymbol{T}\boldsymbol{S} & \boldsymbol{\Phi}_{\boldsymbol{q}}\boldsymbol{B}\boldsymbol{T}\boldsymbol{R} \\ \boldsymbol{P}\boldsymbol{S} & \boldsymbol{P}\boldsymbol{R} \end{bmatrix} = \begin{bmatrix} \boldsymbol{I} & \boldsymbol{0} \\ \boldsymbol{0} & \boldsymbol{I} \end{bmatrix} \tag{5.56}$$

Equation (5.56) implies that $\boldsymbol{\Phi}_{\boldsymbol{q}}\boldsymbol{B}\boldsymbol{T}\boldsymbol{R} = \boldsymbol{0}$. It is therefore possible to say that the columns of $\boldsymbol{R}$ pertain to and generate the nullspace of $\boldsymbol{\Phi}_{\boldsymbol{q}}\boldsymbol{B}\boldsymbol{T}$ and that $\boldsymbol{\Phi}_{\boldsymbol{q}}\boldsymbol{B}\boldsymbol{T}$ and $\boldsymbol{R}$ are orthogonal. It is worth noting that the term $\boldsymbol{R}\,\boldsymbol{z}$ represents a general solution of the homogeneous velocity equation, while the term $\boldsymbol{S}\,\boldsymbol{b}$ represents a particular solution

of the complete equation in the case of rheonomic constraints, that is, when the term $\boldsymbol{\Phi}_t$ is not null.

A second differentiation of the constraint equations brings to:

$$\ddot{\boldsymbol{\Phi}} = \boldsymbol{\Phi}_{\boldsymbol{q}}\ddot{\boldsymbol{q}} + \dot{\boldsymbol{\Phi}}_{\boldsymbol{q}}\dot{\boldsymbol{q}} + \dot{\boldsymbol{\Phi}}_{\boldsymbol{t}} = \boldsymbol{0} \tag{5.57}$$

If the definition of $\ddot{\boldsymbol{q}}$ is introduced in Equation (5.57) and Equation (5.52) is considered, it is possible to write:

$$\begin{bmatrix} \boldsymbol{\Phi}_{\boldsymbol{q}}\boldsymbol{B}\boldsymbol{T} \\ \boldsymbol{P} \end{bmatrix} \dot{\boldsymbol{y}} = \begin{bmatrix} \boldsymbol{c} \\ \dot{\boldsymbol{z}} \end{bmatrix} \tag{5.58}$$

in which $\boldsymbol{c} = -\dot{\boldsymbol{\Phi}}_{\boldsymbol{q}}\boldsymbol{B}\boldsymbol{T}\boldsymbol{y} - \boldsymbol{\Phi}_{\boldsymbol{q}}\boldsymbol{B}\dot{\boldsymbol{T}}\boldsymbol{y} - \boldsymbol{\Phi}_{\boldsymbol{q}}\dot{\boldsymbol{B}}\boldsymbol{T}\boldsymbol{y} - \dot{\boldsymbol{\Phi}}_{\boldsymbol{t}}$. Inversion of matrix of Equation (5.58) permits the evaluation of the vector of joint accelerations:

$$\dot{\boldsymbol{y}} = \boldsymbol{R}\,\dot{\boldsymbol{z}} + \boldsymbol{S}\boldsymbol{c} \tag{5.59}$$

Substituting equation (5.42) into Equation (5.51) and premultiplying by $\boldsymbol{R}^T$, equations of motion of the system can be written as:

$$\boldsymbol{R}^T\boldsymbol{T}^T\bar{\boldsymbol{M}}\boldsymbol{T}\boldsymbol{R}\dot{\boldsymbol{z}} + \boldsymbol{R}^T\boldsymbol{T}^T\boldsymbol{B}^T{\boldsymbol{\Phi}_{\boldsymbol{q}}}^T\boldsymbol{\lambda} = \boldsymbol{R}^T\boldsymbol{T}^T\bar{\boldsymbol{Q}} - \boldsymbol{R}^T\boldsymbol{T}^T\bar{\boldsymbol{M}}\dot{\boldsymbol{T}}\boldsymbol{y} - \boldsymbol{R}^T\boldsymbol{T}^T\bar{\boldsymbol{M}}\boldsymbol{T}\boldsymbol{S}\boldsymbol{c} \tag{5.60}$$

Exploiting the relationship $\boldsymbol{\Phi}_{\boldsymbol{q}}\boldsymbol{B}\boldsymbol{T}\boldsymbol{R} = \boldsymbol{0}$ obtained from Equation (5.56), Equation (5.60) can be written as:

$$\begin{cases} \dot{\boldsymbol{q}} = \boldsymbol{B}\boldsymbol{T}\boldsymbol{y} \\ \boldsymbol{R}^T\boldsymbol{T}^T\bar{\boldsymbol{M}}\boldsymbol{T}\boldsymbol{R}\dot{\boldsymbol{z}} = \boldsymbol{R}^T\boldsymbol{T}^T\left(\bar{\boldsymbol{Q}} - \bar{\boldsymbol{M}}\left(\dot{\boldsymbol{T}}\boldsymbol{y} + \boldsymbol{T}\boldsymbol{S}\,\boldsymbol{c}\right)\right) \end{cases} \tag{5.61}$$

with $\boldsymbol{y} = \boldsymbol{R}\boldsymbol{z} + \boldsymbol{S}\boldsymbol{b}$. Equation (5.61) represents the equations of motion of the multibody system in independent relative joint coordinates. Furthermore, it forms a set of ODEs, so that no specific solver is required and high computational effciency can be obtained. If the system is formed by rigid bodies, mass matrix $\bar{\boldsymbol{M}}$ is constant and can be inverted off-line. This is possible also if the variation of the inertial properties of a deformable body is neglected.

Lagrange multipliers are not present in the formulation. Once the vector of dependent accelerations $\dot{\boldsymbol{y}}$ has been determined however, they can be evaluated by solving the linear system obtained by pre-multiplying equations of motion of (5.51) by matrix $\boldsymbol{S}^T$.

Many methods for the generation of matrix $\boldsymbol{P}$ and, as a consequence, for the definition of the kinematic characteristics $\boldsymbol{z}$ have been proposed, see Section 4.8. It is here assumed that it is possible to identify a set of independent velocities that always remain independent. In this case, $\boldsymbol{P}$ is considered a constant boolean matrix formed by a set of ones and zeros, so that it extracts $n - m$ components of $\dot{\boldsymbol{q}}$ as independent

coordinates $\dot{\boldsymbol{z}}$. This method is the simplest, and it is almost always the most efficient one, [84].

Further techniques are implemented in order to improve the overall computational efficiency of the described method. As an example, the evaluation of matrix $\boldsymbol{R}$ is performed by exploiting Equations (5.54) and (5.55). The columns of $\boldsymbol{R}$ are given by the solutions of the linear system of (5.34) obtained by assigning independent vectors to $\boldsymbol{z}$. The simplest way of creating a set of independent vector is the use of unitary constant vectors. In other words, it is:

$$\begin{bmatrix} \boldsymbol{\Phi_q B T} \\ \boldsymbol{P} \end{bmatrix} \boldsymbol{R}_i = \begin{bmatrix} \boldsymbol{b} \\ \boldsymbol{I}_i \end{bmatrix} \tag{5.62}$$

in which i goes from 1 to $n-m$ and the subscripts indicate the columns respectively of matrix $\boldsymbol{R}$ and of $\boldsymbol{I}$, which is a $(n-m) \times (n-m)$ identity matrix. The efficiency of this technique can be further improved by means of a matrix triangularisation.

In a similar way, the product $\boldsymbol{S}\,\boldsymbol{b}$ can be evaluated by solving the linear system (5.54) when $\boldsymbol{z} = \boldsymbol{0}$ and $\boldsymbol{S}\,\boldsymbol{c}$ solving the (5.58) when $\dot{\boldsymbol{z}} = \boldsymbol{0}$. This is particularity important because the evaluation of matrix $\boldsymbol{S}$ is usually computationally intensive and because the explicit evaluation of matrix $\boldsymbol{S}$ is not necessary.

Matrix $\boldsymbol{\Phi_q}$ is a function of time and therefore also $\boldsymbol{R}$ is time dependent. As a consequence, matrix $\boldsymbol{R}$ has to be evaluated at each time step. However, methods in which the null space matrix $\boldsymbol{R}$ is kept constant for a certain number of time steps and is recalculated at regular intervals, have been developed, [105]. This possibility will be later further investigated.

The solution of the obtained equation of motion allows the evaluation of the vector of generalised coordinates $\boldsymbol{q}$. A problem that might occur during numerical integration of the equations of motion is that numerical errors in the constraint equations may accumulate with the effect of reducing the efficiency of the simulation. This is avoided by implementing a positional error check and correction routine. Thanks to the presence of the constraint Jacobian $\boldsymbol{\Phi_q}$ however, the application of an iterative method, e.g. a Newton-Raphson method, is straightforward.

5.6 Implementation

A symbolic multibody library based on the kinematics and dynamics relationships described in Sections 5.2-5.5 has been developed. The library is based on the computer algebra tool Maple and makes an extensive use of its capabilities. In this sense, it is similar to the reviewed library MbSymba, [4], with the difference that flexible bodies can be included.

The library contains a set of commands that permit the description of a multibody system and the generation of the equations of motion in a symbolic form. The whole

system, including the modal parameters defining body flexibility, is therefore built in a symbolic and parametric manner.

A brief explanation of the commands available for the description of the multibody system is presented in Table 5.1. Table 5.2 reports the commands available for the generation of the equations of motion.

Table 5.1: Available commands for the definition of multibody systems.

Command	Description
`> defineframe(q,options)`	defines a reference system having Cartesian coordinates described by vector `q`
`> definerigidbody(F,m,I,options)`	defines a rigid body having mass `m` and inertia tensor `I` using the reference frame `F`
`> defineflexbody(F,M,p,options)`	defines a flexible body having modal properties described in `M` and modal coordinates `p`
`> definepoint(B,c,options)`	defines a point located on body `B` and local coordinates `c`
`> definemarker(P,d,options)`	defines a marker centred on point `P` having orientation `d`
`> definelinkj(P,Q,l,options)`	defines a link joint between points `P` and `Q` having length `l`
`> definerevj(P,Q,d,options)`	defines a revolute joint between points `P` and `Q` having axis orientation `d`
`> definesphj(P,Q,options)`	defines a spherical joint connecting points `P` and `Q`
`> defineindv(q)`	declares the velocity corresponding to the degree of freedom associated with `q` as independent

The obtained equations can be inspected, manipulated and simplified by hand or by means of the commands available in Maple. Furthermore, the library can automatically generate all the computational routines necessary for the numerical integration of the equations of motion of the system. A brief description of the available routines is presented in Table 5.3.

Table 5.2: Available commands for the generation of the equations of motion of the multibody system.

Command	Description
`> mapq(C,F)`	creates the map between coordinates `C` and reference frames `F`
`> makebodies(C,F,B)`	generates equations of motion for bodies `B` using coordinates `C` and reference frames `F`
`> makepoints(C,F,B,P)`	generates equations for points `P` belonging to bodies `B` using coordinates `C` and reference frames `F`
`> makeconstr(C,F,Phi)`	generates constraint equations
`> makeconstr(C,F,Vi)`	generates matrices for coordinate reduction using independent velocities `Vi`

Once the computational routines are generated, an external Fortran program is employed in order to assign numeric values to the computational routines and to evaluate the external loads. First, the main program includes a module capable of reading input data from a Matlab file. The numerical solution of the differential equations of Expression (5.61) is then obtained by using an available ODE solver. The computation is performed as follows:

1. start at a point in which $\boldsymbol{q}$ and $\boldsymbol{y}$ are known;
2. given $\boldsymbol{q}$ evaluate constraint equations $\boldsymbol{\Phi}$ and Jacobian $\boldsymbol{\Phi_q}$;
3. check error on $\boldsymbol{\Phi}$ and eventually correct it;
4. evaluate matrices $\boldsymbol{B}$ and $\boldsymbol{T}$;
5. use Equation (5.54) to calculate projection matrices $\boldsymbol{R}$ and $\boldsymbol{Sb}$ and Equation (5.58) to obtain $\boldsymbol{Sc}$;
6. evaluate joint velocities $\boldsymbol{y}$, $\bar{\boldsymbol{v}}$, $\dot{\boldsymbol{q}}$ using, respectively, Equations (5.55) and (5.49);
7. evaluate matrices $\dot{\boldsymbol{B}}$ and $\dot{\boldsymbol{T}}$;
8. calculate external forces $\bar{\boldsymbol{Q}}_{\boldsymbol{e}} = f(\boldsymbol{q}, \bar{\boldsymbol{v}}, t)$ and internal forces $\bar{\boldsymbol{Q}}_{\boldsymbol{i}} = f(\boldsymbol{q}, \bar{\boldsymbol{v}})$;
9. solve Equation (5.61) to obtain $\dot{\boldsymbol{z}}$;
10. obtain vectors $\boldsymbol{q}_{t+\Delta t}$ and $\boldsymbol{z}_{t+\Delta t}$; upon convergence return to point 2.

At the end of the simulation, the program automatically writes the results in a Matlab file which is then analysed through the use of specifically-developed routines.

Table 5.3: Computational routines.

Command	Description
`> M = pM(q,par)`	computes the mass matrix of the system
`> Qi = pQi(q,v,par)`	computes the internal, elastic and gravitational forces
`> B = pB(q,par)`	computes the velocity matrix
`> T = pT(q,par)`	computes the recursion matrix
`> P = pP()`	evaluates the boolean matrix for velocity transformation
`> X = pX(q,delta,par)`	evaluate the position of marker points
`> Phi = pPhi(X,par)`	computes the constraint equations
`> Tdot = pTdot(q,qdot,par)`	computes the derivative of matrix T
`> Bdot = pBdot(q,qdot,par)`	computes the derivative of matrix B
`> dXdq = pdXdq(q,delta,par)`	computes the derivative of marker position versus generalised coordinates
`> dXddelta = pdXdd(q,delta,par)`	computes the derivative of marker position versus time-dependent inputs

5.7 Example

In this section, the functionality of the described library is demonstrated by deriving the equations of motion of a planar compound double pendulum. The system is composed of two rigid bodies having respectively masses m_1 and m_2 and inertia J_1 and J_2, see Figure 5.2.

The commands for describing the system and deriving the equations of motion are reported below.

```
> F1 := defineframe(q1, q2, 0, 0,q3, 0, 1)
> F2 := defineframe(q4, q5, 0, 0, q6, 0, 1)
> B1 := definerigidbody(F1, m1, J1, 0, 0, 0, 0, 0)
> B2 := definerigidbody(F2, m2, J2, 0, 0, 0, 0, 0)
> P1 := definepoint(B1, 0, 0, a1)
> P2 := definepoint(B1, 0, 0, -(l1-a1))
> P3 := definepoint(B2, 0, 0, a2)
> z1 := defineindc(q3)
> z2 := defineindc(q6)
> C1 := definerevj(P0,P1,1,0,0)
```

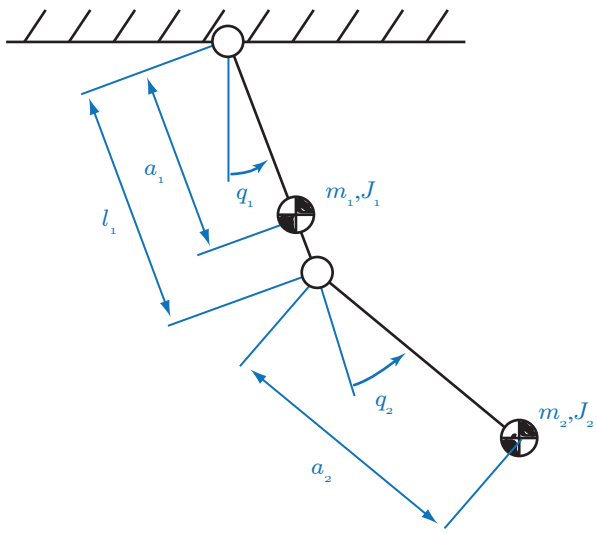

Figure 5.2: Compound planar double pendulum.

```
> C2 := definerevj(P2,P3,1,0,0)
> frames := [F1, F2]
> coords := [q1, q2, q3, q4]
> bodies := [B1, B2]
> points := [P1, P2, P3]
> indc := [z1, z2]
> constr:= [C1, C2]
> θ1:=q3
> θ2:=q6-q3
> mapq(coords, frames)
> makebodies(coords, frames, bodies);
> makepoints(coords, frames, bodies, points);
> makeconstr(coords, points, constr);
> makered(coords, indc);
```

The code automatically generates the matrix of the system $\bar{\boldsymbol{M}}$, the velocity map matrix $\boldsymbol{B}$ and vectors of external and internal forces $\bar{\boldsymbol{Q}}_{\boldsymbol{e}}$ and $\bar{\boldsymbol{Q}}_{\boldsymbol{i}}$. Thanks to the open-loop topology, the projection matrix $\boldsymbol{R}$ can be evaluated in an explicit form. Results are presented by the symbolic code in the following form:

```
      [ J1+a1^2m1+J2+a2^2m2+l1^2m2+2a2l1m2cos(θ2)        J2+a2^2m2+a2l1m2cos(θ2) ]
> M = [                                                                          ]
      [ J2+a2^2m2+a2l1m2cos(θ2)                          J2+a2^2m2               ]
```

$$
> \mathtt{Q_i} = \begin{bmatrix} \mathtt{a_2 l_1 m_2 \omega_2^2 sin(\theta_2) + 2 a_2 l_1 m_2 \omega_1 \omega_2 sin(\theta_2)} \\ \\ \mathtt{-a_2 l_1 m_2 \omega_1^2 sin(\theta_2)} \end{bmatrix}
$$

$$
> \mathtt{Q_e} = \begin{bmatrix} \mathtt{-(a_1 m_1 + l_1 m_2) g\, sin(\theta_1) - a_2 m_2 g\, sin(\theta_1 + \theta_2)} \\ \\ \mathtt{-a_2 m_2 g\, sin(\theta_1 + \theta_2)} \end{bmatrix}
$$

The obtained equations are coincident with those found in the literature, see for example [88, 92]. Although flexible bodies are not included, the present example permits to highlight the validity of the developed multibody library and the fact that it constitutes a valuable tool for the analysis and simulation of mechanical systems.

5.8 Concluding remarks

A symbolic multibody library for modelling flexible multibody systems has been introduced in the present chapter. The need for this novel tool originated from the observation that a symbolic tool for the generation of the equations of motion of systems with flexible bodies does not exist.

The library implements advanced techniques available for the analysis of multibody systems. Body kinematics is described in an efficient and straightforward manner through the use of reference point Cartesian dependent coordinates. From these, equations of motion of rigid and flexible bodies are written in a descriptor form. A moving reference frame, beneficial from the efficiency point of view, is then introduced. A proven modal technique that guarantees good computational efficiency and accuracy is used in order to represent the deformation of flexible bodies.

The library also includes a general semi-recursive formulation which permits the exploitation of the topology of the multibody system. Thanks to the use of dependent joint coordinates, both open- and closed-loop systems can be analysed.

Differential algebraic equations that arise from the formulation of the equations of motion are transformed into a set of ordinary differential equations through the use of a velocity transformation technique. This technique permits the avoidance of the use of specific low-efficiency numerical solvers and, coupled with the recursive formulation, helps obtaining a simulation model that can be inspected and manipulated by the user. Furthermore, the use of a powerful and established computer algebra software as Maple permits any further manipulation, simplification, linearisation and export of the obtained routines.

In conclusion, the adopted formulations coupled with the complete symbolic generation of the equations of motions constitutes a suitable basis for the development of efficient simulation codes. This has been partially demonstrated by means of a

simple application example, reported in the last section of the chapter. A more complex multibody model, consisting of an advanced vehicle model that includes chassis flexibility, is described in Chapter 6.

Chapter 6

A vehicle model with a flexible chassis

The present chapter introduces a novel vehicle model for the analysis of the effects of chassis compliance on vehicle dynamics. In the first part of the chapter, a description of the underlying assumptions of the formulation adopted, of the external routines and of the general implementation is provided. Data of a real vehicle that will be used for further analyses are then introduced. A finite element model of its chassis is then presented and a modal reduction performed. In the second part of the chapter a model developed in the Adams/Car environment is presented and used as a validation tool. Finally, considerations regarding the adopted modelling approach are presented and discussed.

6.1 Model description

6.1.1 Introduction

The literature review and the preliminary analysis presented in Chapter 3 have shown that a detailed analysis of the effects of chassis compliance on vehicle dynamics requires the development of an advanced vehicle model. To this purpose, a symbolic multibody library for flexible multibody systems has been introduced in Chapter 5. From this, a novel vehicle model is developed.

The vehicle model comprises a flexible body representing the sprung mass, four unsprung masses and four rotating wheels, for a total of nine bodies. Given the constraints acting between the bodies, the system has fourteen rigid body degrees of freedom and a variable number of modal coordinates that represent chassis compliance. Under the assumption that the weight of the suspensions and of other moving parts is negligible when compared to the weight of the other bodies, suspension components are modelled as rigid and massless links.

Table 6.1: Vehicle bodies.

Body	Coordinates	Independent coordinates
Sprung mass	$\boldsymbol{q}_1 \dots \boldsymbol{q}_6$	$\boldsymbol{y}_1 \dots \boldsymbol{y}_6$ (3 translations and 3 rotations)
Front left unsprung mass	$\boldsymbol{q}_7 \dots \boldsymbol{q}_{12}$	$\boldsymbol{y}_9$ (vertical motion)
Front right unsprung mass	$\boldsymbol{q}_{13} \dots \boldsymbol{q}_{18}$	$\boldsymbol{y}_{15}$ (vertical motion)
Rear right unsprung mass	$\boldsymbol{q}_{19} \dots \boldsymbol{q}_{24}$	$\boldsymbol{y}_{21}$ (vertical motion)
Rear left unsprung mass	$\boldsymbol{q}_{25} \dots \boldsymbol{q}_{30}$	$\boldsymbol{y}_{27}$ (vertical motion)
Front left wheel	$\boldsymbol{q}_7 \dots \boldsymbol{q}_{10}, \boldsymbol{q}_{31}, \boldsymbol{q}_{12}$	$\boldsymbol{y}_{31}$ (wheel spin)
Front right wheel	$\boldsymbol{q}_{13} \dots \boldsymbol{q}_{16}, \boldsymbol{q}_{32}, \boldsymbol{q}_{18}$	$\boldsymbol{y}_{32}$ (wheel spin)
Rear right wheel	$\boldsymbol{q}_{19} \dots \boldsymbol{q}_{22}, \boldsymbol{q}_{33}, \boldsymbol{q}_{24}$	$\boldsymbol{y}_{33}$ (wheel spin)
Rear left wheel	$\boldsymbol{q}_{25} \dots \boldsymbol{q}_{28}, \boldsymbol{q}_{34}, \boldsymbol{q}_{30}$	$\boldsymbol{y}_{34}$ (wheel spin)
Chassis deformation	$\boldsymbol{q}_{35} \dots \boldsymbol{q}_{44}$	$\boldsymbol{y}_{35} \dots \boldsymbol{y}_{44}$ (all independent)

6.1.2 Kinematics

System coordinates

The kinematics of each of the nine bodies that compose the model is described by means of six reference point coordinates, see Section 5.2. For each body a vector containing the coordinates of its centre of gravity and the rotation parameters is defined as in Equation (5.1). The barycentric coordinates of the wheels, as well as their toe and camber angles, are considered coincident with those of the related unsprung mass. As a consequence, the system is described by means of 34 dependent coordinates, shown in Table 6.1.

Table 6.1 reports the components of the vector of dependent coordinates $\boldsymbol{q}$ and the corresponding independent joint coordinates $\boldsymbol{y}$ for each body. The first six coordinates, all independent, are assigned to the sprung mass; six different coordinates are then assigned to each of the unsprung masses, among them only those relating to the vertical displacement are considered independent. All the others are in fact constrained by the suspension geometry. Finally, a set of independent coordinates, in this case 10, is reserved to modal coordinates for chassis deformation.

All translations are referred to the inertial reference system while rotations are described using a body reference system. A local reference system is defined for each of the bodies, see Figure 6.1. All the coordinates of the wheels, except for the rotation about the y-axis, are coincident with those of the unsprung masses.

The reference system of the sprung mass is aligned in such a manner that when the vehicle is in rest position, both its x_S- and y_S-axes are horizontal and they

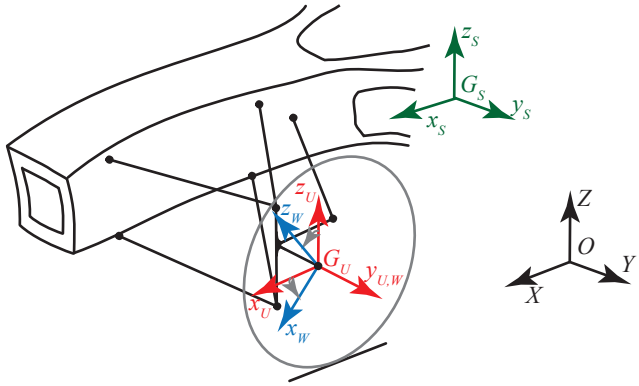

Figure 6.1: Coordinate reference systems.

point respectively forwards and leftwards while the z_S-axis is vertical and pointing upwards. The centre of gravity of each unsprung masses is considered coincident with the corresponding wheel centre. The local y_U-axis is considered coincident with the rotation axis of the wheel, the x_U-axis horizontal and pointing forward and the z_U-axis pointing upwards. The wheel reference system (subscript W) is obtained from the unsprung mass reference system by means of a rotation about the wheel axis.

Different rotation sequences are employed for the evaluation of the rotation matrices of the bodies. The rotation matrix of the sprung mass is obtained using the standard yaw–pitch–roll sequence, described in Equation (5.5). For the unsprung masses and the wheels, the rotation about the y^*-axis follows the one about the x^*-axis so that the toe–camber–spin sequence is respected.

Suspension geometry

The vehicle is assumed to be equipped with double wishbone suspensions with push rod/pull rod type suspension and rocker arm. Other suspensions could be considered, the methodology being the same. As the suspension components are considered massless, they are modelled as ideal links that constrain the relative motion of the sprung and of the unsprung mass. In order to model the suspension kinematics, it is possible to define for each corner 14 hard points that describe its geometry. This is represented in Figure 6.2 and described in Table 6.2.

Some of the suspension hard points belonging to the sprung or to the unsprung mass will be used for the definition of the constraints, they are therefore called connecting points. They are points A, B, C, E, F, H, L and M. Other points are located on parts which are not modelled as real bodies. They will be used for the evaluation of the suspension loads.

While points belonging to the sprung masses are defined by their position in the

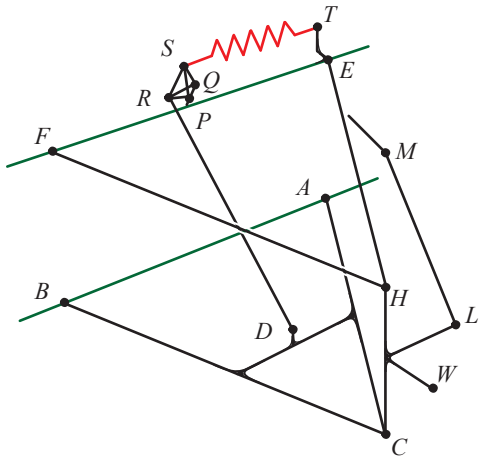

Figure 6.2: Double wishbone suspension geometry and hard points.

local reference frame, points on the unsprung mass also require a subset of modal shapes to be defined so that, once the modal coordinates are evaluated, the deformation vector can be evaluated. This is achieved by defining, in the symbolic code, a relationship between modal shapes and point markers. The steering system is modelled as a purely kinematic system capable of moving points M along the y-axis direction of the sprung mass. Under the assumption of a constant rack ratio k_{stw}, a lateral displacement of $\pm k_{stw}\delta_{stw}$ is therefore superimposed to the position of point M given by the kinematic relationship of Equation (5.6).

6.1.3 Constraints

Both the wishbones and the track rods are modelled by means of rigid and massless link joints, see Section 5.3. Each of the wishbones is modelled by means of two link joints that connect its pivot points to the unsprung mass. This approximation is valid under the assumption that a lateral force applied to the wishbone is transmitted to the chassis by two components which are aligned with the members of the wishbone itself.

The concept is represented in Figure 6.3. If the wishbone is considered as a single body, Figure 6.3a, a force perpendicular to its pivot axis, defined by the points A and B, only generates reactions that are perpendicular to the pivot axis. If the wishbone is instead considered as a composition of two distinct rods, Figure 6.3b, the reaction forces are aligned with the rods and have a component parallel to the pivot axis. The total reaction force is equal in the two cases but the load distribution is different. Due to the structure of the suspensions of race cars, it is reasonable to assume that wishbones tend to be more correctly described by the second model.

Table 6.2: Hard points of the front left suspension.

Point	Description	Body
A	lower wishbone rear pivot	sprung mass
B	lower wishbone front pivot	sprung mass
C	lower wishbone outer ball joint	unsprung mass
D	push rod wishbone end	lower wishbone
E	upper wishbone rear pivot	sprung mass
F	upper wishbone front pivot	sprung mass
H	upper wishbone outer ball joint	unsprung mass
L	inner track rod ball joint	sprung mass
M	outer track rod ball joint	unsprung mass
P	rocker axis 1^{st} point	sprung mass
Q	rocker axis 2^{nd} point	sprung mass
R	push rod rocker end	rocker arm
S	damper to rocker point	rocker arm
T	damper to body point	sprung mass

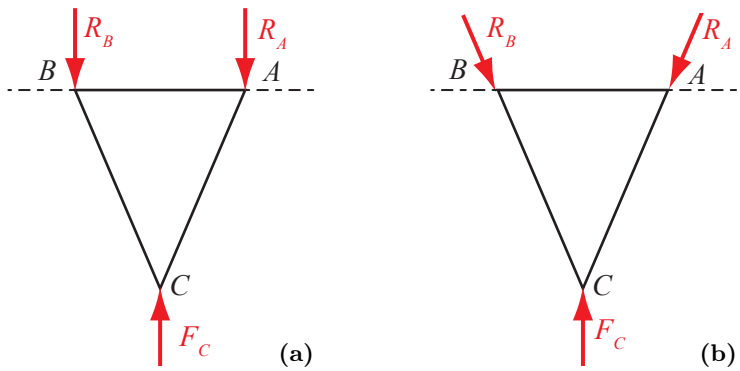

Figure 6.3: Transmission of lateral forces over a suspension wishbone. (a) Single body assumption. (b) Double body assumption.

By definition, massless links are not capable of transmitting external forces to the bodies they connect; a particular treatment is therefore needed for modelling the wishbones to which a push rod or a pull rod is connected. Further details on this subject are presented in Section 6.1.5.

Table 6.3 reports a description of the links employed for the definition of the suspension geometry. Each link is characterised by a constant length and removes one

Table 6.3: Links of the double wishbone suspension.

Link	1^{st} point	2^{st} point
lower wishbone rear side	A	C
lower wishbone front side	B	C
upper wishbone rear side	E	H
upper wishbone front side	F	H
track rod	L	M

degree of freedom. The length of each link is evaluated in a preprocessing routine on the basis of the at-rest configuration of the vehicle. This modelling approach guarantees both the exact modelling of the suspension kinematics and the possibility of evaluating the forces acting on the chassis. The latter point is particularly important when the flexibility of the chassis is included. Globally, 20 degrees of freedom are removed by the constraints; according to the Equation (4.5), the system has therefore 14 degrees of freedom.

It is worth noting that the constraint equations not only depend on the position of the connecting points, which in turn depend on the vector of generalised coordinates $\boldsymbol{q}$, but also on the steering angle input δ_{stw}. Thus, the system is rheonomic.

6.1.4 Dynamics

Each of the nine bodies is assigned a mass matrix which is defined in the local reference system. The rigid part of the sprung mass of the vehicle is considered symmetric with respect to a longitudinal plane. As a consequence, all the terms outside the main diagonal of the inertia tensor, except for those relative to the product of inertia about the $x-z$ plane, are considered equal to zero, [25]. Let m_s be the vehicle sprung mass, J_{xs}, J_{ys} and J_{zs} respectively, the body moments of inertia about the x-, y- and z-axes. The rigid part of the mass matrix of the sprung mass is then:

$$\bar{\boldsymbol{M}}_s = \begin{bmatrix} m_s & 0 & 0 & 0 & 0 & 0 \\ 0 & m_s & 0 & 0 & 0 & 0 \\ 0 & 0 & m_s & 0 & 0 & 0 \\ 0 & 0 & 0 & J_{xs} & 0 & J_{xzs} \\ 0 & 0 & 0 & 0 & J_{ys} & 0 \\ 0 & 0 & 0 & J_{xzs} & 0 & J_{zs} \end{bmatrix} \tag{6.1}$$

Because of body flexibility, a set of deformation-dependent terms is automatically added to the matrix of Equation (6.1), see Equation (5.37). Due to the symbolic and

parametric definition of the vehicle properties however, the possibility of changing important vehicle parameters by tuning single body properties is retained.

Every vehicle corner is composed of two bodies: an unsprung mass and a wheel. The former has the mass, the cambering and the yawing inertia of all the corner. Its polar moment of inertia relative to the y-axis, here called pitching moment, is equal to the corner inertia when all the rotating parts, including the wheel, are removed. The reference system is considered to be coincident with the principal axes of inertia, so that the constant mass matrix of a generic unsprung mass is diagonal. For the front left unsprung mass for example, it is:

$$\bar{\boldsymbol{M}}_{uFL} = \begin{bmatrix} m_{uFL} & 0 & 0 & 0 & 0 & 0 \\ 0 & m_{uFL} & 0 & 0 & 0 & 0 \\ 0 & 0 & m_{uFL} & 0 & 0 & 0 \\ 0 & 0 & 0 & J_{xuFL} & 0 & 0 \\ 0 & 0 & 0 & 0 & J_{yuFL} & 0 \\ 0 & 0 & 0 & 0 & 0 & J_{zuFL} \end{bmatrix} \tag{6.2}$$

in which J_{xuFL}, J_{yuFL} and J_{zuFL} represent, respectively, the cambering, the pitching and the yawing moments of inertia of the unsprung mass.

Wheels are considered massless discs and have only one term of the inertia tensor that is different from zero: the polar moment I_{wFL}. The constant mass matrix of a generic wheel is therefore:

$$\bar{\boldsymbol{M}}_{wFL} = \begin{bmatrix} 0 & 0 & 0 & 0 & 0 & 0 \\ 0 & 0 & 0 & 0 & 0 & 0 \\ 0 & 0 & 0 & 0 & 0 & 0 \\ 0 & 0 & 0 & 0 & 0 & 0 \\ 0 & 0 & 0 & 0 & J_{wFL} & 0 \\ 0 & 0 & 0 & 0 & 0 & 0 \end{bmatrix} \tag{6.3}$$

After the definition of the geometric and inertial properties of the bodies that compose the vehicle model, the total mass matrix of the system is automatically assembled by means of the command `makebodies`, see Table 5.2. Interestingly, as far its projection over matrix $\boldsymbol{TR}$ is invertible, a singular mass matrix does not constitute a problem. This means that it is possible, for example, to use null values of I_{xu}, I_{yu} or I_{zu}. It is worth mentioning that the majority of the models available in the literature consider a constant mass matrix. During roll motion however a large movement of the rotation axis of the unsprung mass may occur and the difference between the real mass matrix and the constant one can be substantial. The complete vehicle is considered symmetric so that the parameters of two unsprung masses or wheels of the same axle are considered equal. As a consequence, only 15 rigid body inertial parameters are left: 5 for the sprung mass, 4 for the front unsprung mass, 4 for the rear one and 4 for the wheels.

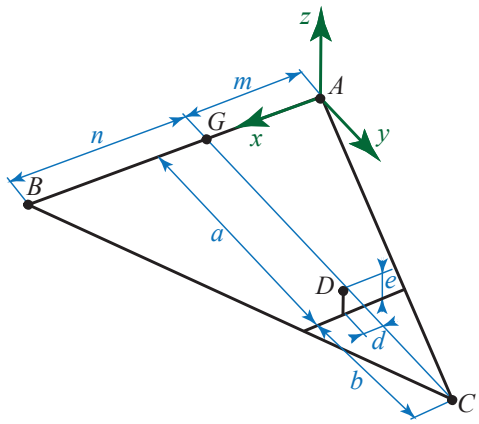

Figure 6.4: Lower wishbone geometry.

6.1.5 External loads

The numerical solution of the equations of motion requires the definition of the set of external loads the multibody system is subject to. The forces considered are those applied by the suspension, by the tyres, by the powertrain unit and by the aerodynamics elements.

Suspension forces

Suspension forces are generated by the spring-damper unit and transmitted through the rocker arm and the lower wishbone to the sprung and unsprung masses. The system can be seen as a kinematic and force loop and it is entirely described in the sprung mass reference system. With the knowledge of the position and of the velocity of the lower wishbone, it is possible to calculate the position and the velocity of the push rod and of the rocker arm. From this, the displacement and the velocity of the spring-damper unit and, in turn, the forces generated can be evaluated. These forces are then applied, through the rocker arm and the push rod, to the lower wishbone and from this to the sprung and unsprung masses. The analytical derivation of the process is rather long; only the most important parts are therefore reported.

Wishbone geometry. The wishbone of the front left suspension is represented in Figure 6.4. The geometry is parametric so that it is possible to develop the calculations analytically. The values of the parameters are calculated on the basis of the input configuration of the vehicle. The wishbone is connected through points A and B to the chassis and through point C to the unsprung mass. Point D is the connection point of the push rod.

A local coordinate system of the wishbone is designated as follows. The x-axis is

placed along the joint axis that connects its pivot points, the y-axis is chosen along the line perpendicular to the x-axis and lying in the plane ABC. The z-axis is located perpendicular to xy-plane and directed upwards. The origin of the reference system is considered point A. A set of three Euler angles, based on the yaw–pitch–roll sequence and described by the angles α_z, α_y, α_x describes the transformation from the sprung mass reference system to the local one.

The positions of points A, B and C are provided by the main multibody code. Point D however is not part of any of the real bodies and its position has to be determined in a different manner. To this purpose, it is possible to use Equation (5.6) once the position of point A, the rotation matrix of the wishbone and its geometry are known.

In order to evaluate the rotation matrix, the three rotation parameters of the wishbone have to be derived. The position of point B, expressed in the sprung mass reference system, can be written as:

$$ {}_S\boldsymbol{x}_B = {}_S\boldsymbol{x}_A + {}_S\boldsymbol{A}_W \, {}_W\boldsymbol{x}_B \tag{6.4} $$

where ${}_S\boldsymbol{A}_W$ denotes the rotation matrix of the transformation from the sprung mass reference system to the wishbone one while ${}_W\boldsymbol{x}_B$ is the position of point B in the wishbone reference system. From this, it follows that:

$$ {}_S\boldsymbol{A}_W \, {}_W\boldsymbol{x}_B = {}_S\boldsymbol{x}_B - {}_S\boldsymbol{x}_A \tag{6.5} $$

The chosen reference system makes ${}_W\boldsymbol{x}_B = [m+n \quad 0 \quad 0]^T$; as a consequence Equation (6.5) is equivalent to:

$$ \begin{bmatrix} \cos\alpha_z \cos\alpha_y & -\sin\alpha_z & \cos\alpha_z \sin\alpha_y \\ \sin\alpha_z \cos\alpha_y & \cos\alpha_z & \sin\alpha_z \sin\alpha_y \\ -\sin\alpha_y & 0 & \cos\alpha_y \end{bmatrix} \begin{bmatrix} m+n \\ 0 \\ 0 \end{bmatrix} = \begin{bmatrix} {}_Sx_B - {}_Sx_A \\ {}_Sy_B - {}_Sy_A \\ {}_Sz_B - {}_Sz_A \end{bmatrix} \tag{6.6} $$

From this:

$$ \begin{cases} \sin\alpha_y = -\dfrac{{}_Sz_B - {}_Sz_A}{m+n} \\ \\ \cos\alpha_y = \sqrt{1 - sin^2\alpha_y} \end{cases} \qquad \begin{cases} \sin\alpha_z = -\dfrac{{}_Sz_B - {}_Sz_A}{(m+n)\cos\alpha_y} \\ \\ \cos\alpha_z = \sqrt{1 - sin^2\alpha_z} \end{cases} \tag{6.7} $$

It should be noticed that, as the wishbone rotates about its x-axis, the values of α_z and α_y are constant and their computation is needed just once. It is therefore computed during the preprocessing of the input data.

A similar procedure is adopted in order to find the third rotation angle, α_x. As the coordinates of point C in the wishbone reference system are ${}_W\boldsymbol{x}_C = [m \;\; a+b \;\; 0]^T$, it is possible to derive an expression similar to Equation (6.6), and, as a consequence,

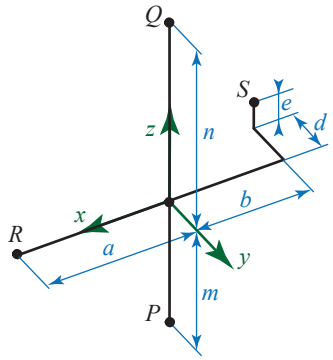

Figure 6.5: Rocker arm geometry.

the values of $\sin\alpha_x$ and $\cos\alpha_x$. These expressions are not reported here for the sake of brevity. The angle α_x is not constant and it is evaluated at each time step. Due to the analytical nature of the calculations however, its computational cost is very small.

The rotation matrix ${}_S\boldsymbol{A}_W$ can then be completed and the relative position of point D evaluated as:

$$ {}_S\boldsymbol{x}_D = {}_S\boldsymbol{x}_A + {}_S\boldsymbol{A}_W\, {}_W\boldsymbol{x}_D \tag{6.8} $$

Rocker arm and push rod. The rocker arm is considered as a massless body and has the geometry of Figure 6.5. Points P and Q define its rotation axis while points R and S indicate, respectively, the push rod and the spring-damper unit connection points. In order to identify the position of point S, a procedure similar to the one adopted for point D is employed. Three rotation parameters define the coordinate transformation from the chassis reference system to the rocker arm one. The first two parameters are determined in the preprocessing routine. The third parameter, the one related to the rotation of the rocker arm about its axis, depends on the position of the lower wishbone, to which the rocker arm is connected by means of the push rod.

Because of the presence of the push rod, the distance between points D and R is constrained. The value of the rotation angle of the rocker arm can be found imposing the following constraint:

$$ \| {}_S\boldsymbol{x}_D - {}_S\boldsymbol{x}_R \| = l_p \tag{6.9} $$

where l_p represents the length of the push rod. As the problem is non-linear, it is solved iteratively using a Newton-Raphson method. Note that, as the model is symbolically developed, it is possible to calculate the gradient of the error function in a straightforward manner so that the iterative method is particularly efficient. Furthermore, in order to improve the computational efficiency, the position evaluated at the previous time step of the simulation is used as a starting point of the iteration.

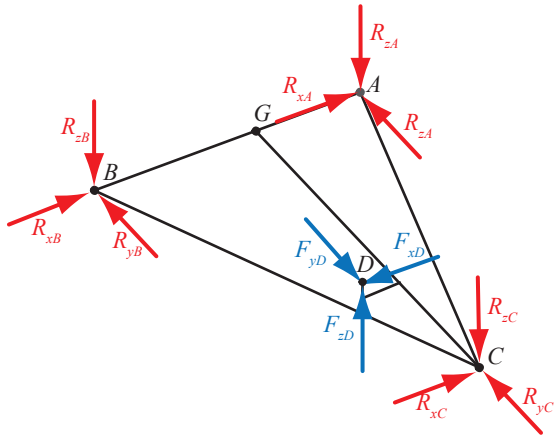

Figure 6.6: Lower wishbone free body diagram.

The evaluation of the rotation angle of the rocker allows the evaluation of position and velocity of point S which is connected to the spring-damper unit. It is therefore straightforward to evaluate the spring length and its time derivative, respectively $l_s = l_s(\boldsymbol{q})$ and $\dot{l}_s = \dot{l}_s(\boldsymbol{q}, \dot{\boldsymbol{q}})$.

Spring-damper unit. The force generated by a generic spring-damper unit can be modelled by means of the equation:

$$F = F(l_s, \dot{l}_s) \tag{6.10}$$

Linear or non-linear models can be found in the literature, the one here adopted is based on non-linear look-up tables.

Rocker arm and push rod forces. The force F of Equation (6.10), generated by the spring-damper unit, is applied to the vehicle body at point T and to the rocker arm at point S, see Figure 6.2. The force applied to point S of the rocker arm is balanced by the reactions of points P and Q and by the force applied by the push rod at point R. The first two points allow the rocker arm to rotate about its axis and constrain any axial movement. A moment equilibrium equation about the rotation axis of the rocker arm permits the evaluation of the force applied to the push rod.

Lower wishbone forces. The push rod transmits the rocker arm force to the lower wishbone. The force is applied at point D and withstood at points A, B and C of Figure 6.6. Because of their nature, however, the links used to model the suspension wishbone only transmit the forces necessary for the system to satisfy the constraint equations and cannot transmit any external force.

In this area, an interesting development was shown by Sohn et al., [145, 146]. Forces acting on the links were resolved and transmitted to the attachment points with a quasi-static assumption. The lower wishbone was modelled by superimposing a massless body capable of transmitting external forces onto the described links that connect the unsprung mass and the sprung mass. Because of the parametric geometry of the lower wishbone model, simple and generic equations can be derived.

Firstly, it is possible to merge points A and B into point G and to consider the whole wishbone as a beam lying in the plane $x-y$ and having the inner end fixed (at point G both rotation and translation are constrained) and the outer end simply supported (at point C only the translation is constrained). The beam is then loaded with an intermediate force and a moment which derives from the transposition of the push rod forces to the GC line.

Under the assumption of a constant beam section and elastic material, the components F_x, F_y and F_z of the push rod force can be distributed between points G and C. The following analytical expressions for the reactions are derived, [147]:

$$\begin{cases} R_{xG} = \dfrac{b}{2l^3}(3l^2 - b^2)F_{xD} + \dfrac{3d}{2l^3}(l^2 - b^2)F_{yD} \\ R_{yG} = \dfrac{b}{l}F_{yD} \\ R_{zG} = \dfrac{b}{l}F_{zD} + \dfrac{e}{l}F_{yD} \\ M_{zG} = \dfrac{b}{2l^2}(l^2 - b^2)F_{xD} - \dfrac{3d}{2l^2}(l^2 - b^2)F_{yD} \end{cases} \quad \begin{cases} R_{xC} = \dfrac{a^2}{2l^3}(3l - a)F_{xD} + \\ \qquad -\dfrac{3d}{2l^3}(l^2 - b^2)F_{yD} \\ R_{yC} = \dfrac{a}{l}F_{yD} \\ R_{zC} = \dfrac{a}{l}F_{zD} - \dfrac{e}{l}F_{yD} \end{cases} \tag{6.11}$$

where $l = a + b$. If the plane $x-z$ is considered, it is possible to distribute the reaction calculated for point G to the real hard points A and B:

$$\begin{cases} R_{xA} = \dfrac{n}{p}\, R_{xG} \\ R_{yA} = \dfrac{n}{p}\, R_{yG} + \dfrac{1}{p}\, M_{zG} \\ R_{zA} = \dfrac{n}{p}\, R_{zG} + \dfrac{e}{p}\, F_{xD} \end{cases} \quad \begin{cases} R_{xB} = \dfrac{m}{p}\, R_{xG} \\ R_{yB} = \dfrac{m}{p}\, R_{yG} - \dfrac{1}{p}\, M_{zG} \\ R_{zB} = \dfrac{m}{p}\, R_{zG} - \dfrac{e}{p}\, F_{xD} \end{cases} \tag{6.12}$$

where $p = m + n$. The described procedure is valid for all the four lower wishbones and permits to distribute the force of the push rods to the sprung and unsprung masses in a simple and efficient way. The forces applied by the suspension components to the points A, B, C, P, Q and T of Figure 6.2 are therefore evaluated.

Tyres

Tyres are fundamental components that are responsible for the generation of the forces between the vehicle and the road. An extensive research activity has resulted in several tyre models, a review of which can be found in [148]. As in many other cases, the complexity of the tyre model to be adopted is related to the particular application. For vehicle handling simulations, the Pacejka, the Fiala or other semi-empirical tyre models are usually adopted. They all consist of routines that calculate the forces and the moments applied to the wheel centre and control the movement of the vehicle. As stated in [148], for handling simulations the vertical, the longitudinal and the lateral forces, as well as the aligning moment have to be considered. In the present model, the road is treated as planar and horizontal, the normal to the road plane is therefore coincident with the z-axis of the inertial reference system.

All the available tyre models require as inputs the normal force applied to the contact patch, the tyre side slip angle, its camber angle and the longitudinal slip. While the vertical force acting on the tyre contact patch is given by a stiffness and a damping contribution, the other required inputs are evaluated by using position and velocity values extracted from the multibody code. For sake of brevity, their expressions are not here reported. Lateral and longitudinal forces, as well as aligning moments, are evaluated by means of the 1996 Pacejka Magic Formula, [73].

It has been shown that tyre lag is an important phenomenon when the transient response of the vehicle is analysed, [43, 149, 150]. This phenomenon is described by means of a first order lag applied to the inputs of the Magic Formula. Two relaxation lengths are considered: σ_α for the side slip input and σ_κ for the longitudinal slip.

Powertrain

In order to generate realistic loads on tyres and on suspensions, a powertrain model is introduced. It is not among the objectives of the present activity to build a complete and detailed model of the engine and of the vehicle driveline; a simplified PID controller capable of controlling the torque applied to the rear driving wheels is therefore adopted.

Aerodynamics

In general, six aerodynamic loads are applied to a ground vehicle, [20, 25]. In the present work, only three of them are considered: the drag force, the down force and the pitching moment. All of them are evaluated as a function of the velocity of the vehicle with respect to the wind by means of interpolation functions. The calculated values are then applied to the sprung mass.

Driver model

In order to ease the execution of the simulations, a driver model is included. It consists of a logic unit capable of controlling the simulation inputs according to open- or closed-loop predetermined laws. In this manner, most of the manoeuvres commonly used for vehicle dynamics simulations can be reproduced.

6.2 Vehicle data

6.2.1 General data

Data of the 2009 Formula Student vehicle of the University of Surrey are used for the simulations. The vehicle has front and rear double wishbone suspension, a 600cc engine and it is characterised by total mass of 290 kg including driver. Data are reported in Appendix B. Table B.1 reports the general vehicle data while Tables B.2 and B.3 describe the position of the hard points of the front and rear left suspensions expressed using a local reference system. The vehicle is equipped with Goodyear FSAE 20.0x7.0-13 D2692 tyre, described in Table B.4. Coefficients for the Pacejka tyre model were derived from experimental data available through the Formula Student Tyre Consortium, graphs reporting tyre characteristics are included in Figure B.1.

6.2.2 Chassis

The chassis of the vehicle consists of a tubular space frame made from high strength steel and welded brackets. In this sense, the considered chassis is not a true space frame, partly because of several design constraints, partly because of lack of optimisation. The chassis weights 23.5 kg and has a measured torsional stiffness of 360 Nm/deg, [151].

Finite element model

The analysis of the chassis is carried out through the use of a finite element model built in the Ansys environment. The geometry is imported from an available CAD model; a mesh is then created by using the Ansys PIPE16 and BEAM4 elements. The BEAM4 element is a uniaxial element with tension-compression, torsion, and bending capabilities. The element is defined by two nodes with six degrees of freedom each: translations in the nodal x, y, and z directions and rotations about the nodal x, y, and z axes, [152]. While structures with a non-circular section are modelled by means of the BEAM4 element, the others are meshed by means of the PIPE16 element. This is based on the same beam element BEAM4 and includes simplifications due to its circular section. A representation of the finite element model of the chassis is reported in Figure 6.7.

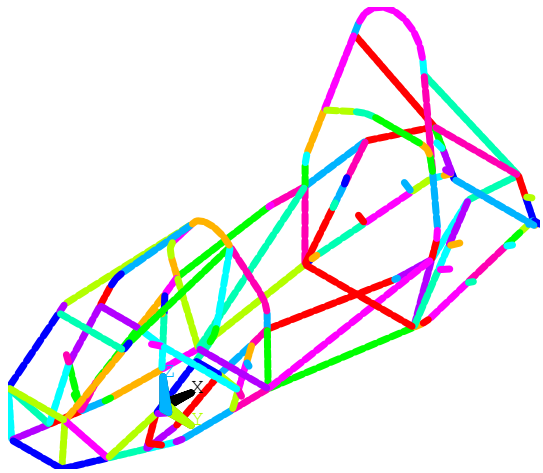

Figure 6.7: Finite element model of the chassis.

The static torsional stiffness of the chassis was previously measured, [151]. The procedure implies two points of the rear part of the chassis lying symmetrically with respect to the longitudinal plane of the vehicle and a point at the front of the chassis to be simply constrained to the ground. A vertical load is then applied to a point opposite to the third one and the deflection of several points of the chassis measured, see Section 2.1.4. From this test a value of torsional stiffness of 360 Nm/deg was measured. Although a detailed estimate of the accuracy of the measure was not carried out, it is reasonable to assume it within 5%. An equivalent set-up is reproduced within the finite element model. The deflection of the nodes receiving the load is measured and the chassis torsional stiffness calculated. The value of chassis torsional stiffness obtained through the finite element model is 385 Nm/deg; a value that is consistent with experimental results.

Modal reduction

A modal reduction technique is employed for the inclusion of chassis compliance within the vehicle model. To this end, files containing the mass and stiffness matrices, tables containing the positions of the nodes and key points and mapping files are exported from the finite element code. A set of routines that evaluate a reduced order model was then implemented in the Matlab environment. In particular, two of the most widely used techniques, namely modal truncation and component mode synthesis were implemented.

Modal truncation. The modal truncation technique requires the modal basis to be formed by a set of eigenvectors corresponding to the lower natural frequencies of

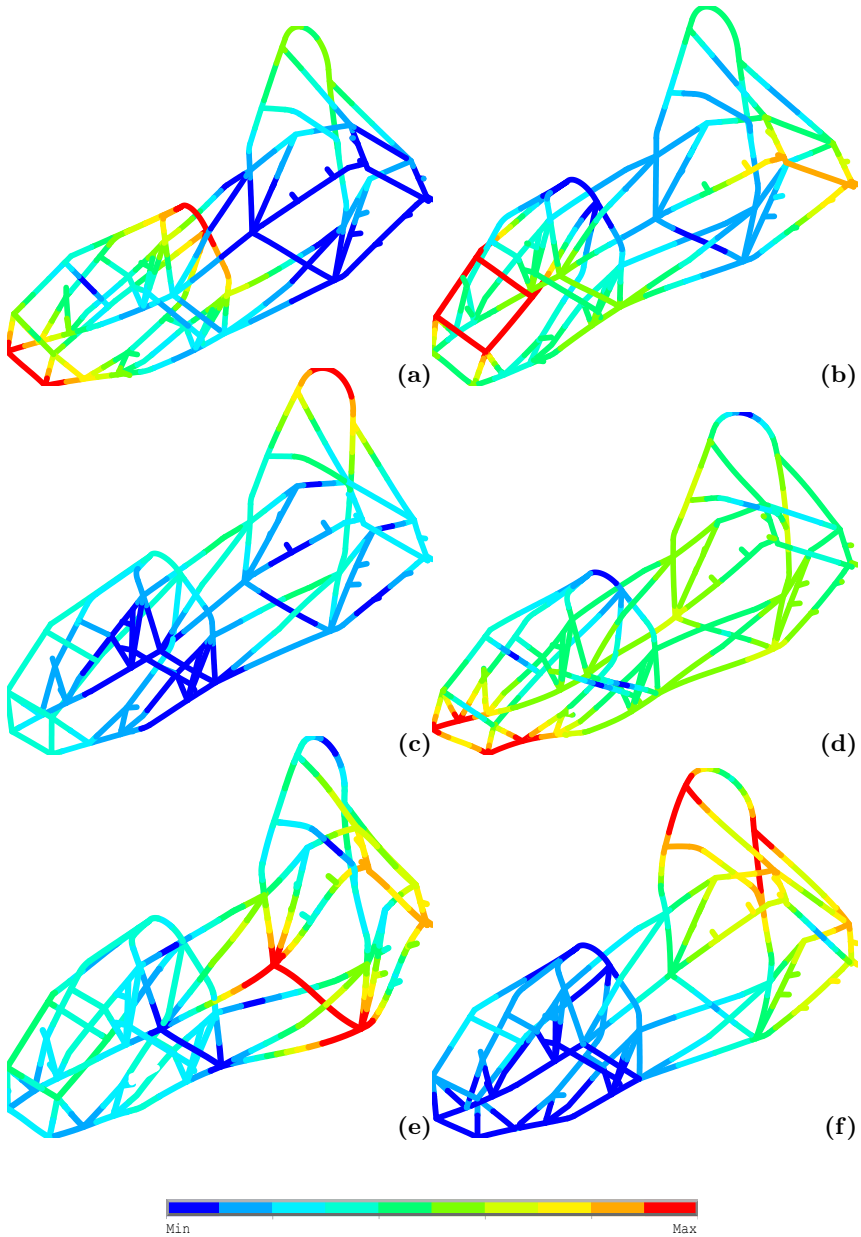

Figure 6.8: Six lowest modes of the chassis. (a) Mode 1, natural frequency 38.35 Hz. (b) Mode 2, natural frequency 54.88 Hz. (c) Mode 3, natural frequency 63.92 Hz. (d) Mode 4, natural frequency 79.23 Hz. (e) Mode 5, natural frequency 92.42 Hz. (f) Mode 6, natural frequency 103.21 Hz.

the component. It has been shown that this approach often requires the use of a high number of modes and that, when stiffly constrained systems are considered, it is inadequate. When a vehicle chassis is considered, it appears that the constraints acting on the chassis, e.g. the suspension system, can be considered weak. As a

Table 6.4: Natural frequencies and modes of vibration of the chassis.

Mode	Frequency [Hz]	Mode description
1	38.35	Front torsion
2	54.88	Lateral bending
3	63.92	Vertical bending
4	79.23	Horizontal losenging
5	92.42	Rear losenging
6	103.21	Rear torsion

consequence, the use of a limited set of free-free modes can be considered as a valid approach for modal representation of chassis compliance. This approach was also successfully employed for the analysis of the effects of chassis compliance on vehicle handling in [59].

According to this approach, eigenvalues and eigenvectors are extracted from the mass and stiffness matrices of the finite element model. After elimination of the null-energy modes, a set of the lowest natural frequencies and corresponding modes of vibration is extracted. As an example, the first six modes are represented in Figure 6.8. The analysis of the modal shapes permits to assign each of the modes main deformation characteristics. For example, mode 1 mainly corresponds to a torsional deformation of the front part of the chassis, mode 2 to a lateral bending and mode 3 to a vertical bending. Further details are shown in Table 6.4.

Component modal synthesis. Component modal synthesis, also known as the Craig-Bampton method, represents the most widespread modal reduction technique currently employed in multibody system dynamics. As described in Section 4.6.2, this approach involves the definition of a set of master nodes that represents the points at which external loads or constraints are attached. To this purpose, all the suspension attachment points are defined as master nodes, for a total of 32 master nodes. All the other nodes are therefore defined as slaves.

After extraction, the generated Craig-Bampton modal basis is transformed into an equivalent, orthogonal basis with modal coordinates. The orthogonalized Craig-Bampton modes are not eigenvectors of the original system. They are eigenvectors of the Craig-Bampton representation of the system and as such have a natural frequency associated with them. Constraint modes are replaced with boundary eigenvector while fixed-boundary modes are replaced with an approximation of the eigenvectors of the unconstrained body. This is an approximation because it is based only on the Craig-Bampton modes. Six of these modes are usually the rigid body modes and can

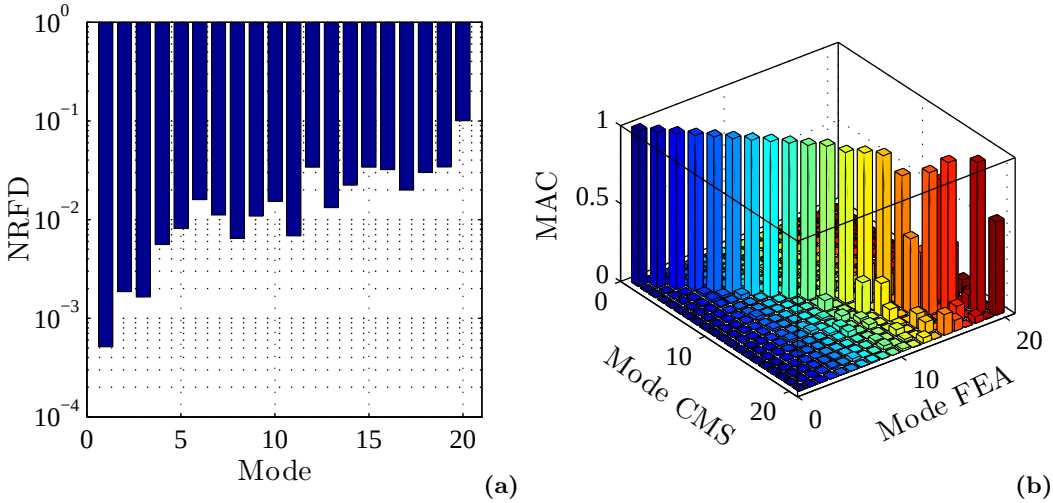

Figure 6.9: Comparison between modal truncation and component mode synthesis. (a) Normalised Relative Eigenfrequency Difference. (b) Modal Assurance Criterion.

be eliminated. Although the removal of any mode constrains the body from adopting the shape associated with it, removing some high-frequency modes is much more tolerable than the removal of any constraint modes because it does not prevent the associated boundary node from moving relative to its neighbours but it only prevents boundary edges from reaching a certain configuration. It is therefore possible to reduce the number of modal variables.

A comparison between the first 20 modes generated by the modal truncation and component mode synthesis techniques is presented in Figure 6.9. Values of normalised relative eigenfrequency difference (NRFD) are reported in Figure 6.9a. The graph reveals that low values of NRFD, smaller than 10^{-2}, are found for the first 10 modes; low eigenfrequencies calculated by means of the two methods are therefore very similar. The correlation between the relative eigenvectors is high.

Values of modal assurance criterion (MAC) between the two techniques are reported in Figure 6.9b. This criterion consists of a mass-normalised measure of the dot product of two eigenvectors; values of MAC=0 and MAC=1 can therefore be interpreted respectively as null and total correlation between the eigenvectors. According to the graph, a high correlation exists for the lowest ten modes; starting from mode 12, correlation is less pronounced. Good correlation found in graphs of Figure 6.9 suggests that, in the considered frequency range, the impact of the internal modes of the chassis is limited and that, as a consequence, the set of free-free modes obtained through the modal truncation technique can be employed. Furthermore, several trials have shown that no additional benefit is obtained if more than six modes are used. As a consequence, all the results presented in Chapter 7 have been obtained under the assumption of free-free boundaries.

Table 6.5: Comparison of CPU time for different solvers.

Manoeuvre	Steering step	Steering ramp	Steering sweep
Duration [s]	5	25	120
CPU time [s]			
RK9ST	2.5	2.5	29.0
DLSODE	1.0	2.3	21.0
DLSODI	2.5	1.8	27.0
DASSKR	0.7	2.1	9.4

6.3 Model Implementation

6.3.1 Main program

The vehicle model is generated by means of the described symbolic multibody library. A first version of the model was exported in Matlab language and introduced in a Simulink model through the use of a Matlab S-function. Although this solution fully exploits the capabilities of Matlab, it proved to be particularly inefficient from the computational point of view. For this reason, a purpose-developed Fortran program is employed. The program includes a set of routines for importing simulation data and exporting simulation results, it includes the solver routine and the computational routines generated by means of the Maple scripts. Initial trials revealed that, compared to a Matlab Simulink implementation, the use of a native code leads to a computational efficiency generally 50 times higher.

6.3.2 ODE Solver

One of the advantages offered by the chosen implementation is that a variety of solver routines is available. On the basis of the literature review, a set of the most widespread solvers for the numerical integration of the derived differential equations was chosen. The first of the solvers considered, RK9ST, is based on a Runge-Kutta-Merson method and is capable of solving non-stiff and middle-stiff ODE systems. The solvers DLSODE and DLSODI instead are, respectively, an explicit and implicit implementation of the original LSODE routine, see Section 4.10. Similarly to the DASSL solver on which it is based, the routine DASSKR consists of an implicit solver based on an implicit backward differentiation formula. Computational time for a steering step manoeuvre, for a steering ramp and for a steering sweep are reported in Table 6.5; all simulations are run at a constant speed of 50 km/h. Relative error tolerance is set to 0.1% and a computer equipped with an Intel Core 2 Duo processor and with 2Gb of RAM

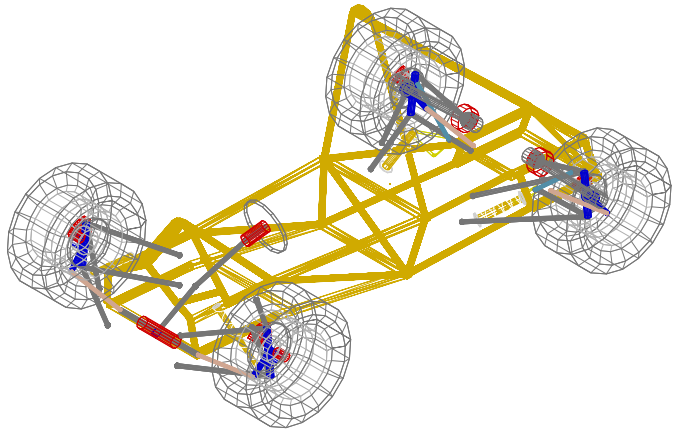

Figure 6.10: Adams/Car multibody model of the vehicle.

is employed.

Although it was originally developed for differential-algebraic problems, data of Table 6.5 show that DASSKR generally performs better than the other codes. Furthermore, trials have shown that the routine is capable of maintaining its computational advantages when the tolerance is decreased, the stiffness of the problem is increased or its damping is decreased. For these reasons, all the results are obtained by means of this solver.

Computational efficiency of flexible multibody systems is largely affected by the amount of modal damping introduced, [59, 153]. Even if the internal damping of materials is usually low, it is common practice to introduce a certain amount of modal damping in order to improve computational efficiency. According to the literature, no significant impact on the simulation results is observed if the numerical damping is kept small, [153]. Proportional damping is introduced according to the definition $\boldsymbol{D} = \alpha \boldsymbol{M} + \beta K$. Trials have shown that the combination of $\alpha = 0$ and $\beta = 1\%$ is sufficient to guarantee good computational performance. For comparison, in [59], values of $\alpha = 2\%$ and $\beta = 5\%$ had to be used.

6.4 Rigid model verification

6.4.1 Adams/Car model

A comparison between the developed 14-degrees-of-freedom vehicle model and an equivalent model developed within the Adams/Car environment is presented here. Although a module which allows the use of flexible bodies is available, chassis flexibility has not been included. The model is based on available templates and is composed of 69 rigid bodies for a total of 414 dependent coordinates and 14 degrees of freedom; a

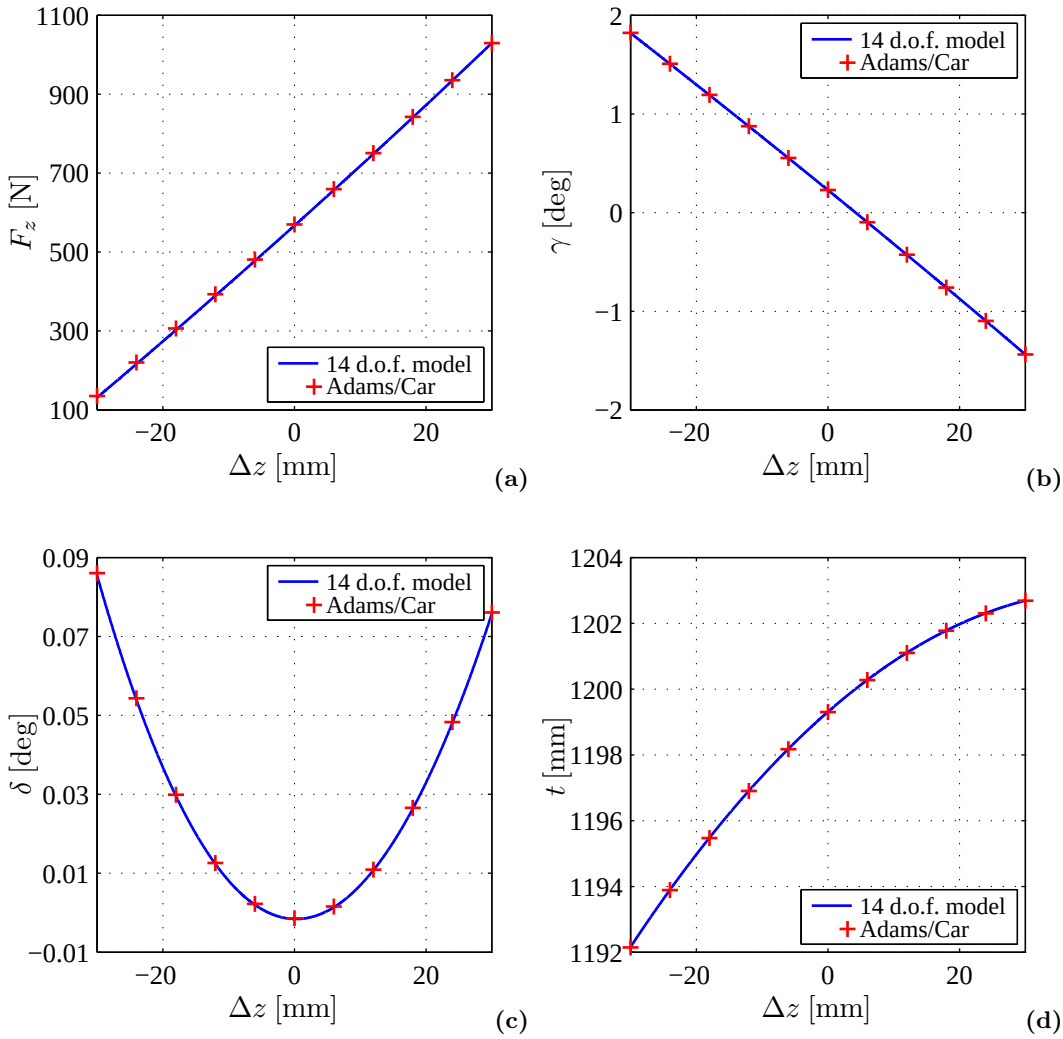

Figure 6.11: Comparative responses of the 14 d.o.f. model and Adams/Car during a bump test of the front suspension. (a) Tyre vertical load. (b) Camber angle. (c) Toe angle. (d) Total track width.

simplified representation is shown in Figure 6.10. Note that the graphical representation of the chassis is not intended to reflect its real shape. Geometry, inertial and tyre properties are relative the same as discussed in Section 6.2. More details are described in Appendix B.

6.4.2 Suspension kinematics

The multibody code Adams/Car offers a variety of routines that exercise suspension systems according to predetermined motion patterns. Among others, bump and steering tests are chosen. A specialised routine for suspension analysis is included

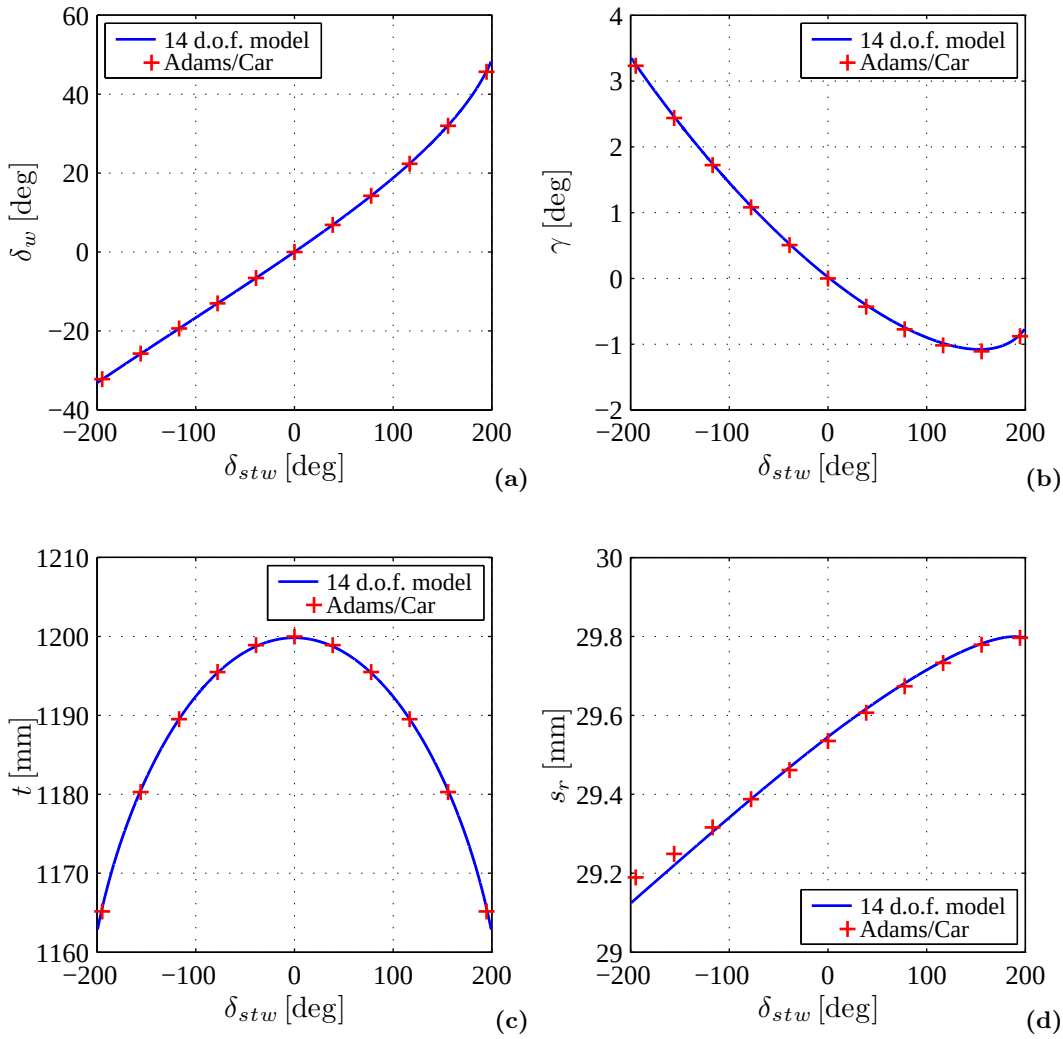

Figure 6.12: Comparison between of the 14 d.o.f. model and Adams/Car during a steering test. (a) Steer angle. (b) Camber angle. (c) Total track width. (d) Scrub radius.

in the developed 14-degrees-of-freedom vehicle model. This routine is capable of controlling the motion of the sprung mass while a suspension or the steering system is exercised.

Figures 6.11 compares the results obtained by means of the two models during a bump test of the front suspension. The variation of tyre vertical load, camber angle, toe angle and track width of the front and rear suspension versus body vertical motion are plotted. Similarly, steer angle, camber angle, total track width and scrub radius versus steering wheel angle during a steering test are shown in Figure 6.12; similar results can be produced for the rear suspension. As good agreement between the two simulation tools is found in all the cases, the kinematic model of the suspension

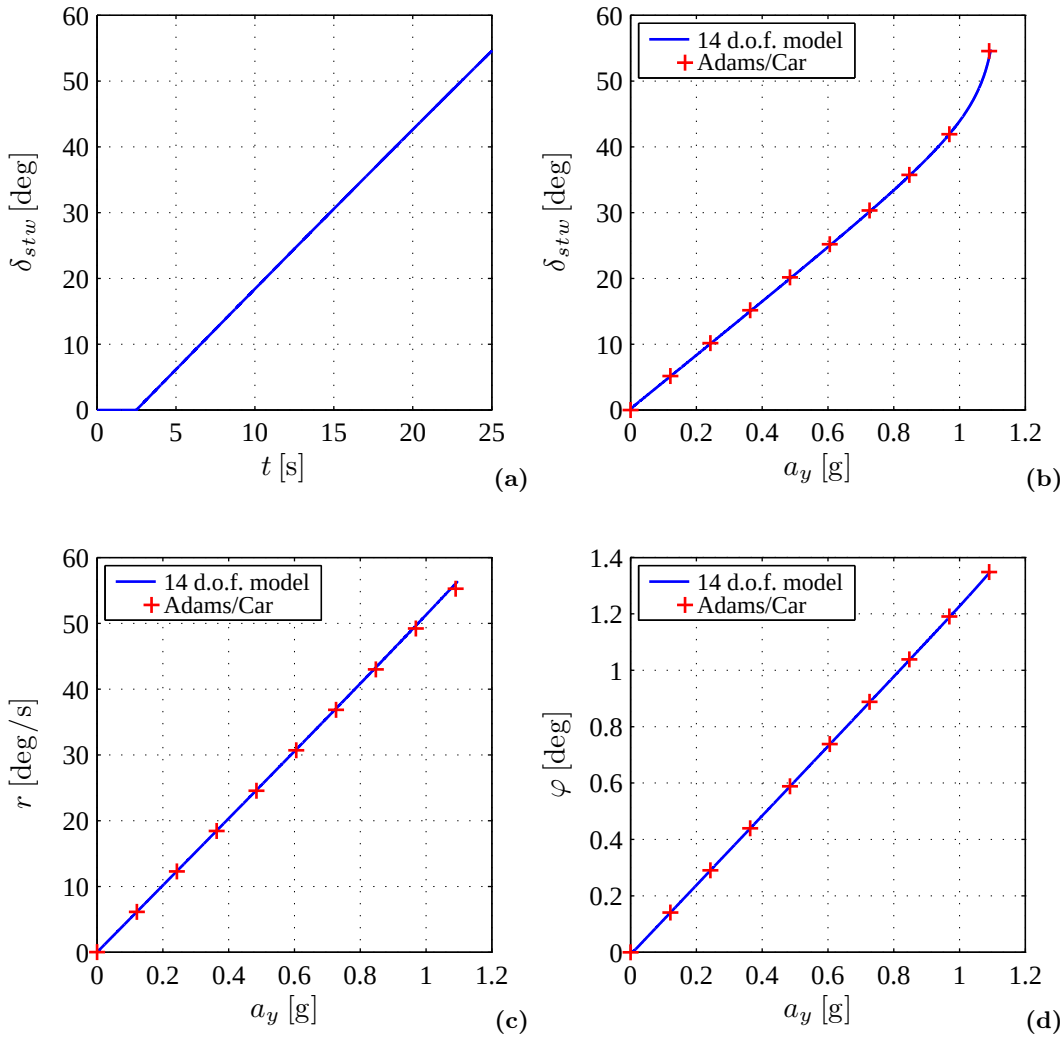

Figure 6.13: Comparative responses of the 14 d.o.f. model and Adams/Car during a ramp steer manoeuvre at 40 km/h. (a) Steering wheel input. (b) Lateral acceleration. (c) Yaw rate. (d) Roll angle.

system can be considered valid.

The technique adopted for the calculation of suspension displacements based on a preliminary calculation of the displacement of the sprung mass from integration of its velocities and a position correction routine offers important advantages in terms of computational efficiency and precision. Analysis of the simulation behaviour reveals that, even when tight tolerances are used, positional error correction is rarely required. When necessary, convergence occurs in 1 to 3 iterations.

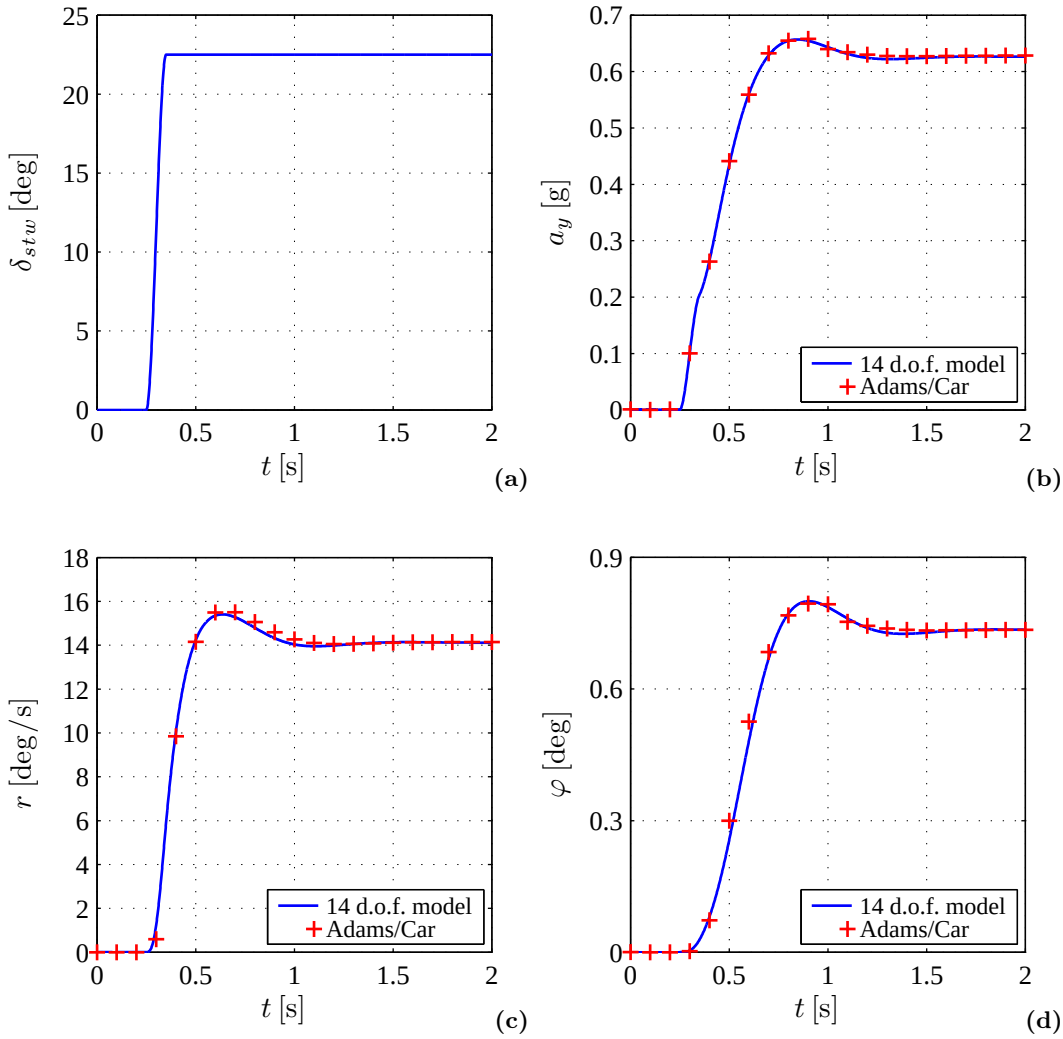

Figure 6.14: Comparative responses of the 14 d.o.f. model and Adams/Car during a step-steer manoeuvre at 40 km/h. (a) Steering wheel input. (b) Lateral acceleration. (c) Yaw rate. (d) Roll angle.

6.4.3 Vehicle behaviour

Steady-state vehicle behaviour is verified through the simulation of an open-loop ramp-steer manoeuvre. The manoeuvre is performed at a constant speed of 40 km/h while the steering wheel angle is increased according to a ramp-like profile. A comparison of the values of lateral acceleration, yaw rate and roll angle are reported in Figure 6.13. Good agreement between the two models is found.

Transient behaviour is compared through the analysis of the vehicle response when subjected to a steer-step input. During the simulation, the vehicle speed is kept constant while the steering input is varied from zero to a predetermined final value.

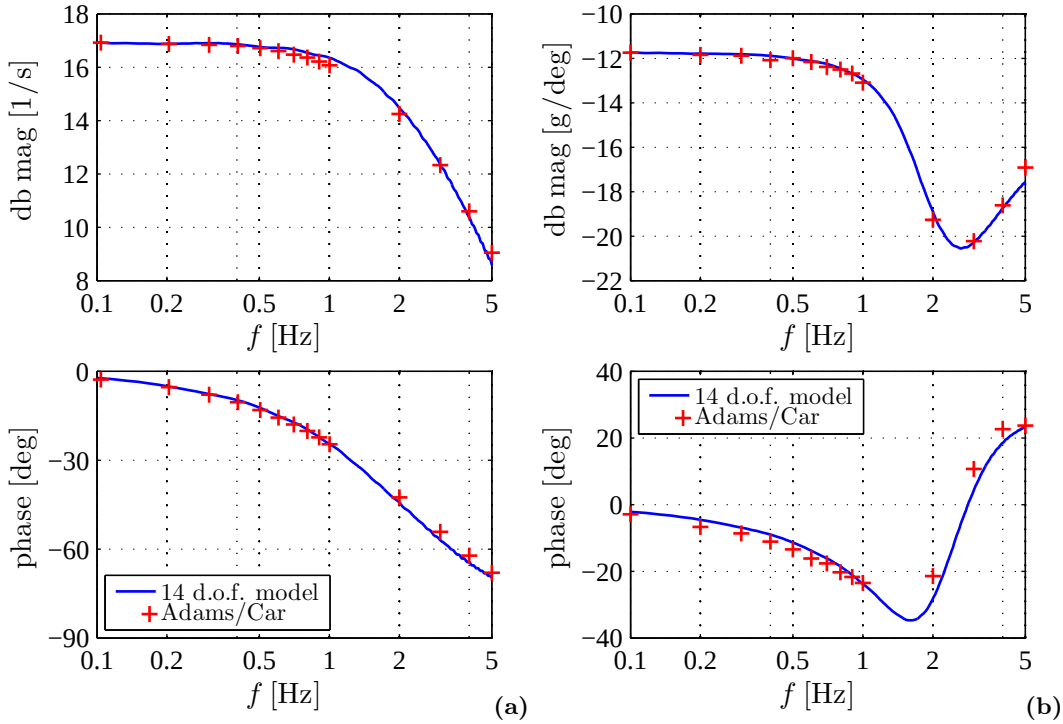

Figure 6.15: Comparison between the frequency response of the vehicle obtained by using the 14 d.o.f. model and Adams/Car. (a) Yaw rate. (b) Lateral acceleration.

In both Adams/Car and in the 14 d.o.f. model, the step function is approximated by means of a cubic polynomial with continuous first and second time derivatives. A comparison between the results obtained is presented in Figure 6.14.

A comparison between results obtained by means of the Adams/Car model and the developed model during a swept steer manoeuvre is shown in Figure 6.15. To this purpose, a sinusoidal steering wheel input having an amplitude of 5 deg and a frequency linearly varying from 0 to 15 Hz is used. Frequency response diagrams are calculated by means of an FFT algorithm. In order to improve the quality of the results, all the the signals are filtered using a Gaussian window filter with a standard deviation of 0.5.

Figures 6.13-6.15 show that good agreement between the two models exists. Due its proven capabilities, Adams/Car can be considered as a valid benchmark for the developed model; it is therefore possible to conclude that the proposed modelling approach is capable of describing the behaviour of the vehicle in an accurate manner.

Table 6.6: Comparison of CPU time, 14-degrees-of-freedom model versus Adams/Car.

Manoeuvre	Steering step	Steering ramp	Steering sweep
Duration [s]	5	25	120
CPU time [s]			
14 d.o.f.	1.1	4.1	6.1
Adams/Car	22.4	72.2	114.4

6.4.4 Computational efficiency

A main difference between the two codes lies in their computational efficiency. As an example, Table 6.6 reports the CPU time for each of the reported manoeuvres. All simulations were run on a standard desktop computer equipped with a 2.4 GHz Intel Core 2 Duo processor and 2 Gb of RAM. Output frequency was set at 1 kHz while a relative tolerance of 0.5% was used in all the cases. Results show that, while giving accurate results, the proposed modelling methodology generally offers higher computational efficiency. Furthermore, trials have shown that the performance of the developed code is only marginally affected by the tolerance required while the efficiency of Adams/Car is sensibly decreased when tight tolerances are required. It is very likely that the reason of this behaviour lies in the fact that Adams/Car solves a set of DAE instead of a set of ODE.

6.5 Concluding remarks

A fourteen-degrees-of-freedom vehicle model suitable for the analysis of the effects of chassis compliance on vehicle dynamics has been introduced in the present chapter. The model includes a modal representation of chassis flexibility, a physical description of suspension kinematics, a detailed tyre model and subroutines for the inclusion of the aerodynamic and powertrain inputs. Using the symbolic multibody library developed in Chapter 5, equations representing the kinematics and the dynamics of the system have been derived in a symbolic form and exported into a Fortran program for their numerical evaluation.

In the second part of the chapter, real vehicle data have been introduced. A finite element model of the structure of its chassis has been presented and a reduced order model has been derived through the implementation of modal truncation and of component mode synthesis techniques. Because of the limited frequency range, results show that the former approach is suitable for vehicle dynamics studies. Also, it appears that a limited number of modal shapes, generally smaller than 10, is sufficient.

In the final part of the chapter, a multibody model developed in the Adams/Car environment is introduced. The model, which represents the same vehicle as the developed fourteen-degrees-of-freedom model, is employed as a validation tool. Results show that good agreement between the two tools is achieved for both the kinematics and the dynamics parts of the model. Furthermore, it has been shown that, due to the formulation adopted, the derived model generally exhibits a very high computational efficiency.

While its high computational efficiency makes it suitable for real-time simulation and for optimisation analysis, the symbolic development, together with the semi-recursive and projection techniques, makes the model a parametric and "essential" tool suitable for research purposes. These characteristics will be thoroughly exploited in Chapter 7, where a detailed analysis of the effects of chassis compliance on vehicle dynamics is introduced.

Chapter 7

Chassis flexibility and vehicle dynamics

This chapter presents a more detailed investigation of the influence of chassis compliance on vehicle dynamics. The analysis intends to demonstrate the application of the described model to a real test case and to assess several aspects of vehicle behaviour. A comparison against the preliminary model described in Chapter 3 and considerations on the achieved computational efficiency are also included.

7.1 Steady-state behaviour

7.1.1 Analysis of modal coordinates

The effect of chassis flexibility on vehicle steady-state characteristics is investigated through the analysis of the results of a skid-pad test with a constant radius of 50 m. Data introduced in Chapter 5 are used for all the simulations. A plot of the first six modal coordinates evaluated during the manoeuvre is reported in Figure 7.1a.

Because of the modal representation of chassis deformation, modal coordinates can be considered as weighting functions of modal shapes. As a consequence, their absolute values cannot be compared; it is however possible to notice that two groups exist. The first group is characterised by a linear or quasi-linear dependency on lateral acceleration and includes modes 1, 2, 4, 5 and 6. The second group includes the modes that do not depend on lateral acceleration, in this case, only mode 3. Referring to Table 6.4 and to Figure 6.8, it is found that the first of the two groups includes modal coordinates corresponding to the torsional, lozenging and lateral bending modes while mode 3 corresponds to a vertical bending.

A linear dependency between modal coordinate 3 and the sprung mass can be noticed in Figure 7.1b where absolute values of modal coordinates obtained under a constant lateral acceleration $a_y = 0.3$g are plotted. The graph also shows a dependency

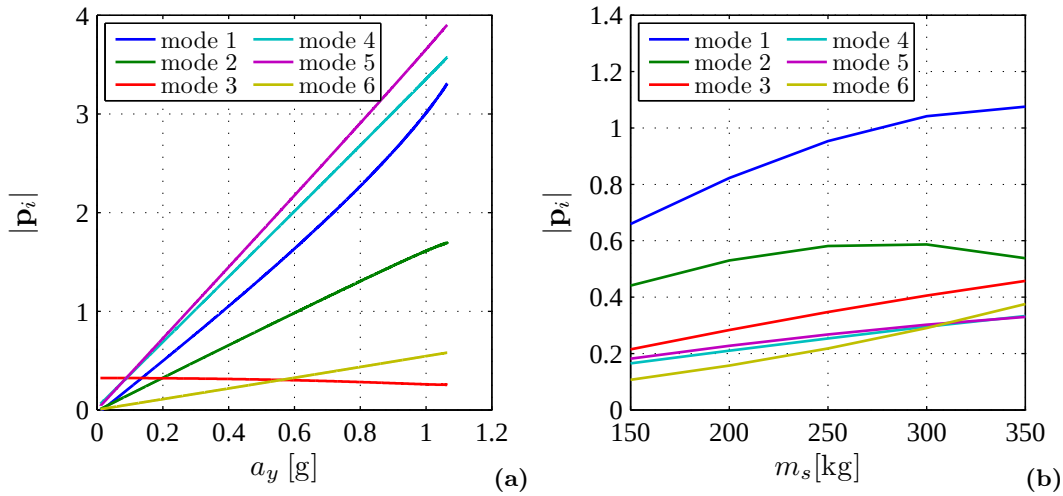

Figure 7.1: Modal coordinates. (a) Modal coordinates versus lateral acceleration. (b) Modal coordinates versus sprung weight at $a_y = 0.5$g.

of modal coordinates versus sprung mass weight; it is therefore appropriate to define the first group as lateral and vertical force-dependent.

7.1.2 Lateral load transfer distribution

Lateral load transfer distribution plays a fundamental role in the definition of the steady-state behaviour of the vehicle. A first attempt at evaluating the effect of chassis torsional flexibility on vehicle behaviour has been presented and discussed in Section 3.1. A more detailed analysis based on the developed multibody vehicle model is presented here.

As expected, simulations have shown a linear relationship between lateral load transfer and lateral acceleration. As an example, Figure 7.2a reports values of lateral load transfer at the front axle predicted by means of the advanced multibody model and by means of the analytical model. Good agreement between the two models can be found.

A lateral load transfer distribution parameter, represented by symbol χ, is defined as the ratio between the lateral load transfer withstood by the front axle and the total lateral load transfer. Dependency of lateral load transfer distribution on normalised roll stiffness distribution $\lambda = k_F/(k_F + k_R)$ is investigated in Figure 7.2b. As in Figure 3.3a, a point exists where the lines representing rigid and flexible chassis hypotheses intersect. For comparison, values obtained by means of Equation (3.6) are also included. A good agreement between the two models can be found in the region of $\lambda = 0.4 - 0.6$; some discrepancies appear at both lower and higher values of λ.

The dependency of lateral load transfer distribution parameter χ on the number

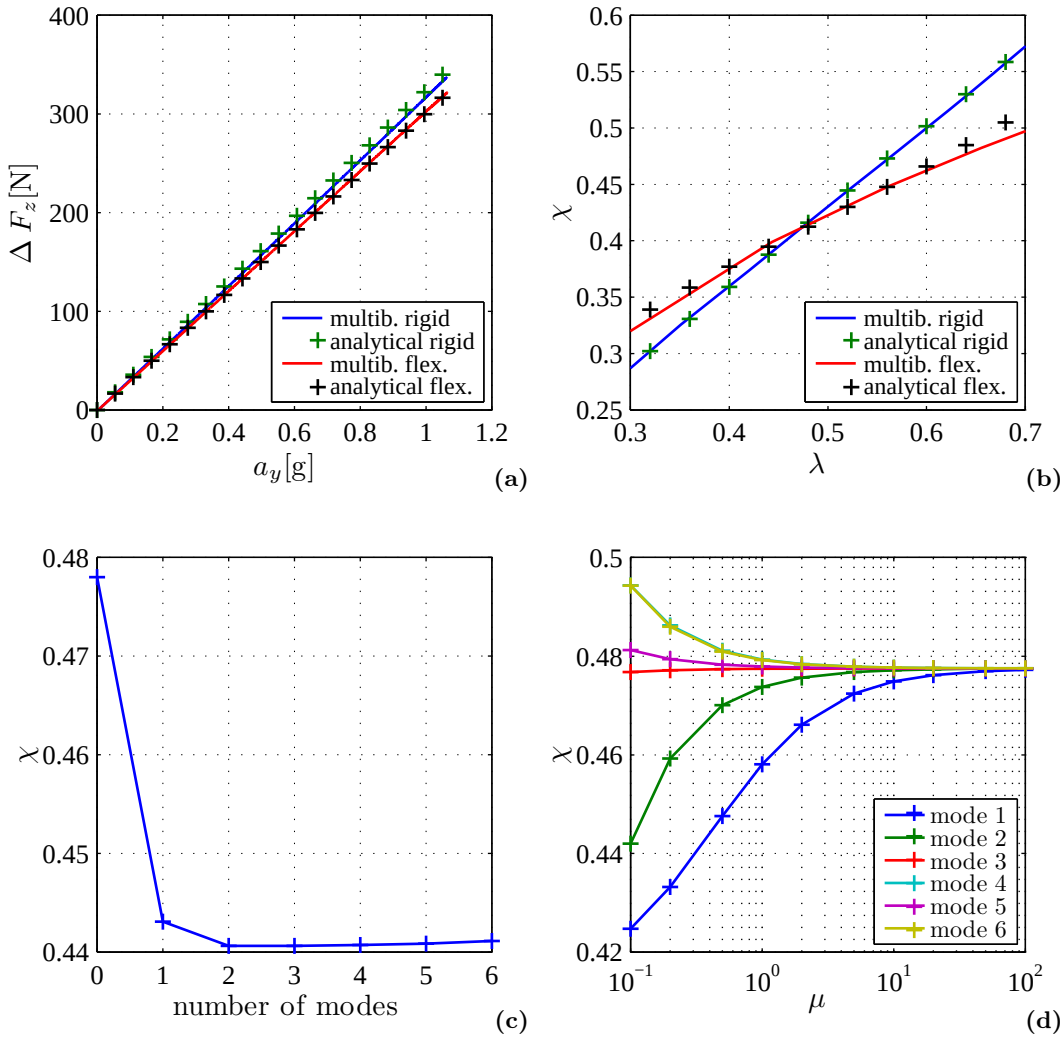

Figure 7.2: Effect of chassis flexibility on lateral load transfer distribution. (a) Front lateral load transfer, comparison between different models. (b) Lateral load transfer distribution versus roll stiffness distribution. (c) Lateral load transfer distribution versus number of modes employed. (d) Lateral load transfer distribution versus individual modal stiffness.

of considered modes is depicted in Figure 7.2c. The graph shows how the lateral load transfer distribution is mainly controlled by mode 1, corresponding to the first torsional mode, and to a lesser extent, by mode 2. The effect of the other modes appears to be negligible. Furthermore, the value of $\chi = 0.441$ found from the graph is in good agreement with the value of $\chi = 0.445$ found by means of Equation (3.6) with $\lambda = 0.54$. It appears therefore that the simplified model presented in Section 3.1 is sufficient for the estimation of the the effect of chassis flexibility on lateral load transfer.

Figure 7.2d reports, for each mode, the variation of the lateral load transfer distribution as a function of a modal stiffness multiplying factor μ. Modes are considered singly. The graph highlights the contribution of each of the individual modes to the loss of lateral load transfer distribution control. Once a target in terms of lateral load transfer distribution is set, the graph can therefore be used as a design tool in order to estimate the required value of stiffness for each of the modes. Interestingly, it appears that while low values of modal stiffness of modes 1 and 2 make χ decrease, modes 5 and 6 induce the opposite effect. This fact seems to suggest that it is possible to counterbalance the effects of mode 1 and 2 by lowering the stiffness associated with modes 5 and 6.

7.1.3 Suspension kinematics

Besides lateral load transfer distribution, suspension kinematics is the second main area of influence of chassis flexibility. The preliminary analysis carried out in Section 3.4 has shown that even if only the roll steer mechanism is introduced, an effect on vehicle handling due to the alteration of the suspension kinematics induced by chassis compliance can be clearly noticed. A more detailed analysis of these effects is presented here.

Use of projection matrix

A novel tool for the analysis of the effects of chassis compliance on suspension kinematics is proposed here. The method is possible thanks to the combination of the adopted semi-recursive formulation and coordinate reduction technique.

It has been shown in Equation (5.61) that the time derivative of generalised coordinates can be written as $\dot{\boldsymbol{q}} = \boldsymbol{BTy}$ with $\boldsymbol{y} = \boldsymbol{Rz} + \boldsymbol{Sb}$. Neglecting the significance of vector $\boldsymbol{Sb}$, vector $\boldsymbol{z}$ represents the set of independent relative velocities, $\boldsymbol{T}$ the recursion matrix while matrix $\boldsymbol{B}$ projects the velocity vector onto the body reference system. In the rest configuration, matrix $\boldsymbol{B}$ can be approximated by an identity matrix. It is therefore:

$$\dot{\boldsymbol{q}} \approx \boldsymbol{TRz} \tag{7.1}$$

If vector $\boldsymbol{z}$ is considered as time derivative of a set of independent relative coordinates so that $\boldsymbol{z} = \dot{\boldsymbol{s}}$, it is possible to write:

$$\frac{\mathrm{d}\boldsymbol{q}}{\mathrm{d}t} \approx \boldsymbol{TR}\frac{\mathrm{d}\boldsymbol{s}}{\mathrm{d}t} \tag{7.2}$$

From this, it is:

$$\frac{\mathrm{d}\boldsymbol{q}}{\mathrm{d}\boldsymbol{s}} \approx \boldsymbol{TR} \tag{7.3}$$

Matrix $\boldsymbol{TR}$ therefore represents the local Jacobian of the vector of generalised dependent coordinates versus the independent joint coordinates. By definition, suspension

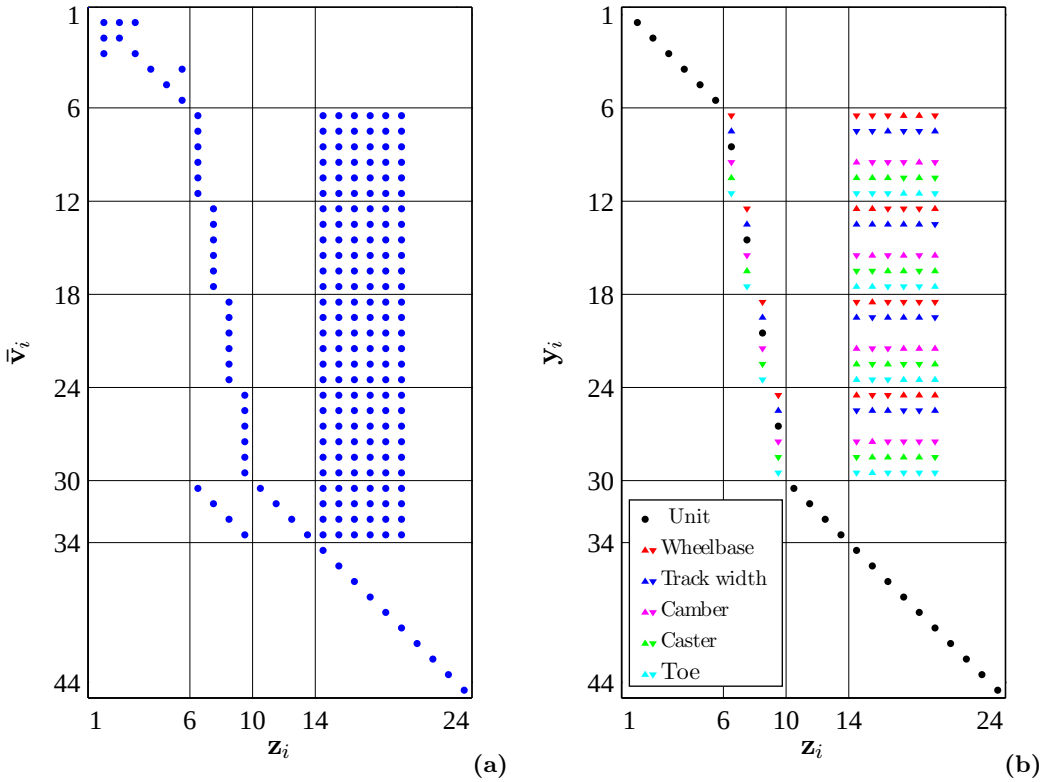

Figure 7.3: Sparsity pattern for reduction matrices. (a) Map of non-zero entries of product $\boldsymbol{RT}$. (b) Map of non-zero entries of matrix $\boldsymbol{R}$. Upward and downward pointing triangles indicate, respectively, positive and negative values; colours indicate the relative wheel parameters.

characteristics parameters are contained in vector $\boldsymbol{q}$; values of suspension vertical displacement are contained in vector $\boldsymbol{s}$. As a consequence, the entire suspension kinematics can be predicted from Equation 7.3.

A map of non-zero elements of matrix product $\boldsymbol{TR}$ is shown in Figure 7.3a. The matrix has been obtained for conditions of constant longitudinal speed and zero lateral acceleration. Horizontal partitions divide sets of dependent coordinates belonging to different bodies, vertical partitions are introduced to divide sets of independent joint coordinates belonging to different bodies. Data relative to the coordinates of the sprung mass are included in rows 1-6 while data relative to the front left, front right, rear right and rear left sprung masses are, respectively, in rows 7-12, 13-18, 19-24 and 25-30. Rows 30-34 and 34-44 refer, respectively to wheel rotations and to chassis modal coordinates. Similarly, the vertical partitions contain, in order from the right, the non-zero data relative to the degrees of freedom of the sprung mass, the unsprung masses, the wheel rotations and to the modal coordinates.

Furthermore, a map of non-zero elements of the reduction matrix $\boldsymbol{R}$ is represented in Figure 7.3b. The matrix is partitioned in the same manner as the one in Figure 7.3a. While the matrix $\boldsymbol{RT}$ expresses the suspension gradients in an absolute frame, the matrix $\boldsymbol{R}$ fully exploits the use of relative kinematics and expresses suspension gradients in the body reference frame.

The structure of matrix $\boldsymbol{R}$ helps highlight the advantages related to the use of a reduction technique coupled with a velocity projection technique. The use of relative velocities eliminates the dependency between the coordinates of the sprung masses and the degrees of freedom of the sprung mass and makes it possible to describe the kinematics of the suspension system by a set of vectors containing the gradients of the suspension characteristic parameters, like wheel base, track width, toe and camber angles, with respect to the degrees of freedom of the system, independent of their nature.

As an example, gradients related to the bump motion are entirely described by lines 7-12 of column 7; those related to chassis deformation are contained in columns 15-24. Matrix $\boldsymbol{R}$ therefore includes a set of synthetic parameters, such as kinematic and deformation gradients that can be used to analyse the effect of chassis flexibility on suspension kinematics.

Coloured triangles are also included in the map of Figure 7.3b. A suspension characteristic parameter is assigned to each colour, as reported in the legend. An upward pointing triangle is assigned to positive values, a downward pointing one to negative values. Kinematics gradients are expressed as a function of bump motion with known sign. As a consequence, their signs can be read directly from the map. For example, from columns 7-10 it is possible to say that positive bump motion induces wheelbase decrease and track width increment, camber reduction and so on.

Because of the modal definition of the deformation coordinates, the signs of the deformation gradients of a single suspension do not have physical meaning. However, if the signs of the gradients of an axle are considered, the nature of each of the modes can be highlighted. For example analyse the effect of the first mode on the front axle, displayed in rows 6-18 and column 15. When this mode is activated, a decrease of wheelbase and half track of the left wheel will induce an increase of those of the right wheel and vice versa. Similarly, positive camber or toe variation of one side will involve negative variations on the other side. The multi-axial torsional nature of the mode can be detected from these considerations. In comparison, the signs of the left and right gradients relative to the third mode are coincident.

A second important advantage of the adopted formulation is that a projection matrix derived by means of another analysis technique can be introduced through the use of look-up tables very similar to those generally employed in lumped parameters models. The use of a projection matrix at the relative-velocities level can therefore be seen as a link between a complete multibody and a lumped parameters representation

Table 7.1: Kinematic gradients from projection matrix analysis.

Description	Front axle	Rear axle
Camber change [deg/g]	-0.190	0.015
Toe change (toe-in) [deg/g]	-0.077	0.105

of a vehicle system. Suspension compliances can be introduced following the same approach.

Furthermore, as matrix $\boldsymbol{R}$ only introduces relative coordinates, it is possible to assume that, under certain circumstances it does not need to be recomputed at each time step. From this, a gain in computational efficiency can be obtained.

Finally, it is worth noting that, in case absolute coordinates are used, the projection matrix obtained is equivalent to matrix $\boldsymbol{RT}$ of Figure 7.3a. As this matrix is dependent on the absolute coordinates of the bodies, no gradient analysis could be carried out, nor data originated from other analyses could be used.

Kinematic gradients

As shown in Figure 7.1a, a linear dependency between modal coordinates and lateral acceleration exists. Also, it has been shown in Section 7.1.3 that suspension kinematics gradients can be deduced from the analysis of matrix $\boldsymbol{R}$. It is therefore possible to represent the suspension gradients as a function of lateral acceleration. This is obtained by representing modal coordinates as linear functions of lateral acceleration and premultiplying a vector containing these gradients by matrix $\boldsymbol{R}$. From this, a vector of gradients of kinematic parameters versus lateral acceleration is obtained. Gradients corresponding to front and rear camber and toe angles are reported in Table 7.1.

As an example, camber and toe angle variations due to chassis flexibility obtained by means of the complete model are compared in Figure 7.4 with those obtained by means of a linear model based on the suspension gradients of Table 7.1. It appears from the graphs that in most cases the estimate provided by the linear approximation is sufficiently accurate. Furthermore, in combination with matrix $\boldsymbol{R}$, the graphs can be used for design and optimisation purposes.

If the particular vehicle is considered, more information can be gained from Figure 7.4. For example, while a decrease of camber and toe angle is present at the front axle, an increase is present at the rear axle. This might be due to the reduction in roll angle occurring at the front axle as a consequence of chassis flexibility.

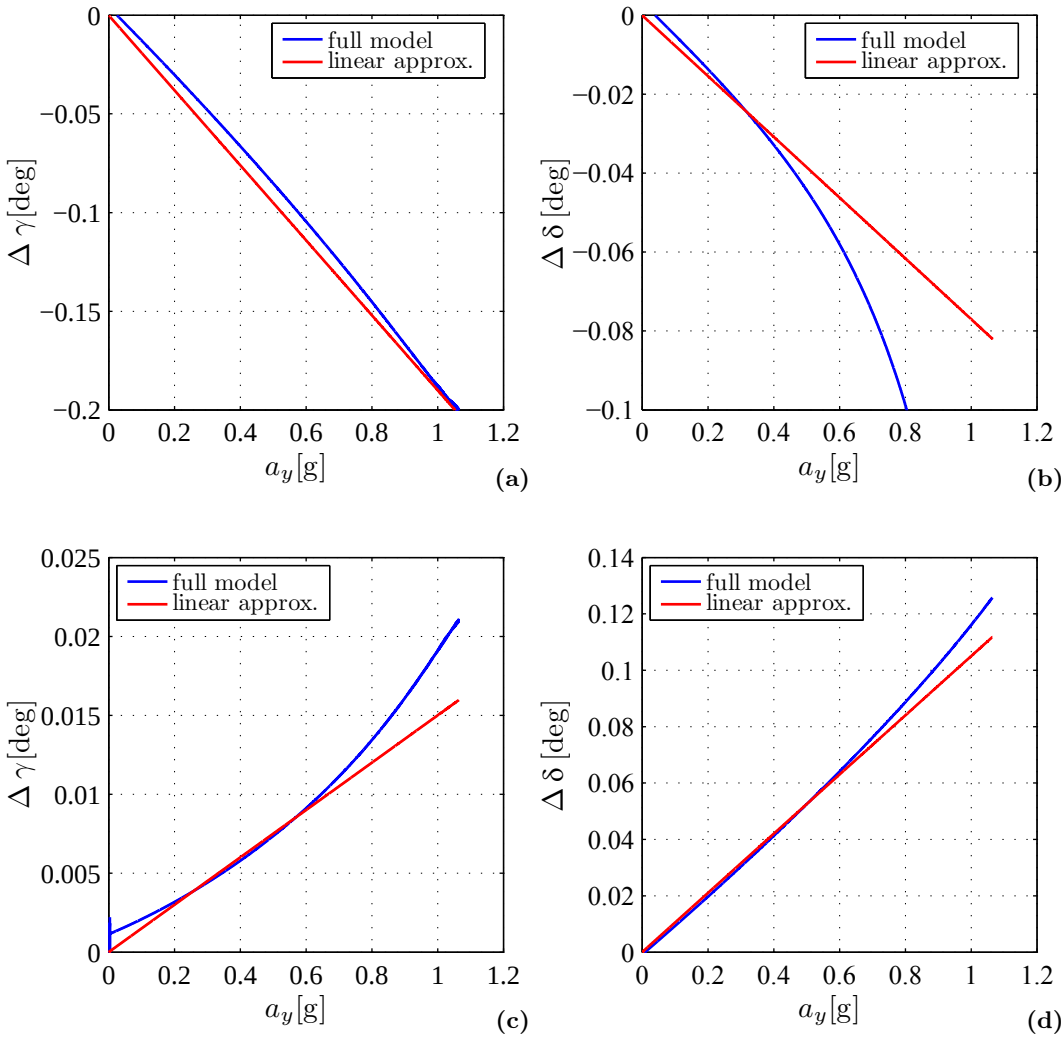

Figure 7.4: Effect of chassis flexibility on suspension kinematics, comparison between complete model and linear approximation. (a) Front left camber angle. (b) Front left toe angle. (c) Rear left camber angle. (d) Rear left toe angle.

7.1.4 Handling characteristics

The handling characteristics obtained from the simulation of a skid-pad test with a radius of 50 m are presented in Figure 7.5. Figure 7.5a compares values of dynamic steering angle versus lateral acceleration obtained from the multibody model versus values obtained from the analytical models of Chapter 3. While a general agreement between the results exists, some differences emerge from the analysis of the graph of the steering sensitivity reported in Figure 7.5b.

Because of the fact that the vehicle considered has limited suspension movement, the effect of suspension kinematics on the overall vehicle behaviour is limited. As

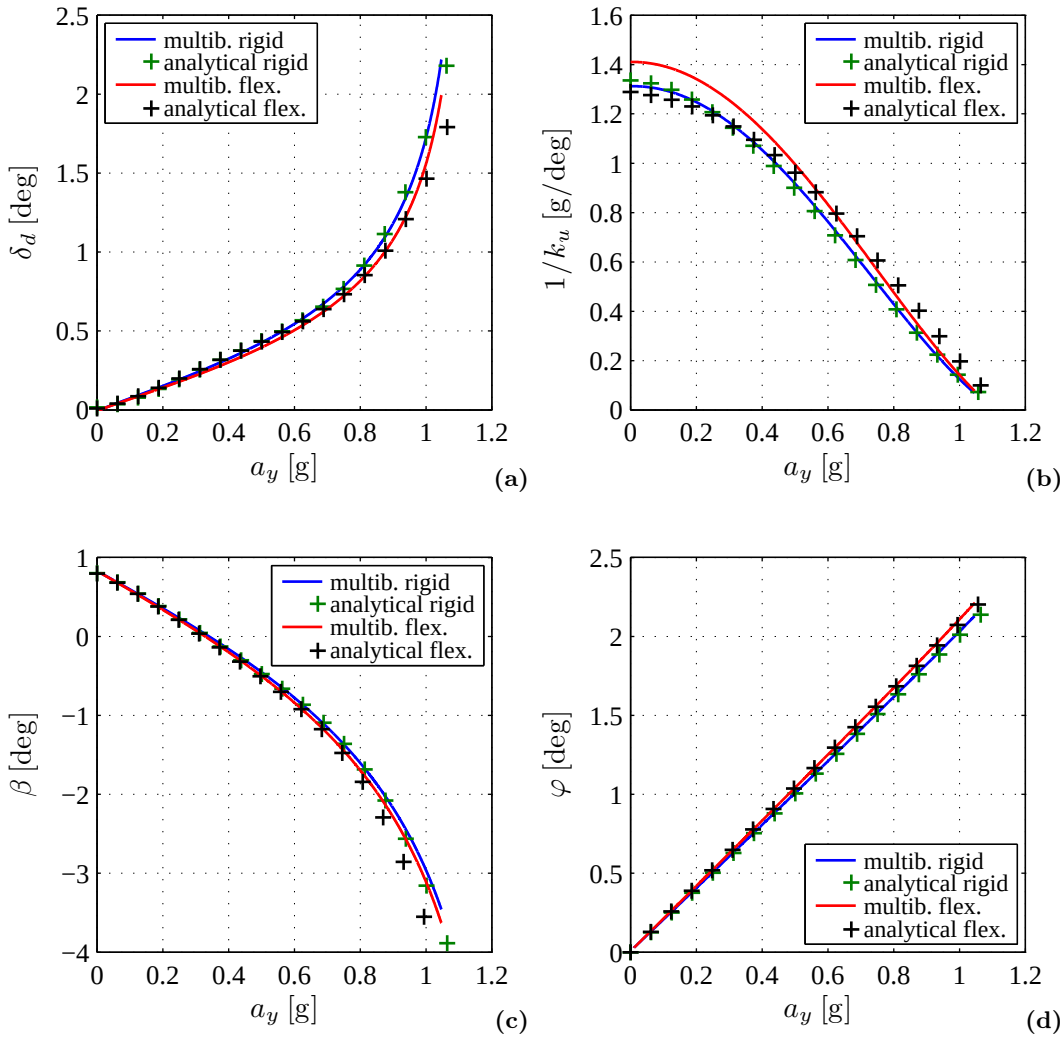

Figure 7.5: Vehicle steady-state characteristics during a skid pad test, comparison between multibody and analytical models under the hypotheses of rigid and flexible chassis. (a) Dynamic steer angle versus lateral acceleration. (b) Steering sensitivity versus lateral acceleration. (c) Body sideslip angle. (d) Roll angle.

a consequence, the analytical model is capable of describing the behaviour of the rigid vehicle in an accurate manner. When chassis flexibility is introduced, however it appears from Figure 7.5b that the accuracy of the simplified model is not sufficient. This is particularly true at low values of lateral acceleration, where the effect of suspension kinematics is predominant. For high values of lateral acceleration, the effect of lateral load transfer is predominant. As shown, there is a good agreement between lateral load transfer distribution evaluated by means of the two models; as a consequence, good agreement on limit behaviour is found. Similar considerations are

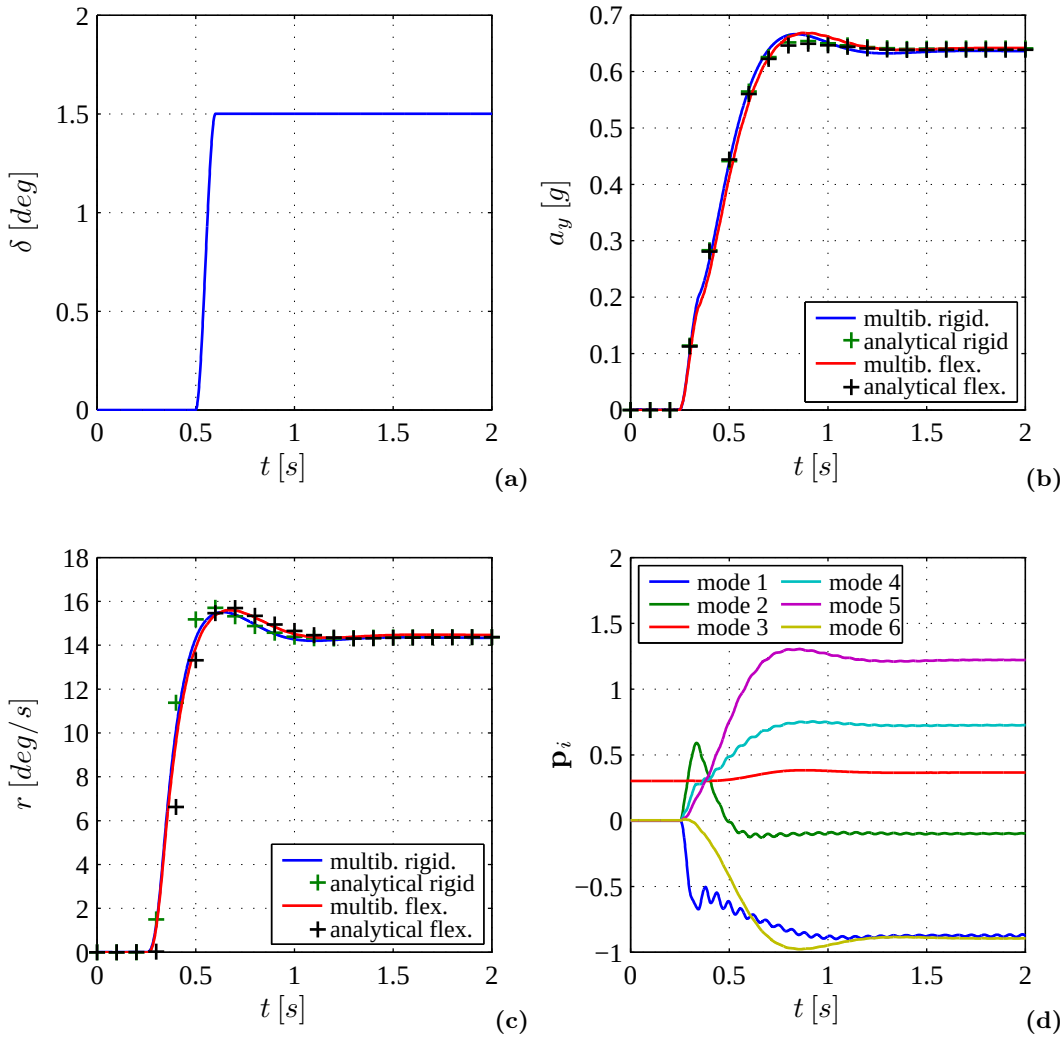

Figure 7.6: Effect of chassis flexibility on steering step response at 90km/h, comparison between multibody and analytical model under the assumptions of rigid and flexible chassis. (a) Steering input. (b) Lateral acceleration. (c) Yaw rate. (d) Modal coordinates.

valid for the analysis of vehicle sideslip and roll angles, represented in Figures 7.5c and 7.5d.

7.2 Transient dynamics

In accordance with the analysis of Section 3.3, vehicle transient dynamics is evaluated through the simulation of a steering step manoeuvre carried out at a constant speed of 90km/h. Results are reported in Figure 7.6; for comparison, results obtained by means of the simplified analytical model of Chapter 3 are also plotted.

The steering input is generated by means of a cubic polynomial with continuous first derivative. The resulting lateral acceleration is reported in Figure 7.6b. It appears from the results that the response obtained by means of the multibody model is marginally more oscillatory. Also, the difference between the rigid and the flexible model appears to be more significant. More specifically, both the response time and the peak time are increased. Similar considerations are valid for the yaw rate response, plotted in Figure 7.6c. In this case however, in accordance with the simplified model, the overshoot ratio is also increased. Chassis flexibility therefore implies a general loss of vehicle responsiveness to the driver inputs.

Curves representing modal coordinates are represented in Figure 7.6d. The graph shows how sustained oscillations affect the modal coordinates and, as a consequence, chassis deformation. While dynamics of modes 4, 5 and 6 appears to be strictly coupled with the lateral acceleration response and mode 3 is only marginally affected, a different behaviour can be noticed for modes 1 and 2.

While the dynamics of mode 1 appears to be dominated by the value of lateral force generated by the front axle, the dynamics of lateral bending mode (mode 2) can be linked to the difference between front and lateral cornering force. This fact can be better understood by observing that in the first phase of the manoeuvre lateral force is generated by the front axle only, in the second part the force generated by the rear axle is prevailing.

When results obtained by means of the multibody model are compared against those obtained by means of the model of Chapter 3, it appears that, although the second is capable of predicting the main effects of chassis compliance, its accuracy is not entirely satisfactory.

7.3 Root locus analysis

Root locus analysis is carried out by means of a linearised version of the model. A linearisation about a steady-state configuration corresponding to null lateral acceleration is introduced.

Results of the root locus analysis are presented in Figure 7.7. Figure 7.7a and 7.7b report the root locus of the system when the full, partial and total coupling between chassis and vehicle dynamics is considered. This is obtained by multiplying vectors containing modal shapes data by a factor that varies from 0 to 1. In order to improve legibility, the eigenvalues relative to chassis deformation modes are reported in Figure 7.7a while those relative to vehicle motion are reported in Figure 7.7b.

From Figure 7.7a, it is possible to say that in absence of coupling, the natural frequencies of the chassis correspond to those shown in Table 6.4. Given that only the modal damping is present, the relative eigenvalues lie on the line corresponding to $\zeta = 0.025$. The graph shows that the coupling between chassis deformation and

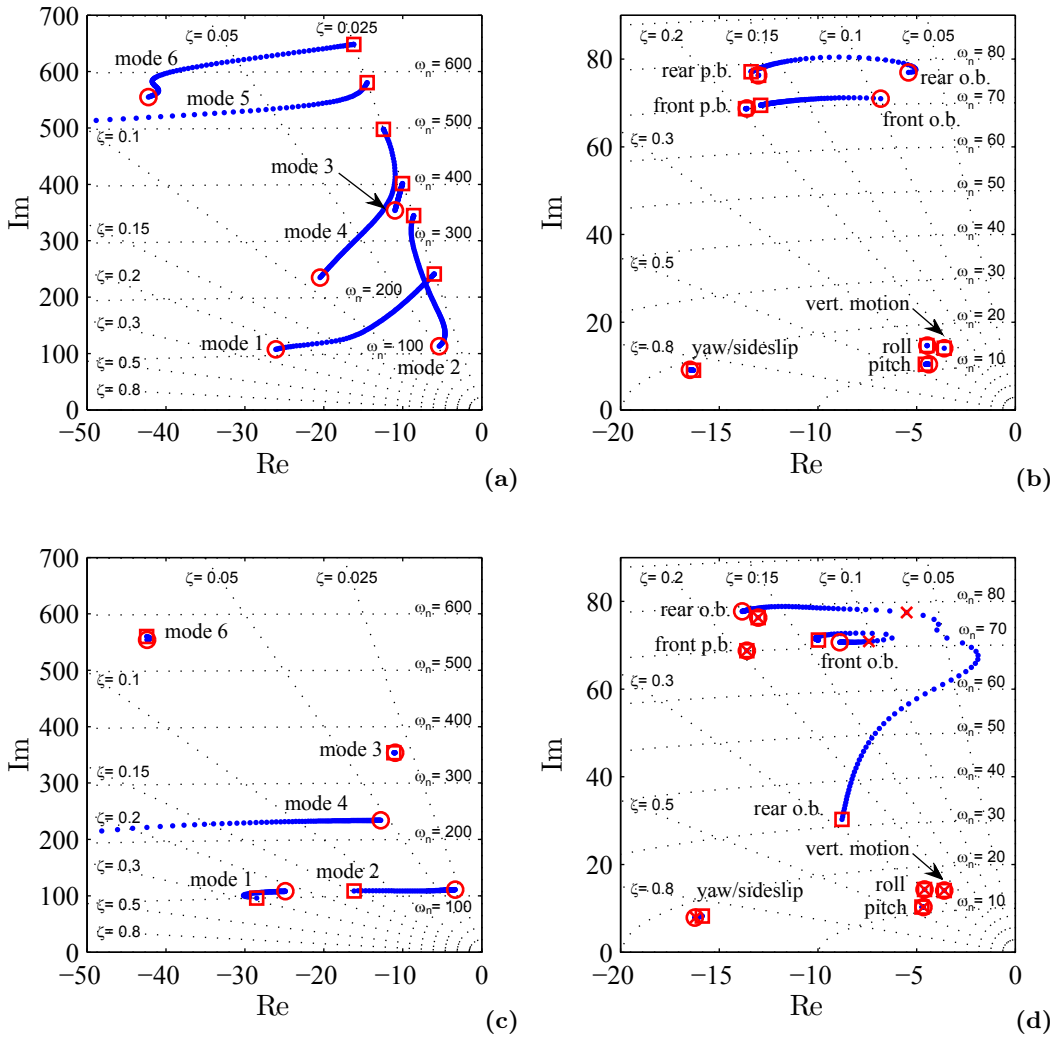

Figure 7.7: Root locus plots of the system. (a) Variation of the position of the eigenvalues relative to chassis deformation from null (□) to full coupling (○) at $v = 50$ km/h. (b) Variation of the position of the eigenvalues relative to sprung and unsprung masses when null (□) or full coupling (○) are considered, $v = 50$ km/h. (c) Root locus as a function of vehicle longitudinal speed, varied from 5 (□) to 120 km/h (○). (d) Root locus for the sprung and unsprung masses as a function of first natural frequency of the chassis, varied from 12 (□) to 120 Hz (○). Symbol (×) indicates its nominal value of 38 Hz.

vehicle dynamics modes causes a decrease of the natural frequencies associated with each of the deformation modes. Also, modal shapes are transformed from pure chassis deformation ones to a combination of chassis deformation and other components. As an example, while the first natural frequency of the free chassis is found at 38Hz, full coupling makes it appear at about 17 Hz. Similarly, the eigenvector corresponding to mode 2 is lowered from 54 to 17 Hz. Furthermore, the graph shows that modal

damping associated with these modes is always higher than the internal damping. In other words, the strict coupling between chassis deformation and vehicle dynamics provides sufficient damping for the internal modes of the chassis itself.

The other vehicle modes are shown in Figure 7.7b. Three of them are those related to vertical, roll and pitch motion of the sprung mass, one describes the yaw and sideslip motion while the remaining four modes describe the parallel or opposite bump motions of the unsprung masses. To this purpose, labels "p.b." and "o.b." are used. Negligible variations in the positioning of the eigenvectors relative to the yaw/sideslip mode and to the rigid motion of the sprung mass can be noticed. When modes relative to the unsprung masses are considered, results show a sensible decrease of the damping associated with the antisymmetric modes. An analysis of the relative eigenvectors shows that this is mainly due to the involvement of the chassis torsional mode. This fact is surely of interest for the analysis of the ride performance of the vehicle, it is however also of interest for the analysis of tyre vertical forces and, as a consequence, for the analysis of the vehicle handling.

An analysis of the variation of the root locus of the system with speed is reported in 7.7c. Only the eigenvalues related to the chassis deformation are plotted. Results show that damping coefficients of high-order modes, such as modes 5 and 6, are minimally affected by speed. Damping of modes 1, 2 and 4 instead sensibly decreases with speed. In particular, high speed damping of modes 2 and 4 decreases to values that are close or lower than the value of the internal damping. When these results are compared with those of Figure 3.9b, it is possible to notice that a similarity between the torsional mode predicted by the analytical model and mode 1 exists. It is worth noticing however that, from the stability point of view, mode 2 appears to be more important than mode 1.

Root locus plots are sensibly affected by the natural frequencies of the chassis. As an example, Figure 7.7d reports the variation of the positioning of the eigenvectors relative to sprung and unsprung masses when the modal stiffness, and as a consequence the natural frequency of the first mode, is varied. In agreement with the graph of Figure 7.7c, it appears that the most affected modes are those relative to antisymmetric bump motions.

7.4 Frequency response

7.4.1 Driver input

In addition to the analysis of Section 3.3.5, frequency response of the vehicle subject to driver inputs is also analysed. Yaw rate and lateral acceleration responses are reported in Figure 7.8.

On the basis of Figure 7.7, it is possible to say that frequencies higher than those

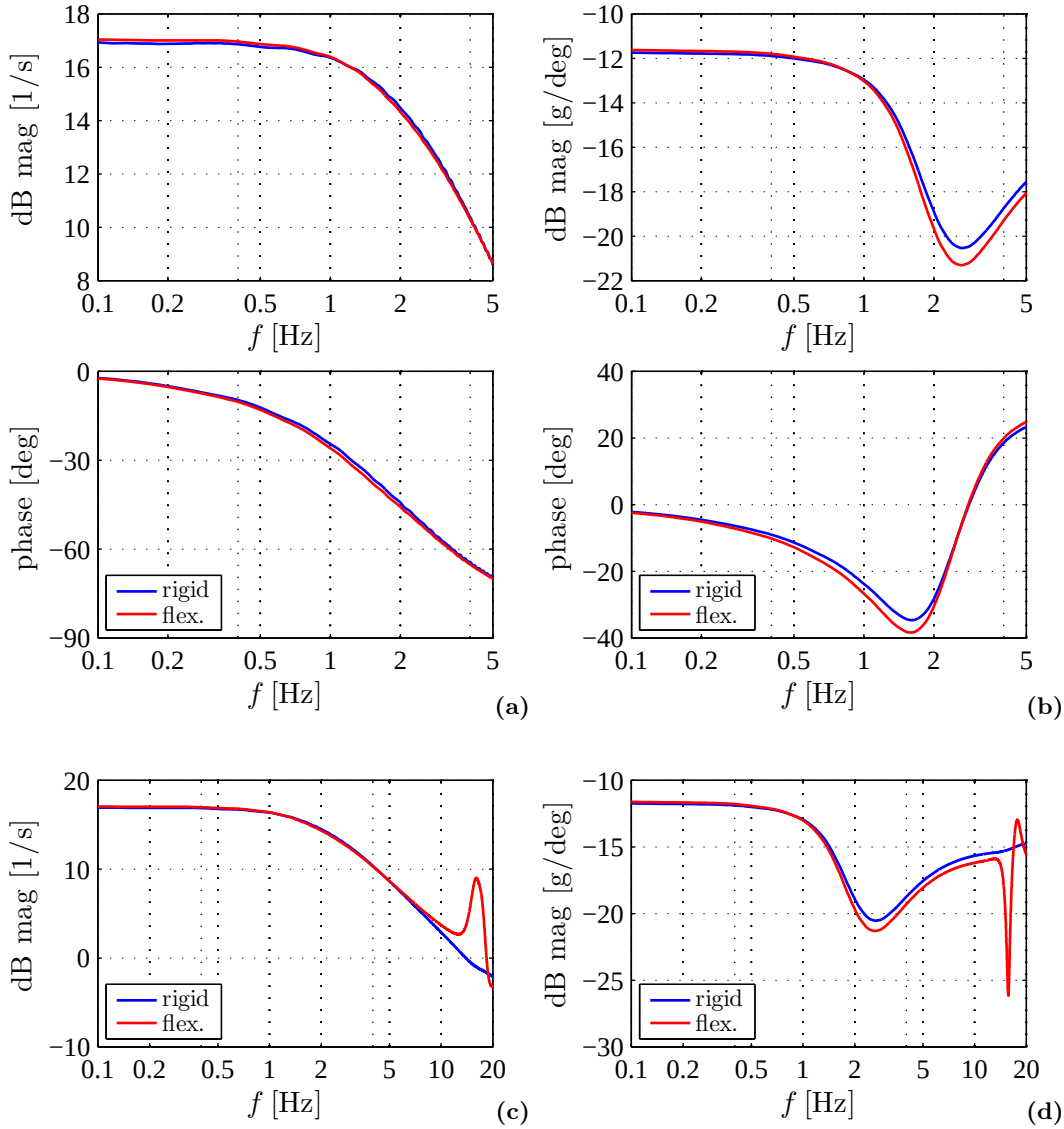

Figure 7.8: Frequency response to steering input at 50 km/h. (a) Yaw rate response. (b) Lateral acceleration response. (c) Extended plot of yaw rate response. (d) Extended plot of lateral acceleration response.

a driver is capable of are required in order to excite one of the modes of the chassis. In accordance with this, a marginal effect of chassis flexibility on yaw rate response is noted, see Figure 7.8a. However, the graph of lateral acceleration response of Figure 7.8b shows how, starting from a frequency of 2 Hz, chassis flexibility causes a faster decay of the vehicle response and a higher phase delay.

This difference can be justified by means of Figures 7.8c and 7.8d where the frequency range is extended in such a way that the first natural frequency of the

chassis is included. A comparison between the two graphs shows the more important effect of chassis flexibility on lateral acceleration response rather than on yaw rate response is due to the fact that for a generic rigid vehicle high frequency response of lateral acceleration does not decay as the yaw rate one. As a consequence, changes in the high frequency response due to chassis flexibility are also noticed in the low frequency range.

When these results are compared against those obtained by means of the simplified model in Section 3.3.5, it is possible to notice that, although there is a good agreement between the rigid models, the simplified model does not predict the impact of chassis flexibility on the frequency response of the vehicle in an appropriate manner.

7.4.2 Road input

The root locus analysis has shown that, although small variations can be noticed in the vehicle response to driver inputs, most of the effects of chassis flexibility can be noticed on the dynamics of the unsprung masses. Besides driver controls, road surface constitutes another important source of loads and deformations. Road input signals are richer in high frequency content than driver inputs.

The chassis response plays an important role in the definition of ride and comfort properties of the vehicle; these aspects are however not treated here. However, because of the substantial dependency of tyre lateral and longitudinal forces on contact patch normal load, the response to road surface inputs also affects the handling qualities of the vehicle. Response to road surface input is experimentally analysed by means of four- and seven-post test rigs on which either track profiles or sinusoidal inputs are reproduced, [154–156]. A first attempt at analysing these influences is presented here.

Simulations are performed in which sinusoidal inputs of increasing frequency are fed to the tyres as vertical displacement of the contact patch. In the first case all the displacements of the contact patches are considered in phase; in the second one lags of 180° between displacements of contact patches belonging to the same axle are then introduced while diagonal symmetry is maintained. All the inputs consist of sinusoidal frequency sweeps having constant amplitude and frequencies up to 30 Hz. Results are presented in Figure 7.9.

In the first case neither the dynamics of sprung and unsprung masses, nor the contact patch load are affected by chassis flexibility. As an example, frequency responses of the contact patch load of the front left tyre evaluated by means of the rigid and flexible models are compared in Figure 7.9a. Furthermore, all chassis coordinates have low response values, see Figure 7.9b.

The effect of chassis flexibility can instead be noticed in the second case. Figure 7.9c reports the frequency response of the front left contact patch vertical load; in this case, the peak occurring in correspondence of the natural frequency of the sprung mass is

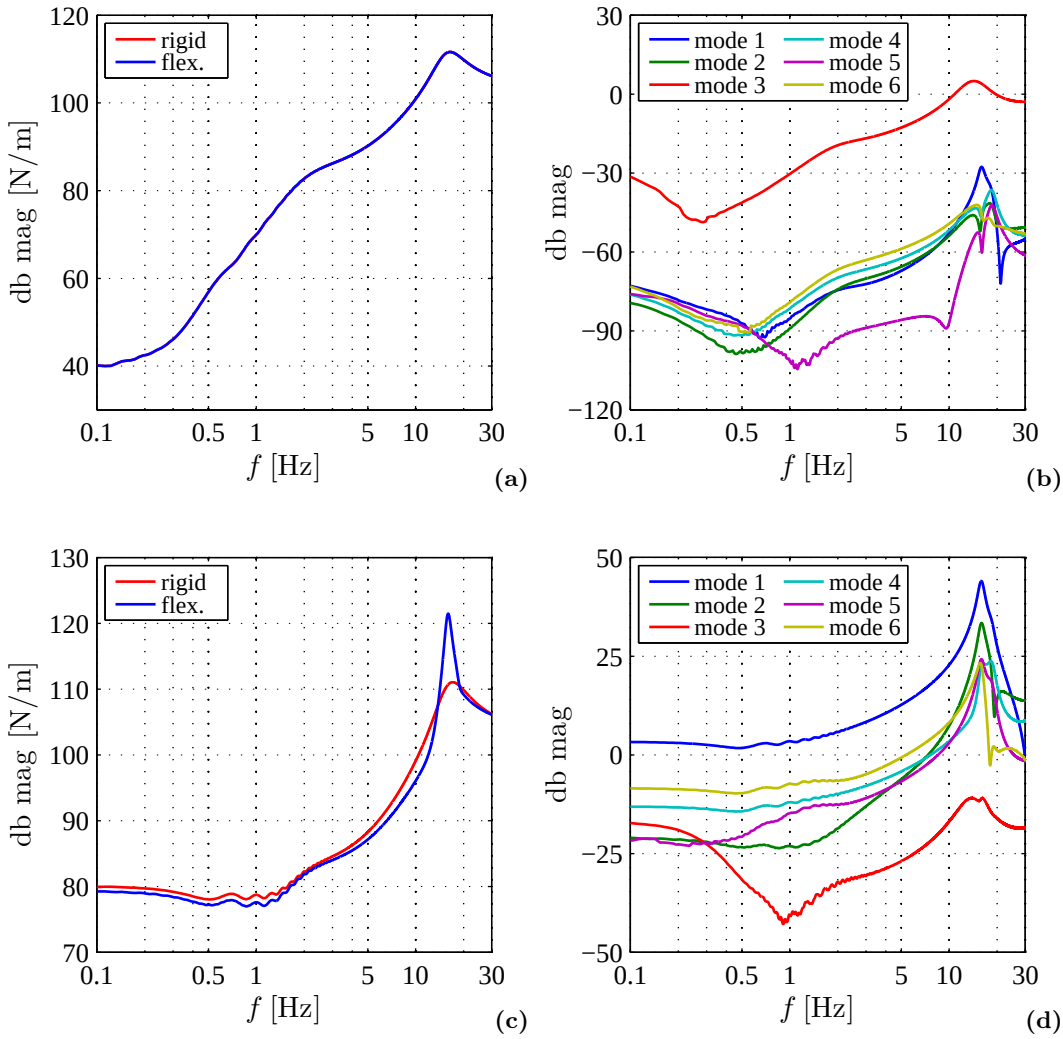

Figure 7.9: Frequency response to road input. (a) Response of front contact patch load to road displacement in case of symmetric input. (b) Response of modal coordinates contact patch load to road displacement in case of symmetric input. (c) Response of front contact patch load to road displacement in case of antisymmetric input. (d) Response of modal coordinates contact patch load to road displacement in case of antisymmetric input.

significantly increased. This peak has a negative impact on tyre r.m.s and therefore on vehicle handling performance. Analysis of the response of modal coordinates, reported in Figure 7.9d shows that at this frequency, the majority of the antisymmetric modes is excited by the bounce motion of the sprung mass. More specifically, the effect of modes 1 and 2, corresponding to torsion and lateral bending, is predominant.

In conclusion, although simplified test cases are examined, results show that a strict interaction between chassis flexibility and unsprung mass dynamics exists. The

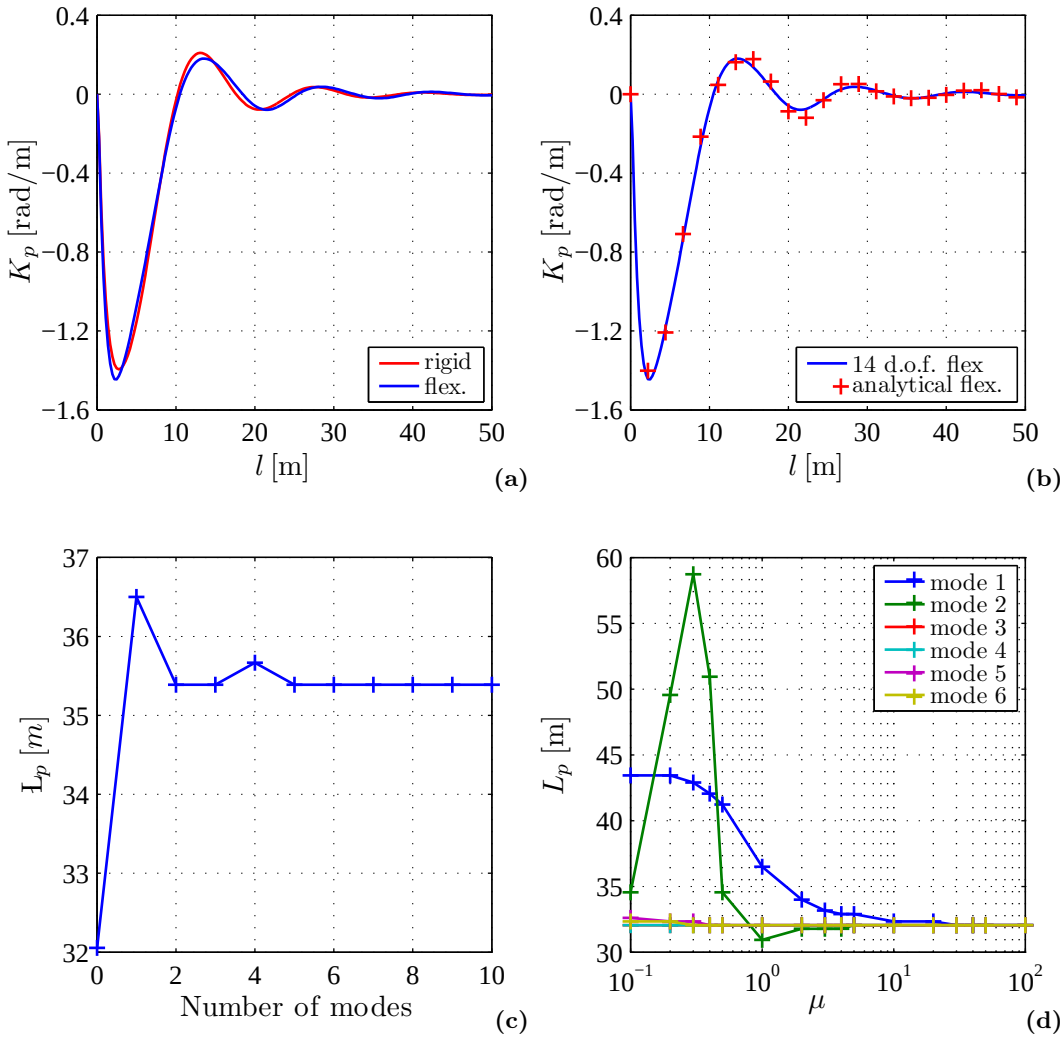

Figure 7.10: Effect of chassis flexibility on TI-optimal controls at $v = 100$ km/h. (a) TI-optimal preview gains. (b) Comparison between the 14 d.o.f model and the analytical preliminary model. (c) Preview distance versus number of modes employed. (d) Preview distance versus modal stiffness.

effect is due to the fact that, in this case, the natural frequency of the unsprung mass and the first two natural frequencies of the installed chassis are similar.

7.5 Optimal controls

Similarly to the analysis presented in Section 3.3.6, optimal controls are here derived for the complete vehicle model. To this purpose, a linearisation about a steady-state configuration corresponding to null lateral acceleration is introduced. Referring to

the exposed theory, all the results have been obtained by using 250 preview points, a discrete time interval of 0.01s and a weighting factor for the tracking error of 1000. The problem can therefore be thought of as a tight path-following one.

Figure 7.10a reports TI-optimal preview gains corresponding to a vehicle velocity of 100 km/h. As already suggested by the preliminary results of Figure 3.12, chassis flexibility requires the driver to generate a marginally more oscillatory control with a marginally lower frequency.

A comparison between the results of the multibody model and those of the analytical model is presented Figure 7.10b. It appears from the graph that, while a general good agreement between the two models exists, some discrepancies can be found.

Preview distance is plotted versus the number of modes employed in Figure 7.10c. Beside a small influence of mode 4, modes 1 and 2 are responsible for most of the variation of L_p due to chassis compliance. The first mode, corresponding to a torsional deformation, induces an increment of the preview length while the second one tends to limit the effects of the first one.

The effect of each of the modes is analysed individually in Figure 7.10d where TI-optimal preview gains are plotted versus a multiplying factor of modal stiffness μ. While a clear inverse relationship between modal stiffness of mode 1 and preview length exists, and while the effect of modes 3-6 is limited, the effect of modal stiffness of mode 2 is more complex. In particular, there exists a configuration ($\mu = 0.3$) for which the value of the preview distance is greatly increased. It might be that this is due to the effect of modal deformation on suspension kinematics; no general conclusion however can be drawn.

A general agreement between Figure 7.10d and Figure 3.11d can be found. Because of its nature however, the simplified model is not capable of capturing the interaction between the chassis deformation and suspension kinematics. As a result, the predicted TI-preview gain sequence and the calculated preview length might differ, depending on the particular suspension geometry.

7.6 Computational aspects

7.6.1 Effect of chassis deformation on inertial forces

The mass matrix of a flexible body contains non-constant terms that depend on the body displacement. Aside from the mathematical details reported in Chapter 5, it is intuitive that these terms describe the variation of the inertia properties of the flexible body due to its own deformation.

Depending on the magnitude of the deformations and on the nature of the problem, these effects might or might not be relevant. When a vehicle is considered, it seems

reasonable to assume that the movements of the driver and of the vehicle fluids contribute to the variation of the inertia properties of the vehicle chassis in a more significant way than the chassis deformation itself. Trials have confirmed this hypothesis. In this case, using the adopted Newton-Euler approach, the mass matrix of the multibody system is constant and can be inverted off-line. As a consequence, an advantage in terms of computational efficiency can be obtained. Similar considerations are valid for the gyroscopic effects due to rotational and elastic coordinates of Equation (5.45).

7.6.2 Influence of coordinate reduction

As shown in Chapter 5, the adopted coordinate reduction method requires the evaluation of terms that include the first and second derivative of the constraint equations versus time. These depend, respectively, on steering wheel angle velocity and acceleration.

Simulation results have shown that no significant effect is found if vector $\boldsymbol{c}$ of Equation (5.61) is neglected. This fact can be associated with the use of relative coordinates for modelling the suspension kinematics; the use of absolute coordinates would involve significant variations in the projection matrices simply due to vehicle motion.

Similarly, trials have shown that vector $\boldsymbol{b}$ of Equation (5.54) only marginally affects the simulation results. In this case however, evaluation of steering angles due to steering wheel change is completely left to the kinematic error correction routine. As a consequence, a higher number of iterations is required and the computational advantage of neglecting $\boldsymbol{b}$ is limited.

7.6.3 Computational efficiency

The proposed modelling approach achieves a better computational efficiency than commercial multibody codes. Reasons for this lie in the use of a moving reference frame for the sprung mass and of relative coordinates for the unsprung masses, in the implementation of a velocity projection techniques capable of transforming the DAE problem arising from the multibody approach into a set of ODEs, and in the symbolic development. Furthermore, the reduced number of modal shapes minimises the computational cost due to the inclusion of chassis flexibility.

As an example, Table 7.2 reports CPU times required for some of the simulations presented when the described simplifications are introduced. All simulations have been performed on a standard PC equipped with a 2.4 GHz processor and 2 Gb of RAM. A relative tolerance of 10^{-4} and a sampling frequency of 1 kHz have been used. The table shows that in every case, the simulation time is considerably smaller than the duration of the manoeuvre; as a consequence the proposed model is suitable for real-time applications. Furthermore, simulations have shown that the computational burden

Table 7.2: Comparison of computational efficiency.

Manoeuvre	St. step	Skid-pad	St. sweep
Duration [s]	5	60	120
CPU time [s]			
Complete model, rigid chassis	0.7	2.1	9.4
Complete model, flexible chassis	0.9	2.4	10.0
Constant mass matrix	0.8	2.3	9.6
Neglect terms $\boldsymbol{G_r}$ and $\boldsymbol{G_e}$ of Eq. (5.45)	0.8	2.2	9.5
Neglect vector $\boldsymbol{c}$ of Eq. (5.58)	0.6	2.0	9.4

associated with chassis flexibility is limited and that the additional computational effort can be balanced by introducing a series of simplifications that do not affect simulation results.

It is worth noting that the whole Fortran program has been implemented without the use of any of the latest advances in software engineering such as parallelisation, multi-threading, or graphical processor unit computing, [157]. Despite this, the program has proven to be exceptionally efficient from the computational point of view. This fact makes it suitable for optimisation tasks and for all those applications in which high accuracy and computational efficiency are required.

7.7 Concluding remarks

Some results obtained from a multibody vehicle model have been presented in this chapter.

Simulations of steady-state vehicle behaviour have demonstrated that chassis deformation can either be written as a function of lateral acceleration or as a constant term due to weight of the sprung mass. While the latter has a negligible impact on vehicle behaviour, this is not the case for the former.

The analysis of the influence of chassis flexibility on lateral load transfer distribution has shown good agreement between the results of the analytical model presented in Chapter 3 and those of the more complex multibody model. Also, it has been shown that, although the torsional mode is responsible for most of the effects of chassis compliance on lateral load transfer distribution, minor effects due to higher order modes can be found.

The effect of chassis stiffness on suspension kinematics strongly depends on the nature of the modal shapes and on the geometry of the suspension system. A novel

analysis technique based on the use of relative coordinates and of a velocity projection matrix has been introduced in order to assess the effect of each of the single modes on suspension kinematics. This technique describes changes in suspension kinematics in a synthetic and efficient manner and highlights unwanted effects. Furthermore, this capability can be used for design and optimisation purposes.

Analysis of steady-state vehicle behaviour partially confirms the conclusions drawn in Section 3.4. More specifically, simulations show that while the effect of chassis flexibility on the lateral load transfer mechanism is responsible for the limit behaviour, changes in suspension kinematics are responsible for vehicle behaviour in the linear region. As representation of the effects of suspension kinematics in the preliminary model is limited, discrepancies between the two models can be found.

Analysis of transient behaviour has shown that impulsive manoeuvres can induce structural vibrations within the chassis that are responsible for a decay of the response of the vehicle.

Root locus analysis has been carried out by using a linearised version of the multibody model. Simulations have shown that the coupling between chassis and vehicle dynamics is responsible for lowering the frequency at which the first chassis mode is excited. On the other hand, this coupling increases internal chassis damping. Furthermore, dependency between internal damping and vehicle speed has been demonstrated.

Analysis of the frequency response to driver input has shown that, because of the limited bandwidth of the steering wheel input, effects on vehicle response are limited. When road inputs are considered however, simulations have shown that strong interaction between chassis and unsprung mass dynamics can occur. More specifically, resonance effect can be noticed if the anti-symmetric modes are excited.

It has been shown in the last part of the analysis that the multibody model can be employed within an existing framework for the derivation of time-invariant optimal controls. Results have shown a general agreement against the predictions of the preliminary model of Chapter 3. In particular, a strong dependency of the preview length on modal stiffness has been found.

Finally, a brief analysis of the achieved computational efficiency has been presented. In conclusion, the model has proven to be an efficient and effective tool for the analysis of several aspects of the impact of chassis flexibility on vehicle dynamics.

Chapter 8

Conclusions and future work

This Chapter summarises the main findings of the described work and includes recommendations for further research.

8.1 Conclusions

A literature review on the influence of chassis flexibility on vehicle dynamics has been introduced in the first part of the thesis. The analysis has revealed that, although the importance of the influence of chassis stiffness on vehicle dynamics is generally recognised, a systematic and complete study of its effects is not available.

Models currently employed for vehicle dynamics simulation have been reviewed; two distinct types exist. The first includes all those purpose-developed and often hand-derived models that follow the path that can be traced back to the work presented in 1956 by Segel et al., [34]. The second group, developed from the 1970s, is based on the use of multibody systems. The analysis of the positive and negative characteristics of each has revealed that, while multibody models generally permit to obtain very detailed results, purpose-developed analytical models are of great advantage for a first assessment of the considered problem.

On the basis of the literature review, an analytical model for a preliminary analysis of the impact of chassis flexibility on vehicle dynamics has been developed. Simulations have shown that chassis flexibility mainly affects the linear region of the vehicle behaviour through its effects on suspension kinematics and the limit region through its effects on lateral load transfer distribution. From this, it has been shown how both error and sensitivity maps can be derived and employed for vehicle design and tuning. Also, results have shown that chassis oscillations have a negative influence on the dynamic response of the vehicle and that the damping associated with chassis flexibility decreases with speed.

A review of the available techniques for multibody simulation has highlighted that

an efficient and effective model for the analysis of the influence of chassis flexibility on vehicle dynamics requires the implementation of a set of advanced methods. A novel symbolic multibody library that satisfies this requirement has been presented in Chapter 5. In this library, equations of motion are written according to a Newton-Euler formulation in a moving reference frame; a semi-recursive formulation is used for the description of the kinematics of the vehicle suspension and a coordinate reduction technique is implemented so that a set of minimal coordinates is obtained. Also, body flexibility is introduced through the use of a modal approach. The library, developed in the computer algebra environment Maple, is suitable for the analysis of generic mechanical systems and, in particular, of ground vehicles.

A vehicle model for the analysis of the effects of chassis flexibility on vehicle dynamics has been built using the multibody library. The model includes a detailed description of suspension kinematics and dynamics, a detailed tyre model and subroutines for the inclusion of aerodynamic and powertrain inputs.

Chassis flexibility has been included in the symbolic formulation of the multibody system through the use of modal shapes. Non-constant terms of the mass matrix and gyroscopic effects of rotational coordinates on body deformation coordinates have been included; the analysis has however shown that most of them can be safely neglected. Modal shapes have been obtained from a finite element model of an available vehicle by means of a modal truncation technique.

Good agreement between the developed model and an equivalent Adams/Car model has been found. The symbolic multibody formulation guarantees that the model is as accurate as those obtained by means of numeric multibody codes while a full and intrinsic parametrisation is included. The high computational efficiency makes the model suitable for optimisation, lap time analysis and hardware- or driver-in-the-loop simulation.

The multibody model has been demonstrated by using a set of data of a real vehicle. The analysis of the steady-state behaviour of the vehicle has partially confirmed the results obtained from the preliminary model. More specifically, it has been shown that the impact of chassis flexibility on lateral load transfer distribution can be correctly analysed by means of a relatively simple analytical model in which only the chassis torsional stiffness is included. The preliminary model however is of limited use for the analysis of the impact of chassis flexibility on suspension kinematics. These effects have been analysed by means of a novel technique based on the use of the velocity projection matrix. This technique permits the evaluation of the effects of each deformation mode of the chassis on suspension kinematics.

Root locus analysis has shown that the coupling between chassis and vehicle dynamics lowers the natural frequencies of the chassis while increasing modal damping. As shown by the preliminary model however, damping of chassis oscillations decreases with speed. As a result, chassis flexibility endangers vehicle stability at high speed.

Simulation of the response of the vehicle during a four-post test has highlighted that resonance effects between chassis and unsprung mass dynamics are generated if the relevant natural frequencies are close. In this case, both ride and handling qualities are sensibly affected.

It is common belief that vehicles with excessive chassis compliance do not inspire confidence into the driver. Due to their nature, both open- and closed-loop simulation methods cannot find a quantifiable correspondence to these considerations. Optimal control theory seems to address, at least partially, this problem. Its application to the developed vehicle model has shown that chassis flexibility is detected by the driver as the need for a more oscillatory control and for a longer preview distance.

Some considerations on the modelling approach are possible. Aside from the problem of modelling chassis flexibility, the proposed model might be seen as an attempt at bridging the gap between purpose-developed and commercial multibody models. Indeed, the implemented velocity projection technique coupled with the semi-recursive formulation permits a detailed description of suspension kinematics while enabling inspection of the projection matrix. As this matrix contains a synthetic description of the entire suspension kinematics, a link between the two types of models can be established. More specifically, not only data contained in the matrix are useful for a detailed evaluation of suspension kinematics gradients that can be used for a more simplified analysis but also the matrix itself can be derived from other models or from experimental data.

Considering the problem of modelling chassis flexibility for vehicle dynamics studies, the complication of hand-derivation of the equations of motion prevents any extensive development. Apart from a limited discussion presented in [24], modelling chassis compliance has never been attempted without the use of numeric multibody tools. The model presented intends to overcome some of the limitations generally linked to these tools and to offer a novel modelling perspective.

On the question of "how much stiffness is enough?", it appears from the analysis that an answer in absolute terms does not exist. On the contrary, it is important to distinguish the various aspects of vehicle dynamics, to set targets in terms of handling qualities, weight and costs and to analyse benefits and drawbacks of each design solution.

From the designer point of view, the analysis has shown that the effect of chassis flexibility on lateral load transfer distribution, which is very often the only mentioned one, does not constitute a major problem. As far as chassis flexibility is known, maps for tuning the roll stiffness distribution can be produced by using a simplified model. On the contrary, the analysis of the effects on suspension kinematics requires the use of more advanced modelling tools. Also, careful analysis on the interaction between the dynamics of the chassis and of the unsprung masses is recommended. It is worth noting that, because of the coupling between chassis and vehicle dynamics, analysis of

natural frequencies of the chassis alone is not sufficient. Finally, the described use of optimal control theory offers a novel tool for the evaluation of the impact of chassis flexibility on driver control.

8.2 Future work

Although it has proven to be a valid tool for the generation of the equations of motion of the complete vehicle, further work is recommended on the multibody library presented in Chapter 5. More specifically, documentation should be produced and user friendliness should be improved so that the library could be used for other modelling purposes within the research group. Also, a more complete set of joints should be generated. It is worth noting that, although other similar libraries exist, none of them is capable of including flexible bodies, of using relative coordinates and of implementing a velocity projection technique.

Regarding the vehicle modelling approach, further enhancements could include a more detailed modelling of chassis mass distribution, the possibility of including suspension compliances and the inclusion of powertrain loads. Also, it would be of interest to verify the capabilities of the developed model within a real-time or hardware-in-the loop system and to validate it against experimental data.

It is worth noting that the majority of the commercial multibody codes offer a limited choice in terms of modal description of flexible bodies. For example, Adams/Car only supports the use of Craig-Bampton bases. As a consequence, the use of some reduction techniques, e.g. the Krylov and Serep ones, has never been verified within a multibody system for vehicle dynamics simulation. Due to its formulation, the proposed model is compatible with any reduction technique; a systematic analysis of the performance of the available reduction techniques within the multibody code is therefore recommended.

Also, a full parametrisation of a limited set of modal shapes is possible. This would permit not only the evaluation of their effect on vehicle dynamics but also a further optimisation of the structure of the vehicle. A very limited analysis in this sense has been presented in [61] and, in a broader sense, in [62]. Further research in this sense is strongly recommended.

Further work on the analysis of the dynamics of vehicles with a flexible chassis is also recommended. As stated by Milliken, [20], excessive chassis flexibility induces problems in the field of lateral load transfer, suspension kinematics and unwanted vibrations. While effects on lateral load transfer are known, further work in understanding the effects on suspension kinematics is suggested. A further development of the analysis based on the use of the projection matrix, coupled with a parametrisation of the modal shapes, could be of advantage.

Although simulations have shown that damping induced by the coupling between

chassis and vehicle dynamics is generally high, this effect is reduced at high speed. As a consequence, chassis internal damping is critical for high-speed stability of vehicles with a flexible chassis. Further analysis in this area is recommended.

The same coupling between chassis and vehicle dynamics might trigger unwanted interactions between chassis and unsprung masses dynamics. Results have shown that the consequent underdamped vibrations sensibly increase the variation of the vertical load of the tyre contact patch. This problem can be avoided by increasing chassis stiffness or by lowering suspension natural frequency. It might also be possible to limit this interaction by using other techniques, for example by installing additional vibration absorbers. Also, a better understanding of the parameters that cause the reduction of chassis natural frequency could help mitigate these effects.

The analysis has exploited the potential of optimal control theory in a very limited manner. Recent works have shown that a detailed vehicle model can be employed for the evaluation of optimal controls in the non-linear region of the vehicle behaviour, [66, 158]. The inclusion of the proposed vehicle model within this framework would permit the assessment of the influence of chassis flexibility on optimal controls in a more realistic way.

Finally, despite the low computational cost of the model, further work on its computational efficiency is recommended. This should try to take advantage of the latest developments in the field of parallelisation and Graphics Processing Unit-based computing. Thanks to the adopted formulation, parallel implementation of the multibody model would lead to a further sensible improvement of its computational efficiency.

Appendix A

Input data for the preliminary model of Chapter 3

Table A.1: Vehicle data, baseline configuration.

Data	Description	Value	Unit
m	vehicle total mass	290	kg
m_s	sprung mass	225	kg
m_{uF}	front unsprung mass	28	kg
m_{uR}	rear unsprung mass	37	kg
h_G	vehicle c.g. height	295	mm
a	distance of vehicle c.g from front axle	843	mm
b	distance of vehicle c.g from rear axle	712	mm
a_s	distance of sprung mass c.g from front axle	830	mm
b_s	distance of sprung mass c.g from rear axle	725	mm
l	wheelbase	1555	mm
t	front and rear track width	1210	mm
h_{sF}	height of front sprung mass c.g.	295	mm
h_{sR}	height of rear sprung mass c.g.	315	mm
h_{uF}	height of front unsprung mass c.g.	255	mm
h_{uR}	height of rear unsprung mass c.g.	255	mm
z_F	front roll centre height	25	mm
z_R	rear roll centre height	45	mm
k_F	front roll stiffness	205	Nm/deg
k_R	rear roll stiffness	175	Nm/deg
c_F	front roll damping	225	Nms/deg
c_R	rear roll damping	270	Nms/deg
k_C	chassis torsional stiffness	380	Nm/deg

Data	Description	Value	Unit
c_C	chassis torsional damping	0	Nms/deg
k_{stw}	steering ratio	12	-
J_{rF}	front half roll inertia	30	kg m^2
J_{rR}	front half roll inertia	35	kg m^2
J_z	total yaw inertia	165	kg m^2
ε_F	front roll steer coefficient	0.05	-
ε_R	rear roll steer coefficient	0.1	-

Appendix B

Input data for the vehicle model of Chapter 4

Table B.1: Vehicle data.

Data	Description	Value	Unit
a	distance of vehicle c.g from front axle	1000	mm
b	distance of vehicle c.g from front axle	700	mm
h_{CG}	vehicle centre of gravity height	295	mm
m_s	sprung mass	225	kg
J_{xs}	sprung mass roll inertia	65	kgm^2
J_{ys}	sprung mass pitch inertia	90	kgm^2
J_{zs}	sprung mass yaw inertia	130	kgm^2
J_{xzs}	sprung mass $ox - oz$ product of inertia	20	kgm^2
m_{uF}	front single unsprung mass	14	kg
J_{xuF}	front unsprung mass cambering moment of inertia	0.2	kgm^2
J_{yuF}	front unsprung mass pitching moment of inertia	0.2	kgm^2
J_{zuF}	front unsprung mass yawing moment of inertia	0.6	kgm^2
m_{uR}	rear axle unsprung mass	18.5	kg
J_{xuR}	rear unsprung mass cambering moment of inertia	0.3	kgm^2
J_{yuR}	rear unsprung mass pitching moment of inertia	0.3	kgm^2
J_{zuR}	rear unsprung mass yawing moment of inertia	0.5	kgm^2
J_{wF}	front wheel spin moment of inertia	0.25	kgm^2
J_{wR}	rear wheel spin moment of inertia	0.25	kgm^2
t_F	front track width	1260	mm
t_R	rear track width	1210	mm
δ_F	static front toe angle	0	deg
δ_R	static rear toe angle	0	deg

Data	Description	Value	Unit
γ_F	static front camber angle	0	deg
γ_R	static rear camber angle	0	deg

Table B.2: Front left suspension hard points, rest configuration.

Point	Description	X	Y	Z	Unit
A	lower wishbone rear pivot	-280.0	249.7	145.0	mm
B	lower wishbone front pivot	80.0	249.7	145.0	mm
C	lower wishbone outer ball joint	5.0	585.6	140.0	mm
D	push rod wishbone end	5.0	550.5	165.0	mm
E	upper wishbone rear pivot	-280.0	259.7	345.0	mm
F	upper wishbone front pivot	80.0	259.8	345.0	mm
H	upper wishbone outer ball joint	-5.0	560.9	380.3	mm
L	inner track rod ball joint	-61.0	248.8	315.0	mm
M	outer track rod ball joint	-61.0	540.0	344.0	mm
P	rocker axis 1st point	100.0	210.0	432.7	mm
Q	rocker axis 2nd point	100.0	310.0	595.8	mm
R	push rod rocker end	158.0	250.0	475.0	mm
S	damper to rocker point	100.0	160.0	530.0	mm
T	damper to body point	-170.0	160.0	530.0	mm

Table B.3: Rear left suspension hard points, rest configuration.

Point	Description	X	Y	Z	Unit
A	lower wishbone rear pivot	-280.0	249.7	145.0	mm
B	lower wishbone front pivot	80.0	249.7	145.0	mm
C	lower wishbone outer ball joint	5.0	585.6	140.0	mm
D	push rod wishbone end	5.0	550.5	165.0	mm
E	upper wishbone rear pivot	-280.0	259.7	345.0	mm
F	upper wishbone front pivot	80.0	259.8	345.0	mm
H	upper wishbone outer ball joint	-5.0	560.9	380.3	mm
L	inner track rod ball joint	-61.0	248.8	315.0	mm
M	outer track rod ball joint	-61.0	540.0	344.0	mm
P	rocker axis 1st point	100.0	210.0	432.7	mm
Q	rocker axis 2nd point	100.0	310.0	595.8	mm
R	push rod rocker end	158.0	250.0	475.0	mm
S	damper to rocker point	100.0	160.0	530.0	mm
T	damper to body point	-170.0	160.0	530.0	mm

Table B.4: Tyre data.

Data	Description	Value	Unit
k_z	vertical stiffness	150000	N/m
c_z	vertical damping	50	Ns/m
σ_k	longitudinal slip relaxation length	0.3	m
σ_α	side slip relaxation length	0.3	m

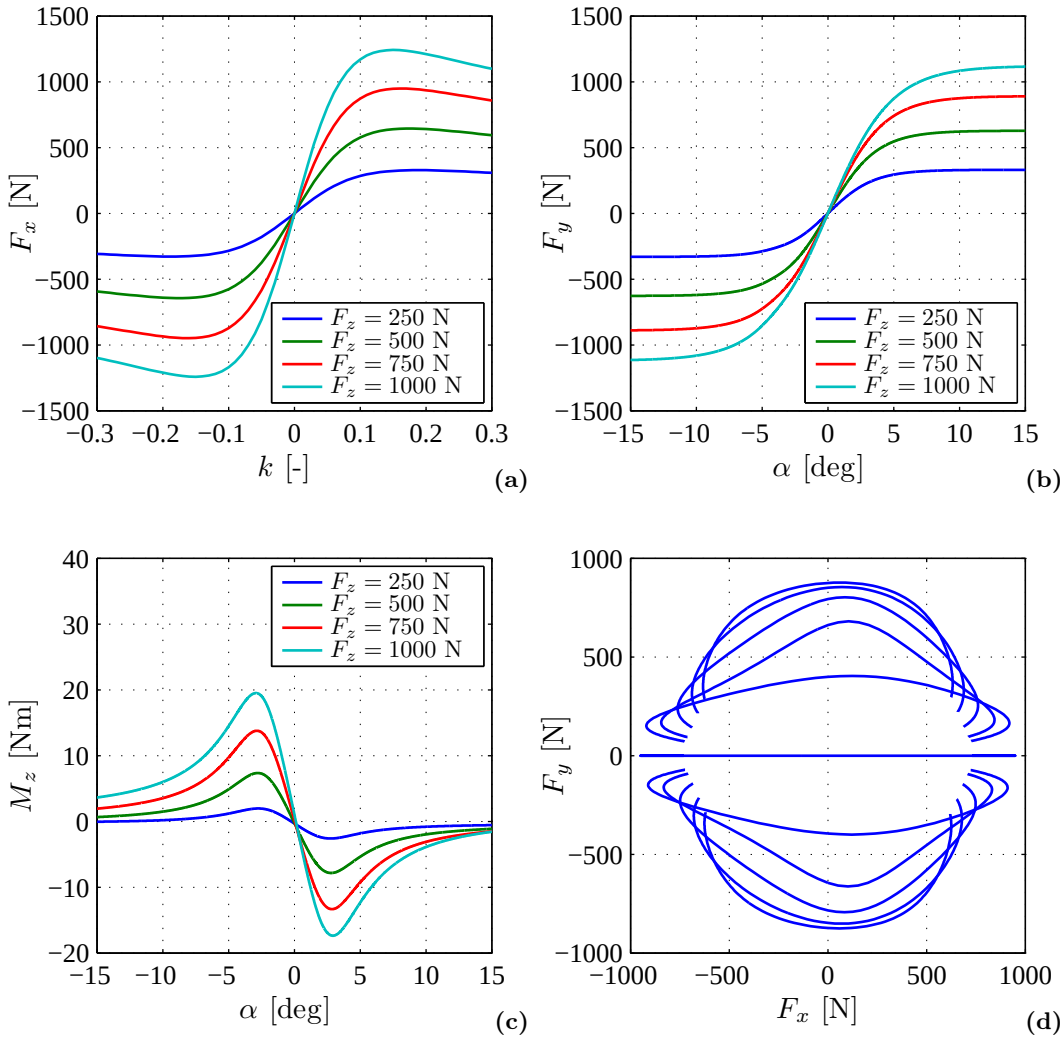

Figure B.1: Tyre force characteristics. (a) Longitudinal force versus longitudinal slip at different normal loads and null camber angle. (b) Lateral force versus slip angle at different normal loads and null camber angle. (c) Aligning torque versus slip angle at different normal loads and null camber angle. (d) Combined lateral and longitudinal forces at $F_z = 750$ N and null camber angle.

References

[1] D. Sperling and D. Gordon. *Two billion cars: driving toward sustainability.* Oxford University Press, New York Oxford, 1st ed., 2009.

[2] D. A. Crolla. Vehicle dynamics - theory into practice. *Proceedings of the Institution of Mechanical Engineers, Part D: Journal of Automobile Engineering*, 210 (2), pp. 83–94, 1996.

[3] R. S. Sharp. Application of multi-body computer codes to road vehicle dynamics modelling problems. *Proceedings of the Institution of Mechanical Engineers, Part D: Journal of Automobile Engineering*, 208 (1), pp. 55–61, 1994.

[4] R. Lot and M. Da Lio. A symbolic approach for automatic generation of the equations of motion of multibody systems. *Multibody System Dynamics*, 12 (2), pp. 147–172, 2004.

[5] M. Trzesniowski. *Rennwagentechnik: Grundlagen, Konstruktion, Komponenten, Systeme.* Vieweg Teubner Verlag, Wiesbaden, 1st ed., 2008.

[6] C. T. Onions. *Oxford dictionary of English etymology.* Oxford University Press, 1966.

[7] M. Costin and D. Phipps. *Racing and sports car chassis design.* Batsford, London, 2nd ed., 1974.

[8] D. Bastow. Car chassis frame design. *Proceedings of the Institution of Automobile Engineers*, 40 (1), pp. 147–165, 1946.

[9] J. C. Brown, A. J. Robertson and S. T. Serpento. *Motor vehicle structures: concepts and fundamentals.* Butterworth-Heinemann, Oxford, 2002.

[10] A. G. Booth. Factory experimental work and its equipment. *Proceedings of the Institution of Automobile Engineers*, 33 (1), pp. 503–581, 1939.

[11] M. E. Biancolini, F. Renzi and G. Rizzoni. Design of a lightweight chassis for the land speed record vehicle Buckeye Bullet 2. *International Journal of Vehicle Design*, 44 (3-4), pp. 379–402, 2007.

[12] H. Heisler. *Advanced vehicle technology.* Butterworth-Heinemann, Oxford, 2nd ed., 2002.

[13] T. Keer and R. Sturt. Automotive structures. American Society of Civil Engineers, Reston, 2007.

[14] D. Casanova, R. S. Sharp and P. Symonds. Minimum time manoeuvring: the significance of yaw inertia. *Vehicle System Dynamics*, 34 (2), pp. 77–115, 2000.

[15] D. Casanova. *On minumum time vehicle manoeuvring: the theoretical optimal lap.* PhD thesis, Cranfield University, 2000.

[16] A. Deakin, D. A. Crolla, J. P. Ramirez and R. Hanley. The effect of chassis stiffness on race car handling balance. In *2000 SAE Motorsports Engineering Conference Proceedings*, Dearborn, 2000. SAE paper 2000-01-3554, SAE International, Warrendale, 2000.

[17] W. B. Riley and A. R. George. Design, analysis and testing of a Formula SAE car chassis. In *2002 SAE Motorsports Engineering Conference Proceedings*, Indianapolis, 2002. SAE paper 2002-01-3300, SAE International, 2002.

[18] L. L. Thompson, P. H. Soni, S. Raju and H. E. Law. The effects of chassis flexibility on roll stiffness of a Winston Cup race car. In *1998 SAE Motorsports Engineering Conference Proceedings*, Dearborn, 1998. SAE paper 983051, SAE International, Warrendale, 1998.

[19] J. C. Dixon. *Tires, suspension and handling.* SAE International, Warrendale, 1996.

[20] W. F. Milliken and D. L. Milliken. *Race car vehicle dynamics.* SAE International, Warrendale, 1st ed., 1995.

[21] L. L. Thompson, S. Raju and H. E. Law. Design of a Winston Cup chassis for torsional stiffness. In *1998 SAE Motorsports Engineering Conference Proceedings*, Dearborn, 1998. SAE paper 983053, SAE International, Warrendale, 1998.

[22] L. L. Thompson, J. K. Lampert and H. E. Law. Design of a twist fixture to measure the torsional stiffness of a Winston Cup Chassis. In *1998 SAE Motorsports Engineering Conference Proceedings*, Dearborn, 1998. SAE paper 983054, SAE International, Warrendale, 1998.

[23] J. He and Z. F. Fu. *Modal analysis.* Butterworth-Heinemann, Oxford, 2001.

[24] G. Genta and L. Morello. *The automotive chassis. Volume 2: system design.* Springer, Dordrecht, 2009.

[25] G. Genta. *Motor vehicle dynamics: modeling and simulation.* World Scientific, Singapore, 1st ed., 1997.

[26] S. C. Southward and C. M. Boggs. Comparison of the performance of 7-post and 8-post dynamic shaker rigs for vehicle dynamic studies. In *2008 SAE Motorsports Engineering Conference Proceedings*, Concord, 2008. SAE paper 2008-01-2966, SAE International, Warrendale, 2008.

[27] D. Hancock. Testing partnership. *Racecar engineering*, 16 (1), pp. 42–44, January 2006.

[28] M. Blundell and D. Harty. *The multibody systems approach to vehicle dynamics.* Butterworth-Heinemann, Oxford, 1st ed., 2004.

[29] E. M. Lowndes. *Development of an intermediate DOF vehicle dynamics model for optimal design studies.* PhD thesis, North Carolina State University, 1998.

[30] P. Riekert and T. Schunck. Zur Fahrmechanik des gummibereiften Kraftfahrzeugs. *Ingenieur-Archiv*, 11, pp. 210–224, 1940.

[31] Y. Rocard. Les mefaits du roulement, auto-oscillations et instabilité de route. *La Revue Scientifique*, 84 (45), 1946.

[32] W. F. Milliken and D. W. Whitcomb. General introduction to a programme of dynamic research. *Proceedings of the Institution of Mechanical Engineers, Automobile Division*, 1956 (1), pp. 287–309, 1956.

[33] D. W. Whitcomb and W. F. Milliken. Design implications of a general theory of automobile stability and control. *Proceedings of the Institution of Mechanical Engineers, Automobile Division*, 1956 (1), pp. 367–425, 1956.

[34] L. Segel. Theoretical prediction and experimental substantiation of the response of the automobile to steering control. *Proceedings of the Institution of Mechanical Engineers, Automobile Division*, 1956, pp. 310–330, 1956.

[35] W. Bergman. Considerations in determining vehicle handling requirements. *SAE Journal*, SAE paper 690234, 1968.

[36] D. H. Weir and R. J. Di Marco. Correlation and evaluation of driver/vehicle directional handling data. *SAE Journal*, SAE paper 780010, 1978.

[37] R. R. McHenry. An analysis of the dynamics of automobiles during simultaneous cornering and ride motions. In *Proc. Handling of Vehicles under Emergency Conditions, IMechE Symposium*, Loughborough, 1969.

[38] R. S. Sharp and J. R. Goodall. A mathematical model for the simulation of vehicle motions. *Journal of Engineering Mathematics*, 3 (3), pp. 219–238, 1969.

[39] N. O. Tiffany, G. A. Cornell and R. L. Code. Hybrid simulation of vehicle dynamics and subsystems. *SAE Journal*, SAE paper 700155, 1970.

[40] F. H. Speckhart. A computer simulation for three dimensional vehicle dynamics. *SAE Journal*, SAE paper 730526, 1973.

[41] W. R. Garrott, D. L. Wilson and R. A. Scott. Digital simulation for automobile maneuvres. *Simulation*, 37 (3), pp. 83–91, 1981.

[42] W. R. Allen and T. J. Rosenthal. Vehicle and tire modeling for dynamic analysis and real-time simulation. In *2000 SAE World Congress & Exhibition Proceedings*, Detroit, 2000. SAE paper 2000-01-1620, SAE International, Warrendale, 2000.

[43] G. J. Heydinger, W. R. Garrott and J. P. Chrstos. The importance of tire lag on simulated transient vehicle response. In *1991 SAE International Congress & Exposition Proceedings*, Detroit, 1991. SAE paper 910235, SAE International, Warrendale, 1991.

[44] C. L. Clover and J. E. Bernard. The influence of lateral load transfer distribution on directional response. In *1993 SAE International Congress & Exposition Proceedings*, Detroit, 1993. SAE paper 930763, SAE International, Warrendale, 1993.

[45] W. R. Allen, B. L. Aponso, J. P. Chrstos and D. C. Lee. Driver/vehicle modelling and simulation. In *2002 SAE World Congress & Exhibition Proceedings*, Detroit, 2002. SAE paper 2002-01-1568, SAE International, Warrendale, 2002.

[46] K.-P. Schnelle, A. Van Zanten and M. Hiller. Simulation of nonlinear vehicle dynamics with the modular simulation package FASIM. *Vehicle System Dynamics*, 20 (Suppl.1), pp. 551–565, 1991.

[47] M. Hiller, K.-P. Schnelle and A. Van Zanten. FASIM - A modular program for simulation of nonlinear vehicle dynamics. *Vehicle System Dynamics*, 22 (Suppl.1), pp. 69–73, 1993.

[48] D. Horton. VDAS - Vehicle dynamics analysis software. *Vehicle System Dynamics*, 22 (Suppl. 1), pp. 130–133, 1993.

[49] A. A. Shabana and R. A. Wehage. Coordinate reduction technique for dynamic analysis of spatial substructures with large angular rotations. *Journal of Structural Mechanics*, 11 (3), pp. 401–431, 1983.

[50] T. W. Chu and R. P. Jones. Analysis and simulation of nonlinear handling characteristics of automotive vehicles with focus on lateral load transfer. *Vehicle System Dynamics*, 46 (Suppl. 1), pp. 17–31, 2008.

[51] L. L. Thompson, G. P. Herrick and H. E. Law. The effects of local spring perch flexibility on suspension geometry of a Winston Cup race car. In *1998 SAE Motorsports Engineering Conference Proceedings*, Dearborn, 1998. SAE paper 983032, SAE International, Warrendale, 1998.

[52] R. Baudille, M. E. Biancolini and L. Reccia. Load transfers evaluation in competition go-kart. *International Journal of Vehicle Systems Modelling and Testing*, 2 (3), pp. 208–226, 2007.

[53] G. Mirone. Multi-body elastic simulation of a go-kart: Correlation between frame stiffness and dynamic performance. *International Journal of Automotive Technology*, 11 (4), pp. 461–469, 2009.

[54] S. Hasegawa, Y. Kusahara and Y. Watanabe. Influence of vehicle body torsional stiffness on the vehicle controllability and stability of medium duty trucks. In *1989 SAE International Congress & Exposition Proceedings*, Detroit, 1989. SAE paper 891295, SAE International, Warrendale, 1989.

[55] S. Hasegawa, Y. Kusahara and Y. Watanabe. Influence of vehicle body torsional stiffness on vehicle roll characteristics of medium duty trucks. In *1990 SAE International Congress & Exposition Proceedings*, Detroit, 1990. SAE paper 902267, SAE International, Warrendale, 1990.

[56] S. Miki. Method for evaluating stability and handling of a truck considering body torsional rigidity. In *1988 SAE International Congress & Exposition Proceedings*, Detroit, 1988. SAE paper 881870, SAE International, Warrendale, 1989.

[57] S. J. Randle. Concept and design of the McLaren F1 suspension system. Birmingham, 1993. Mechanical Engineering Publications.

[58] Y. Y. Tong. Vehicle dynamic simulations based on flexible and rigid multibody models. In *2000 SAE World Congress & Exhibition Proceedings*, Detroit, 2000. SAE paper 2000-01-0114, SAE International, Warrendale, 2000.

[59] J. A. C. Ambrósio and J. P. C. Gonçalves. Complex flexible multibody systems with application to vehicle dynamics. *Multibody System Dynamics*, 6 (2), pp. 163–182, 2001.

[60] S. Azadi, M. Vaziri and M. Hoseini. Vehicle dynamic control of a passenger car applying flexible body model. *Vehicle System Dynamics*, 48 (5), pp. 587–617, 2010.

[61] S. H. Woo, C. S. Kim and C. Kim. The procedure for improving R&H performance of the new 2010 Hyundai Sonata by modal parameter modification of its body. In *2010 SAE World Congress & Exhibition Proceedings*, Detroit, 2010. SAE paper 2010-01-1136, SAE International, Warrendale, 2010.

[62] T. Tamarozzi, G. Stigliano, M. Gubitosa, S. Donders and W. Desmet. Investigating the use of reduction techniques in concept modeling for vehicle body design optimization. In *ISMA2010 International Conference on Noise and Vibration Engineering*, Leuven, 2010.

[63] B. Chaturvedi, R. Mugundaram and D. Rana. Correlation of vehicle dynamics & NVH performance with body static & dynamic stiffness through CAE and experimental analysis. In *2010 SAE World Congress & Exhibition Proceedings*, Detroit, 2010. SAE paper 2010-01-1137, SAE International, Warrendale, 2010.

[64] I. M. Ibrahim, D. A. Crolla and D. C. Barton. Effect of frame flexibility on the ride vibration of trucks. *Computers and Structures*, 58 (4), pp. 709–713, 1996.

[65] M. Mahinzaeim, J. M. Halelb, D. C. Swailes, R. Schmidt and B. Johanning. The application of an active vibration regulation system to improving driving comfort in convertible vehicles: a comparative Study of regulator design methodologies. *Applied Mechanics and Materials*, 7-8 (1), pp. 277–282, 2007.

[66] D. P. Kelly and R. S. Sharp. Time-optimal control of the race car: A numerical method to emulate the ideal driver. *Vehicle System Dynamics*, 48 (12), pp. 1461–1474, 2010.

[67] S. Moss and L. Pomeroy. *Design and behaviour of the racing car*. William Kimber, London, 1963.

[68] M. Abe and W. Manning. *Vehicle handling dynamics: theory and application*. Butterworth-Heinemann, Oxford, 2009.

[69] H. Kwakernaak and R. Sivan. *Linear optimal control systems*. Wiley-Interscience, New York - London, 1972.

[70] R. S. Sharp and V. Valtetsiotis. Optimal preview car steering control. In P. Lugner and K. Hedrick (editors), *International Congress of Theoretical and Applied Mechanics*, Chicago, 2000. Swets & Zeitlinger.

[71] R. S. Sharp. Driver steering control and a new perspective on car handling qualities. *Proceedings of the Institution of Mechanical Engineers, Part C: Journal of Mechanical Engineering Science*, 219 (10), pp. 1041–1051, 2005.

[72] M. Thommyppillai, S. Evangelou and R. S. Sharp. Car driving at the limit by adaptive linear optimal preview control. *Vehicle System Dynamics*, 47 (12), pp. 1535–1550, 2009.

[73] H. B. Pacejka. *Tyre and vehicle dynamics*. Elsevier, Oxford, 2nd ed., 2006.

[74] J. Wittenburg. *Dynamics of systems of rigid bodies*. Teubner, Stuttgart, 1977.

[75] P. E. Nikravesh. *Computer-aided analysis of mechanical systems*. Prentice-Hall, Englewood Cliffs, 1988.

[76] E. J. Haug. *Computer aided kinematics and dynamics of mechanical systems*. Prentice Hall, Boston, 1989.

[77] W. Schiehlen (editor). *Advanced multibody system dynamics: simulation and software tools*. Kluwer Academic, 1993.

[78] R. Von Schwerin. *Multibody system simulation: numerical methods, algorithms, and software*. Springer-Verlag, Berlin, 1999.

[79] R. Schwertassek and O. Wallrapp. *Dynamik flexibler Mehrkörpersysteme*. Vieweg Verlagsgesellschaft, Braunschweig - Wiesbaden, 1999.

[80] R. Huston. *Multibody dynamics*. Butterworth-Heinemann, Stoneham, 1990.

[81] A. A. Shabana. *Computational dynamics*. Wiley, New York, 1st ed., 2001.

[82] A. A. Shabana. *Dynamics of multibody systems*. Cambridge University Press, Cambridge, 3rd ed., 2005.

[83] A. A. Shabana. Flexible multibody dynamics: review of past and recent developments. *Multibody System Dynamics*, 1 (2), pp. 189–222, 1997.

[84] J. García de Jalón and E. Bayo. *Kinematic and dynamic simulation of multibody systems: the real-time challenge*. Springer-Verlag, New York, 1st ed., 1994.

[85] W. Schiehlen. Multibody system dynamics: Roots and perspectives. *Multibody System Dynamics*, 1 (2), pp. 149–188, 1997.

[86] W. Kortüm and W. Schiehlen. General Purpose Vehicle System Dynamics Software Based on Multibody Formalisms. *Vehicle System Dynamics*, 14 (4), pp. 229–263, 1985.

[87] W. Kortüm and R. S. Sharp. Multibody computer codes in vehicle system dynamics. *Vehicle system dynamics*, 22 (Suppl. 1), pp. 1–267, 1993.

[88] R. S. Sharp. Multibody dynamics applications in vehicle engineering. In *Institution of Mechanical Engineers Conference Transactions 1998*, London, 1998.

[89] J. I. Rodriguez, J. M. Jimenez, J. F. Funes and J. García De Jalón. Recursive and residual algorithms for the efficient numerical integration of multi-body systems. *Multibody System Dynamics*, 11 (4), pp. 295–320, 2004.

[90] M. A. Serna, R. Avilés and J. García De Jalón. Dynamic analysis of plane mechanisms with lower pairs in basic coordinates. *Mechanism and Machine Theory*, 17 (6), pp. 397–403, 1982.

[91] T. M. Wasfy and A. K. Noor. Computational strategies for flexible multibody systems. *Applied Mechanics Reviews*, 56 (6), pp. 553–613, 2003.

[92] H. Bremer. *Elastic multibody dynamics: a direct Ritz approach.* Springer, Dordrecht, 2008.

[93] O. Wallrapp. Standardization of flexible body modeling in multibody system codes, Part I: Definition of standard input data. *Mechanics of Structures and Machines*, 22 (3), pp. 283–304, 1994.

[94] J. O. Song and E. J. Haug. Dynamic analysis of planar flexible mechanisms. *Computer Methods in Applied Mechanics and Engineering*, 24 (3), pp. 359–381, 1980.

[95] R. Schwertassek, O. Wallrapp and A. A. Shabana. Flexible multibody simulation and choice of shape functions. *Nonlinear Dynamics*, 20 (4), pp. 361–380, 1999.

[96] P. Koutsovasilis and M. Beitelschmidt. Comparison of model reduction techniques for large mechanical systems. *Multibody System Dynamics*, 20 (2), pp. 111–128, 2008.

[97] R. R. Craig and M. C. C. Bampton. Coupling of substructures for dynamic analyses. *AIAA Journal*, 6 (7), pp. 1313–1319, 1968.

[98] S.-S. Kim and E. J. Haug. A recursive formulation for constrained mechanical system dynamics, Part I: open-loop systems. *Mechanics of Structures and Machines*, 15 (3), pp. 359–382, 1987.

[99] S.-S. Kim and E. J. Haug. A recursive formulation for constrained mechanical system dynamics, Part II: closed-loop systems. *Mechanics of Structures and Machines*, 15 (4), pp. 481–506, 1987.

[100] S.-S. Kim. A subsystem synthesis method for efficient vehicle multibody dynamics. *Multibody System Dynamics*, 7 (2), pp. 189–207, 2002.

[101] A. Eichberger and W. Rulka. Process save reduction by macro joint approach: the key to real-time and efficient vehicle simulation. *Vehicle System Dynamics*, 41 (5), pp. 401–413, 2004.

[102] D. S. Bae, J. M. Han, J. H. Choi and S. M. Yang. A generalized recursive formulation for constrained flexible multibody dynamics. *International Journal for Numerical Methods in Engineering*, 50 (8), pp. 1841–1859, 2001.

[103] J. Goncalves and J. Ambrosio. Advanced modelling of flexible multibody systems using virtual bodies. *Computer Assisted Mechanics and Engineering Sciences*, 9 (3), pp. 373–390, 2002.

[104] E. Hairer and G. Wanner. *Solving ordinary differential equations II: stiff and differential-algebraic problems*. Springer-Verlag, Berlin, 2nd ed., 1996.

[105] A. Laulusa and O. A. Bauchau. Review of classical approaches for constraint enforcement in multibody systems. *Journal of Computational and Nonlinear Dynamics*, 3 (1), pp. 011004/8, 2008.

[106] O. A. Bauchau and A. Laulusa. Review of contemporary approaches for constraint enforcement in multibody systems. *Journal of Computational and Nonlinear Dynamics*, 3 (1), pp. 11005/9, 2008.

[107] C. W. Gear. DIFSUB for solution of ordinary differential equations. *Communications of the ACM*, 14 (3), pp. 185–190, 1971.

[108] J. Baumgarte. Stabilization of constraints and integrals of motion in dynamical systems. *Computer Methods in Applied Mechanics and Engineering*, 1 (1), pp. 1–16, 1972.

[109] U. M. Ascher and L. R. Petzold. Stability of computational methods for constrained dynamics systems. *SIAM Journal on Scientific Computing*, 14 (1), pp. 95–120, 1993.

[110] E. Bayo, J. García De Jalón and M. A. Serna. A modified Lagrangian formulation for the dynamic analysis of constrained mechanical systems. *Computer Methods in Applied Mechanics and Engineering*, 71 (2), pp. 183–195, 1988.

[111] R. A. Wehage and E. J. Haug. Generalized coordinate partitioning for dimension reduction in analysis of constrained dynamic systems. *Journal of Mechanical Design*, 104 (1), pp. 247–255, 1982.

[112] G. A. Maggi. *Principii della teoria matematica del movimento dei corpi: corso di meccanica razionale*. Ulrico Hoepli, Milan, 1896.

[113] G. A. Maggi. Di alcune nuove forme della equazioni della dinamica applicabile ai sistemi anolonomi. *Atti della Reale Academia Nazionale dei Lincei, Serie V*, 10 (2), pp. 287–291, 1901.

[114] J. I. Neimark and N. A. Fufaev. *Dynamics of nonholonomic systems.* American Mathematical Society, Providence, 1972.

[115] M. Borri, C. Bottasso and P. Mantegazza. Equivalence of Kane's and Maggi's equations. *Meccanica*, 25 (4), pp. 272–274, 1990.

[116] A. Kurdila, J. G. Papastavridis and M. P. Kamat. Role of Maggi's equations in computational methods for constrained multibody systems. *Journal of Guidance, Control, and Dynamics*, 13 (1), pp. 113–120, 1990.

[117] T. R. Kane and D. A. Levinson. *Dynamics: theory and applications.* McGraw-Hill, New York, 1985.

[118] M. W. Sayers. Vehicle models for RTS applications. *Vehicle System Dynamics*, 32 (4-5), pp. 421–438, 1999.

[119] M. W. Sayers and D. Han. Generic multibody vehicle model for simulating handling and braking. *Vehicle System Dynamics*, 25 (Suppl.1), pp. 599–613, 1996.

[120] F. E. Udwadia and R. E. Kalaba. A new perspective on constrained motion. *Proceedings of the Royal Society of London, Series A*, 439 (1906), pp. 407–410, 1992.

[121] C. C. Pantelides. The consistent initialization of differential-algebraic systems. *SIAM Journal on Scientific and Statistical Computing*, 9 (2), pp. 213–231, 1988.

[122] T. Kurz, P. Eberhard, C. Henninger and W. Schiehlen. From Neweul to Neweul-M^2: symbolical equations of motion for multibody system analysis and synthesis. *Multibody System Dynamics*, 24 (1), pp. 25–41, 2010.

[123] R. S. Sharp. Optimal stabilization and path-following controls for a bicycle. *Proceedings of the Institution of Mechanical Engineers, Part C: Journal of Mechanical Engineering Science*, 221 (4), pp. 415–428, 2007.

[124] R. S. Sharp, S. Evangelou and D. J. N. Limebeer. Advances in the modelling of motorcycle dynamics. *Multibody System Dynamics*, 12 (3), pp. 251–283, 2004.

[125] C. W. Mousseau, M. W. Sayers and D. J. Fagan. Symbolic quasi-static and dynamic analyses of complex automobile models. *Vehicle System Dynamics*, 20 (Suppl.1), pp. 446–459, 1992.

[126] V. Cossalter, R. Lot and M. Massaro. The influence of frame compliance and rider mobility on the scooter stability. *Vehicle System Dynamics*, 45 (4), pp. 313–326, 2007.

[127] V. Cossalter, R. Lot and M. Massaro. An advanced multibody code for handling and stability analysis of motorcycles. *Meccanica*, August 2010, pp. 1–16, 2010.

[128] G. K. Gupta, R. Sacks-Davis and P. E. Tischer. A review of recent developments in solving ODEs. *Computing Surveys*, 17 (1), pp. 5–47, 1985.

[129] E. Hairer, S. P. Nø rsett and G. Wanner. *Solving ordinary differential equations I: nonstiff problems*. Springer-Verlag, Berlin, 2nd ed., 1993.

[130] P. Henrici. *Discrete variable methods in ordinary differential equations*. Wiley, New York, 1962.

[131] L. Petzold. Automatic selection of methods for solving stiff and nonstiff systems of ordinary differential equations. *SIAM Journal on Scientific and Statistical Computing*, 4 (1), pp. 136–148, 1983.

[132] K. E. Brenan, S. L. Campbell and L. R. Petzold. *Numerical solution of initial-value problems in differential algebraic equations*. Society for Industrial and Applied Mathematics, Philadelphia, 1996.

[133] C. Orlandea and N. V. Orlandea. Description of the general three-dimensional computer program 3D-MCADA. *Vehicle System Dynamics*, 22 (Suppl.1), pp. 83–86, 1993.

[134] C. W. Gear and L. R. Petzold. ODE methods for the solution of differential–algebraic systems. *SIAM Journal on Numerical Analysis*, 21 (4), pp. 716–728, 1984.

[135] C. W. Gear. Simultaneous numerical solution of differential algebraic equations. *IEEE Transactions on circuit theory*, 18 (1), pp. 85–95, 1971.

[136] C. W. Gear. Differential algebraic equations, indices, and integral algebraic equations. *SIAM Journal on Numerical Analysis*, 27 (6), pp. 1527–1534, 1990.

[137] C. W. Gear. Differential algebraic equation index transformations. *SIAM Journal on Scientific and Statistical Computing*, 9 (1), pp. 39–47, 1988.

[138] L. R. Petzold. Automatic selection of methods for solving stiff and nonstiff systems of ordinary differential equations. *SIAM Journal on Scientific and Statistical Computing*, 4 (1), pp. 136–148, 1983.

[139] L. R. Petzold. Differential algebraic equations are not ODE's. *SIAM Journal on Scientific and Statistical Computing*, 3 (3), pp. 367–384, 1982.

[140] K. Burrage and L. R. Petzold. On order reduction for Runge–Kutta methods applied to differential algebraic systems and to stiff systems of ODEs. *SIAM Journal on Numerical Analysis*, 27 (2), pp. 447–456, 1990.

[141] U. M. Ascher, H. Chin, L. R. Petzold and S. Reich. Stabilization of constrained mechanical systems with DAEs and invariant manifolds. *Mechanics of Structures and Machines*, 23 (2), pp. 135–157, 1995.

[142] U. M. Ascher and L. R. Petzold. Projected implicit Runge–Kutta methods for differential algebraic equations. *SIAM Journal on Numerical Analysis*, 28 (4), pp. 1097–1120, 1991.

[143] C. W. Gear, B. Leimkuhler and G. K. Gupta. Automatic integration of Euler-Lagrange equations with constraints. *Journal of Computational and Applied Mathematics*, 12-13 (1), pp. 77–90, 1985.

[144] C. Lubich. Extrapolation integrators for constrained multibody systems. *Impact of Computing in Science and Engineering*, 3 (3), pp. 213–234, 1991.

[145] J. H. Sohn, W. S. Yoo, K. S. Kim and J. N. Lee. Force element formulation of bushed massless links for numerical efficiency. *Mechanics of Structures and Machines*, 29 (4), pp. 477–497, 2001.

[146] J. H. Sohn, W. S. Yoo, K. S. Kim and J. N. Lee. Massless links with external forces and bushing effect for multibody dynamic analysis. *KSME International Journal*, 16 (6), pp. 810–818, 2002.

[147] R. G. Budynas. *Advanced strength and applied stress analysis*. McGraw-Hill, New York, 1977.

[148] M. Blundell. The modelling and simulation of vehicle handling, part 3: tyre modelling. *Proceedings of the Institution of Mechanical Engineers, Part K: Journal of Multi-body Dynamics*, 214 (1), pp. 1–32, 2000.

[149] J. S. Loeb, D. A. Guenther, H. H. Fred Chen and J. R. Ellis. Lateral stiffness, cornering stiffness and relaxation length of the pneumatic tire. In *1990 SAE International Congress & Exposition Proceedings*, Detroit, 1990. SAE paper 900129, SAE International, 1990.

[150] G. Mavros. A study on the influences of tyre lags and suspension damping on the instantaneous response of a vehicle. *Proceedings of the Institution of Mechanical*

Engineers, Part D: Journal of Automobile Engineering, 222 (4), pp. 485–498, 2008.

[151] A. Stevenson. Manufacturing, testing and optimisation of the chassis of the 2009 Formula Student vehicle. MSc thesis, University of Surrey, 2009.

[152] *Ansys Elements Reference*. ANSYS, Inc, 2007.

[153] J. A. C. Ambrosio and P. Ravn. Elastodynamics of multibody systems using generalized inertial coordinates and structural damping. *Mechanics of Structures and Machines*, 25 (2), pp. 201–219, 1997.

[154] H. Kowalczyk. Damper tuning with the use of a seven post shaker rig. In *2002 SAE World Congress & Exhibition Proceedings*, Detroit, 2002. SAE paper 2002-01-0804, SAE International, Warrendale, 2002.

[155] J. Kelly, H. Kowalczyk and H. A. Oral. Track simulation and vehicle characterization with seven post testing. In *2002 SAE World Congress & Exhibition Proceedings*, Detroit, 2002. SAE paper 2002-01-3307, SAE International, Warrendale, 2002.

[156] R. Dias Torcato and D. Purdy. Test signals for four post and seven post testing. In *FISITA World Automotive Congress*, Budapest, 2010. Springer Automotive Media.

[157] T. Heyn, A. Tasora, M. Anitescu and D. Negrut. A parallel algorithm for solving complex multibody problems with stream processors. In *7th International Conference on Multibody Systems, Nonlinear Dynamics, and Control*, San Diego, CA, United states, 2009. American Society of Mechanical Engineers.

[158] M. Thommyppillai, S. Evangelou and R. S. Sharp. Advances in the development of a virtual car driver. *Multibody System Dynamics*, 22 (3), pp. 245–267, 2009.